INTERNATIONAL STUDIES IN THE FIELD OF

ENGINEERING

EDITORS

Prof. Dr. Selahattin BARDAK - Doç. Dr. Hilmi ZENK

DECEMBER 2025

gece kitaplığı

İmtiyaz Sahibi / Yaşar Hız
Yayına Hazırlayan / Gece Kitaplığı

Birinci Basım / Aralık 2025 - Ankara
ISBN / 978-625-8570-58-8

Gece Kitaplığı
Kızılay Mah. Fevzi Çakmak 1. Sokak
Ümit Apt No: 22/A Çankaya/ANKARA
0312 384 80 40
www.gecekitapligi.com / gecekitapligi@gmail.com

Baskı & Cilt
Bizim Büro
Sertifika No: 42488

INTERNATIONAL STUDIES IN THE FIELD OF ENGINEERING

DECEMBER 2025

EDITORS

Prof. Dr. Selahattin BARDAK

Doç. Dr. Hilmi ZENK

gece kitaplığı

CONTENTS

CHAPTER 1

VISUAL SENTIMENT ANALYSIS: BRIDGING THE GAP BETWEEN PIXELS AND AFFECT

Arzum KARATAS[1]

1 Asst. Prof. Dr., Department of Computer Engineering, Faculty of Engineering and Natural Sciences, Bandirma Onyedi Eylul University, https://orcid.org/ 0000-0001-6433-3355.

1. Introduction

Visual Sentiment Analysis (VSA) is a specialized branch of computer vision dedicated to predicting the emotional response evoked by visual stimuli. While traditional Object Recognition (OR) seeks to answer the objective question *"What is in this image?"*, VSA addresses the subjective query *"How does this image make the viewer feel?"*.

The distinction is profound. In object recognition, a classifier that identifies a *dog* has succeeded if the pixels correspond to the biological entity *Canis lupus familiaris*. In VSA, the presence of a dog is merely a feature; the goal is to determine whether the dog—perhaps baring its teeth or playing with a ball—conveys *Fear* or *Joy*. Similarly, an image of a thunderstorm may be semantically described as *clouds*, *rain*, and *lightning*, but affectively interpreted as *fear*, *awe*, or *melancholy* depending on the context. This shift from ontology (*what is it*) to affect (*what does it mean*) represents a significant leap in Artificial Intelligence.

1.1 The "Visual Turn" in Digital Communication

The significance of this field has grown in parallel with what sociologists term the 'Visual Turn'. The proliferation of smartphones, high-speed mobile networks, and social media platforms has fundamentally altered the nature of human interaction. Platforms like Instagram, TikTok, Snapchat, and YouTube generate billions of visual data points daily. Unlike the web of the early 2000s, which was predominantly textual, the modern web is visual.

Images are rarely neutral artifacts; they are curated expressions of joy, outrage, sorrow, nostalgia, and irony. Traditional text-based sentiment analysis, which powered web analytics in the 2000s, is no longer sufficient. For example, an image of a burning forest accompanied by the caption "This is fine"—a popular internet meme—would be misclassified as Neutral or even Positive by a text-only model, missing the profound irony and negative sentiment conveyed by the visual context. This illustrates why VSA has emerged as a critical sub-discipline of Affective Computing and Computer Vision (Liu et al., 2023).

1.2 Problem Formulation

Mathematically, Visual Sentiment Analysis (VSA) can be defined as a mapping function f. Given an image I from a visual space v, the goal is to map I to a sentiment label s in a sentiment space S:

$$s = f(I; \theta)$$

where θ represents the learnable parameters of the model. The nature of space S defines the specific VSA task:

1. **Binary Polarity:** $S \epsilon \{Positive, Negative\}$
2. **Discrete Emotion Classification:** $S \epsilon \{Anger, Disgust, Fear, Joy, Sadness, Surprise\}$ (based on Ekman's model).
3. **Dimensional Regression:** $S \epsilon \mathbb{R}^2$ (Valence-Arousal space).

1.1 The Semantic, Affective, and Cultural Gaps

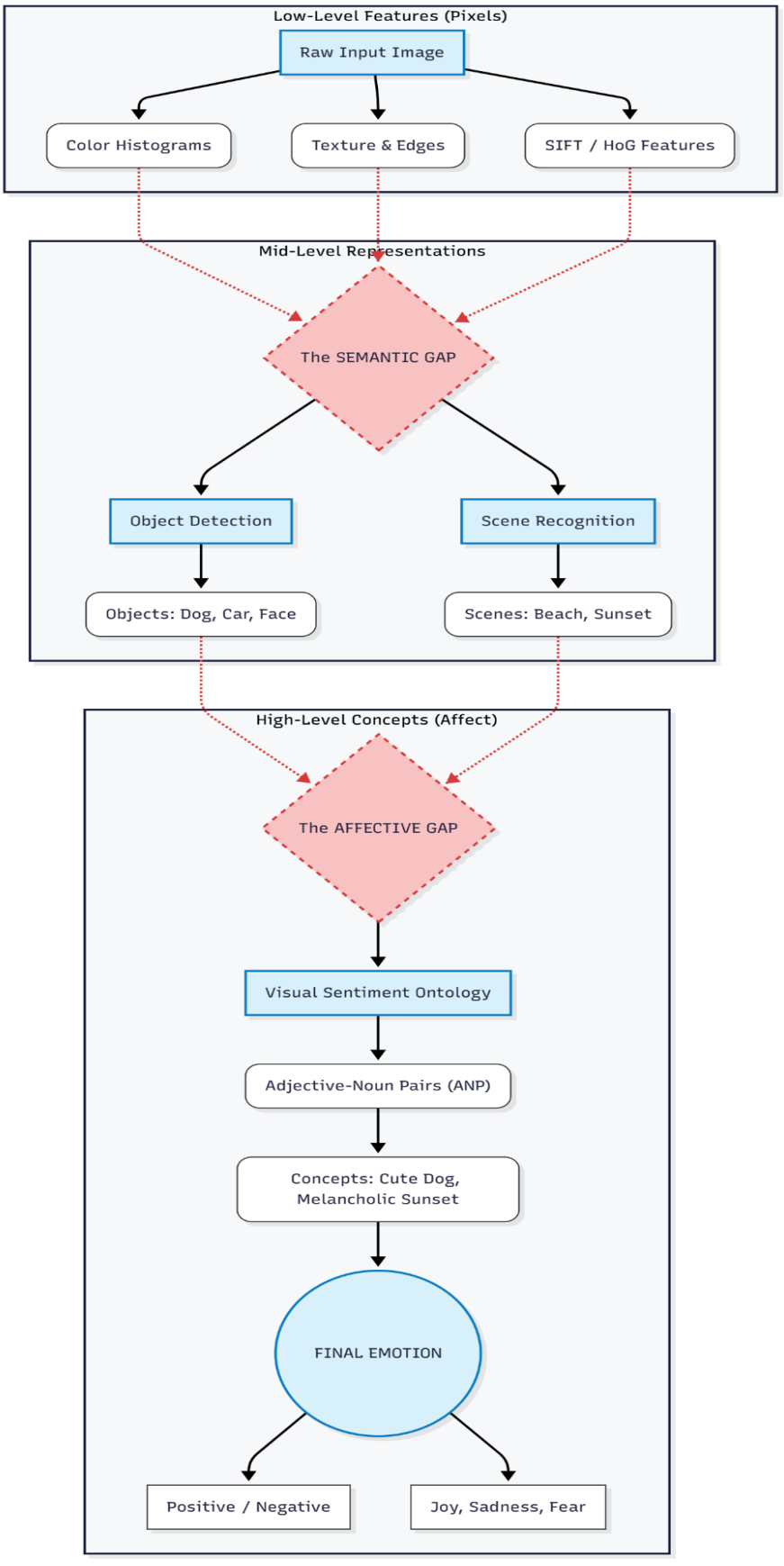

Figure 1. Hierarchical Framework of Visual Analysis

To understand the computational difficulty of Visual Sentiment Analysis (VSA), three critical conceptual hurdles must be defined. These gaps represent the loss of information that occurs when translating human experience into machine-readable data.

- **Semantic Gap:** The disconnect between low-level pixel information (color intensity, texture gradients) and high-level semantic concepts. For a computer, an image is a matrix of numbers (0–255). Mapping these numbers to the concept of a *sunset* illustrates the Semantic Gap. While modern Convolutional Neural Networks (CNNs) have largely bridged this gap for concrete objects, abstract or context-dependent concepts remain challenging.

- **Affective Gap:** The further disconnect between semantic concepts and the subjective emotions they trigger. For instance, the semantic concept *Clown* is objectively defined, yet the affective response varies: joy for a child at a circus, terror for an adult with coulrophobia, or fear in the context of a horror movie. Bridging this gap requires models that integrate visual content with contextual, cultural, and psychological cues (*Zhao et al., 2018*).

- **Cultural Gap:** Emotional interpretation varies across cultures. A gesture, color, or symbol may evoke joy in one culture but sadness or fear in another. Bridging this gap requires culturally adaptive models that account for diversity in affective meaning.

Figure 1 illustrates the transition from pixels to semantics, and semantics to affect, highlighting the challenges noted above. Specifically:

- **Low-Level (Pixel Level):** Raw data perceived by the computer (color, edges, texture).

- **Semantic Gap & Affective Gap:** Shown as red dashed lines, marking the two major hurdles already defined in the literature.

- **Bridging Strategies:** Researchers often employ mid-level representations such as *Adjective–Noun Pairs (ANPs)*. For instance, the sentiment in *Cute Dog* emerges not merely from the object (*dog*), but from the adjectival modifier (*cute*), which conveys affective meaning.

2. Theoretical Foundations: The Psychology of Emotion

Computer vision algorithms are not merely technical operations; they aim to model human biological and psychological processes; they attempt to model biological and psychological processes. Therefore, a robust VSA system must be grounded in established psychological theories of emotion. Two dominant paradigms exist in the literature: *Categorical Emotion Models* (Discrete) and *Dimensional Emotion Models* (Continuous).

2.1 Categorical Emotion Models (Ekman)

The most widely adopted framework in Visual Sentiment Analysis (VSA) datasets is the *Categorical Emotion Model*. Building on Paul Ekman's seminal cross-cultural research on facial expressions, this paradigm assumes that humans universally share six *Basic Emotions*: *Happiness, Sadness, Fear, Anger, Disgust, and Surprise* (Ekman, 1992). Within this framework, VSA tasks are formulated as a *multi-class classification problem*, where each image is mapped to one of these discrete emotional categories.

Formally, the model produces a probability distribution vector $p \in \mathbb{R}^6$, representing the likelihood of each emotion class. Training is typically guided by the *Categorical Cross-Entropy Loss*, which penalizes deviations between predicted probabilities and ground-truth labels. The objective is to learn discriminative features that enable the assignment of a single dominant emotion label to a given image.

$$Categorical\ Cross - Entropy\ Loss = -\sum y_i * log(\hat{y}_i)$$

where y are ground-truth labels and $\hat{y}$ are predicted probabilities. When y is encoded as a *one-hot vector*, the loss reduces to the negative log-likelihood of the predicted probability for the true class, i.e. $L = -log\ (\hat{y}_{true})$. In cases where *soft labels* or distributional annotations are used (e.g., multiple emotions weighted by annotator agreement), the same formulation applies, but the loss aggregates across all classes proportionally to their ground-truth weights. This generalization makes categorical cross-entropy suitable both for strict single-label classification and for probabilistic, multi-annotator scenarios.

2.2 Dimensional Emotion Models (The Circumplex Model)

While categorical frameworks provide discrete labels, they often fail to capture the fluid and overlapping nature of human emotions. To address these limitations, James Russell (1980) introduced the *Circumplex Model of Affect*, which conceptualizes emotions as points in a continuous two-dimensional space. The two axes are:

- **Valence (Pleasant–Unpleasant):** Measures the positivity or negativity of an emotional state.
- **Arousal (Calm–Excited):** Captures the intensity or activation level of the emotion.

In this representation, emotions are not isolated categories but coordinates within a continuous plane. For example, *Joy* corresponds to high valence and high arousal, while *Sadness* corresponds to low valence and low arousal. Mixed or ambiguous emotions, such as *Bittersweetness*, can be represented as intermediate points, offering a more nuanced depiction than categorical models.

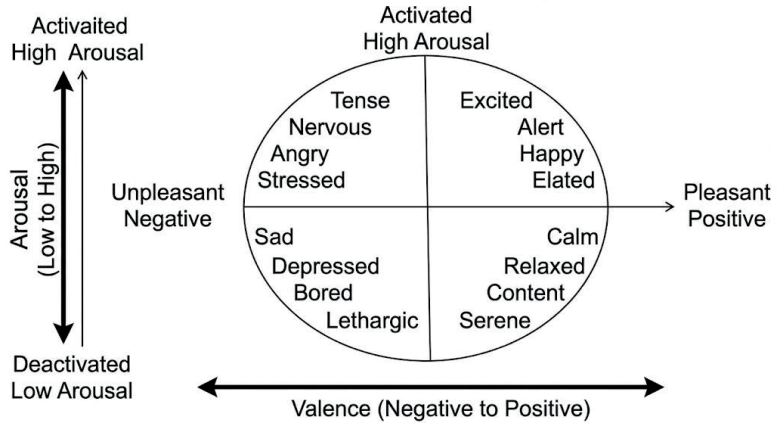

Figure 2. Russell's Circumplex Model of Affect showing Valence and Arousal axes.

From a computational perspective, VSA tasks based on dimensional models are formulated as *regression problems* rather than classification. The model outputs continuous values for valence and

arousal, typically normalized to the range [−1,1]. Evaluation metrics such as the *Concordance Correlation Coefficient (CCC)* are employed to assess both correlation and agreement between predicted and ground-truth values.

This model is particularly useful for measuring subtle shifts in sentiment, a focus of recent automotive and human-computer interaction datasets like MuSe-CaR (Stappen et al., 2021).

3. The Era of Hand-Crafted Features (2010–2013)

Before the dominance of Deep Learning, feature engineering in Visual Sentiment Analysis (VSA) was a manual process. Researchers attempted to design *hand-crafted features* inspired by psychology, art theory, and photography, aiming to correlate visual cues with human emotion. This era was characterized by the extraction of *low-level features* that were computationally efficient but semantically shallow, alongside mid-level aesthetic descriptors that sought to capture compositional quality.

3.1 Low-Level Features: Color and Texture

Color has long been recognized in psychology as a powerful determinant of mood. Machajdik and Hanbury (2010) formalized the use of color features by extracting *3D Color Histograms* in RGB and HSV spaces. They also applied *Itten's Color Theory* to quantify contrasts and harmonic relationships between hues. Mathematically, images were represented by statistical moments of their color distribution:

$$\mu_C = \frac{1}{N}\sum p_{ij}, \qquad \sigma_C = \sqrt{\frac{1}{N}\sum\left(p_{ij} - \mu_C\right)^2}$$

beyond color, *texture analysis* provided additional cues. Smooth textures were often associated with calmness, while chaotic or noisy textures suggested distress. Techniques such as Local Binary Patterns (LBP) and Gabor filters were employed to capture these distinctions. Together, color and texture descriptors offered a primitive but interpretable mapping between visual stimuli and affective states.

3.2 Mid-Level Features: The Aesthetic Hypothesis

Researchers also investigated the relationship between *aesthetics and sentiment*, operating under the so-called *Aesthetic Hypothesis*—the idea that visually pleasing images generally evoke positive emotions. Computational aesthetics involved measuring adherence to photographic rules such as the *Rule of Thirds* (visual balance*), Depth of Field (DoF),* and *symmetry*.

While these methods showed statistical significance on small datasets, they failed to generalize. For example, a beautifully composed photograph of a funeral or a war zone might score highly on aesthetic metrics (composition, lighting) yet be misclassified as *Positive* by an algorithm. This paradox highlighted the limitations of hand-crafted features and underscored the necessity of *semantic understanding*—moving beyond pixels and composition toward contextual meaning.

4. The Semantic Turn: Object-Based Sentiment (2013–2015)

To address the failures of low-level features, the field moved toward Mid-Level Representations. The core idea was that sentiment is carried by the *objects* and *scenes* in the image, not just the colors.

4.1 The Visual Sentiment Ontology (VSO)

In a landmark study, Borth et al. (2013) introduced the Visual Sentiment Ontology (VSO). They argued that nouns alone are insufficient. A "baby" is neutral. A "smiling baby" is positive; a "crying baby" is negative. Thus, the Adjective-Noun Pair (ANP) became the fundamental unit of visual sentiment.

4.2 SentiBank

SentiBank is a visual sentiment analysis framework designed to bridge the "affective gap" between low-level pixel features and high-level emotions by utilizing Adjective-Noun Pairs (ANPs) as mid-level representations. The system operates by first extracting low-level visual features (such as color, texture, and edges) from an input image and feeding them into a bank of *1,200 pre-trained SVM classifiers*, where each detector is specialized to recognize a specific emotionally charged concept (e.g., "beautiful sky" or "sad eyes"). The collective output of these detectors forms a sparse, 1,200-dimensional *"SentiBank vector"* which serves as a semantically rich descriptor that effectively translates visual content into sentiment, allowing a final linear classifier to determine the image's overall polarity (positive or negative) with high accuracy. This method provided high interpretability. Unlike deep neural networks which are 'black boxes', SentiBank allowed researchers to trace a 'Negative' prediction back to specific concepts.

In Figure 3, SentiBank architecture and some examples of ANPs are illustrated. SentiBank leverages deep learning to detect objects and their sentiment-laden attributes, combining them into a rich vocabulary of ANP for image analysis.

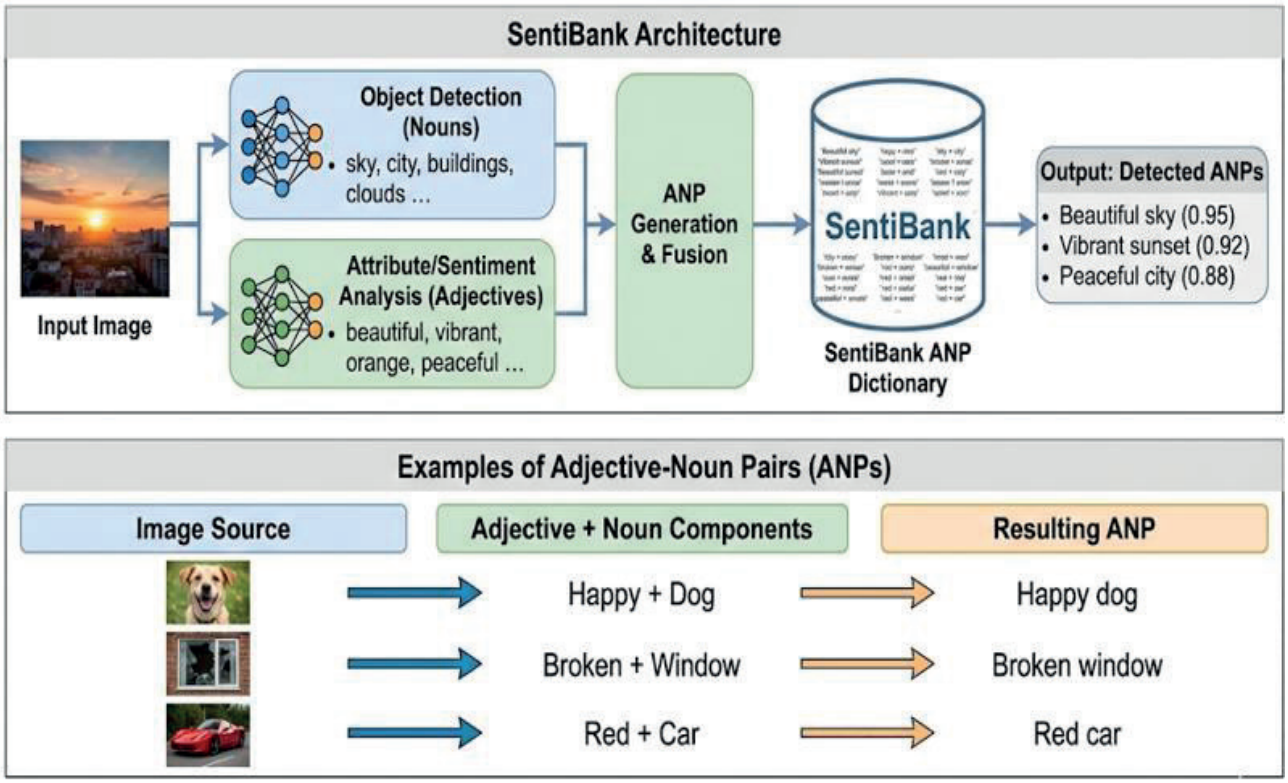

Figure 3. Architecture of SentiBank and examples of Adjective-Noun Pairs (ANPs).

5. The Deep Learning Revolution (2015–2019)

The emergence of Convolutional Neural Networks (CNNs) marked the end of hand-crafted features in Visual Sentiment Analysis (VSA). Unlike manually engineered descriptors, CNNs learn to extract features directly from raw pixel data through backpropagation, building hierarchical representations that capture edges, textures, objects, and eventually affective cues. This paradigm shift rendered manual feature extraction largely obsolete and opened the door to end-to-end learning.

5.1 CNN Architectures: From AlexNet to ResNet

The progression of CNN architectures was rapid and transformative.

AlexNet (2012): Established the baseline with five convolutional layers, demonstrating the power of deep learning on ImageNet.

VGGNet (2014): Increased depth to 19 layers using small 3×3 filters, enabling finer texture capture.

ResNet (2015): Introduced Residual Connections, allowing networks with 50+ layers to be trained effectively by mitigating the vanishing gradient problem.

ResNet-50 remains a standard backbone for VSA tasks due to its balance of depth, efficiency, and trainability. These architectures provided the foundation for sentiment-specific adaptations.

5.2 Transfer Learning and Fine-Tuning

A persistent bottleneck in VSA was the scarcity of large, labeled sentiment datasets. While ImageNet offered 14 million annotated images for object recognition, sentiment datasets typically contained only a few thousand samples. Training a deep CNN from scratch on such limited data led to severe overfitting.

The solution was Transfer Learning (Islam & Zhang, 2016). Researchers utilized pre-trained backbone networks (e.g., VGG-19, ResNet-50) trained on ImageNet and fine-tuned the final layers on sentiment datasets. This approach allowed models to leverage general visual knowledge (edges, shapes, objects) while adapting to the nuances of emotional interpretation. Transfer learning became the de facto strategy for VSA, enabling robust performance despite data scarcity.

5.3 Visual Attention Mechanisms

Another major advancement in this era was the integration of Visual Attention (Yang et al., 2018). Standard CNNs often relied on global average pooling, treating all regions of an image as equally important. However, sentiment is frequently driven by a small focal region.

Attention mechanisms addressed this by generating spatial weight maps, highlighting the pixels most relevant to affective classification. For example, in a crowded street scene, a single crying child may define the overall sentiment. By focusing on such “emotional protagonists” and down-weighting background clutter, attention-based models significantly improved accuracy and interpretability compared to global averaging methods.

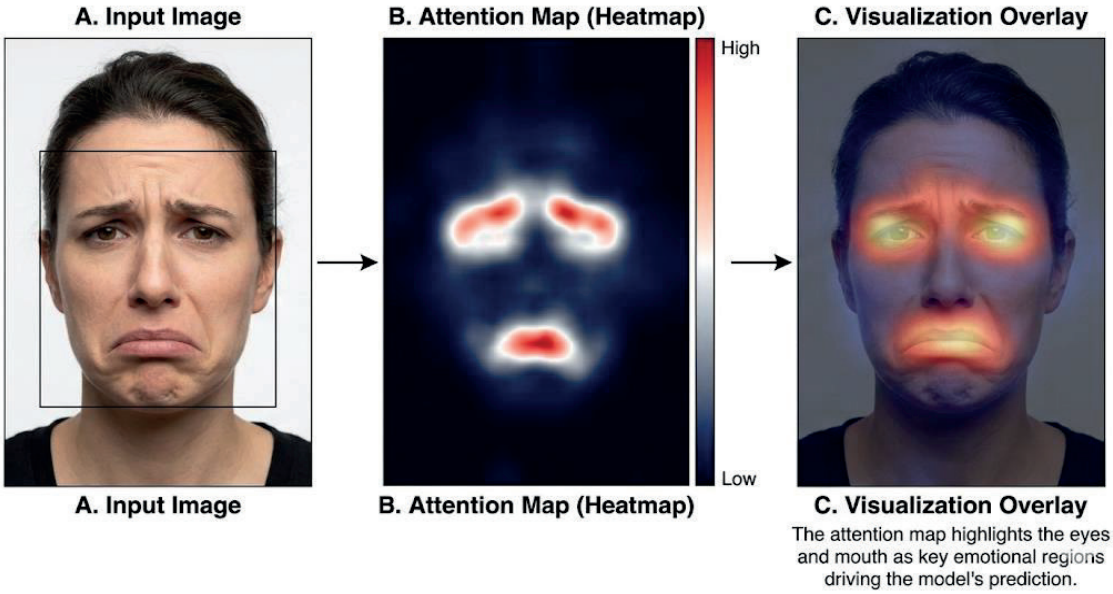

Figure 4. Visualization of Attention Maps highlighting emotional regions in an image

The Deep Learning era fundamentally transformed Visual Sentiment Analysis. CNN architectures provided hierarchical feature extraction that surpassed hand-crafted descriptors, while transfer learning enabled robust performance despite limited sentiment datasets. The integration of attention mechanisms further enhanced interpretability by highlighting emotionally salient regions within complex scenes. Together, these innovations bridged much of the Semantic Gap, allowing models to move beyond superficial cues toward richer affective understanding. Yet, challenges such as subjectivity, cultural variability, and data scarcity persisted, motivating the next wave of research based on Transformers and multimodal learning.

6 The Modern Era: Transformers and Zero-Shot Learning (2020–Present)

In recent years, Visual Sentiment Analysis (VSA) has moved beyond traditional CNN-based approaches toward architectures capable of modeling *global context* and achieving *multimodal alignment*. This transition has been driven by the adoption of Transformer models, which leverage self-attention mechanisms to capture relationships across the entire image and between image–text pairs.

6.1 Vision Transformers (ViT)

While CNNs excel at local feature extraction, they struggle with long-range dependencies. The *Vision Transformer (ViT)* (Dosovitskiy et al., 2021) addresses this limitation by dividing an image into fixed-size patches (e.g., 16×16 pixels) and processing them as a sequence. Through stacked *self-attention layers*, each patch can attend to every other patch, enabling the model to integrate global context.

This capability is crucial for complex sentiment tasks where the relationship between objects defines the emotion. For example, a smiling face may typically signal *positive sentiment*, but if the background depicts a disaster, the overall affective interpretation may shift to *negative*. ViTs thus provide a more holistic understanding of affective cues compared to CNNs.

6.2 Zero-Shot Learning with CLIP

A paradigm shift occurred with the release of *Contrastive Language–Image Pre-training (CLIP)* (Radford et al., 2021). CLIP was trained on 400 million image–text pairs to learn a *shared latent embedding space*, aligning visual and textual representations.

Instead of training a task-specific classifier (e.g., a "sadness detector"), researchers can define a set of text prompts such as *"a joyful child"* or *"a fearful scene."* CLIP compares the image embedding to these textual prompts and selects the closest match. This *Zero-Shot capability* eliminates the need for large labeled sentiment datasets, offering highly flexible sentiment analysis in dynamic environments.

Recent work by Zhang & Zhang (2023) demonstrates that *prompt learning with CLIP* achieves state-of-the-art results in VSA without task-specific training data. Further refinements such as BLIP (Li et al., 2022) extend this alignment, enabling sentiment-aware caption generation and improved multimodal reasoning.

6.3 Toward Multimodal Large Models

Building on CLIP, newer *Large Multimodal Models (LMMs)* such as BLIP-2, LLaVA, and GPT-4V integrate vision and language understanding at scale. These models can interpret irony, sarcasm, and cultural references by jointly analyzing visual cues and textual context, marking a significant step toward bridging the *Affective Gap* and the *Cultural Gap*.

6.4 Key Contributions of Transformers to VSA

Transformers have introduced several pivotal contributions to Visual Sentiment Analysis. By leveraging self-attention, they enable models to capture global context across the entire image, allowing sentiment to be interpreted not only from local features but also from relationships between distant visual elements. This holistic perspective is particularly important in affective tasks where meaning often emerges from the interplay of objects and background.

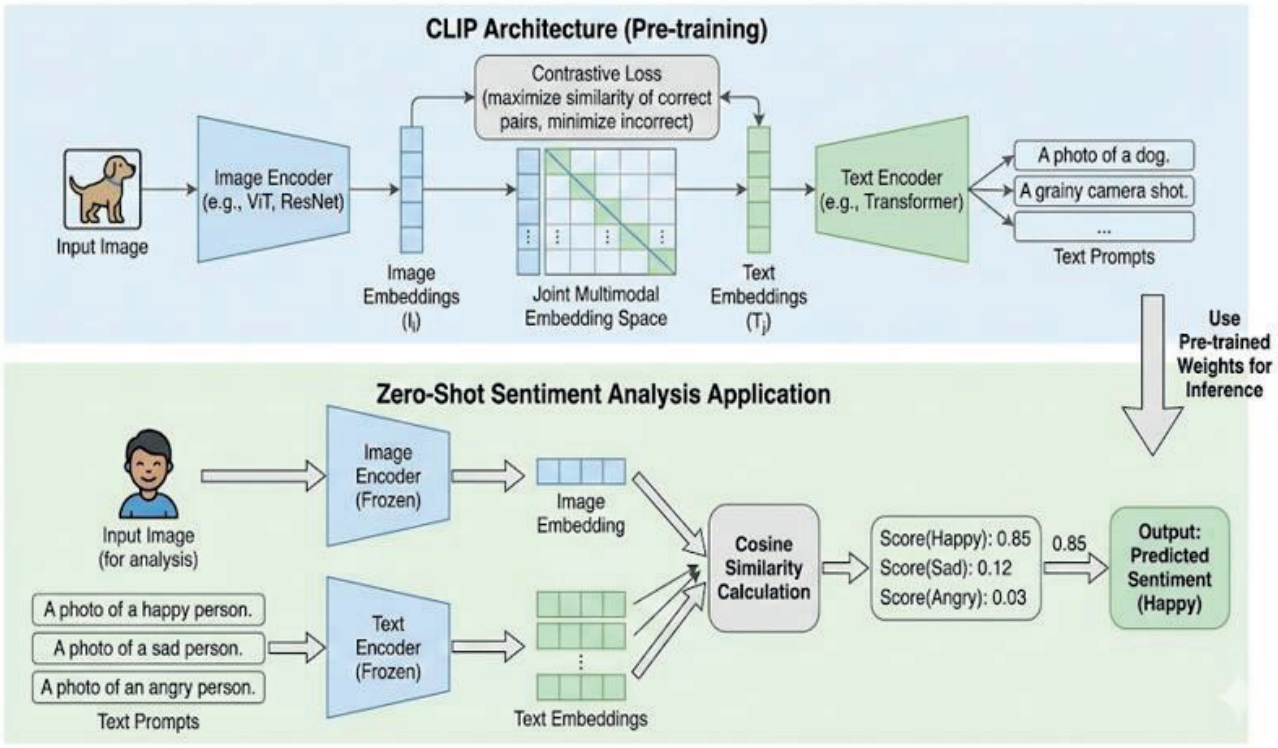

Figure 5. The architecture of CLIP and its application in Zero-Shot Sentiment Analysis

Another major advancement is the ability to perform *zero-shot classification*, which frees researchers from the dependence on large, task-specific labeled datasets. Through models like CLIP, sentiment can be inferred directly from textual prompts aligned with visual embeddings, offering unprecedented flexibility in dynamic environments. The development of *prompt learning* further enhances this capability, enabling models to adapt to new affective tasks with minimal supervision.

Transformers also facilitate *multimodal integration*, combining vision and language representations in a shared embedding space. This allows systems to detect irony, sarcasm, and cultural references that would otherwise be missed by unimodal approaches. Finally, their scalability—driven by pre-training on massive datasets—ensures that these models generalize across diverse domains and cultural contexts, marking a decisive step toward bridging both the Affective and Cultural Gaps in VSA.

7. Subjectivity and Label Distribution Learning

Perhaps the most profound realization in recent Visual Sentiment Analysis research is that *Ground Truth is an illusion*. Emotion is inherently subjective, and the assumption of a single, universally valid label often fails to capture the diversity of human affective perception.

7.1 Label Distribution Learning (LDL)

A major philosophical and technical challenge in VSA is the subjectivity of emotion. Traditional classification approaches assume that a definitive ground truth exists, yet human agreement on sentiment is frequently low. To address this ambiguity, modern approaches employ *Label Distribution Learning (LDL)* (Geng, 2016). Instead of representing the ground truth as a single label y, LDL models it as a probability distribution $\hat{d}$. The task of the model is to predict a distribution $\hat{d}$ that minimizes the *Kullback–Leibler (KL) Divergence* (Zhao et al., 2020).

This formulation allows the model to express uncertainty and nuance. For example, if seven annotators label an image as *Happy* and three as *Neutral*, the resulting distribution becomes {Happy: 0.7, Neutral: 0.3}. Such probabilistic representation enables the AI to state, *"This image is mostly Happy, but has elements of Neutrality,"* thereby mirroring the complexity of human emotional processing (Yang et al., 2021).

7.2 Addressing Dataset Bias

Beyond subjectivity, dataset bias remains a critical obstacle. Standard benchmarks often reflect Western aesthetics, leading models to associate certain low-level features—such as darkness—with negative emotions across all contexts. To mitigate this, the *UnbiasedEmo dataset* (Xiong et al., 2022) was introduced, offering a balanced benchmark that accounts for cultural diversity and prevents spurious correlations.

The evolution of datasets illustrates this trajectory in Table 1. The development of datasets in Visual Sentiment Analysis reflects both the growing scale and the increasing awareness of subjectivity and cultural bias. Early psychology-driven corpora such as *IAPS* (Lang et al., 2005) provided normative affective stimuli, while large-scale web collections like *VSO* (Borth et al., 2013) and *Emotion6* (Peng et al., 2015) expanded the scope to Flickr-based images with adjective–noun pairs and label distribution learning. Social media–oriented datasets such as *FI* (You et al., 2016) and artistic collections like *ArtPhoto* (Machajdik & Hanbury, 2010) introduced more diverse affective contexts.

Table 1. The development of datasets in Visual Sentiment Analysis

Dataset	Year	Size	Labels	Source	Reference
IAPS	2005	1,182	Val/Aro	Psychology	Lang, Bradley, & Cuthbert (2005)
VSO	2013	500K	ANPs	Flickr	Borth, Chen, Ji, & Chang (2013)
Emotion6	2015	1,980	LDL	Flickr	Peng, Chen, Sadovnik, & Gallagher (2015)
FI	2016	23K	Pos/Neg	Social Media	You, Luo, Jin, & Yang (2016)
ArtPhoto	2016	806	8 emotions	Art images	Machajdik & Hanbury (2010)
AffectNet	2017	1M	Val/Aro + 8	Web	Mollahosseini, Hasani, & Mahoor (2017)
UnbiasedEmo	2020	3K	6 Class	Web	Xiong, Wang, & Ji (2022)
MuSe-CaR	2021	40h	Video	YouTube	Stappen, Baird, Schmitt, & Schuller (2021)
MuSe 2025	2025	100K	Multimodal	Benchmark	Schuller, Stappen, Baird, & Weninger (2025)

The release of *AffectNet* (Mollahosseini et al., 2017) marked a turning point, offering over one million facial images annotated with valence–arousal and categorical emotions. More recently, culturally balanced corpora such as *UnbiasedEmo* (Xiong et al., 2022) were designed to mitigate Western-centric biases. In parallel, multimodal benchmarks like *MuSe-CaR* (Stappen et al., 2021) and the latest *MuSe 2025 Challenge* (Schuller et al., 2025) have pushed the boundaries toward understanding affect in complex, real-world video data.

This progression highlights the field's movement from psychology-driven corpora to large-scale, multimodal benchmarks, reflecting both the growing complexity of VSA tasks and the increasing awareness of cultural and subjective dimensions.

8 Multimodal Sentiment Analysis

In real-world scenarios, images rarely appear in isolation. They are typically accompanied by captions, hashtags, and comments. Multimodal Sentiment Analysis (MSA) seeks to fuse visual and textual modalities, enabling models to capture richer affective cues than unimodal approaches. State-of-the-art systems now employ advanced fusion strategies to integrate these modalities effectively.

8.1 Fusion Architectures

Early approaches relied on simple concatenation of features, combining raw vectors from image and text encoders before classification. While straightforward, this *Early Fusion* strategy often failed to capture nuanced interactions. Later methods introduced *Late Fusion*, where separate classifiers were trained for each modality and their prediction scores averaged. More sophisticated approaches such as *Tensor Fusion* explicitly modeled the interactions between modalities, allowing systems to detect conflicts—for example, irony or sarcasm when textual sentiment contradicts visual cues.

Recent architectures like *MISA* (Hazarika et al., 2020) further advanced this paradigm by disentangling modality-invariant features from modality-specific ones, ensuring that the model learns both shared and unique cues from text and image. Comprehensive surveys (Soleymani et al., 2017; Liu et al., 2023) consistently highlight that multimodal models significantly outperform unimodal ones, particularly in challenging cases such as sarcasm detection.

8.2 Large Multimodal Models (LMMs)

The field is now transitioning toward Large Multimodal Models (LMMs) such as *GPT-4V* (OpenAI, 2023) and *LLaVA* (Liu et al., 2024). Unlike traditional classifiers, these models are capable of reasoning about sentiment. They can explain why an image is perceived as funny or sad, integrating vast external knowledge bases into the analysis process. By combining vision, text, and even audio, LMMs promise richer affective reasoning, enabling systems to handle complex cultural references, irony, and subtle emotional cues.

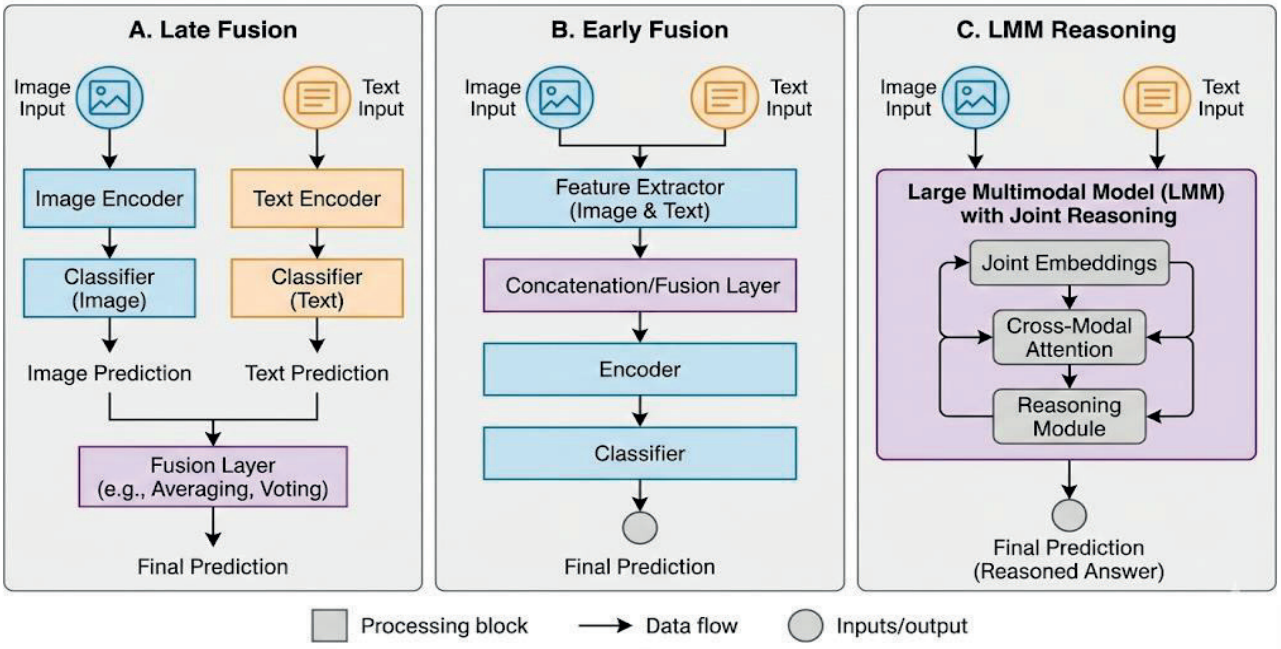

Figure 6. Comparison of Late Fusion vs. Early Fusion vs. LMM Reasoning architectures

While multimodal architectures and large multimodal models have significantly advanced the state of Visual Sentiment Analysis, their effectiveness ultimately depends on rigorous evaluation. To ensure that these systems are not only innovative but also reliable, researchers employ a range of metrics that capture accuracy, sensitivity to class imbalance, and discriminative power. The following section outlines the evaluation metrics used to benchmark VSA models, providing a foundation for transparent and reproducible comparison across approaches.

9. Evaluation Metrics for Visual Sentiment Analysis

Measuring the success of Visual Sentiment Analysis (VSA) models is significantly more complex than tasks with objective *true/false* answers, such as object detection. Due to the inherent subjectivity of emotion and frequent class imbalances (e.g., positive examples outnumbering negative ones), it is necessary to go beyond standard accuracy measurements. In the literature, different sets of metrics have been adopted depending on the structure of the problem addressed—*classification, regression, or retrieval*—while also incorporating measures of subjectivity and annotator agreement.

9.1 Classification-Based Metrics

The most common approach in VSA is to assign images to discrete categories (e.g., Happy, Sad, Angry). While *Accuracy* is the fundamental metric, it can be misleading in imbalanced datasets. For instance, if 80% of a dataset is labeled "Happy," a model that always predicts "Happy" achieves 80% accuracy without meaningful learning.

To measure performance more precisely, *Precision, Recall*, and their harmonic mean, the F1-Score, are used:

$$F1 = 2 \cdot \frac{Precision \cdot Recall}{Precision + Recall}$$

The F1-Score is particularly critical for detecting less frequent emotions such as fear or disgust. *Confusion Matrices* are also preferred to analyze which emotions the model confuses (e.g., "Fear" vs. "Surprise"). For binary sentiment tasks, *ROC-AUC* provides a robust comparison of classifiers.

Additionally, because emotion labeling is subjective, *Cohen's Kappa* is used to measure annotator agreement beyond chance. In *Label Distribution Learning (LDL)* settings, metrics such as *KL Divergence* and *Earth Mover's Distance (EMD)* quantify the distance between predicted and true label distributions, reflecting uncertainty in human perception.

9.2 Dimensional (Regression) Metrics

In dimensional models where emotion is expressed through continuous values such as *Valence* and *Arousal*, the distance between predicted and ground truth values is measured. Common error metrics include *Mean Squared Error (MSE)* and *Mean Absolute Error (MAE)*:

$$MSE = \frac{1}{n}\sum_{i=1}^{n}(y_i - \hat{y_i})^2$$

However, in sentiment analysis, the accuracy of the *trend* is often more important than absolute values. To capture this, the *Pearson Correlation Coefficient (r)* is used, with successful models expected to exhibit low error rates and high correlation ($r \approx 1$).

9.3 Retrieval-Oriented Metrics

Table 2. Problem–Metric Mapping

Problem Type	Common Metrics	VSA Relevance
Classification	Accuracy, Precision, Recall, F1-Score, ROC-AUC, Confusion Matrix, Cohen's Kappa, KL Divergence, EMD	Discrete emotion categories (e.g., Happy, Sad). Handles imbalance and subjectivity.
Regression	Mean Squared Error (MSE), Mean Absolute Error (MAE), Pearson Correlation (r)	Dimensional models (Valence, Arousal). Captures continuous affect trends.
Retrieval	Mean Average Precision (mAP)	Ranking images with specific sentiment (e.g., SentiBank, CLIP). Evaluates retrieval quality.

For approaches aiming to retrieve images with specific sentiments from large databases (e.g., SentiBank or CLIP-based models), *Mean Average Precision (mAP)* is the standard metric. It evaluates how effectively the model ranks relevant images at the top of search results, reflecting retrieval quality in large-scale applications.

In Table 2, problem and metric mapping is given. This mapping highlights that evaluation in VSA is multi-layered. Classification metrics dominate categorical emotion tasks but must be complemented with agreement and distribution-based measures to account for subjectivity. Regression metrics are essential for dimensional affect modeling, while retrieval metrics ensure that large-scale systems can effectively surface sentiment-rich content. Together, these metrics provide a comprehensive framework for benchmarking VSA models across diverse problem structures.

10. Applications of Visual Sentiment Analysis

Visual Sentiment Analysis (VSA) has emerged as a powerful tool across multiple domains, enabling researchers and practitioners to interpret emotional cues embedded in visual content. Its applications extend from commercial contexts to cultural and societal analysis, reflecting the versatility of affective computing.

10.1 Marketing & Advertising

One of the most prominent application areas of VSA is marketing and advertising. By analyzing consumer reactions to campaigns, product designs, and promotional visuals, companies can gain insights into brand perception and emotional resonance. This allows for data-driven optimization of advertisements and more effective audience targeting.

10.2 Healthcare

In healthcare, VSA contributes to the detection of emotional states in patient-shared images, supporting mental health monitoring and therapeutic interventions. Emotion recognition from visual content can provide clinicians with supplementary information about patients' well-being, enabling more holistic approaches to treatment.

10.3 Education

Educational environments increasingly rely on digital platforms, where VSA can help understand student emotions in online learning contexts. By analyzing visual cues in submitted assignments, discussion posts, or learning materials, educators can assess engagement levels and adapt teaching strategies to foster motivation and emotional well-being.

10.4 Cultural Analytics

VSA also plays a role in cultural analytics, where sentiment is studied in art, film, and social media trends. This application enables researchers to explore how visual culture reflects collective emotions, societal values, and aesthetic preferences, offering new perspectives in digital humanities and media studies.

10.5 Social Media Monitoring

Finally, VSA is widely used in social media monitoring. By tracking public mood during events, crises, or political movements, analysts can map emotional dynamics at scale. Such insights are valuable for policymakers, journalists, and organizations seeking to understand societal reactions in real time.

11 Conclusion and Future Directions

Visual Sentiment Analysis has evolved from a field reliant on simple color heuristics to one powered by massive neural networks capable of multimodal reasoning. Early stages focused on hand-crafted descriptors rooted in psychology and art theory, later replaced by deep learning architectures capable of hierarchical feature extraction, and most recently by Transformer-based multimodal systems that integrate vision and language. Each stage of this progression has contributed to narrowing the *Semantic Gap*, yet the *Affective Gap* remains a persistent challenge.

The future of VSA lies in *personalization and context awareness*. As noted by Wang et al. (2024) and Mittal et al. (2022), the next generation of models must account for user demographics and contextual factors—asking not only *"What is in this image?"* but also *"Who is viewing this image?"*. Benchmarks such as the *MuSe 2024 Challenge* (Schuller et al., 2024) continue to push the boundaries toward understanding social perception, humor, and affect in wild, uncurated video data, highlighting the importance of context-sensitive evaluation.

References

Borth, D., Ji, R., Chen, T., Breuel, T., & Chang, S.-F. (2013). Large-scale visual sentiment ontology and detectors using adjective noun pairs. In Proceedings of the 21st ACM International Conference on Multimedia (pp. 223–232). ACM.

Dosovitskiy, A., Beyer, L., Kolesnikov, A., Weissenborn, D., Zhai, X., Unterthiner, T., ... & Houlsby, N. (2021). An image is worth 16x16 words: Transformers for image recognition at scale. In Proceedings of the International Conference on Learning Representations (ICLR).

Ekman, P. (1992). An argument for basic emotions. Cognition & Emotion, 6(3–4), 169–200.

Geng, X. (2016). Label distribution learning. IEEE Transactions on Knowledge and Data Engineering, 28(7), 1734–1748.

Hazarika, D., Zimmermann, R., & Poria, S. (2020). MISA: Modality-invariant and -specific representations for multimodal sentiment analysis. In Proceedings of the 28th ACM International Conference on Multimedia (pp. 1122–1131). ACM.

Islam, J., & Zhang, Y. (2016). Visual sentiment analysis for social images using transfer learning approach. In Proceedings of the IEEE International Conference on Big Data and Cloud Computing (BDCloud) (pp. 124–130). IEEE.

Li, J., Li, D., Xiong, C., & Hoi, S. (2022). BLIP: Bootstrapping language-image pre-training for unified vision-language understanding and generation. In Proceedings of the 39th International Conference on Machine Learning (ICML) (pp. 12888–12900). PMLR.

Liu, H., Li, C., Wu, Q., & Lee, Y. J. (2024). Visual instruction tuning. In Advances in Neural Information Processing Systems (NeurIPS) (Vol. 36).

Liu, Y., Yuan, H., & Pan, S. (2023). Visual sentiment analysis in the era of large multimodal models: A survey. Artificial Intelligence Review, 56, 12345–12389.

Machajdik, J., & Hanbury, A. (2010). Affective image classification using features inspired by psychology and art theory. In Proceedings of the 18th ACM International Conference on Multimedia (pp. 83–92). ACM.

Mittal, T., Guhan, P., & Bhattacharya, U. (2022). Affect2MM: Affective analysis of multimedia content using probabilistic graphical models. In Proceedings of the IEEE/CVF Conference on Computer Vision and Pattern Recognition (CVPR) Workshops (pp. 2345–2354). IEEE.

OpenAI. (2023). GPT-4 technical report (arXiv:2303.08774). arXiv. https://doi.org/10.48550/arXiv.2303.08774

Radford, A., Kim, J. W., Hallacy, C., Ramesh, A., Goh, G., Agarwal, S., ... & Sutskever, I. (2021). Learning transferable visual models from natural language supervision. In Proceedings of the 38th International Conference on Machine Learning (ICML) (pp. 8748–8763). PMLR.

Russell, J. A. (1980). A circumplex model of affect. Journal of Personality and Social Psychology, 39(6), 1161–1178.

Schuller, B. W., Baird, A., Stappen, L., Tzirakis, P., & Cambria, E. (2024). The MuSe 2024 multimodal sentiment analysis challenge: Social perception and humor. In Proceedings of the 32nd ACM International Conference on Multimedia. ACM.

Soleymani, M., Garcia, D., Jou, B., Schuller, B., Chang, S.-F., & Pantic, M. (2017). A survey of multimodal sentiment analysis. Image and Vision Computing, 65, 3–14.

Stappen, L., Baird, A., & Schuller, B. (2021). The multimodal sentiment analysis in car reviews (MuSe-CaR) dataset: Collection, insights and improvements. IEEE Transactions on Affective Computing, 12(4), 1024–1039.

Wang, Z., Wu, S., & Liu, Q. (2024). Personalized visual sentiment analysis: A meta-learning approach. IEEE Transactions on Multimedia, 26, 450–462.

Xiong, J., Cao, H., & Wu, X. (2022). UnbiasedEmo: A balanced visual emotion dataset for reducing bias. In Proceedings of the Asian Conference on Computer Vision (ACCV) (pp. 1230–1246).

Yang, J., She, D., Lai, Y. K., Rosin, P. L., & Yang, M. H. (2018). Weakly supervised coupled networks for visual sentiment analysis. In Proceedings of the IEEE Conference on Computer Vision and Pattern Recognition (CVPR) (pp. 7584–7592). IEEE.

Yang, K., Guo, D., & Zhang, H. (2021). Multi-modal emotion reasoning with label distribution learning. IEEE Signal Processing Letters, 28, 1650–1654.

Zhang, R., & Zhang, W. (2023). Zero-shot visual sentiment analysis with prompt learning. IEEE Transactions on Circuits and Systems for Video Technology, 33(5), 2210–2221.

Zhang, Y., & Zhang, Z. (2023). Context-aware visual sentiment analysis with graph neural networks. Pattern Recognition, 138, 109353.

Zhao, S., Yao, H., Gao, Y., Ji, R., & Ding, G. (2018). Continuous probability distribution prediction of image emotions via multitask shared sparse regression. IEEE Transactions on Multimedia, 20(11), 3072–3081.

Zhao, S., Lin, P., Xu, J., Yao, H., & Ding, G. (2020). Discrete probability distribution prediction of image emotions with shared sparse learning. IEEE Transactions on Affective Computing, 11(4), 574–587.

CHAPTER 2

ENGINEERING-BASED GOVERNANCE OF THE KYOTO PROTOCOL AND ITS GLOBAL IMPLEMENTATION EFFECTS

Şaile Tuba ÖZTÜRK[1], Zeynel Fuat TOPRAK [2]

1 Lecturer Dr., Fırat University, ORCID ID: 0000-0003-0408-5825
2 Prof. Dr., Dicle University, ORCID ID: 0000-0003-0876-1165

1. Introduction

The Kyoto Protocol marks a decisive turning point not only in the evolution of international environmental law but also in the redefinition of the working domains of technical disciplines such as energy, environmental, climate, and hydraulic engineering. Rising global environmental pressures in the final quarter of the twentieth century made it evident that climate change mitigation could no longer be confined to political declarations; instead, the integration of scientific data, advanced modelling techniques, and engineering-based infrastructural solutions into diplomatic processes became imperative (IPCC, 2001; Stern, 2007; Toprak et al., 2013). In this respect, the Protocol represents the first comprehensive international regulation to demonstrate that environmental problems cannot be understood solely through ecological observation or policy texts: diverse engineering fields—including energy production, transportation systems, water-resources management, infrastructure-resilience planning, and industrial design—constitute integral elements of climate governance (Kayan & Küçük, 2022; Gupta, 2010; Agiralioglu et al., 2017).

With Kyoto, climate policy was institutionalized through measurable emission parameters, verifiable engineering outputs, and standardized reporting structures. The establishment of the Measurement–Reporting–Verification (MRV) system enabled the technical auditing of energy efficiency, carbon management, and infrastructure design standards in engineering projects (Grubb, 2003; Böhringer & Löschel, 2003; Öztürk & Toprak, 2024). This approach moved the notion of governance beyond traditional political coordination by placing technical rationality and data-driven engineering planning at the core of global environmental management. Kyoto thus functions not merely as a legal framework but as the starting point of a new global governance model that requires the integrated functioning of engineering, economics, and climate science (Okereke, 2008).

During the Kyoto period, engineering-oriented practices such as energy efficiency, carbon-emission control, waste management, hydrological-cycle analysis, and the strengthening of renewable-energy infrastructures became priority instruments of environmental policy. As a result, climate change debates evolved from a narrow field of political negotiation into a governance structure grounded in engineering disciplines—measurable, verifiable, and supported by technical standards (Kaya, 2020; Kayan & Küçük, 2022; IPCC, 2001; Alashan et al., 2016). In parallel, the notion of "ecological diplomacy" gained prominence in the literature, emphasizing that sustainability goals should not be left solely to political will but should be systematically supported by engineering indicators such as carbon-footprint calculations, energy-intensity coefficients, water-resource renewal rates, infrastructure-resilience metrics, and standardized emission factors (Ürge-Vorsatz et al., 2009).

From the perspective of engineering sciences, the Protocol is particularly distinguished by the institutionalization of the MRV mechanism. Through MRV, emission-reduction strategies, infrastructure projects, and energy-transition plans became technically traceable, establishing an environmental-performance system grounded in international standards (Grubb, 2003; Böhringer & Löschel, 2003; Gupta, 2010; UNFCCC, 2006; Toprak et al., 2013). Karakaya's (2008) holistic assessment of the scientific, economic, and technical dimensions of Kyoto, and of Turkey's climate policy in light of its engineering infrastructure, energy-efficiency capacity, and institutional alignment, underscores that the Kyoto era was not solely an international policy process but was directly linked to countries' technical capacity, standards, and data-production and reporting infrastructures (Öztürk & Toprak, 2024).

The socio-political impact of the Kyoto Protocol extends beyond the redefinition of states' international obligations to include a profound transformation in how sustainable design, energy transition, and environmental performance responsibility are understood within engineering disciplines. The principle of "common but differentiated responsibilities" (CBDR), one of Kyoto's foundational tenets, reveals that environmental justice is anchored in technical infrastructures. While

CBDR acknowledges that all countries must contribute collectively to climate mitigation, it simultaneously requires differentiated obligations in light of disparities in carbon intensity, energy efficiency, industrial infrastructure, and technological capacity (Kayan & Küçük, 2022; Gupta, 2010; Batan & Toprak, 2020). In this sense, the principle of equitable carbon management has evolved from a purely political discourse into an engineering-based balancing system grounded in technical parameters.

Within the Kyoto framework, developed countries were expected to deploy advanced technologies such as carbon capture and storage (CCS), renewable-energy transition systems, smart grids, waste-heat recovery solutions, and high-efficiency industrial processes, whereas developing countries prioritized technology transfer, capacity building, sustainable water management, adaptation infrastructures, and low-cost efficiency solutions. IPCC assessments underline that this differentiation is not just economic but is directly linked to engineering capacity at the implementation level (IPCC, 2014; Agiralioglu et al., 2017). Consequently, environmental justice has increasingly been articulated as a technical compliance process defined by measurable indicators. At the same time, the differentiated-responsibility approach has given rise to debates on "technological inequality" in energy, transport, and industrial engineering: developed countries often claim that flexibilities granted to developing countries distort competitive conditions, while developing countries interpret demands for equal technical investments without accounting for historical emissions as a form of "technological injustice." These tensions constitute one of the most complex and debated dimensions of Kyoto's engineering-based implementation practices.

From a sociotechnical perspective, Kyoto transcends its status as an environmental agreement and constitutes a critical turning point in the institutionalization of green engineering movements, sustainable-technology initiatives, and community-based environmental actions. Since the mid-1990s, universities, research centers, and engineering organizations have built interdisciplinary networks in areas such as energy transition, climate modelling, sustainable-infrastructure design, and environmental risk management, thereby fostering a new global culture of technical cooperation (Khanna, 2001; Mol & Spaargaren, 2000; Alashan et al., 2016). This evolution has transformed engineering from a purely technical problem-solving field into a sociotechnical actor that connects environmental values with society and guides the trajectory of environmental transformation.

The Protocol's influence on public perception has likewise extended beyond raising environmental awareness to reshaping understandings of social responsibility within engineering professions. Following Kyoto's entry into force, climate discourse moved to the center of public debate through the activities of the media, academia, engineering chambers, civil society, and professional organizations. Environmental consciousness thus became embedded in technical decision-making on energy use, water management, infrastructure design, and material selection, making the societal dimension of engineering practice more visible (Bulkeley & Betsill, 2003). Engineering-based environmental awareness materializes through practices such as carbon-footprint and energy-intensity calculations, sustainable material cycles, green-building design, and urban-scale stormwater management (Ürge-Vorsatz et al., 2009; IPCC, 2014; Toprak et al., 2013). In this respect, Kyoto revealed the capacity of technical knowledge to generate public awareness and accelerated the dissemination of engineering-based environmental information through media, civil society, and local governments.

At the level of global governance, the Kyoto period consolidated a multi-layered, technically grounded model of cooperation (Gupta, 2010; Morin et al., 2013; Okereke, 2008). States, international organizations, the private sector, civil society, and universities assumed differentiated roles in shaping and implementing environmental policy by sharing engineering expertise. Academic institutions, engineering chambers, and technical standardization bodies played particularly critical roles by developing guidance on emission modelling, MRV procedures, green-technology criteria,

and data-accuracy protocols, thereby contributing to the institutionalization of the Protocol's technical infrastructure (IPCC, 2007; Ürge-Vorsatz et al., 2009; Öztürk & Toprak, 2024).

Kaya (2020) argues that the shift from the Kyoto Protocol to the Paris Agreement produced dual outcomes from an engineering perspective. On the one hand, voluntary commitment mechanisms under Paris allowed countries to develop more flexible and locally adapted solutions in line with their technical capacities. On the other hand, the weakening of uniform global performance-monitoring, verification procedures, and standardized technical criteria reduced coherence and oversight in global climate governance. Thus, while Kyoto established a more binding, standards-driven technical regime, the Paris era emphasized a more inclusive model that broadened socio-political participation. At the same time, the governance framework shaped by Kyoto strengthened the technical foundations of environmental modernization and positioned engineering solutions as priority instruments of global environmental policy (Mol & Sonnenfeld, 2000).

Kyoto's socio-political impact also extended to the development of an engineering-based conception of global justice. Environmental justice requires that differences in technical capacity, financial resources, and institutional resilience be considered in the planning of energy, water, and infrastructure systems. Regions most severely affected by climate change typically suffer from low infrastructure resilience, inadequate early-warning systems, and limited engineering capacity, conditions that reveal structural inequalities conceptualized as "technological injustice" and, more broadly, "climate injustice" (Kim et al., 2020; Roberts & Parks, 2007; Batan & Toprak, 2020). Through the Kyoto process, these concepts became central to global environmental governance and engineering policy.

Environmental justice during the Kyoto period thus moved beyond ethical discourse to assume concrete technical form in the transformation of energy systems, water management, disaster resilience, and carbon-monitoring infrastructures. The transfer of renewable-energy technologies, clean water and waste-treatment systems, early-warning mechanisms, and carbon-tracking infrastructures to developing countries exemplifies this engineering-oriented justice approach (Sovacool et al., 2019; Agiralioglu et al., 2017). Environmental policy thereby evolved from a matter of individual moral choice to one of collective technical action.

2. The Concept of Global Environmental Governance and the Role of Kyoto

Global environmental governance transcends purely political or diplomatic processes; it constitutes a collective problem-solving effort rooted in scientific data, engineering expertise, and technological capacity. Effective governance in this domain requires the international community to establish shared technical standards, robust monitoring and verification systems, and sustainable infrastructure policies to address transboundary environmental challenges. Consequently, modern environmental governance extends beyond unilateral state action, relying on a multi-actor cooperation model in which engineering organizations, research institutions, the private sector, and civil society collaboratively contribute. This layered structure transforms environmental management into an integrated system in which political, technical, and scientific dimensions operate in concert.

Environmental issues are increasingly understood as technical processes inherently linked to engineering practices such as data-driven modeling, energy-efficiency optimization, hydrological planning, and carbon management. The Kyoto Protocol marked a turning point by institutionalizing this holistic perspective, introducing measurable, reportable, and verifiable (MRV) obligations that cross national boundaries, thereby transforming environmental governance into an engineering-based framework for planning and oversight (Lopez, 2003; Ma, 2010).

The core rationale of global environmental governance is grounded in the fact that sustainability cannot be achieved without technical coordination and data sharing. Since the climate system, hydrological cycles, atmospheric energy transfers, and ecosystem processes involve a high degree of interdependence, it is impossible for any single country to manage these systems on its own. The effective implementation of environmental policies requires the establishment of shared data infrastructures, the standardization of engineering-based modeling tools, and the strengthening of international monitoring and verification mechanisms (Ma, 2010). Within this framework, the Kyoto Protocol stands out as the first international agreement to define legally binding technical obligations. Parties were required to support the specified targets with national engineering-based action plans. The implementation of these plans was secured through international verification mechanisms, thereby transforming environmental governance from a political framework into a management architecture grounded in technical standards. This transformation is also supported by empirical findings that reveal the compliance performance of EU member states with their Kyoto targets (Öztürk & Toprak, 2025).

Empirical evidence supports this approach. Panel-data analyses by Kim et al. (2020) indicate that the Kyoto Protocol significantly reduced greenhouse-gas emissions among party countries, though the effect varied according to technological level, energy infrastructure efficiency, and engineering capacity. These findings underscore that climate policy effectiveness depends not only on political commitment but also on technical capability, innovative engineering solutions, and robust data-management systems.

Traditionally, environmental management operated as a top-down mechanism based on centralized planning, legal sanctions, and state authority. In contrast, global environmental governance emphasizes participation, transparency, data sharing, and technical collaboration. Decision-making is no longer exclusive to states; engineering organizations, research institutes, private sector actors, local governments, and civil society organizations actively shape policy (Lopez, 2003; Ma, 2010). This shift transforms environmental management into a multi-actor governance model grounded in technical indicators, measurable datasets, and engineering-oriented problem-solving.

The Kyoto Protocol operationalized this model, requiring parties to measure and verify emission reductions using scientific and engineering methods and report outcomes to international databases. This verification framework demonstrates that effective environmental policy relies on measurable outputs rather than political declarations alone, employing engineering indicators such as carbon intensity, energy-efficiency coefficients, and sector-specific emission profiles (Kim et al., 2020). In this way, the Protocol converted abstract policy targets into a governance structure grounded in technical data and international oversight.

The MRV mechanism, constituting the Protocol's technical backbone, forms the engineering-based infrastructure of global environmental governance. Each country calculates greenhouse-gas emissions across energy, transport, industry, and building sectors using standardized measurement methods and reports the data to international institutions. Verification is conducted by IPCC and UNFCCC expert groups and independent research centers, ensuring technical reliability and global data integrity. Civil society, universities, and engineering research centers further contribute to scientific and ethical audits, enhancing credibility (Maamoun, 2019). Consequently, environmental governance becomes a multi-layered system jointly supported by technical expertise, scientific communities, and engineering ethics, rather than determined solely by political actors. Kyoto thereby established a networked technical governance model as the foundation of global sustainability.

A key innovation of the Kyoto Protocol is its "flexibility mechanisms"—the Clean Development Mechanism (CDM), Joint Implementation (JI), and Emissions Trading (ET). These

mechanisms linked global governance with an engineering-based carbon economy, transforming environmental policy into a technically and financially grounded system. Under the CDM, energy-efficiency, hydropower, waste-recovery, and renewable-energy projects in developing countries undergo detailed engineering-based carbon-reduction calculations (CERs), which can subsequently be traded on global carbon markets. This approach converted environmental policy from ethical responsibility into a measurable economic strategy, with technical parameters such as energy-conversion coefficients, process efficiency, and fuel consumption directly influencing the global economy (Grubb, 2003).

The Protocol was the first international framework linking environmental goals' financial viability to technical indicators, establishing a governance paradigm in which performance is validated via technical measurements integrated with cost-effectiveness analyses (Grubb, 2003; Maamoun, 2019). It also redefined national sovereignty in terms of collective technical and environmental responsibility, requiring countries to account for global impacts of energy production, water management, industrial processes, and transportation infrastructure using engineering-based indicators (Ma, 2010; Maamoun, 2019).

Kyoto shifted environmental management from a state-centered domain to a multilayered governance system coordinated by international engineering networks and scientific institutions. National emissions inventories, energy-efficiency reports, and carbon-monitoring systems became integrated into international measurement systems standardized by IPCC and UNFCCC, evolving environmental information from political instruments into technical management tools. The Protocol enhanced international awareness, data sharing, and scientific coordination, institutionalizing engineering-based environmental management (Lopez, 2003). However, disparities in technical infrastructure and capacity, particularly in developing countries, limited uniform implementation, highlighting that governance effectiveness depends on technological adequacy, scientific data generation, and engineering innovation.

Global environmental governance, as exemplified by Kyoto, integrates ecological sustainability with technical justice, technology access, and equity principles. The CBDR principle exemplifies engineering-oriented environmental justice, placing greater responsibility on developed countries for high-carbon infrastructures and advanced technologies, while providing support mechanisms for developing nations, including technology transfer, capacity building, and knowledge sharing (Maamoun, 2019). This approach balances ethical imperatives with the correction of technological inequalities, demonstrating that climate policy requires political, technical, and data-driven support.

Kyoto also reconceptualized international technical cooperation, framing the environment as a global engineering system and shared public value (Madubuegw et al., 2021). Scientific data, engineering calculations, and verification systems became integral to policy, transforming governance from value-based to data-driven and technologically informed. Technical indicators such as atmospheric composition, energy balance, hydrological cycles, and land-use changes enable measurable, verifiable, and modelable policy planning. Ma (2010) emphasizes that the Protocol's effectiveness also depends on technology transfer and engineering knowledge-sharing, with institutional limitations in developing countries creating inequalities in global environmental governance.

In the twenty-first century, global environmental governance has evolved into a form of technical soft power, linking engineering-based sustainability achievements to international prestige. The European Union exemplifies this approach by diffusing energy-efficiency standards, carbon-management systems, life-cycle assessments, and verification techniques globally (Maamoun, 2019; Madubuegw et al., 2021). Kyoto's recognition of technical standards within international

environmental law marked a shift from voluntary frameworks to structures grounded in measurable engineering criteria, which was further reinforced by post-Kyoto agreements such as the Paris Agreement. Through mechanisms like the Technology Mechanism, Capacity-Building Framework, and Enhanced Transparency Framework, international governance increasingly relies on technical expertise, data sharing, model standardization, and engineering innovation, solidifying Kyoto's legacy as the institutional infrastructure of global environmental governance.

Despite limitations in compliance, Kyoto's "hidden success" lies in building technical and institutional capacity, standardizing measurement, reporting, and verification systems, and reshaping the culture of international technical governance (Maamoun, 2019). Empirical evidence confirms that the Protocol fostered institutionalized technical frameworks that extend beyond legal obligations, integrating engineering, scientific, and economic dimensions into global climate policy.

3. Environmental Justice, Burden Sharing, and Climate Inequality

The impacts of global climate change have transcended ecological concerns, evolving into a global justice issue that produces deep structural inequalities in engineering infrastructure, energy technologies, disaster-risk management, and natural-resource planning. Consequently, environmental justice emerges as a central principle underpinning both the ethical and technical foundations of the Kyoto Protocol. This concept encompasses not only the equitable distribution of environmental burdens, risks, and damages but also the balanced allocation of sustainable-development resources, including access to technology, financial capacity, engineering expertise, and adaptation infrastructure across societies, regions, and generations (Madubuegw et al., 2021).

This perspective underscores that environmental challenges must be addressed not solely through technical solutions but through a holistic integration of ethical considerations, social equity, and engineering responsibility. The Kyoto Protocol institutionalized this balance by centering environmental justice within global climate governance. Recognizing the historical emission responsibilities of developed countries, the Protocol mandated higher mitigation commitments while providing developing countries with support via technology transfer, capacity building, and financial mechanisms (Maamoun, 2019). In this framework, global climate policy was transformed into a multidimensional justice system evaluated not only by the technical feasibility of emission reductions but also by equality in engineering capacity. Consequently, climate policy acquired an international standard simultaneously defined by technical measurability and ethical responsibility.

Comparative analysis by Madubuegw et al. (2021) highlights significant differences between the Kyoto Protocol and the Paris Agreement regarding the level of technical intervention. Developing countries' structural deficiencies in access to technology, engineering infrastructure, data-generation capacity, and finance limit their effectiveness as global climate actors. This finding demonstrates that environmental justice is not merely a political burden-sharing principle but also closely tied to concrete technical factors, including technological autonomy, engineering-capacity development, and the reinforcement of adaptation infrastructures (Morin et al., 2013).

Kyoto was among the first global agreements to operationalize environmental justice in terms of technical equality, capacity balancing, and knowledge sharing. As such, climate-policy success is measured not only by greenhouse-gas reduction rates but also by objective indicators such as renewable-energy access, enhanced engineering standards for water and waste management, verifiable data production, and technology transfer. Thus, Kyoto provides a foundational framework for subsequent engineering-based environmental governance models.

One key technical dimension of environmental justice is historical responsibility. Historically, developed countries have produced the majority of global carbon emissions through high-energy

industrial infrastructures, fossil-fuel-based transportation systems, and energy-intensive engineering applications, achieving economic growth while externalizing environmental costs onto global ecosystems (Madubuegw et al., 2021; Morin et al., 2013). In contrast, developing countries—despite relatively low emissions—are more vulnerable to climate impacts due to limited infrastructure resilience, technological capacity, and adaptation systems. Consequently, climate change constitutes not only an environmental issue but also a structural inequality rooted in disparities in engineering capabilities.

The Kyoto Protocol institutionalized the principle of Common but Differentiated Responsibilities (CBDR) to address these inequities. CBDR allocates obligations according to historical emissions, the maturity of energy and engineering infrastructures, technological capacity, and adaptive potential (Maamoun, 2019). Thus, environmental responsibility is differentiated based on both historical impact and the technical renewal capacity of national systems, positioning Kyoto as a pioneering framework integrating ethical and technical dimensions in global climate governance.

Burden sharing is both politically and technically contested. To operationalize it, Kyoto divided Parties into Annex I and Non-Annex I countries. Developed economies (Annex I) bear verifiable emission-reduction obligations grounded in scientific measurements and engineering calculations, whereas developing countries participate through engineering projects, technology transfer, and financial-support programs. This distinction reflects a burden-sharing mechanism informed by political ideals, technical capacity, and engineering infrastructure (Morin et al., 2013).

Kyoto also ensured that burden sharing maintained structural stability regarding economic feasibility and engineering sustainability. Developed countries were expected to transform high-emission infrastructures and invest in clean technologies, while developing countries received support for renewable-energy systems, water-resource management, climate-resilient infrastructure, transportation modernization, and waste management. This multidimensional approach recognizes disparities in both technical and economic capacities.

The Protocol's justice-based technical strategy comprises two core elements:

- Countries with high historical emissions undertake extensive engineering transformations.
- Countries with limited technological access receive support through capacity building, technology transfer, and financial assistance.

This approach transforms environmental management from political negotiation into a system based on scientific data, engineering calculations, and measurable performance indicators. Consequently, Kyoto reframed environmental policy as a multilayered governance model integrated with development support and capacity-strengthening mechanisms, linking sustainability goals to technology transfer, institutional capacity building, and technical verification processes.

Morin et al. (2013) characterize this architecture as a multi-actor governance model where international organizations, civil society, engineering institutions, and scientific networks collaborate with states. In this model, emission accounting, energy-balance analyses, hydrological and atmospheric datasets, and standardized reporting protocols become integral to environmental law. Environmental decision-making is institutionalized around technical expertise and scientific verification, rendering environmental responsibility a concrete governance instrument defined by measurable engineering indicators, verifiable datasets, and performance criteria.

Climate inequality manifests both across states and within countries, reflecting disparities in infrastructure quality, engineering capacity, and technology access. Poor and socioeconomically vulnerable communities face disproportionate impacts from floods, droughts, storms, and sea-level

rise yet have limited access to resilient buildings, early-warning systems, water-management infrastructure, and energy-efficiency solutions (Nordhaus & Boyer, 1998). Technology-transfer initiatives, financial support, and capacity-building programs under Kyoto aimed to reduce such disparities; however, infrastructure deficits and limited technical competence persisted, revealing structural barriers to environmental justice.

The concept of climate debt highlights that developed countries' historical growth through high-emission energy and industrial systems generated obligations toward less technologically equipped nations. Climate debt thus encompasses the transfer of clean-energy technologies, sustainable infrastructure, early-warning systems, and engineering knowledge (Morin et al., 2013; Nordhaus & Boyer, 1998). While Kyoto did not explicitly define climate debt, mechanisms such as the Clean Development Mechanism (CDM), green-finance instruments, and technology-transfer programs implicitly operationalize this responsibility. Nevertheless, reliance on voluntary participation limited effectiveness, leaving developing countries disadvantaged in accessing innovative engineering technologies.

Technical inequalities between developed and developing countries affect climate-policy legitimacy. Developed nations' advanced infrastructures and research capabilities facilitate the low-carbon transition, while developing countries remain reliant on carbon-intensive production due to high costs and insufficient engineering infrastructure. Market-based mechanisms, although theoretically fair, often favor countries with stronger technical capacities, reinforcing dependency. Addressing climate debt thus requires not only financial support but also technology sharing, engineering education, research partnerships, and open-data cooperation. Kyoto's approach redefined environmental debt in relation to technical knowledge, energy efficiency, and sustainable infrastructure.

Climate inequality is also intergenerational. Current decisions influence future infrastructure security, water-management capacity, energy systems, and ecological resilience. Kyoto reconceptualized environmental policy as a long-term sustainability responsibility, emphasizing protection of ecological balance, energy infrastructure, water resources, climate adaptation, and ecosystem integrity for future generations (Oxley & Macmillan, 2004). From this perspective, environmental justice embodies "temporal engineering justice," integrating ethical responsibility with technical planning.

Kyoto also pioneered the integration of climate migration and environmental security into global governance from an engineering standpoint. Climate-induced hazards—such as droughts, coastal erosion, water scarcity, infrastructure failures, and energy system vulnerabilities—create both humanitarian and technical challenges (Nordhaus & Boyer, 1998; Oxley & Macmillan, 2004). Recognizing the human–technical nexus, the Protocol linked environmental governance with security and resilience planning, evaluating engineering practices not solely on efficiency but also on social resilience and intergenerational ethics.

Nordhaus and Boyer (1998) highlight that market-based instruments, such as carbon pricing and emissions trading, require technical modeling, optimization, and data-driven assessment to enhance policy effectiveness. Environmental justice debates have revealed the structural power dynamics inherent in access to technology, infrastructure, and engineering capabilities, with developing countries critiquing the perpetuation of "green imperialism." Binding Kyoto targets generated divergent perceptions: while some states view them as promoting equity and technical diffusion, others, especially developing nations, perceive restrictions on autonomy and technical sovereignty (Oxley & Macmillan, 2004).

Achieving equitable environmental policies necessitates integrated assessment of economic development, social welfare, and technical capacity. Kyoto institutionalized this balance, defining sustainability goals through engineering-based transformation strategies in energy, water, transportation, and industrial systems. It demonstrated that environmental protection is both an ethical imperative and a technology-centered development principle, linking sustainability to economic growth.

Debates on climate inequality have also scrutinized international environmental-finance mechanisms, such as the Green Climate Fund (GCF), which aims to support engineering-based projects. Audit gaps and political influences have weakened technical neutrality, highlighting the need for transparent, accountable, and locally responsive mechanisms (Öztürk & Toprak, 2024). The future of global environmental governance requires multilayered engineering solidarity, encompassing financial transfers, knowledge sharing, data infrastructure strengthening, engineering education, and technology dissemination.

Environmental justice extends beyond economic or legal distribution; it is a holistic construct evaluated through cultural rights, social representation, and technical adaptation capacity. Indigenous peoples, small island states, and local communities, despite minimal contributions to global emissions, are disproportionately affected due to fragile infrastructure, energy dependency, and disrupted ecosystem cycles (Oxley & Macmillan, 2004; Öztürk & Toprak, 2024). Kyoto provided the institutional foundation for integrating moral responsibility with technical accuracy, establishing climate justice ethics as a normative framework.

This framework reconceptualizes the human–nature relationship based on mutual protection, intergenerational responsibility, and sustainable design principles, requiring engineering disciplines to embrace ethical responsibility, cultural sensitivity, and ecosystem integrity (Page, 2007). Studies of APEC economies demonstrate that rapid industrialization and fossil-fuel dependence hinder compliance, showing that environmental justice is structurally linked to energy efficiency, technological sophistication, and engineering transformation capacity (Oxley & Macmillan, 2004). Future policies must integrate cultural sustainability with technical equity and engineering ethics within a unified governance framework.

4. Public Perceptions of Kyoto in Media, Academia, and the Public Sphere

With the international adoption of the Kyoto Protocol, climate change evolved beyond intergovernmental diplomatic negotiations and became a multidimensional policy domain situated at the intersection of scientific, technical, and societal awareness. This transformation positioned environmental issues as a shared sphere of responsibility not only for policymakers but also for engineers, academics, civil society organizations, and individuals. Public, media, and academic perceptions of Kyoto have therefore emerged as key dynamics shaping the social legitimacy of global environmental governance (Öztürk & Toprak, 2024; Page, 2007).

The Kyoto Protocol demonstrated that environmental consciousness extends beyond the political and legal domains and permeates technical fields that shape everyday life, including engineering practices, urban planning, energy efficiency, and waste management. Accordingly, environmentally conscious engineering has evolved into not merely a professional standard but also a societal ethical norm. In the post-Kyoto era, knowledge production itself has transformed; engineering research has increasingly integrated environmental economics, data analytics, carbon-monitoring technologies, and energy-modeling systems, elevating environmental governance into a sphere of public awareness grounded in scientific evidence and innovation.

Public perceptions of Kyoto are closely linked to countries' technical capacities, economic structures, and degrees of environmental vulnerability. In developed countries, the Protocol is frequently interpreted as a marker of environmental accountability and engineering performance, and governments are expected to expand renewable energy investments, promote carbon-neutral infrastructures, and lead green-technology innovation (Page, 2007). Conversely, in many developing countries Kyoto is perceived as a regulatory burden that may constrain economic growth, and environmental policies are continually recalibrated in relation to technical development goals due to high investment costs. This pattern reveals that environmental awareness is not solely a political preference but a multidimensional phenomenon shaped by economic capacity, engineering infrastructure, and cultural values.

Media discourse plays a decisive role within this dynamic. Kyoto has at times been idealized as a "technological rescue plan," while at other moments criticized as a diplomatic formality with limited impact. In the age of social media, the popularization of technical debates has increased the density of public information, making the gap between engineering accuracy and popular discourse more visible. Yet the Kyoto process has encouraged the democratization of engineering-based environmental knowledge, transforming environmental policy from an expert-dominated domain into a broader process of collective knowledge production. This development has laid the groundwork for a new model of "science–society partnership," in which environmental governance is intertwined with ethical, social, and cultural dimensions.

From an academic standpoint, the Kyoto Protocol has generated a robust interdisciplinary field connecting the social and technical sciences. International law, economics, political science, environmental engineering, urban planning, energy systems, and data science have each analyzed Kyoto through their respective theoretical and methodological perspectives. As a result, environmental policies have come to be understood not only as legal frameworks but also as systems inseparable from engineering calculations, energy-balance models, and carbon-management metrics. While some scholars argue that Kyoto marked a significant threshold for democratizing governance, enhancing transparency, and institutionalizing science-based decision-making, others contend that market-based mechanisms such as carbon trading and the CDM have not always aligned with principles of environmental justice and have, at times, exacerbated disparities in engineering capacity between countries (Page, 2007; Pardy, 2004).

This academic divergence reveals that climate policy is a multilayered domain shaped not merely by ideological debates but by technological capacity, data infrastructures, institutional coordination, and engineering governance. Examining the case of Turkey, Öztürk and Toprak (2024) show that late accession initially resulted in major deficiencies in emission inventories, carbon-management systems, and reporting infrastructures; however, after 2010, significant improvements in MRV systems, data integrity, and energy–environment engineering capacity led to substantial enhancement in compliance performance. These findings indicate that the success of national environmental policies depends not only on legal provisions but also on concrete implementation dynamics such as technical infrastructure, data quality, institutional coordination, and engineering capacity.

The relationship between public opinion and academic discourse plays a decisive role in shaping the social legitimacy of environmental awareness. Pardy (2004) emphasizes that the media often portrays climate change through emotional, dramatized, and scientifically detached frames, which prevents broad segments of society from adequately understanding climate models, energy systems, and engineering data. As a result, the technical components of the Kyoto Protocol—such as emission-calculation methods, carbon-equivalency mechanisms, and energy-efficiency coefficients—are frequently perceived by the public as abstract, complex, and distant from everyday life. Consequently, contemporary environmental governance increasingly highlights the need for more inclusive

environmental communication strategies that simplify engineering data, employ visualizations, and provide solution-oriented content.

Within this process, the symbolic impact of the Kyoto Protocol has acquired a lasting quality through its cultural diffusion. The Protocol transformed environmental responsibility from an obligation solely imposed on states into an ethical framework encouraging individuals to reassess everyday practices such as energy consumption, water use, recycling habits, and personal carbon footprints. International media has often framed Kyoto with dramatic metaphors such as "the last chance to save the planet," which, while rendering the moral dimension of environmental policy more visible, has at times also contributed to climate fatigue and public disengagement (Peker & Demirci, 2008). From an engineering perspective, however, achieving lasting behavioral change requires balancing crisis-focused rhetoric with feasible technical solutions, benefit-oriented messages, and principles of sustainable design.

Since the mid-2000s, the literature has increasingly highlighted the "Kyoto paradox": despite institutionalizing global environmental governance, the Protocol has been criticized for failing to fully achieve environmental justice in the face of economic interests, national development priorities, and disparities in technical capacity (Peker & Demirci, 2008; Prins & Rayner, 2008). These critiques illustrate that sustainability policies cannot be confined to a diplomatic framework alone; rather, they constitute a multilayered transformation process requiring simultaneous strengthening of infrastructure modernization, scientific capacity building, and engineering capabilities.

5. Perceptual and Systemic Transformation in the Transition to the Paris Agreement

The transition from the Kyoto Protocol to the Paris Agreement fundamentally transformed not only the technical architecture of global environmental governance but also its perceptual, institutional, and normative foundations. Kyoto's rigid, centralized, and mandatory reduction-based structure was replaced in the Paris era by a paradigm of voluntarism, flexibility, adaptability to national capacities, and multi-actor responsibility. This shift reflects the growing recognition that climate issues can no longer be governed through numerical obligations imposed on selected states; instead, they require a holistic global system grounded in shared engineering capacity, data exchange, technological cooperation, and collective action (Prins & Rayner, 2008; Şahin, 2020).

The Paris regime redefined climate action as a network-based governance model in which local governments, the private sector, engineering organizations, research institutions, and individuals themselves became central actors. Renewable energy technologies, smart-grid systems, sustainable urban design, hydrological management approaches, and digital measurement-reporting infrastructures constitute the core engineering components of this new policy framework. This transformation positioned climate action as a global engineering collaboration, a data-driven sustainability strategy, and a multi-actor field of technical governance.

At the perceptual level, the Paris Agreement abandoned Kyoto's crisis- and threat-oriented discourse, instead foregrounding the concepts of solution, adaptation, and transformation (Shishlov et al., 2016). Climate challenges were reframed not merely as zones of risk and cost but as strategic development opportunities intertwined with technological innovation, economic benefits, and social welfare. In contrast to the perception among many developing countries that Kyoto at times constrained the "right to development," the Paris model reconceptualized environmental protection and economic development as mutually reinforcing processes (Şahin, 2020). Concepts such as green growth, circular economy, decarbonized production, and sustainable finance moved to the center of climate politics; the Paris Agreement reframed carbon mitigation not as a constraint on economic output but as a core component of a development paradigm grounded in engineering innovation, energy efficiency, and low-carbon technologies. This approach repositioned environmental policy not

as a burden conflicting with economic order but as a strategic mechanism that accelerates economic transformation (Peker & Demirci, 2008; Thakur, 2021).

Public perception likewise shifted, with the Paris Agreement widely viewed as a more inclusive, flexible, and pragmatic framework compared with Kyoto. Whereas many states remained outside the Kyoto process due to its rigid and binding targets, the voluntary and capacity-sensitive NDC system of the Paris regime encouraged much broader participation in climate policy (Shishlov et al., 2016). Consequently, global climate governance evolved from an elite diplomatic arena into a dynamic system shaped by collective will, data exchange, and multi-actor technical coordination. This new model—referred to in the literature as *multi-level governance*—facilitates the integration of environmental policy with local implementation networks, technical cooperation, and technology transfer beyond national boundaries (Shogren, 1999).

Environmental communication also transformed significantly in the Paris era. Whereas Kyoto-era climate policy predominantly addressed expert communities, the Paris Agreement reached broader public audiences through digital media, youth movements (such as Fridays for Future and Extinction Rebellion), and global environmental campaigns. As a result, environmental consciousness evolved from a technical-bureaucratic discourse into a cultural, ethical, and social form of awareness (Shishlov et al., 2016).

Adaptation became one of the most distinctive features differentiating the Paris regime from Kyoto. While Kyoto primarily emphasized mitigation strategies, Paris placed resilience and adaptive engineering solutions at the core of its climate agenda (Shogren, 1999). Redesigning energy infrastructures, water-resource systems, transportation networks, and urban planning for changing climate conditions positioned environmental engineering as a strategic element of global climate resilience.

Analyses of the limitations of the Kyoto Protocol highlight that it had increasingly become "politically appealing but practically ineffective," failing to achieve the anticipated reductions in global emissions (Prins & Rayner, 2008). In response, the Paris Agreement was designed as a governance model built upon more measurable, data-driven, and adaptive processes.

By democratizing climate governance, the Paris regime fostered a culture of shared responsibility among scientific institutions, engineering communities, the private sector, and individuals (Thakur, 2021). In contrast to Kyoto's externally imposed strict obligations, the Paris framework allowed countries to determine their own Nationally Determined Contributions (NDCs) in accordance with their technical, economic, and cultural conditions. As a result, environmental obligations were reframed not as externally imposed duties but as long-term engineering investments in the common future.

6. Conclusion

The Kyoto Protocol represents far more than a technical regulatory framework for emission reduction in the history of global environmental governance. It established a multilayered governance architecture that approaches climate change through scientific evidence, engineering capacity, technological transformation, and ethical responsibility. In this regard, Kyoto became the first comprehensive global system to transform environmental policy through technical verification processes, measurable performance indicators, and international engineering cooperation. Consequently, environmental management transcended national borders and evolved into a shared sphere of technical responsibility in which the atmosphere, energy cycles, water resources, and ecosystems were redefined as the common engineering domain of the international community.

One of the Protocol's most decisive contributions lies in reframing environmental justice not merely as an ethical or political debate but as a set of concrete engineering parameters shaped by technical capacity, technological access, data generation, and adaptation infrastructure. Within this framework, the principle of "Common but Differentiated Responsibilities" (CBDR) emerged as a technical mechanism aimed at balancing structural inequalities between historical emission profiles and engineering capabilities. However, Kyoto did not fully meet the technology transfer, financial support, and institutional capacity needs of developing countries, resulting in persistent limitations in the practical implementation of environmental justice.

Nevertheless, the Kyoto experience served as a critical learning process that laid the technical and methodological foundations of contemporary global climate governance. Emission inventories, MRV systems, carbon markets, verification protocols, and engineering-based performance indicators were institutionalized during the Kyoto era, providing the structural groundwork for the Paris Agreement. By doing so, the Protocol shifted environmental policy from a peripheral topic of international relations to a central global policy field integrated with energy strategies, economic models, urban planning, infrastructure management, and innovation-oriented engineering practices.

The new era introduced by the Paris Agreement transformed Kyoto's rigid and centralized architecture into a more flexible, inclusive, and capacity-responsive model. Climate action was redefined as a multi-actor technical cooperation arena that extends beyond state-centered obligations, incorporating local authorities, private sector actors, engineering communities, research institutions, and individuals. Adaptation, resilience, data-driven policymaking, digitalized reporting mechanisms, and engineering innovation became the cornerstones of the Paris regime, enabling environmental management to operate through a multilayered governance model combining both top-down and bottom-up approaches.

In conclusion, although the Kyoto Protocol did not achieve the level of global emission reduction initially anticipated, it remains a historic turning point that established the technical, institutional, and normative foundations of international environmental governance. The Protocol provided a unique reference framework that integrated engineering-based environmental management with international law, redefined environmental justice as an issue of technical capacity, and transformed global cooperation into a data-centered system. This legacy continues to shape the foundations of the Paris Agreement and subsequent climate regimes, clearly demonstrating that sustainable development is attainable only through a governance approach in which scientific knowledge, ethical responsibility, and engineering innovation are fully integrated.

References

Agiralioglu, N., Eris, E., Andic, G., Cigizoglu, H. K., Coskun, H. G., Yilmaz, L., Algancı, U., & Toprak, Z. F. (2017). *Practical methods for the estimation of hydroelectric power potential of poorly gauged basins*. Sigma Journal of Engineering and Natural Sciences, 35(2), 347–358.

Alashan, S., Şen, Z., & Toprak, Z. F. (2016). *Hydroelectric energy potential of Turkey: A refined calculation method*. Arabian Journal for Science and Engineering, 41, 3167–3176. https://doi.org/10.1007/s13369-015-1982-5

Aylett, A. (2015). *Institutionalizing the urban governance of climate change adaptation: Results of an international survey.* Urban Climate, 14, 4–16.

Batan, M., & Toprak, Z. F. (2020*). The mutual triggering of drivers and consequences in climate change*, Dicle University Journal of Engineering, 11(2), 759–769. https://doi.org/10.24012/dumf.547015

Bulkeley, H., & Betsill, M. M. (2003). *Cities and climate change: Urban sustainability and global environmental governance.* Routledge.

Bulkeley, H., & Betsill, M. M. (2013). *Revisiting the urban politics of climate change.* Environmental Politics, 22(1), 136–154.

Grubb, M. (2003). *The economics of the Kyoto Protocol.* World Economics, 4(3), 1–14.

Gupta, J. (2010). *A history of international climate change policy.* WIREs Climate Change, 1(5), 636–653. https://doi.org/10.1002/wcc.67

IPCC. (2001). *Climate change 2001: Mitigation. Contribution of Working Group III to the Third Assessment Report of the Intergovernmental Panel on Climate Change.* Cambridge University Press.

IPCC. (2007). *Climate change 2007: Synthesis report. Contribution of Working Groups I, II and III to the Fourth Assessment Report of the Intergovernmental Panel on Climate Change.* IPCC.

IPCC. (2014). *Climate change 2014: Synthesis report. Contribution of Working Groups I, II and III to the Fifth Assessment Report of the Intergovernmental Panel on Climate Change.* IPCC.

Karakaya, E. (Ed.). (2008). *Global warming and the Kyoto Protocol: Scientific, economic, and political analysis of climate change.* Bağlam Publishing.

Kaya, H. E. (2020). *Global climate policies from Kyoto to Paris.* Meriç International Journal of Social and Strategic Studies, 4(10), 165–191.

Kayan, A., & Küçük, A. (2022). *The impact of political decisions on the formation of the global climate crisis.* Dicle University Journal of Social Sciences (DÜSBED), 31, 501–526.

Khanna, N. (2001). *Analyzing the economic cost of the Kyoto Protocol.* Ecological Economics, 38(1), 59–69. https://doi.org/10.1016/S0921-8009(01)00149-9

Kim, Y., Tanaka, K., & Matsuoka, S. (2020). *Environmental and economic effectiveness of the Kyoto Protocol.* PLoS ONE, 15(7), e0236299. https://doi.org/10.1371/journal.pone.0236299

Lopez, T. M. (2003). *A look at climate change and the evolution of the Kyoto Protocol.* Natural Resources Journal, 43(1), 285. https://digitalrepository.unm.edu/nrj/vol43/iss1/9

Ma, Z. (2010). *The effectiveness of the Kyoto Protocol and consummating the legal institution for international technology transfer.* Asian Social Science, 6(4), 80–85.

Maamoun, N. (2019). *The Kyoto Protocol: Empirical evidence of a hidden success.* Journal of Environmental Economics and Management, 95, 227–256. https://doi.org/10.1016/j.jeem.2019.03.001

Madubuegw, C. E., Okechukwu, G. P., Emeka, O., Samuel, N., & Kyrian, U. (2021). *Climate change and challenges of global interventions: A critical analysis of Kyoto Protocol and Paris Agreement.* Journal of Policy and Development Studies, 5(6), 127–140. https://doi.org/10.12816/0059151

Mol, A. P. J., & Spaargaren, G. (2000). *Ecological modernization theory in debate: A review.* Environmental Politics, 9(1), 17–49. https://doi.org/10.1080/09644010008414511

Morin, J.-F., Orsini, A., Trudeau, H., Duplessis, I., Lalonde, S., Van de Graaf, T., De Ville, F., O'Neill, K., Roger, C., Dauvergne, P., Oberthür, S., Biermann, F., Ohta, H., & Ishii, A. (2013). *Insights from global environmental governance.* International Studies Review, 15(4), 562–589.

Nordhaus, W. D., & Boyer, J. G. (1998). *Requiem for Kyoto: An economic analysis of the Kyoto Protocol* (Cowles Foundation Discussion Paper No. 1201). Cowles Foundation for Research in Economics, Yale University.

Okereke, C. (2008). *Global justice and neoliberal environmental governance: Sustainable development, carbon trading and the climate change regime.* Routledge.

Oxley, A., & Macmillan, S. (2004). *The Kyoto Protocol and the APEC economies.* Australian APEC Study Centre ITS Global.

Öztürk, Ş. T., & Toprak, Z. F. (2024). *Evaluation of the Kyoto Protocol and Turkey's adaptation process.* Turkish Journal of Hydraulics, 8(1), 7–18.

Öztürk, Ş. T., & Toprak, Z. F. (2025). *The success of the Kyoto Protocol in reducing carbon emissions in the EU.* International Journal of Global Warming, 36, 53–66.

Page, E. (2007). *Equity and the Kyoto Protocol.* Politics, 27(1), 8–15. https://doi.org/10.1111/j.1467-9256.2007.00273.x

Pardy, B. (2004). *The Kyoto Protocol: Bad news for the global environment.* Journal of Environmental Law and Practice, 14, 27–48.

Peker, O., & Demirci, M. (2008). *Analysis of climate change from the perspectives of science and economics.* Süleyman Demirel University Journal of Economics and Administrative Sciences, 13(1), 239–251.

Prins, G., & Rayner, S. (2008). *The Kyoto Protocol.* Bulletin of the Atomic Scientists, 64(1), 45–48. https://doi.org/10.2968/064001011

Roberts, J. T., & Parks, B. (2007). *A climate of injustice: Global inequality, North–South politics, and climate policy.* MIT Press.

Rogers, M. F., Pfatteicher, S., & Venkataraman, P. (2008). *Engineering citizenship: Engineering ethics for a globalized world.* Journal of Professional Issues in Engineering Education and Practice, 134(2), 102–110. https://doi.org/10.1061/(ASCE)1052-3928(2008)134:2(102)

Şahin, Ü. (2020). *New era in climate policies: The Paris Agreement and rights-based approach.* Toplum ve Hekim, 35(1), 1–12.

Shishlov, I., Morel, R., & Bellassen, V. (2016). *Compliance of the parties to the Kyoto Protocol in the first commitment period.* Climate Policy, 16(6), 768–782. https://doi.org/10.1080/14693062.2016.1164658

Shogren, J. (1999). *The benefits and costs of the Kyoto Protocol.* The AEI Press.

Sovacool, B. K., & Van de Graaf, T. (2018). *Building or stumbling blocks? Assessing the performance of the EU emissions trading system.* Energy Policy, 145, 111–123.

Sovacool, B. K., Linnér, B.-O., & Goodsite, M. E. (2019). *The political economy of climate adaptation.* Nature Climate Change, 9, 616–623.

Stern, N. (2000). *Public commentary on climate economics.* Oxford University Press.

Stern, N. (2007). *The economics of climate change: The Stern Review.* Cambridge University Press.

Toprak, Z. F., Hamidi, N., Toprak, Ş., & Şen, Z. (2013). *Climatic identity assessment of the climate change*. International Journal of Global Warming, 5(1), 30–45. https://doi.org/10.1504/IJGW.2013.051480

Thakur, S. (2021). *From Kyoto to Paris and beyond.* India Quarterly, 77(3), 366–383. https://doi.org/10.1177/09749284211044272

UNFCCC. (2006). *Manual for compliance with the Kyoto Protocol.* United Nations Framework Convention on Climate Change.

Ürge-Vorsatz, D., Koeppel, S., & Mirasgedis, S. (2009). *Appraisal of policy instruments for reducing buildings' CO_2 emissions.* Building Research & Information, 37(4), 247–266. https://doi.org/10.1080/09613210902899798

CHAPTER 3

STRUCTURE AND FUNCTION OF DYE-SENSITIZED SOLAR CELLS

Olcay GENÇYILMAZ[1], Aicha Rouffa ABDALLAH[2]

1 Prof. Dr., Çankırı Karatekin University, Pyhsics, Materials and Materials Processing Technologies, ORDIC ID: 0000-0002-7410-2937
2 Çankırı Karatekin University, Graduate School of Education, Pyhsics

1. Introduction

A Dye Sensitized Solar Cell (DSSC) is a system that converts sunlight directly into electrical energy. The cell consists of several components. Conductive glass (FTO, ITO, etc.) is characterized by its ability to provide a transparent and conductive surface, thereby enabling light to penetrate and facilitating electrical conductivity. The oxide film (ZnO, TiO2, etc.) that is coated onto the substrate creates an extensive interface for the purpose of holding the dye and conducting electrons.The dye, a pivotal component of the system, exhibits photosensitivity and functions as the initiator of electron production by means of the absorption of incoming sunlight. The counter electrode (Pt, C, Pd, etc.) is responsible for ensuring the completion of the generated charges, supporting the electron flow, and providing an efficient energy conversion. The electrolyte between these electrodes is responsible for the transportation of ions, thus ensuring the maintenance of electrical charge balance and facilitating the process of energy conversion. The gasket is vital in this regard, as it acts as an adhesive, binding the two electrodes together. This prevents the leakage of liquid electrolyte and ensures the longevity of the cell. This configuration enables DSSC to function as a cost-effective and eco-friendly energy solution, thereby facilitating the transformation of sunlight into electricity (Pekuslu, 2022). Figure 1 shows the fundamental structures that constitute this system.

Figure 1.

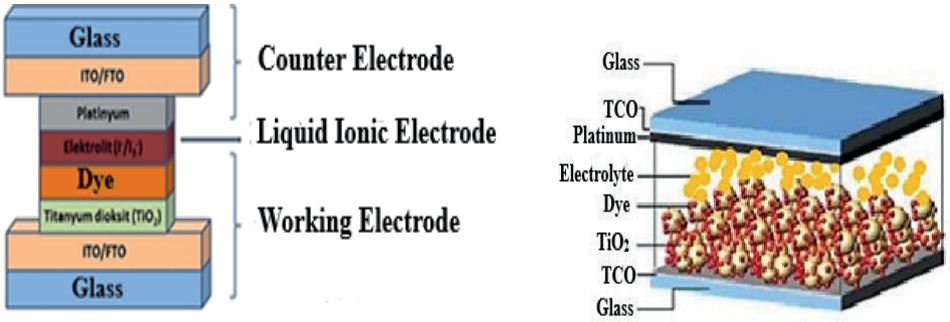

Schematic illustrations of the basic structure of DSSC components (Gezgin, 2024; Özel, 2017)

1.1 Conductive glass layer

Conductive glasses are utilized in dye-sensitized solar cells to facilitate electrical conductivity and optical transparency. Typically, this is accomplished by physical vapor deposition (PVD), a process that involves the application of tin oxide layers doped with various elements to the glass surface. Depending on the dopant, there are ITO (indium-doped tin oxide), CTO (chlorine-doped tin oxide), and FTO (fluorine-doped tin oxide). FTO is a predominantly utilized conductive glass and has higher conductivity than CTO. Within materials research and engineering, ITO is the preferred material for its ability to provide both high conductivity and optical transparency. However, given the significant expense associated with this approach, there is an ongoing investigation into potential alternatives. Double layer coatings (ITO/SnO_2 and FTO/ITO) have been developed to improve conductivity and temperature resistance. ITO's fragility and exorbitant production costs have led to the emergence of carbon nanotube coatings as a viable alternative. These materials are less costly

and offer superior mechanical properties in comparison to ITO. The thickness is typically optimized through the use of ITO or FTO, thereby enhancing electrical efficiency (Seçkin, 2010).The most commonly utilized ITO and FTO glass shapes are depicted in Figure 2 below.

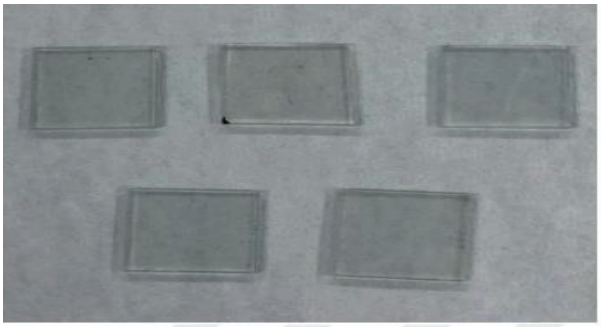

Figure 2. Conductive glass layers FTO and ITO (Pekuslu, 2022)

1.2 Dye

The performance of the cells is facilitated by a sensitizing dye that absorbs light. This dye's functionality is enabled by its ability to capture energy through sunlight absorption. The captured energy subsequently facilitates the passage of electrons toward the TiO2 semiconductor layer through the formation of chemical bonds (Cesur, 2019). Sensitizing dyes, which are employed in dye-sensitized solar cells, facilitate energy production through the absorption of light. However, for a given treatment to be considered effective, it must meet specific criteria. First, it is imperative that the dye exhibit effective uptake of photons across the luminous band of solar radiation and the near-infrared (IR) region. This phenomenon enables the collection of a greater quantity of light energy. It is imperative that the dye be firmly bonded to the semiconductor surface, such as TiO_2. In order to establish and fortify this bond, it is necessary for the dye molecule to possess carboxylate, sulfonate, or phosphate groups. For electron transfer to be effective, the LUMO (lowest empty molecular orbital) excited-state threshold of the dye must exceed transport band of the semiconductor.This phenomenon facilitates the transmission of electrons, thereby enhancing the overall conductivity of the material. It is imperative that oxidation state of the dye exceed the potential of the redox electrolyte.This process enables the dye to revert to its original state, thereby facilitating the continuity of the energy production process. Furthermore, the dye must demonstrate chemical and thermal stability, as well as resistance to light (Ünlü, 2017).

Metal complex dyes play a pivotal role in light absorption and electron transfer process. These dyes contain binding and auxiliary ligands. The presence of binding ligands enables the dye to adhere to the semiconductor surface. Auxiliary ligands have also been shown to improve the system's optical and electrical properties. Metal complex dyes exhibit a broad light absorption spectrum and demonstrate remarkable chemical stability. This wide absorption ability is attributable to the redistribution of electrons across the metal site and the bound ligand. In the field of DSSCs, ruthenium-based metal–ligand frameworks reveal the

preferred configuration. Ruthenium complexes, including N3, N719, and N749, have been observed to yield approximately 10% of the total yield. Despite its high efficiency, ruthenium is a rare and expensive metal. It is imperative to note that the compounds present in this substance have the potential to be carcinogenic. Consequently, transition metal complexes, including osmium, rhenium, and platinum, have been examined as potential alternatives. However, due to the high costs and low yields of these metals, ruthenium has not been fully replaced. Additionally, the investigation encompassed copper and iron complexes, which were considered more economical alternatives. However, these alternatives also exhibited inadequate yields. Alternatively, phthalocyanines and porphyrins have been utilized in DSSCs. Phthalocyanines (Pc) and porphyrins (Por) are organometallic compounds can be used. These compounds are particularly advantageous in solar energy devices because of their capacity for photon capture across the NIR spectral range and their thermal stability. Phthalocyanines are distinguished by their capacity to absorb infrared light, a property attributable to their substantial conjugation structure. However, these compounds tend to aggregate, have low LUMO levels, and lead to some disadvantages due to solubility problems. To address these challenges, the utilization of functional groups and co-adsorbent materials has been employed to impede aggregation. Furthermore, the enhancement of LiI content within the electrolyte has been demonstrated to facilitate enhanced electron transfer. However, the utilization of excess LiI has been observed to cause a lowering of the open-circuit voltage, necessitating meticulous optimization. Symmetric phthalocyanines (A4 type) were the inaugural phthalocyanines adopted. These compounds are typically composed of tetracarboxy or tetrasulfo Pc moieties. These compounds, which yield approximately 4% of the desired product, are scarcely soluble in organic solvents due to their low solubility. As a result, they present significant challenges in synthesis and purification processes. Additionally, their inadequate capacity to adsorb on the semiconductor surface can have an adverse impact on the efficiency of DSSCs, leading to a decline in yield. Asymmetric phthalocyanines (A3B type) are extensively employed and continue to be a subject of research. The functionalization of these molecules with ter-butyl groups has been shown to enhance their solubility in organic solvents and reduce their propensity for aggregation. These enhancements have led to a notable boost in current density measured at short-circuit state, ranging from 20% to 80%, and a corresponding rise in the open-circuit potential (Voc) of DSSCs, with a range of 2.4% to 12%, when compared to symmetric phthalocyanines. In 2007, significant advancements were made in the field of peripheral functionalization studies, which played a pivotal role in enhancing the efficiency of phthalocyanines. In this process, phthalocyanines functionalized with ter-butyl groups were rendered more stable by reducing their aggregation tendency. By concentrating the electron density in the donor groups, the "push-pull" mechanism was enhanced and charge transfer was rendered more efficient. In the present studies, phthalocyanines such as PCH001 and TT1 have been utilized as lead compounds. Through the strategic functionalization of phthalocyanines with diverse auxiliary and linker groups, the efficiency of DSSCs has been enhanced, achieving a maximum yield of up to 12%. Porphyrins are macromolecules with broad conjugation that are analogous to phthalocyanines. However, a distinguishing feature of these compounds is their composition, which consists of four pyrrole units. In their initial implementation, aggregation issues were encountered in DSSCs. To address these challenges, porphyrins with a D-π-A structure analogous to metal-free organic dyes were synthesized. In 2010, a porphyrin known as YD2 was synthesized. The molecule under consideration contains a bis(4-hexylphenyl)amine donor group and a 4-ethynylbenzoic acid linker group. YD2 has demonstrated high performance,

exhibiting 11% efficiency in solar cells (Ünlü, 2024). As demonstrated in Figure 3, metal complex dyes that demonstrate optimal efficiency for DSSCs are predominantly ruthenium-based.

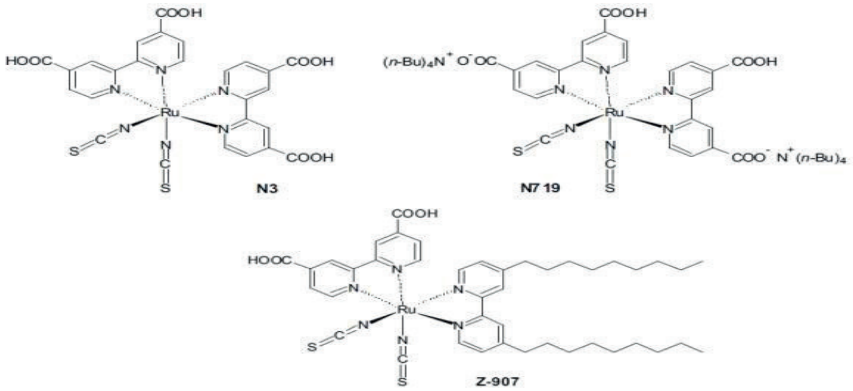

Figure 3. Molecular structures of the most commonly used Ru complexes (Ünlü, 2017)

Metal-free organic dyes exhibit certain advantages over metal complexes utilized in solar cells. These materials are characterized by their ease of design and synthesis, cost-effectiveness, and environmental sustainability. Moreover, given their high molar extinction coefficients, they are particularly well-suited for thin-film and solid dye-sensitized solar cells (DSSC) (Ünlü, 2017). Metal-free organic dyes are highly relevant within photovoltaic research owing to their distinctive structural characteristics, which exhibit a D-π-A configuration.The structure of the compound under consideration consists of three primary components: an electron donor (D), an electron donor (D), an electron-conducting bridge (π), and an electron acceptor (A). This feature has been demonstrated to accelerate charge transfer and elevate the functional output of solar cell systems. Compounds such as diphenylamine and triphenylamine are utilized as donors in this process. These groups assist solar cells in producing greater amounts of energy by facilitating enhanced light absorption. Aromatic π-bridges have been shown to accelerate electron flow, thereby enhancing the efficiency of charge transfer. Fused aromatic systems are of particular interest in scientific research due to their effectiveness under visible light conditions. Carboxylic acids and their derivatives have been identified as critical acceptors, facilitating the channeling of electrons toward the outer layer of titanium dioxide (TiO_2). Cyanoacrylic acid is among the most prevalent acceptors, and through specific chemical modifications, its application can enhance the efficiency of photovoltaic. The productivity of dye-sensitized solar cells (DSSCs) prepared using metal-free organic dyes exhibits significant variability. Recent studies have demonstrated that such solar cells have the potential to achieve efficiencies ranging from 12% to 13%. However, the synthesis and purification processes for metal-free organic dyes are complex and multi-step, which constitutes a significant disadvantage. Figure 4 shows the design scheme of dyes with D-π-A structure.

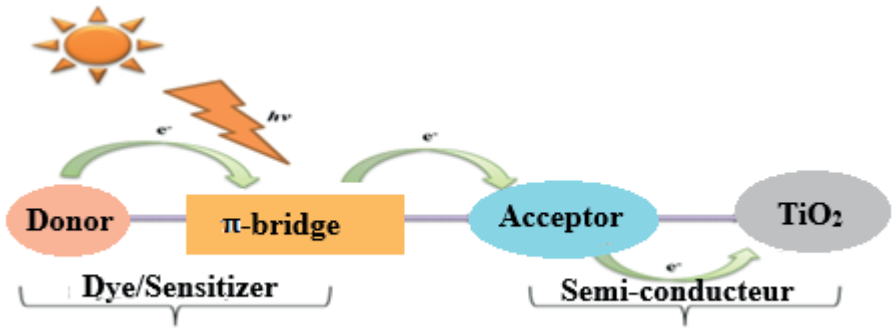

Figure 4. Design scheme of dyes with D-π-A structure (Gezgin, 2024; Ünlü, 2024)

Natural dyes are environmentally friendly colorants derived from the fruits, leaves, roots, and stems of plants. These materials are utilized as a substitute within photovoltaic devices owing to their absence of harmful metals. While transition-metal dye constructs and non-metallic dye molecules are the preferred choice in conventional dye-sensitized solar cells, they are costly and laborious to produce. Consequently, natural dyes present an economically viable and sustainable alternative. However, the efficiency of natural dyes in solar cells exhibits variability, ranging from 0.5% to 2%. This efficiency has been augmented to up to 2% through the application of diverse natural dye mixtures (Çakar, 2017). The pigments present in plant life that are utilized in the fabrication of natural solar cells include chlorophyll, carotene, anthocyanin, lutein, rutin, and betalain. Chlorophyll is a natural pigment that efficiently absorbs sunlight and plays an important role in the photosensitization process. When utilized in conjunction with nanostructured TiO_2, it has been evidenced to elevate the functional output of photovoltaic systems by optimizing the conversion of light energy into electrical energy. Solar cells that are based on chlorophyll and carotenoids exhibit high efficiencies by emulating the light harvesting mechanism that is observed in the natural context of the photosynthetic apparatus of plants. Carotenoids function in conjunction with chlorophyll to facilitate the process of photosynthesis, broaden the spectrum of light absorbed, and enhance the productivity of solar energy conversion. Anthocyanins are water-soluble pigments belonging to the flavonoid class that are found in a wide variety of plants and exhibit a broad light absorption spectrum. The absorption of light at varying wavelengths confers a distinct advantage in the utilization of a broader spectrum of light in solar cells. These pigments, which manifest in colors such as red, violet, and blue, act as fundamental drivers in advancing the output of photovoltaic devices with respect to electron transfer and energy levels. A 2015 study demonstrated that anthocyanin pigments present in sweet pomegranate have a positive effect on solar cell efficiency, indicating a significant potential for these natural compounds in photovoltaic applications (Battal, 2020).

1.3 Counter Electrode

The counter electrode is the component that forms the positive end of an electrical circuit. The structure generally comprises a conductive layer that is coated on a glass or plastic surface. It has been verified that the device receives electrons from the external circuit and subsequently transmits them back to the electrolyte, thereby ensuring the uninterrupted operation of the system (Özkacar, 2021). In the context of solar cells, counter electrodes play a pivotal role in facilitating the transmission of photocurrent. It is anticipated that these materials will exhibit high conductivity and reduce redox pairs with low voltage. The counter electrodes utilized in DSSC systems must possess both high current density and low charge transfer resistance. Platinum (Pt) is a preferred catalyst for I^- reduction due to its effectiveness

in this process (Cesur, 2019). Despite its high conversion efficiency, platinum is being studied as an alternative material due to its high cost and instability in redox electrolytes. In the pursuit of enhanced cost-effectiveness, research is underway on alternative materials such as carbon black, graphene, and graphite for this purpose. In a 2011 study, eight distinct carbon electrodes were examined as counter electrodes in DSSC systems, exhibiting conversion efficiencies ranging from 2.8% to 7.5%. Among these materials, well-ordered porous carbon emerged as a particularly promising candidate, exhibiting catalytic properties analogous to those of platinum. As illustrated in Table 1, a comparative analysis of photovoltaic parameters has been conducted on eight distinct carbon electrodes. These electrodes have been proposed as potential alternatives to platinum in DSSCs.

Table 1. Photovoltaic parameters of eight types of carbon electrodes used as alternatives to platinum in DSSCs (Demirci, 2022)

Counter Elektrode	Redox Pair	Dye (V)	Voc	Jsc (ma/Cm^2) FF	η (%)
Platinum	I^-/I_3^-	N719	0.799	13.71 0.682	7 .5
Carbon Black	I^-/I_3^-	N719	0.805	12.30 0.631	6.3
Carbon Dye	I^-/I_3^-	N719	0.809	13.38 0.697	7.5
Carbone Nanotube	I^-/I_3^-	N719	0.808	13.25 0.656	7.0
Carbone Fiber	I^-/I_3^-	N719	0.806	13.20 0.625	6.7
Well Sorted Parous carbon	I^-/I_3^-	N719	0.807	14.40 0.646	7.5
Activated Carbon	I^-/I_3^-	N719	0.802	13.07 0.626	6.6
Fulleren (c_{60})	I^-/I_3^-	N719	0.750	11.60 0.323	2.8
Printer toner	I^-/I_3^-	N719	0,780	12.02 0.455	4.3

An investigation was conducted into the utilization of Fe-Ni alloys as a substitute for the costly and unstable platinum (Pt) electrode that is utilized in dye-sensitized solar cells. The

production of Fe-Ni alloys involved mechanical ball milling, and the alloys were subsequently tested for their potential as solar cell counter electrode materials. The solar cell fabricated with these new electrodes achieved a power conversion efficiency of 3.28%. Fe-Ni electrodes have been demonstrated to be a cost-effective and easily producible alternative for solar cells (Akin & Akman, 2022).

1.4 Photoanode

In dye-sensitized solar cells, the semiconductor metal oxide films form the negative end of the battery, otherwise known as the anode, which is the photoanode part. The photoanode contains a conductive glass (TCO) and a semiconductor layer (TiO_2) that can transmit light (Tutar, 2019). Semiconductor oxide films applied in dye-sensitized solar cells must possess a substantial bandgap to facilitate efficient light transmission. Additionally, these materials must exhibit resistance to photocorrosion when exposed to sunlight. In dye-sensitized solar cells (DSSCs), the lowest excited level linking the dye and the conduction band limit energy must be compatible for the purpose pertaining to electron flow from the excited state of the dye into the conduction band of TiO_2. In the event that the conduction band energy is excessively high, electron injection becomes challenging, thus prompting the preference for low band edge energies. However, while low band energy facilitates electron passage, the open-circuit potential (V_{oc}) may undergo a decline, leading to diminished peak power generation of the cell.Consequently, the bandgap of the semiconductor must be meticulously selected in conjunction with other factors that determine the overall performance of the solar cell (Seçkin, 2010). A variety of semiconductor oxides are utilized in the fabrication of solar cells, including titanium dioxide (TiO_2), zinc oxide (ZnO), niobium oxide (Nb_2O_5), and tin dioxide (SnO_2) (Cesur, 2019). However, due to their wide band gap, titanium dioxide (TiO_2) and zinc oxide (ZnO) semiconductor materials are widely used. The band gaps of the semiconductors utilized are showed in (Figure 5).

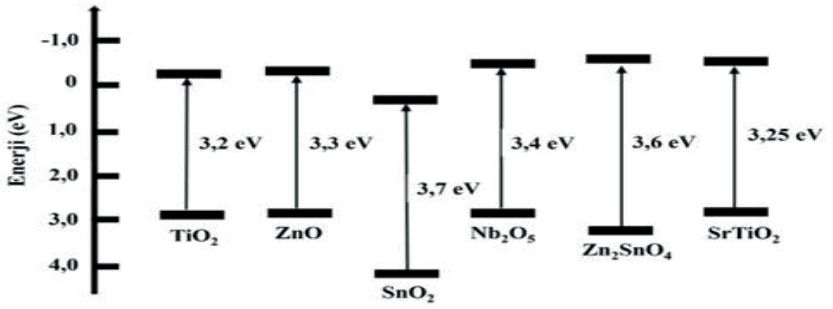

Figure 5. Some photoanode materials used in DSSCs and their band gaps (Ünlü, 2024)

Titanium dioxide (TiO_2) has the distinction of being the most widely used semiconductor material in dye-sensitized solar cells. This stems from its broad bandgap, has been extensively researched, is inexpensive and readily available, and poses no threat to health. The function of titanium dioxide (TiO_2) within the cell is to facilitate the transfer of electrons from the dye substance to the conductive glass. The wide band gap property of the material functions to impede the spontaneous generation of electrons by TiO_2 during its active state. The substantial surface area of TiO_2 facilitates the binding of a greater quantity of dyestuff. Titanium dioxide (TiO_2) is known to exist in three distinct crystal structures: Rutile, Anatase, and Brucite. Rutile, a crystal structure that forms at high temperatures and exhibits minimal light

absorption, is not a preferred material in dye-sensitized solar cells due to its suboptimal photovoltaic properties. Anatase is the most suitable crystal structure for dye-sensitized solar cells because it has a wider bandgap and high photoactivity. The utilization of brucite is precluded due to its scarcity and its inability to absorb UV light. Anatase is the preferred photocatalyst for these solar cells due to its superior photocatalytic properties, which facilitate the acceleration of photoreactions. The titanium dioxide (TiO_2) anode constitutes a pivotal element in the composition of a dye-sensitized solar cell. A considerable amount of scientific work has indicated that enhancing the surface area can lead to a tenfold increase in efficiency. Conventionally, the synthesis of nano-sized TiO_2 powders entails sintering, wherein the initial coating on the surface of conductive glass is subjected to thermal treatment (see Figure 6). The thickness of these coatings can vary between 5 and 20 microns, and their density can range from 1 to 4 milligrams per square centimeter (Seçkin, 2010; Özel, 2017).

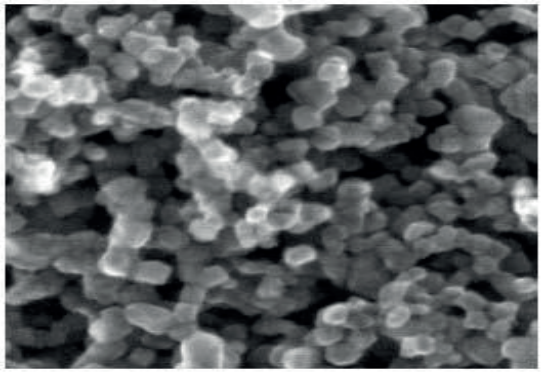

Figure 6. FESEM image of a nanocrystalline TiO_2 film with a pore diameter of 15 nm (Seçkin, 2010)

Zinc oxide (ZnO) is the second most commonly used semiconductor material in dye-sensitized solar cells. However, in comparison to TiO_2, it exhibits reduced chemical stability. Consequently, the dye molecules exhibit a diminished capacity to bind to the surface. The electron transport capability of ZnO is higher, enabling electrons to traverse the circuit with greater velocity. However, it is important to note that the material may experience dissolution problems in acidic and basic environments. The efficiency of solar cells can be influenced by the morphology of ZnO. Research findings indicate that cell efficiency levels for studies employing N719 ruthenium dye range from 1% to 7%. Research concentrating on electron transport and dye adhesion capacity aims to enhance cell efficiency. According to the extant research, ZnO nanolayered structures exhibit the highest efficiency (Çakar, 2017).

Tin oxide (SnO_2) has been identified as a promising material for use as a photoanode in dye-sensitized solar cells (DSSCs). This is due to its high electron mobility and broad optical transparency. This material is particularly fitting for contexts that necessitate strong electrical conductivity and transparency. However, due to inherent limitations, such as reduced conduction band energy and isoelectric point, its photoconversion efficiency is comparatively lower than that of more prevalent alternatives, such as TiO_2. In order to reduce recombination, studies have focused on strategies such as increasing dye uptake, raising the Fermi energy level, and enhancing surface roughness. These advancements have led to a resurgence of interest in SnO_2-based DSSCs, as evidenced by their ability to exhibit open-circuit voltages

comparable to those of TiO_2 and superior short-circuit current performance. Research continues to explore how to best utilize the advantages of SnO_2 to produce more efficient DSSCs (Esen, 2024).

1.5 Electrolyte

In dye-sensitized solar cells, the electrolyte solution between the working electrode and the counter electrode is critical to ensure the efficient operation of the system. The electrolyte plays a pivotal role in facilitating the continuous renewal of the dye and serves as a conduit for electrical charges between the two electrodes. Consequently, this configuration enables the maximization of energy yield from sunlight. This process directly affects the photovoltaic performance of the solar cell, thereby enabling electricity generation (Özel, 2017). The electrolytes utilized in DSSCs must possess critical properties to ensure the effective functioning of the solar cell. The material should exhibit high electrical conductivity and low viscosity to ensure rapid electron transfer. The electrolyte is responsible for facilitating the effective operation of the system by ensuring adequate contact between the semiconductor film and the counter electrode. It should also prevent the degradation of the dyestuff and not absorb visible light (Arslan, 2018). The electrolyte must be chosen judiciously to avoid reactions with the photoanode and dye, as these reactions can lead to a decline in solar cell efficiency. Consequently, it is imperative to select an appropriate electrolyte (Pekuslu, 2022).

The classification of electrolytes utilized in dye-sensitized solar cells is comprised of three primary categories. These electrolytes can be categorized as liquid, solid, or semi-solid. Liquid electrolytes play a pivotal role in DSSCs, functioning as the chemical components that facilitate the operation of the battery. These electrolytes are composed of organic solvents, redox couples, and additives. The most frequently utilized organic solvents include acetonitrile, valeronitrile, 3-methoxypropionitrile, and ethylene carbonate. The efficiency of the battery is influenced by factors such as viscosity and dielectric constant, which are inherent to these solvents. Redox pairs facilitate electron exchange, thereby enabling the battery to function. The most frequently utilized redox couples in DSSCs are iodide/iodine (I^-/I_3^-) and cobalt (Co(II)/Co(III)) compounds. These pairs are recognized as the most efficient chemicals. The addition of these substances enhances the battery's efficiency. Nitrogen-containing compounds, such as pyridine and its derivatives, have been shown to enhance the current and voltage of the battery by impeding recombination reactions. The most prevalent additives are 4-tert-butylpyridine and N-methylbenzimidazole. The iodide/triiodide (I^-/I_3^-) redox couple is the most commonly used liquid electrolyte in DSSCs. This electrolyte is preferred due to its ability to facilitate rapid electron transfer. The electron injection process onto the TiO_2 surface is recognized to transpire at a frequency much faster than the rate of recombination with I_3^-. Consequently, during operation of the battery, electrons exhibit high velocity movement towards the surface of the TiO_2, thereby enhancing energy production efficiency. Instead of combining with oxidized dye molecules, the electrons react with I^-, thereby maintaining the system in equilibrium. The I_3 present within the electrolyte serves as the conduit for the transfer of electrons to the cathode, where they undergo a process of conversion back into I^- ions. This process ensures the continuous operation of the battery, thereby facilitating the generation of energy. However, the concentration of iodide and triiodide must be meticulously calibrated. In the event that the amount of iodine is insufficient, the conductivity of the electrolyte is reduced, thereby impeding the rapid execution of redox reactions and, consequently, diminishing the efficiency of the battery. Conversely, elevated iodine concentrations can lead to electron losses on the TiO_2 surface, thereby compromising the battery's performance. Furthermore, an excess of iodine has been

shown to enhance light absorption, a phenomenon that can lead to unanticipated outcomes. However, liquid electrolytes are not without their drawbacks. The solvents utilized in the process tend to evaporate at elevated temperatures, impeding the battery's ability to function reliably. The leakage of electrolytes has been demonstrated to disrupt the operation of the battery, as well as to potentially compromise the environment and human health. Furthermore, elevated temperatures can induce degradation of the chemical composition of the electrolyte, resulting in the release of noxious gases. The implementation of sealing is a critical measure undertaken to avert the aforementioned complications. Sealing plays a crucial role in preventing electrolyte leakage by enveloping the electrodes with a specialized material. However, this process necessitates the use of additional materials and energy, resulting in increased costs. A schematic representation of the sealing process is provided in (Figure 7).

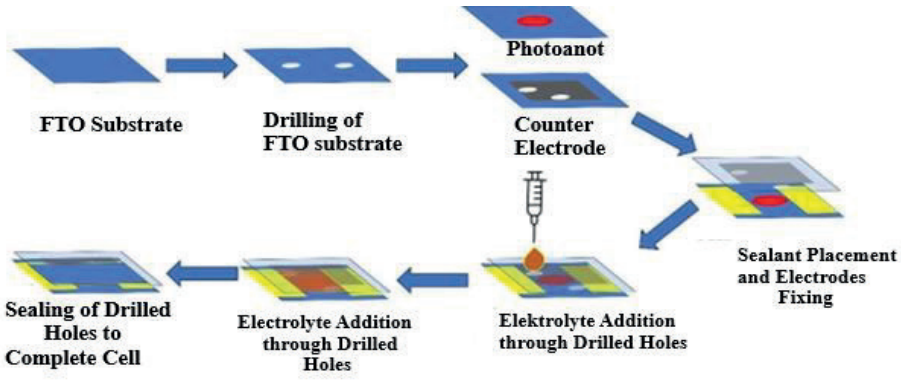

Figure 7. Schematic representation of the sealing process for liquid electrolytes

Solar cells utilize phase materials to address the limitations of liquid electrolytes. Solid-phase dye-sensitized solar cells (DSSCs) utilize solid electrolytes in lieu of liquid electrolytes. Despite their ability to prevent issues such as leakage or evaporation, solid electrolytes often exhibit suboptimal interfacial properties that compromise their efficiency, particularly when compared to liquid electrolytes. Semi-solid electrolytes present a compelling alternative, exhibiting characteristics of both liquid and solid states. Their conductivity is comparable to that of liquid electrolytes, and they demonstrate remarkable stability over extended periods (Ünlü, 2024; Yilan, 2023).

1.6 Operating Principle of Dye-Sensitized Solar Cells

Dye-sensitized solar cells (DSSCs) function by emulating the process of photosynthesis in nature. Plants are capable of capturing sunlight due to the presence of pigments known as chlorophyll, which facilitate the conversion of carbon dioxide and water into nutrients that provide energy (glucose) and oxygen. This process occurs within specialized organelles known as chloroplasts, located in the leaves of plants. DSSCs utilize a comparable principle, with specialized dyes capturing light energy and converting it into electrical energy. DSSCs are composed of four primary components. These components include the photoanode, counter electrode, dye, and electrolyte (Tutar, 2019). DSSCs are based on the principle of exciting electrons by absorbing sunlight, as illustrated in (Figure 8).

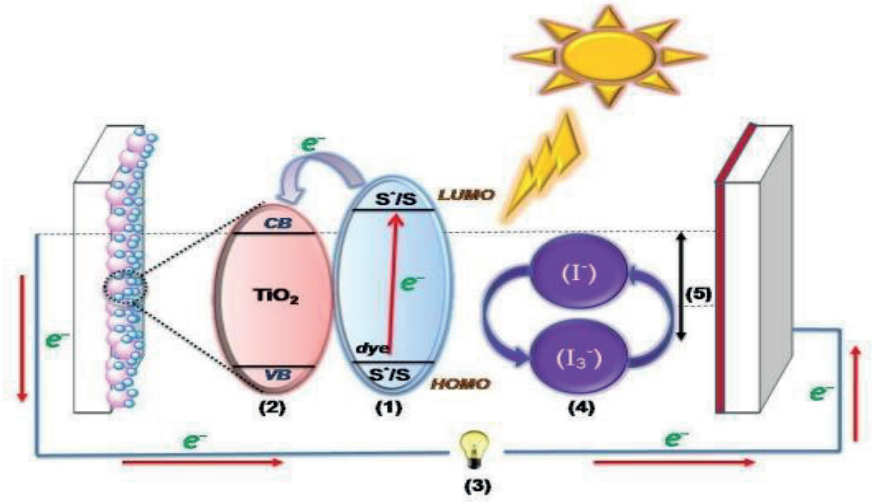

Figure 8. Operating principle of dye-sensitized solar cells (Demirci, 2022)

The dye molecule absorbs sunlight, which causes an excitation in which electrons are transferred from the HOMO (highest occupied molecular orbital) level to the LUMO (lowest unoccupied molecular orbital) level. This process occurs when a molecule absorbs light energy and the electrons reach a higher energy level. Upon attaining this elevated energy state, the electrons are transferred directly to the conduction band of the semiconductor, which can be represented by TiO_2 or ZnO. During this transition, the dye molecule undergoes oxidation, resulting in electron deficiency. The electrons accumulated in the photoanode move along the external circuit, first to the cathode and then to the electrolyte system. Consequently, the solar cell circuit maintains continuous electricity generation. The oxidized dye molecule reverts to its original state by accepting electrons from the iodide (I^-) ions present within the electrolyte. Concurrently, the iodide ions undergo a loss of electrons, resulting in their conversion to triiodide (I_3^-). The process of conversion involves the transfer of electrons from the cathode to the triiodide, resulting in the restoration of its original state as iodide. Consequently, the electrolyte is replenished, and the circuit persists in generating energy through continuous operation (Öztürk, 2022).

The electrical mechanism of DSSC is as seen in the following reactions. (1) reaction is described as absorption, (2) electron conduction in the semiconductor, (3) energy generation in the semiconductor, (4) dye regeneration, (5) iodide regeneration.

$$D + \text{light} \rightarrow D^* \quad (1)$$

$$D^* + \text{semiconductor} \rightarrow D^+ + e^- \quad (2)$$

$$\text{Counter electrode (C. E)} + e^- (\text{semiconductor}) \rightarrow \text{Semiconductor} + e^-_{(\text{C.E})} \quad (3)$$

$$D^* + \frac{3}{2} I^- \rightarrow D + \frac{1}{2} I_3^- \quad (4)$$

$$\frac{1}{2} I_3^- + e^-_{(\text{K.E})} \rightarrow \frac{3}{2} I^- + \text{cathode electrode (C. E)} \quad (5)$$

1.7 Photovoltaic Performance Parameters of Dye-Sensitized Solar Cells

The performance values of DSSCs are determined by four basic parameters. The parameters in question are open circuit voltage (Voc), short circuit current (Jsc), charging factor (FF), and energy conversion efficiency (η). Open circuit voltage (Voc) is defined as the maximum voltage value that the battery reaches when the load is not connected. This term refers to the disparity in energy between the semiconductor's conduction band and the redox potential of the electrolyte. Short-circuit current (Jsc) is defined as the photocurrent per unit area and is influenced by the interaction of TiO_2 with the dye and the absorption coefficient. The filling factor (FF) is a critical parameter that quantifies the quality of the battery's power supply and indicates the proximity of the solar cell to its optimal operating conditions. Energy conversion efficiency (η) is defined as the ratio of the maximum power produced by the solar cell, contingent on the incident irradiance. This parameter is employed to compare the efficiency of disparate DSSCs. These parameters are used as a basis for evaluating the overall performance of the cell and making improvements to increase efficiency (Güngör, 2021). The determination of these parameters is derived from current-voltage curves, as illustrated in (Figure 9).

$$FF = \frac{P_{max}}{P_T} = \frac{I_{max} \times V_{max}}{I_{SC} \times V_{OC}} \quad (1)$$

$$\eta = \frac{P_{max}}{P_{in}} = \frac{I_{max} \times V_{max}}{P_{in}} = \frac{I_{SC} \times V_{OC} \times FF}{P_{in}} \quad (2)$$

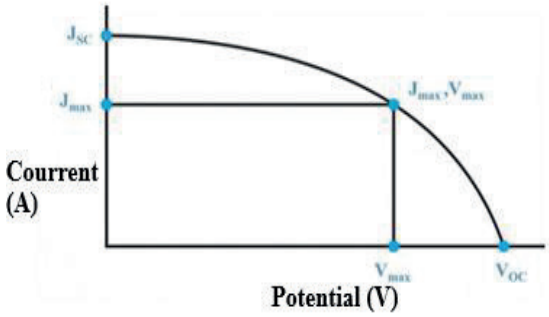

Figure 9. Current–voltage curve of dye-sensitized solar cells (Ünlü, 2024)

1.8 Efficiency

The efficiency of DSSCs has seen significant improvements over time, and this development has paralleled a growth in research activity in this field. Furthermore, the analysis examined the efficiency of various dyes used in dye-sensitized solar cells. There has been a considerable increase in efficiency, rising from 6.4% in 1991 to 11.1% in 1997. Although there were minor advances between 2006 and 2011, an overall upward trend has been observed. Between 2012 and 2019, there was a more pronounced increase, attributable to significant advances in materials and production technologies. Efficiency reached 12.3% in 2019 and rose to 13% in 2020, showing a significant increase. Furthermore, it was determined

tha the efficiency of Ru dye ranged between 7.1% and 7.9%. Over the years, numerous studies have been conducted using a variety of paints in the process. The highest productivity, 13% was achieved using SM315 paint.

CONCLUSION

As the world's energy demands continue to escalate, the importance of renewable resources is increasing. Solar energy has been identified as a sustainable, eco-friendly, and cost-effective energy source. Consequently, photovoltaic technologies are undergoing a period of accelerated proliferation. One such technology is dye-sensitized solar cells, which are photovoltaic systems that utilize dyes to absorb sunlight and convert it into electrical energy. In comparison to alternative batteries, it has the capacity to generate electrical energy at reduced temperatures. Dye-sensitized solar cells (DSSCs) are poised to play a significant role in future energy solutions, owing to their cost-effectiveness and adaptability. Their efficient operation, especially in low light conditions, provides an advantage in the field of sustainable energy. Nevertheless, ongoing development efforts persist on matters such as electrolyte stability and prolonged utilization. Furthermore, the utilization of natural dyes is intended to mitigate the occurrence of toxic effects, while concurrently promoting the development of a more sustainable energy production. In the context of DSSCs, meticulous examination of the primary components that constitute these batteries has been demonstrated to enhance their efficiency. Consequently, it is hypothesized that enhanced efficiency can be attained through the refinement of the types of photoanode and their respective effects, in addition to the exploration of diverse electrolyte types. This research area remains a subject of ongoing investigation.

REFERENCES

Akin, S., Akman, E. (2022). Investigation of the counter electrode potential of economical Fe@Ni alloys produced by ball milling in dye-sensitized solar Cells. El-Cezeri, Volume 9, Issue 1, 24–34.

Arslan, H. (2018). Synthesis, characterization, and use of Europium (Eu^{+3})-doped TiO_2 thin films as photoanodes in dye-sensitized solar cells. Master's thesis, Selçuk University, Institute of Natural Sciences, Department of Physics, Turkey.

Battal, G. (2020). A study on organic dye-sensitized solar cells. International Journal of Sustainable Engineering and Technology,Volume 4, Issue 1, 1–6.

Cesur, M. (2019). Investigation of the use of Berberis vulgaris extracts as photosensitizers in dye-sensitized solar cells. Master's thesis, Sakarya University, Institute of Natural Sciences, Department of Chemistry, Sakarya.

Çakar, S. (2017). Development of dye-sensitized solar cells based on tannin using new approaches. Doctoral thesis, Sakarya University, Institute of Natural Sciences, Department of Chemistry, Division of Physical Chemistry, Sakarya.

Demirci, Y. C. (2022). Development of phthalocyanine dyes for dye-sensitized solar cells. Master's thesis, Sakarya University, Institute of Natural Sciences, Department of Chemistry, Division of Physical Chemistry, Sakarya.

Esen, S. (2024). The effect of different photoanodes on cell efficiency in dye-sensitized solar cells (DSSC). Master's thesis, Van Yüzüncü Yıl University, Institute of Natural Sciences, Department of Physics, Van.

Gezgin, M. (2024). Investigation of the use of metal-free synthetic and commercial dyes as co-sensitizers in solar cells. Doctoral thesis, Sakarya University, Institute of Natural Sciences, Department of Chemistry, Sakarya.

Güngör, M. (2021). Development of a new paint for dye-sensitized solar cells and calculation of their electronic properties. Master's thesis, Karamanoğlu Mehmetbey University, Institute of Natural Sciences, Department of Technologies, Turkey.

Mahadik, S. A., Pathan, H. M., Salunke-Gawali, S. (2024). An overview of metal complexes, metal-free and natural photosensitizers in dye-sensitized solar cells. ES Energy & Environment, 24, 1078.

Özel, K. (2017). Synthesis, characterization, and efficiency improvement of ZnO-layered, TiO_2-based dye-sensitized organic solar cells. Master's thesis, Ankara University, Institute of Natural Sciences, Department of Electrical and Electronics Engineering, Ankara.

Özkacar, T. (2021). Investigation of the effect of photoanode annealing temperature and electrolyte type on the performance of dye-sensitized solar cells. Master's thesis, Düzce University, Institute of Natural Sciences, Department of Physics, Düzce.

Öztürk, Ö. (2022). Synthesis and characterization of asymmetric TiO (iv) phthalocyanines used as photosensitizers in solar cells.

Pekuslu, A. (2022). Effect of different dyes on the efficiency of ZnO-based dye-sensitized solar cells. Master's thesis, Eskisehir Technical University, Graduate School of Education, Department of Physics, Eskişehir.

Seçkin, E. (2010). Production and Efficiency Characterization of Dye-Sensitized Solar Cell Using Titanium Anodization Method. Master's Thesis, Istanbul Technical University, Institute of Science, Department of Advanced Technologies, Istanbul.

Tutar, Ö. F. (2019). Investigation of the use of pigments obtained from the Phylotacca americana plant in dye-sensitized solar cells. Master's thesis, Sakarya University, Institute of Natural Sciences, Department of Chemistry, Sakarya.

Ünlü, B. (2017). Development of ditizone metal complex dyes for dye-sensitized solar cells. Master's thesis, Sakarya University, Institute of Natural Sciences, Department of Chemistry, Division of Physical Chemistry, Sakarya.

Ünlü, B. (2024). Development of dyes and electrolytes for dye-sensitized solar cells. Doctoral thesis, Sakarya University, Institute of Natural Sciences, Department of Chemistry, Division of Physical Chemistry, Sakarya.

Yilan, D. (2023). Investigation of the use of indoline and benzothiadiazole-based dyes in solar cells. Master's thesis, Sakarya University, Institute of Natural Sciences, Department of Chemistry, Division of Physical Chemistry, Sakarya.

CHAPTER 4

POST-KYOTO ERA: AN ENGINEERING-ORIENTED FRAMEWORK FOR ENVIRONMENTAL IMPLEMENTATION AND FUTURE PERSPECTIVES

Şaile Tuba ÖZTÜRK[1], Zeynel Fuat TOPRAK [2]

1 Lecturer Dr., Fırat University, ORCID ID: 0000-0003-0408-5825
2 Prof. Dr., Dicle University, ORCID ID: 0000-0003-0876-1165

1. Introduction

The period between the entry into force of the Kyoto Protocol in 2005 and the completion of its first commitment period in 2012 functioned not only as an implementation phase but also as an experimental laboratory for global environmental governance (Babiker, Jacoby, Reilly, & Reiner, 2002; Dessai, Lacasta, & Vincent, 2003; Maamoun, 2019; Depledge, 2022). The experience gained during this interval yielded critical insights into which institutional and technical dimensions of future climate regimes required strengthening, particularly with respect to the design of obligations, the effectiveness of compliance mechanisms, and the performance of flexibility instruments (Güneş, 2011; Shishlov, Morel, & Bellassen, 2016). As a result, the post-Kyoto era made increasingly clear the need for an environmental governance architecture that is more flexible, inclusive, and adaptive (Bulkeley & Moser, 2007; Gupta, 2010; Hongyuan, 2015). In this context, the future of global environmental policy is no longer determined solely by diplomatic commitments, but also by technological innovation capacity, societal awareness, ethical value frameworks, and the dynamics of low-carbon economic transformation (Türk, 2008; Karakaya, 2008; Kaya, 2020). Accordingly, the post-Kyoto period is widely described as a paradigmatic restructuring phase in which environmental consciousness and governance models have been both normatively and institutionally redefined (Morin et al., 2013; Thakur, 2021).

One of the most notable developments in this period has been the reframing of environmental policy from a domain of international competition to a field of shared interest. Whereas the Kyoto Protocol was organized around binding, country-specific emission reduction targets, subsequent evolution of the regime saw cooperation move beyond the doctrine of "common but differentiated responsibilities" toward a broader notion of "shared global responsibility" (Page, 2007; Ma, 2010; Madubuegw et al., 2021). This shift repositioned environmental policy from a perceived constraint on national interests to a foundational pillar of international stability, economic prosperity, and social well-being (Kaya, 2020; Thakur, 2021).

Concurrently, environmental governance moved away from a state-centric and hierarchical configuration toward a multi-actor, network-based, and solidarity-oriented model. The private sector, civil society organizations, academic institutions, local governments, and individuals ceased to act merely as passive implementers and instead emerged as active participants in the design, implementation, and monitoring of policy (Bulkeley & Moser, 2007; Auer, 2000; Morin et al., 2013). This multilayered model integrates engineering expertise with social responsibility mechanisms, thereby fostering advances in climate technologies, data sharing, systems modeling, and environmental innovation (Türkeş, 2006; Wijen, Zoeteman, & Pieters, 2005; Coskun et al., 2010).

Shogren's (1999) cost–benefit analysis suggests that, although the direct impact of the Kyoto Protocol on aggregate emission reductions was limited, it marked a historical turning point by consolidating the institutional foundations of international environmental policy. This institutional threshold prepared the ground for the emergence of a more comprehensive model of environmental management—one rooted in economic efficiency, scientific data governance, robust MRV (measurement, reporting, verification) systems, and engineering-driven innovation (Böhringer & Vogt, 2003; Kim, Tanaka, & Matsuoka, 2020; Maamoun, 2019; Shishlov, Morel, & Bellassen, 2016; Toprak et al., 2009). The post-Kyoto period should therefore be understood not simply as a phase that corrected earlier shortcomings, but as a critical transition that shaped

the engineering-oriented climate strategies, multi-actor governance processes, and scientific data infrastructures of the future (Gupta, 2010; Hongyuan, 2015; Kaya, 2020).

Technological change has played a decisive role in this structural transformation. Digitalization, energy-efficiency applications, renewable energy technologies, carbon-monitoring infrastructures, sensor networks, and AI-based environmental analytics have become key instruments enhancing both the effectiveness and verifiability of environmental policies (Karakaya, 2008; Kaya, 2020). These technologies reinforce transparency, data integrity, and comparability in emission monitoring and reporting, allowing Kyoto's MRV architecture—central to its compliance regime—to function in a more reliable and sophisticated manner (Güneş, 2011; Shishlov, Morel, & Bellassen, 2016). By facilitating knowledge sharing at a global scale, they also constitute the technical backbone of the multi-actor governance model (Morin et al., 2013). Satellite-based observation systems, the Copernicus program, ERA5-Land reanalysis datasets, remote sensing technologies, and high-resolution sensor networks have rendered ecological processes quantitatively measurable, observable, and modelable (Kim, Tanaka, & Matsuoka, 2020; Maamoun, 2019; Egorov et al., 2021; Algancı et al., 2009).

In parallel, the economic dimension of environmental policy has become a defining feature of the post-Kyoto landscape. As the global economy shifts from carbon-intensive production toward a low-carbon development paradigm, fundamental economic parameters—such as energy security, competitiveness, production costs, and employment—have been reconfigured (Türkeş, 2006; Türk, 2008). Within this context, the green economy has emerged as a holistic development framework that simultaneously targets ecological balance, social justice, regional resilience, and macroeconomic stability (Kaya, 2020). This evolution has attenuated the longstanding tension between environmental policy and economic growth, fostering a more coherent and sustainable interaction between the two domains.

Sustainable finance mechanisms have provided the economic backbone of this transformation. Green bonds, carbon credit systems, climate funds, and environmental risk assessment standards have become strategic tools that integrate environmental management into financial systems (Bayrak, 2012; Akagündüz, 2022). Thakur (2021) argues that the transition from Kyoto's centralized, target-driven, and strictly binding model to the more flexible, participatory, and incremental framework of the Paris Agreement constitutes a paradigmatic shift in global governance. In this context, sustainable finance instruments have redefined environmental management from a cost-intensive obligation into a development pathway that generates innovation, employment, and competitive advantage; sustainability has thus evolved from a question of "cost accounting'' into a key driver of economic growth and technological progress (Böhringer & Vogt, 2003; Kim, Tanaka, & Matsuoka, 2020; Maamoun, 2019).

The future of global environmental governance is closely tied to states' capacity for multilateral cooperation and their ability to institutionalize such cooperation domestically and locally. In the post-Kyoto era, the Conference of the Parties (COP) meetings under the UNFCCC have become the principal decision-making fora for climate policy, while the practical viability of these decisions depends increasingly on countries' economic strength, social support, and political stability (Türkeş, Sümer, & Çetiner, 2000; Hongyuan, 2015). This evolution has shown that environmental policies must be institutionalized not only at the international level but also across national, regional, and local scales (Gupta, 2010; Morin et al., 2013). Nationally Determined Contributions (NDCs), prepared in line with each country's socioeconomic conditions, function as structural bridges between global targets and local

realities. This framework transforms environmental governance from a top-down model into a networked partnership system rooted in bottom-up participation (Auer, 2000; Bulkeley & Moser, 2007). As a result, environmental management now operates within a multilayered governance structure that brings together international coordination and local adaptability, with urban planning, engineering practice, and societal awareness emerging as crucial determinants of policy sustainability (Kaya, 2020).

During the post-Kyoto era, environmental awareness has deepened not only at institutional and diplomatic levels but also throughout everyday social life. Environmental policy has ceased to be solely a governmental responsibility and has become embedded in individual lifestyles, consumption patterns, and ethical orientations (Bulkeley & Moser, 2007; Auer, 2000). The widespread adoption of recycling, energy efficiency practices, sustainable consumption, green transport systems, and environmentally friendly technologies has become a visible manifestation of this growing societal consciousness (Türkeş, 2006). Enhanced public awareness has, in turn, exerted pressure on political decision-makers, contributing to more determined, enduring, and accountable environmental policies (Morin et al., 2013).

A further hallmark of the period is the rising prominence of climate justice. Low-income countries, small island states, and other vulnerable communities that are disproportionately affected by climate change have gained increased visibility at the center of global environmental governance (Gökpınar, 2020; Madubuegw et al., 2021). This development underscores that environmental justice must be addressed not only as an ecological principle but also in conjunction with economic, social, and political equality (Page, 2007). Climate finance, technology transfer, and capacity-building policies have thus become key institutional instruments of environmental justice (Türkeş, Sümer, & Çetiner, 2000; Bayrak, 2012). Financial support provided by developed countries to developing nations through green funds, carbon credit mechanisms, and technology-sharing arrangements is regarded as a significant step toward global solidarity and more equitable burden sharing (Akagündüz, 2022; Maamoun, 2019).

In this evolving context, the notion of a "sustainability culture" has become a defining dimension of environmental governance. Sustainability is no longer merely a policy target; it has emerged as a cultural norm shaping societal lifestyles, production systems, and ethical values (Uysal, 2009; Bulkeley & Moser, 2007). From educational curricula and media narratives to urban planning and production processes, sustainability principles increasingly guide both individual behavior and institutional practice (Auer, 2000; Morin et al., 2013).

Another striking development has been the integration of environmental policy into broader digitalization processes, often referred to as the "green digital transition." This transformation encompasses the deployment of digital infrastructures that enable the collection, analysis, dissemination, and policy use of environmental data. Satellite observations, sensor-based monitoring systems, AI-assisted data analytics, and big data modeling tools are making environmental management more dynamic, transparent, and evidence-based (Shishlov, Morel, & Bellassen, 2016; Kim, Tanaka, & Matsuoka, 2020; Coskun et al., 2010; Algancı et al., 2009). These technologies allow emission-monitoring systems to produce real-time data and make policy implementation verifiable through quantitative indicators. At the same time, blockchain-based verification infrastructures are enhancing transparency and trust in carbon markets and green finance, thereby reinforcing the accountability of environmental governance.

Within this broader trajectory, Türkeş (2006) discusses climate change scenarios and the historical role of the Kyoto Protocol, arguing that the rise in anthropogenic greenhouse gas emissions has irreversibly disrupted climatic balance, while Kyoto—though belated—constituted a highly symbolic turning point in slowing this trend. The digital, technical, and cultural transformations of the post-Kyoto era have reinforced this symbolic threshold, propelling environmental governance toward a holistic paradigm shaped at the intersection of engineering, information technologies, and ethical norms.

The future of global climate policy in the post-Kyoto context is increasingly being redefined around education, awareness, and the active engagement of younger generations. Young people have come to perceive the climate crisis not merely as a historical legacy, but as an immediate threat to their own life prospects, and have translated this awareness into political mobilization at a global scale. Youth movements such as “Fridays for Future” and the “Youth Climate Movement” have strengthened societal participation in environmental governance and injected new momentum into democratic processes (Morin et al., 2013).

Embedding environmental awareness in education from an early age helps consolidate a durable culture of sustainability and transforms environmental governance into a system that protects not only present conditions but also the fundamental rights of future generations (Uysal, 2009). This approach institutionalizes environmental consciousness as an intergenerational responsibility and a shared ethical inheritance, extending sustainability beyond its technical and economic dimensions and contributing to the reconstruction of societal values (Karakaya, 2008; Kaya, 2020).

Finally, the post-Kyoto period has witnessed the strengthening of regional solidarity and the diffusion of multilevel governance models. The regionally differentiated impacts of global environmental problems have highlighted the importance of local dynamics and cultural diversity in designing effective responses. Kyoto’s legacy has been reinterpreted and carried forward by regional entities such as the European Union (EU), ASEAN, the African Union, and Latin American initiatives, which have deepened cooperation through climate funds, renewable energy platforms, emission-reduction programs, and technology-transfer networks (Hongyuan, 2015; Bayrak, 2012). These regional approaches forge more flexible and culturally adaptive linkages between global objectives and local realities.

In this multilevel architecture, local governments, regional institutions, and civil society organizations assume active roles in producing engineering-based solutions for the implementation of global environmental policies (Türk, 2008; Türkeş, Sümer, & Çetiner, 2000; Madubuegw et al., 2021). As the climate crisis intensifies, climate finance has emerged as one of the most contested domains of the post-Kyoto regime. Developing countries’ growing need for financial support to implement sustainable transformation projects has spurred institutions such as the Green Climate Fund, the World Bank, and regional development banks to strengthen the financial underpinnings of environmental initiatives (Bayrak, 2012; Akagündüz, 2022). Yet persistent challenges regarding the effectiveness, transparency, and equity of fund distribution highlight critical justice gaps. Wijen, Zoeteman, and Pieters (2005) and Uysal (2009) argue that the unjust management of environmental finance undermines the realization of global environmental justice, while Page (2007) and Madubuegw et al. (2021) show that inequalities in climate finance weaken the adaptive capacities of vulnerable communities.

In this light, the success of environmental policy in the post-Kyoto era depends not only on the development of new technologies but also on their global accessibility. Institutionalizing

technology transfer and expanding capacity-building programs are crucial for reducing both environmental and economic inequalities (Egorov et al., 2021; Ma, 2010; Türk, 2008). Renewable-energy infrastructures—especially hydropower systems—have become central to this effort, with numerous studies demonstrating the role of hydrological modelling and refined calculation methods in enhancing technical capacity and supporting sustainable development (Alashan, Şen, & Toprak, 2016; Agiralioglu et al., 2017). Future environmental governance therefore treats financial inclusiveness and access to technology as core domains of ethical responsibility. Climate finance is not merely an economic tool; it is a concrete expression of global solidarity, equitable burden sharing, and environmental equality.

2. The Legacy of the Kyoto Protocol: The Paris Agreement and the COP Processes

The Kyoto Protocol, signed in 1997, was not merely an environmental agreement but a historical turning point that laid the institutional foundations of modern environmental governance. With this protocol, binding commitments were for the first time introduced in the global fight against climate change, marking a structural paradigm shift in international environmental law (Lopez, 2003; Dessai, Lacasta & Vincent, 2003). The most enduring legacy of Kyoto is the cognitive and normative transformation that reframed climate change not as a local or national issue, but as a shared responsibility of humankind. This understanding directly shaped the design of the Paris Agreement and the decision-making logic of the COP processes; the institutional experience accumulated during the Kyoto period became a reference point for all subsequent climate regimes (Babiker et al., 2002; Hongyuan, 2015).

The governance legacy of the Kyoto Protocol is most evident in the institutionalization of monitoring, reporting, and verification (MRV) mechanisms. Kyoto demonstrated that environmental policy cannot rely solely on voluntary declarations, thereby institutionalizing international oversight, transparent reporting, third-party verification, and performance assessment processes (Güneş, 2011; Shishlov, Morel & Bellassen, 2016). This structural discipline strengthened the technical infrastructure of global governance in terms of environmental data standardization and accountability, and it provided the institutional basis for the Nationally Determined Contributions (NDC) model introduced under the Paris Agreement (Egorov et al., 2021). The Paris model softened Kyoto's centralized and mandatory structure, developing a more flexible and inclusive approach grounded in voluntary participation (Kaya, 2020; Thakur, 2021). Nevertheless, the Paris system was built on the institutional knowledge base, monitoring standards, and environmental accounting mechanisms established during the Kyoto era. For this reason, although the Paris Agreement reshaped Kyoto's governance legacy into a more democratic, flexible, and multi-actor framework, it remains a direct technical and institutional continuation of Kyoto (Maamoun, 2019; Yalçın, 2010).

One of the most influential outcomes of the Kyoto Protocol was its transformation of climate diplomacy into a continuous and institutionalized negotiation process. Prior to Kyoto, environmental summits generally consisted of one-time political declarations; however, the post-Kyoto period established an ongoing, learning, and increasingly deepening negotiation tradition through the annual COP meetings (Wijen et al., 2005; Yalçın, 2010). These conferences transformed climate policy from a static document into a dynamic governance process, with each new COP meeting developing new targets and strategies based on lessons from previous experiences. Thus, Kyoto became the starting point of an institutional framework that reshaped environmental governance into an evolutionary, adaptive, and multi-actor system.

In this context, Türkeş, Sümer, and Çetiner (2000) note that the flexibility mechanisms envisioned under Kyoto—Emissions Trading, Joint Implementation, and the Clean Development Mechanism—sought to balance environmental objectives with economic efficiency, although institutional capacity constraints in developing countries limited their implementation. Kyoto is widely considered the first comprehensive example demonstrating that environmental policy can be integrated with economic systems. Through these mechanisms, carbon became not only a pollutant but also a measurable, priceable, and tradable economic commodity. This transformation laid the foundation for the carbon-neutral economic vision of the Paris Agreement; today, green bonds, carbon markets, sustainable investment funds, and environmental finance models are regarded as continued extensions of Kyoto's economic approach (Akagündüz, 2022).

Another lasting influence of Kyoto is that it brought environmental justice debates to the agenda of international law. The principle of "common but differentiated responsibilities (CBDR)" recognizes historical emission burdens and differences in economic capacity, emphasizing that developed countries should bear greater responsibility (Akagündüz, 2022; Akın, 2016). The Paris Agreement did not abandon this principle; rather, it reinterpreted it through a more flexible and inclusive framework that accounts for variables such as economic capacity, technological capability, and national circumstances. Thus, Kyoto's justice-based normative legacy continues in the Paris era, albeit through a more pragmatic and adaptive approach.

The success of the Paris Agreement rests largely on the institutional and methodological lessons derived from the Kyoto experience. One of the major criticisms directed at the Kyoto Protocol was that its obligations applied to only a limited number of countries, and that developing nations were insufficiently represented in the process. The Paris model addressed this shortcoming by adopting the principle of universal participation and inclusiveness, thereby transforming global climate governance from an intergovernmental structure into a multi-actor, horizontal, and participatory system (Akın, 2016). Nevertheless, at the core of this inclusive structure lies the methodological and technical framework developed during the Kyoto period. The monitoring, reporting, and verification (MRV) standards created under Kyoto provided the normative basis for the technical functioning of the Paris Agreement and established the institutional infrastructure that made the NDC system operational (Akın, 2016; Aksoy, 2020). In this respect, Kyoto is regarded as the invisible backbone of modern environmental governance.

The current structure of the COP processes is also an extension of Kyoto's understanding of multilateral diplomacy, science-based decision-making, and data-driven policy design. With Kyoto, climate diplomacy evolved into a knowledge regime organized around scientific data, comparable indicators, performance monitoring, and international reporting systems. The use of IPCC reports as the primary reference documents in COP summits represents one of the most prominent manifestations of this institutional transformation (Aksoy, 2020). In the Paris era, this science-based approach became even stronger; climate policies increasingly adopted a data-driven, accountable, and transparent governance model. In this regard, the Kyoto Protocol is not merely a historical agreement but the foundational document of a holistic governance architecture that enables the interconnected functioning of environmental engineering, economics, and international law in the 21st century. The rational, data-oriented, and multilateral diplomatic culture initiated by Kyoto continues to serve as a systemic precursor shaping the core operational principles of contemporary climate regimes.

The legacy of the Kyoto Protocol extends beyond institutional structures to shaping the intellectual, methodological, and development-oriented direction of contemporary environmental policy. With Kyoto, the environment ceased to be an external component of economic growth and became central to development strategies; thus, environmental policy emerged as a defining axis of economic and social sustainability. This perspective grew even stronger during the Paris era and merged with the United Nations Sustainable Development Goals (SDGs), creating a holistic development framework that integrates environmental integrity, economic growth, and social justice (Aldemir & Kaypak, 2008). This integration demonstrates that environmental governance is no longer confined to carbon reduction, but has become a key determinant of multidimensional transformation—from production systems to social lifestyles, from energy security to the structure of global trade. In this sense, Kyoto constitutes the foundational document that laid the conceptual basis of the sustainable growth paradigm.

Another key contribution of the Kyoto Protocol is the institutional integration of environmental sciences and engineering-based data analysis into policymaking processes. Before Kyoto, environmental policies largely relied on technical reports, whereas the adoption of the protocol marked the beginning of a phase in which IPCC assessments became the principal reference documents of international environmental diplomacy (Aksoy, 2020; Aldemir & Kaypak, 2008). This shift ensured that environmental decision-making became grounded in scientific evidence, making policies measurable, comparable, verifiable, and accountable. In the post-Kyoto period, this approach was institutionalized through the Paris process; scientific knowledge became not only an input guiding decision-making but also a strategic element that provided legitimacy to environmental governance. This rationalization process transformed environmental policy from an emotional or ideological domain into a data-driven, accountable, and manageable governance system.

Uysal (2009), in his doctoral research, conceptualized climate change as a multidimensional transformation process that simultaneously affects ecological, economic, and social systems on a global scale. Uysal emphasized that while the Kyoto Protocol did not fully meet expectations in terms of ecological sustainability, it nevertheless played a pioneering role in institutionalizing sustainability consciousness. This finding demonstrates that Kyoto was not merely a technical regulation but also an instrument that constructed a normative awareness, an ethical responsibility framework, and a sustainability vision for global environmental policy.

In conclusion, the Kyoto Protocol not only provided a legal basis for environmental policy but also established the foundation of a multilayered governance approach that incorporates a science-based decision-making culture, an ethical and normative responsibility framework, and a vision of sustainable development. This intellectual, methodological, and normative legacy of Kyoto continues to play a decisive role in shaping contemporary environmental policymaking.

3. Statistical and Structural Assessments of Kyoto's Effectiveness

The success of the Kyoto Protocol is assessed not only by the extent to which participating countries fulfilled their legal obligations but also by the structural transformation and measurable statistical impacts it generated at the international level. Kyoto heightened global awareness in the fight against climate change and opened a new chapter in environmental governance by establishing the first systematic and comparable mechanisms for measuring, reporting, and reducing greenhouse gas emissions (Aldemir & Kaypak, 2008). In this respect,

the Protocol is widely regarded as the beginning of the “age of accountability” in global environmental management.

The regional effectiveness of the Kyoto Protocol is particularly evident in the case of the European Union. In their empirical analysis of the EU-27, Öztürk and Toprak (2025) demonstrate that during the Kyoto period, the EU not only exceeded its reduction targets but also achieved emission cuts significantly above the global average. Their study shows that strengthened energy efficiency policies, accelerated investment in renewable energy, and the effective functioning of the EU Emissions Trading System (EU ETS) were key determinants of this success. These findings strongly confirm that Kyoto provided a technically feasible, economically transformative, and institutionally sustainable framework—especially within the EU context.

Prior to Kyoto, national emission inventories exhibited substantial inconsistencies, and measurement systems lacked internationally verifiable standards. With the entry into force of the Protocol, a common reporting format, standardized greenhouse gas inventories, and a monitoring infrastructure based on third-party verification were established; this ensured data comparability across countries and made it possible to track global climate policies on a statistical basis. The technical infrastructure built under Kyoto directly formed the foundation for the MRV (Measurement, Reporting and Verification) system of the Paris Agreement and has become the institutional source of today’s transparency and accountability standards in climate governance.

Statistical evaluations indicate that during its first commitment period (2008–2012), the Kyoto Protocol enabled developed countries to reduce their total greenhouse gas emissions by an average of 22 percent. This reduction far exceeded the initial global target of 5.2 percent. Countries such as the European Union, Japan, and Norway met the majority of their commitments through strengthened energy efficiency policies, increased renewable energy investments, and low-carbon industrial transformation. In contrast, Canada failed to meet its targets due to economic and political considerations and withdrew from the Protocol in 2011. These divergent experiences demonstrate that Kyoto’s effectiveness is directly linked to national policy capacity, economic structure, and levels of societal support. Anderson (1998) similarly emphasizes that the Protocol’s feasibility ultimately depends on the institutional capacity and political commitment of the contracting parties.

The IPCC’s 2014 Assessment Report confirms that the global rate of emission growth slowed significantly during the Kyoto period. While the annual average global emission growth rate was 2.1 percent between 1990 and 2000, it dropped to 1.6 percent between 2000 and 2010. This deceleration not only demonstrates the effectiveness of the policy tools implemented under Kyoto, the investments in low-carbon technologies, and the market-based mechanisms, but also reveals the maturation of data-driven decision-making structures in international climate governance (Aldemir & Kaypak, 2008). These findings indicate that Kyoto was not merely a legal arrangement but a powerful governance instrument capable of statistically influencing global emission trajectories.

The structural success of the Kyoto Protocol extends far beyond the reduction of greenhouse gas emissions. By establishing an institutional and economic framework within which environmental governance could operate, the Protocol fundamentally transformed the policy instruments of modern environmental management. The three principal market mechanisms introduced under Kyoto—Emissions Trading (ET), Joint Implementation (JI), and

the Clean Development Mechanism (CDM)—represent a significant turning point in global environmental economics. Through these mechanisms, environmental policy evolved from a structure based solely on mandatory legal regulations into a multidimensional system supported by economic incentives, innovative technologies, and market-based models. Anderson (1998) likewise emphasizes that Kyoto introduced a new institutional logic and a set of economic instruments to international environmental policy.

With this transformation, carbon ceased to be perceived merely as a pollutant and became a global economic asset that could be priced, measured, and traded. By 2011, the global carbon market had reached an estimated value of approximately $176 billion; and under the CDM, more than 4,000 projects implemented across over 90 countries prevented an average of 1 billion tons of CO_2-equivalent emissions annually. These figures clearly demonstrate that the Kyoto Protocol fostered lasting ecological awareness by supporting environmental objectives with market-based instruments and initiated a structural transformation that integrated carbon management into the global economy.

In their comprehensive work *A Handbook of Globalization and Environmental Policy*, Wijen, Zoeteman, and Pieters (2005) evaluate the Kyoto Protocol as the most concrete model transforming the interaction between globalization processes and national environmental policies. The authors argue that Kyoto created the first viable framework for global environmental governance by integrating environmental policy with economic systems and emphasize that this structure played a critical role in aligning national policy frameworks with international economic processes. This analysis clearly illustrates that Kyoto was not merely a technical regulation, but a paradigmatic step toward the institutionalization of environmental economics within the international system.

4. Energy, Legal, and Geographical Dimensions of the Kyoto Protocol's Effectiveness

The effectiveness of the Kyoto Protocol is reflected not only in its greenhouse gas mitigation outcomes but also in the momentum it generated for the global transition to renewable energy. With the Protocol's entry into force, carbon pricing instruments, green incentives, and market-based regulations significantly reshaped global investment patterns. Renewable energy investments, which totaled approximately USD 45 billion in 2004, rose to USD 280 billion by 2012—a clear indication that Kyoto's economic tools initiated a structural transformation in global energy markets. According to International Energy Agency (IEA) data, energy efficiency in OECD countries increased by roughly 17 percent between 1990 and 2010, demonstrating that Kyoto's influence extended beyond climate mitigation into broader energy strategies and industrial restructuring. In doing so, the Protocol institutionalized the linkage between energy efficiency, renewable energy expansion, and low-carbon growth, providing the foundational architecture for today's low-carbon economic transition (Aldemir & Kaypak, 2008).

A central criticism of the Kyoto Protocol concerned its exclusion of developing countries from binding emission-reduction commitments. Rapidly industrializing economies such as China, India, Brazil, and South Africa increased their share of global emissions from approximately 35 percent in 1997 to nearly 55 percent in 2012. This shift underscored the asymmetric distribution of mitigation responsibilities between developed and developing nations and highlighted the limited inclusiveness of Kyoto's architecture. As a result, the Paris

Agreement adopted a broader and more equitable burden-sharing framework that incorporates all parties while acknowledging national circumstances.

Nonetheless, the monitoring, reporting, and verification (MRV) mechanisms pioneered during the Kyoto era were expanded under the Paris regime into a global infrastructure applicable to all parties. These institutional and technical innovations now serve as the backbone of contemporary emission-monitoring systems, enabling comparable, verifiable, and transparent data generation essential to modern environmental governance (Aldemir & Kaypak, 2008).

Another structural contribution of the Kyoto Protocol was the establishment of environmental obligations as binding legal norms within the international system. With Kyoto, environmental responsibility ceased to be merely moral or political—it became a matter of enforceable law, facilitating the consolidation of international environmental jurisprudence (Auer, 2000; Anderson, 1998). The MRV mechanisms devised under Kyoto later evolved into the Paris Agreement's "transparency framework," now central to maintaining the integrity and continuity of global climate regimes (Güneş, 2011; Shishlov, Morel & Bellassen, 2016).

Kyoto also reshaped the traditionally state-centric nature of environmental governance by creating a multi-actor architecture that incorporated the private sector, civil society, and scientific institutions into policy-making processes. This shift transformed global climate governance from a purely intergovernmental negotiation forum into a multi-level, participatory, and inclusive system (Wijen, Zoeteman & Pieters, 2005; Bulkeley & Moser, 2007). Thus, Kyoto marks not only the rise of technical environmental regulation but also the democratization of environmental diplomacy.

The Protocol's effectiveness is evaluated through both quantitative emission outcomes and qualitative indicators such as governance capacity, normative awareness, and political influence (Atabey & Toprak, 2024; Auer, 2000; Hongyuan, 2015). Kyoto integrated environmental diplomacy into the strategic and institutional fabric of international relations. Prior to the Protocol, environmental issues were typically subordinate to development, energy, or trade agendas; after Kyoto, they became standalone policy domains embedded in states' foreign-policy frameworks (Kaya, 2020; Akın, 2016).

The incorporation of explicit climate objectives into national development strategies worldwide exemplifies Kyoto's enduring structural impact. Similarly, the proliferation of national emissions-trading schemes, the institutionalization of carbon pricing, and the integration of environmental policy into economic planning reflect the Protocol's lasting influence on global policy systems (Kim, Tanaka & Matsuoka, 2020; Böhringer & Vogt, 2003).

Geographical variation is a key factor in evaluating Kyoto's performance. European countries—benefiting from strong regional coordination, proactive renewable-energy policies, and significant advances in efficiency—surpassed their Kyoto targets. By contrast, North American and Oceanian states struggled to meet their commitments due to fossil-fuel dependency, political resistance, and structural economic factors. The United States' refusal to ratify the Protocol and withdrawal from the process in 2001 constituted one of the most significant obstacles to achieving global mitigation goals, particularly given that the country accounted for roughly 25 percent of global emissions at the time (Auer, 2000). Its absence thus structurally constrained Kyoto's overall effectiveness.

In this context, the European Union played an important compensatory role by operationalizing Kyoto's market-based approach at a regional scale. The EU Emissions Trading System (EU ETS) emerged as the most institutionalized expression of Kyoto's flexibility mechanisms and today remains the world's largest carbon market (Wijen, Zoeteman & Pieters, 2005; Shishlov, Morel & Bellassen, 2016). The EU ETS demonstrates that Kyoto's economic instruments can evolve into durable, technically sophisticated governance models.

Policy durability constitutes another key indicator of Kyoto's success (Ayhan, 2010). The Protocol's impact is measured not only by compliance during its commitment periods but also by the extent to which its governance practices persisted afterward. The continuity of national mitigation targets beyond the Protocol's formal implementation period illustrates that Kyoto fostered a lasting governance culture rather than a temporary diplomatic arrangement. This reflects a deeper cognitive and administrative shift through which environmental policy became embedded in states' bureaucratic and political systems (Auer, 2000; Ayhan, 2010; Hongyuan, 2015).

Thus, Kyoto transformed environmental governance from a time-bound treaty into an administrative norm. The Paris Agreement's inclusive architecture—firmly rooted in the institutional and ideological foundations laid during Kyoto—makes the Protocol's structural legacy unmistakably clear (Akın, 2016; Aksoy, 2020).

World Bank and OECD sustainability indicators show a 15–25 percent reduction in energy intensity across many developed economies during the Kyoto period. This improvement is closely linked to increased reliance on renewable energy, the diffusion of clean industrial technologies, and strengthened energy regulations (Ayhan, 2010; Aldemir & Kaypak, 2008). Likewise, Europe's nearly 19 percent reduction in per capita CO_2 emissions since 1990 demonstrates that Kyoto was not merely a legal instrument but a governance framework that generated measurable gains in environmental performance and energy transition.

External factors influencing Kyoto's outcomes must also be acknowledged. The 2008 global financial crisis led to temporary emission reductions due to declining industrial activity. As Azad (2025) notes, these reductions stemmed from economic contraction rather than structural policy success. Similarly, Shishlov, Morel, and Bellassen (2016) argue that economic cycles can cause short-term fluctuations in emission trends. Importantly, however, many countries did not revert to carbon-intensive production patterns after recovery; instead, they continued to adopt low-carbon technologies. This indicates that Kyoto produced a structural transformation resilient to economic shocks (Hongyuan, 2015; Aksoy, 2020). The persistence of energy-efficiency investments, the expansion of emissions-trading systems, and long-term declines in renewable-energy costs further confirm the durability of Kyoto's governance framework.

5. Emission Projection Models for 2050

In planning the future of global climate policy, estimating the potential trajectory of greenhouse gas emissions is one of the key tools shaping both national strategies and international agreements. Modeling studies conducted in the aftermath of the Kyoto Protocol and the Paris Agreement have strengthened the analytical and science-based dimension of environmental policy, establishing a new methodological framework grounded in data-driven decision-support systems (Aksoy, 2020). Emission projection models for 2050 examine variables such as energy transition, population growth, economic development, urbanization

dynamics, and technological innovation in an integrated manner, providing a multidimensional perspective to climate scenarios. These models demonstrate a shift away from intuitive approaches toward the institutionalization of predictive policy design in environmental governance. The methodological transformation initiated under Kyoto grew even stronger during the Paris era and has now become a standard practice in contemporary climate science (Hongyuan, 2015).

Among the most widely used methods in emission projections is time series analysis, particularly ARIMA (Autoregressive Integrated Moving Average) models. ARIMA models utilize historical emission data to produce probabilistic forecasts, capturing trends, seasonality, and structural policy shifts statistically (Yalçın, 2010). In this respect, ARIMA is a powerful analytical tool that renders the future impacts of climate policies comparable within a broader governance context rather than solely as mathematical outputs.

ARIMA-based analyses of global emission data for the period 1970–2020 indicate that, in the absence of policy intervention, CO_2 emissions could increase by 30–40 percent by 2050. Under the same assumption, global warming is likely to reach 2.5–3°C. These findings mathematically confirm that the climate crisis could accelerate under scenarios in which current energy policies remain insufficient. Although ARIMA models operate under the assumption of the continuity of historical trends, they can incorporate the effects of policy changes, thereby providing quantitative evidence on the speed and scope at which climate strategies must be updated.

Thus, ARIMA and similar time series methods have become one of the most important components of the data-driven governance paradigm that emerged in the post-Kyoto era. This methodological framework clearly demonstrates that the future success of climate policy depends not only on diplomatic will but also on scientific projections and analytical decision-support systems. While ARIMA models are effective in identifying linear trends, hybrid approaches based on nonlinear learning algorithms have been developed to more accurately represent the complex and multivariate nature of environmental systems. In this context, Artificial Neural Networks (ANNs), with their ability to learn nonlinear relationships among multiple variables—such as economic growth, energy consumption, population increase, and industrial production—can generate more realistic projections (Azad, 2025; Babuş, 2005). ANN models reveal hidden patterns that classical statistical methods cannot detect, expanding the decision-making space of policymakers and offering a more flexible, dynamic, and adaptive forecasting framework for climate policy design.

Current ANN-based projections estimate that, under a continuation of existing policy trends, global emissions will increase by an average of 1.7 percent annually until 2050. By contrast, a green transition scenario—characterized by rapid expansion of renewable energy use and reductions in fossil fuel consumption—suggests that emissions will plateau after 2035 and gradually decline toward 2050 (Babuş, 2005; Kim et al., 2020). These results demonstrate that the energy efficiency paradigm established during the Kyoto era plays a decisive long-term role in maintaining global carbon stability.

Hybrid ARIMA–ANN models combine the short-term trend detection capacity of time series methods with the learning power of artificial intelligence, producing multidimensional and highly accurate forecasts. While the ARIMA component statistically captures trends and seasonality, the ANN component is capable of learning structural breaks, stochastic effects, and nonlinear relationships. Hybrid simulations developed for the 2020–2050 period indicate that

if investments in sustainable energy are maintained, emissions will peak around 2030 and enter a gradual decline after 2040. When combined with strong global policies and technological transformations, this trajectory aligns with the Paris Agreement's 2050 carbon-neutrality objective (Babuş, 2005; Babiker et al., 2002; Maamoun, 2019).

In addition, methods such as multiple linear regression, the Grey Prediction Model (GM), and Support Vector Machines (SVM) are also widely used in climate projections. These approaches evaluate variables simultaneously—such as economic indicators, population density, energy supply-demand balance, and carbon pricing—to generate projections with high policy sensitivity. SVM-based analyses show that a 10 percent increase in energy demand raises emissions by an average of 6–7 percent, whereas the implementation of an effective carbon pricing mechanism reduces this effect to below 3 percent (Babiker et al., 2002). These findings highlight the critical importance of advanced learning models in evaluating the long-term policy impacts of the carbon market mechanisms developed during the Kyoto era.

Projections for 2050 are highly sensitive to regional differences. ARIMA- and ANN-based studies indicate that emissions may stabilize after 2035 in Europe and North America; by contrast, in the Asia-Pacific region, rapid economic growth and a fossil-fuel-intensive energy system are likely to sustain the upward trajectory (Bayrak, 2012). This divergence is directly related to factors such as energy mix, technology transfer capacity, carbon pricing effectiveness, and policy feasibility.

In this context, the Clean Development Mechanism (CDM), developed during the Kyoto period, regains critical importance. The transfer of low-carbon technologies to developing countries emerges as one of the most influential mitigation parameters in hybrid modeling for 2050 projections. Thus, the results of these models not only provide numerical estimates for the future but also identify where, in which sectors, and within which time frames stronger policy interventions are required (Babiker et al., 2002; Bayrak, 2012).

6. International Cooperation, Technology Transfer, and Sustainability Policies

The global environmental governance architecture established by the Kyoto Protocol demonstrated unequivocally that climate change cannot be addressed without robust cross-border cooperation. Because greenhouse gas accumulation generates transboundary impacts, effective climate governance requires international solidarity. Consequently, the post-Kyoto climate regime has been shaped by three mutually reinforcing pillars—global cooperation, technology transfer, and sustainability-oriented development—which continue to form the institutional foundation of the Paris Agreement and subsequent COP processes (Böhringer & Vogt, 2003; Brulle, 2022).

A core contribution of the Kyoto Protocol was the operationalization— for the first time in binding international law—of the principle of Common but Differentiated Responsibilities (CBDR). By recognizing disparities in economic capacity and development levels, CBDR sought to distribute mitigation obligations equitably while simultaneously safeguarding the development rights of poorer countries. In doing so, Kyoto institutionalized justice as a practical governance norm, laying the conceptual groundwork for all modern climate regimes (Buanawatyy & Hastiadi, 2017; UNFCCC, 1998).

Kyoto's flexibility mechanisms—including the Clean Development Mechanism (CDM) and Joint Implementation (JI)—served as concrete embodiments of CBDR. They enabled

developed countries to meet part of their mitigation commitments through projects abroad while fostering the diffusion of low-carbon technologies in developing states. CDM's catalytic role in expanding renewable energy, energy-efficiency measures, and methane-reduction technologies is widely documented in IPCC assessment reports (IPCC, 2007; IPCC, 2014).

Technology transfer emerged as one of Kyoto's most transformative features. By aligning environmental mitigation with development objectives, it advanced a paradigm in which low-carbon technologies address both ecological and socioeconomic inequalities. Renewable energy systems, efficiency technologies, and carbon capture and storage (CCS) infrastructures exemplify the tangible outputs of this process (UNFCCC, 2015). The networks established during Kyoto were later formalized in the Paris Agreement through the Technology Mechanism—comprising the Technology Executive Committee (TEC) and the Climate Technology Centre and Network (CTCN)—which expands developing countries' access to green technologies via technical expertise, capacity-building, and financial assistance (UNFCCC, 2014).

The effectiveness of technology transfer hinges not only on financial flows but also on knowledge exchange, institutional strengthening, and human-resource development. Organizations such as UNEP, UNDP, and the Global Environment Facility (GEF) have supported these dimensions by providing technical training, advisory services, and infrastructure financing (UNDP, 2018; UNEP, 2019). These initiatives reveal that environmental governance is grounded as much in education, institutional empowerment, and social capacity as in technology and finance.

Increasingly, local and Indigenous knowledge systems have complemented global scientific frameworks. Traditional ecological practices—ranging from sustainable land use to low-carbon production—highlight that cultural diversity is integral to environmental sustainability (Berkes, 2012; Agrawal, 1995). Accordingly, post-Kyoto technology transfer has evolved from a one-directional technical exchange into a multidirectional, collaborative, and culturally adaptive learning process.

Kyoto's financial architecture also extended beyond carbon markets to encompass energy transition, water management, agricultural sustainability, and disaster-risk reduction. By transforming environmental measures from economic burdens into investment opportunities, Kyoto anchored climate action within a durable financial framework. Contemporary instruments such as carbon pricing, green bonds, and sustainable finance mechanisms reflect the ongoing influence of this paradigm (OECD, 2017; World Bank, 2020).

Sustainable development policies, particularly under the Paris Agreement and the SDGs, have since become a central axis of environmental governance. Environmental policy has expanded from a narrow focus on emissions to a multidimensional agenda addressing energy, food, water, health, and social equity. Kyoto provided the initial institutional foundation for this integration, and current green-growth strategies, carbon-neutrality visions, and circular-economy policies build directly on this legacy (Brulle, 2022; IPCC, 2014).

With the global institutionalization of sustainability, post-Kyoto governance increasingly emphasizes the interdependence of environmental protection, economic stability, and social well-being. As Bulkeley and Moser (2007) note, principles forged during the Kyoto era have become embedded in national strategies for energy security, food systems, urban planning, and industrial transformation. Environmental policy has therefore evolved from a

sector-specific field into a core pillar of national development planning, supported by the flexible and inclusive governance framework of the Paris Agreement (UNFCCC, 2015).

The incorporation of international cooperation and technology transfer into sustainability frameworks has generated a multilayered system in which private actors, local governments, and civil society play growing roles. The NDC structure enables states to design climate and sustainability strategies tailored to national conditions, enhancing policy ownership and implementation effectiveness (Buanawatyy & Hastiadi, 2017; Bulkeley & Moser, 2007).

Technology transfer remains essential for global sustainability, particularly through the spread of low-carbon production systems, renewable energy technologies, waste-management solutions, and CCS methods (Caneill & Cassen, 2025; Brulle, 2022). Its success depends on the integration of technical solutions with planning, regulation, financing, and human-capital development. Post-Kyoto cooperation has therefore expanded to involve knowledge sharing, training, and governance experience, in alignment with CBDR and the imperative of strengthening institutional capacity in developing countries (Uysal, 2009).

The digitalization of climate governance—through satellite observations, big-data analytics, sensor networks, and real-time monitoring—has intensified the data-driven character of international cooperation (Bulkeley & Moser, 2007). This shift represents a technologically enhanced extension of Kyoto's MRV architecture adapted to the digital age (Depledge, 2022). Under the Paris Agreement, digital governance has been further institutionalized through the Technology Framework and the Technology Mechanism, which integrate technology deployment with financial tools and structured capacity-building initiatives (UNFCCC, 2018). These developments have produced an innovation-supporting ecosystem in which local governments, academic institutions, and the private sector play critical roles.

The green economy—a model built on efficient resource use, low-impact production, circular-economy practices, and renewable-energy investment—now constitutes a central pillar of post-Kyoto climate governance (Bulkeley & Moser, 2007; Caneill & Cassen, 2025). Countries are restructuring their industrial strategies around energy efficiency, recycling, carbon neutrality, and sustainable urbanization, simultaneously enhancing environmental sustainability and economic resilience (OECD, 2011). Renewable energy deployment, smart-grid development, energy-storage technologies, and CCS infrastructures have become key indicators of sustainability performance and are indispensable for achieving carbon neutrality by 2050 (IRENA, 2023).

Ultimately, the evolution of energy and sustainability policies into domains requiring collective global action underscores that climate challenges are transboundary in nature and cannot be addressed through isolated national efforts. The technology-development, financing, and capacity-building mechanisms of the Paris Agreement thus represent a direct institutional continuation of the cooperative foundations laid during the Kyoto era (UNFCCC, 2018).

7. Conclusion

The global environmental governance process initiated by the Kyoto Protocol has evolved into a multidimensional transformation, deepened today through an engineering-based implementation framework. The monitoring, reporting, and verification (MRV) mechanisms established under Kyoto ensured that data-driven analysis, accountable performance metrics, and scientific standardization became fundamental components of environmental policy. In the post-Kyoto era, this rational approach has triggered structural change not only in international law and diplomacy, but across all engineering disciplines—energy technologies, infrastructure planning, water and agricultural management, transportation systems, and disaster risk reduction.

From an engineering perspective, Kyoto's legacy has been translated from abstract policy aspirations into concrete and measurable implementation programs. Renewable energy investments, smart grid systems, energy storage technologies, carbon capture and storage (CCS) infrastructures, low-carbon production processes, and sustainable urban planning models represent contemporary reflections of the technical transformation whose foundations were laid during the Kyoto period. Likewise, the Clean Development Mechanism (CDM) and technology transfer initiatives have played a critical role in disseminating engineering-based solutions at the global scale, reducing capacity disparities among countries.

Today, environmental decision-making processes are increasingly supported by artificial intelligence, big data, and remote sensing technologies—representing a digitalized and advanced extension of Kyoto's data-oriented paradigm. Emission projections for 2050 generated through ARIMA, Artificial Neural Networks, and hybrid analytical models demonstrate that the pace of energy transition, the level of technological uptake, and the strength of international cooperation are key determinants of the future global carbon balance. These models clearly show that technical capacity and data-driven policy design are essential for achieving sustainability objectives.

A defining feature of the post-Kyoto era is the emergence of a multi-actor and multi-level structure in environmental governance. Collaboration among states, local governments, the private sector, academic institutions, and civil society has demonstrated that environmental challenges can only be addressed through the coordinated contributions of engineering, economics, and the social sciences. This holistic governance model—reinforced by the Paris Agreement and the Sustainable Development Goals—illustrates that environmental implementation lies at the center of national development policies and long-term infrastructure strategies.

In conclusion, the Kyoto Protocol has gone beyond serving as an initial climate policy document; it has provided the normative, institutional, and technical foundations for engineering-based environmental implementation. Contemporary approaches such as the green economy, carbon neutrality, digital environmental governance, and multi-level climate governance are all built upon the scientific and institutional trajectory initiated by Kyoto. From a future-oriented perspective, a sustainable world appears possible only through technological innovation, science-based decision-making, and the integrated contributions of engineering disciplines. Therefore, the post-Kyoto vision of environmental governance should be understood not merely as a climate policy, but as a long-term engineering project for global welfare, ecological integrity, and societal resilience.

References

Agiralioglu, N., Eris, E., Andic, G., Cigizoglu, H. K., Coskun, H. G., Yilmaz, L., Alganci, U., & Toprak, Z. F. (2017). *Practical methods for estimating the hydroelectric power potential of poorly gauged basins.* Sigma Journal of Engineering and Natural Sciences, 35(2), 347–358.

Agrawal, A. (1995). *Dismantling the divide between indigenous and scientific knowledge.* Development and Change, 26(3), 413–439.

Akagündüz, H. K. (2022). *Green economy on the path to sustainable development: An empirical study on Turkey.* Master's thesis, Bursa Uludağ University, Institute of Social Sciences, Department of Economics, Bursa.

Akın, M. S. (2016). *Insights from the Kyoto Protocol, Paris Agreement, and marketing field in the context of climate change.* Turkish Journal of Marketing, 1(1), 12–29.

Aksoy, Ö. B. (2020). *The impact of the Kyoto Protocol on solving climate change problems within a common property framework.* Akdeniz Journal of Economics and Administrative Sciences, 20(2), 169–184. https://doi.org/10.25294/auiibfd.827487

Alashan, S., Şen, Z., & Toprak, Z. F. (2016). *Hydroelectric energy potential of Turkey: A refined calculation method.* Arabian Journal for Science and Engineering. https://doi.org/10.1007/s13369-015-1982-5

Aldemir, Ş., & Kaypak, Ş. (2008). *Eco-economy approach, the Kyoto Protocol process, and Turkey.* In Globalization, Democratization and Turkey International Symposium Proceedings (pp. 486–496). Akdeniz University.

Alganci, U., Coskun, H. G., Eris, E., Agiralioglu, N., Cigizoglu, H. K., Yilmaz, L., & Toprak, Z. F. (2009). *Determining the hydroelectric potential of ungauged river basins using remote sensing and GIS-based hydrological modelling*. HKM Journal of Geodesy, Geoinformation and Land Management, THBTK 2009(3) Special Issue, 1–5.

Anderson, J. W. (1998). *The Kyoto Protocol on climate change: Background, unresolved issues, and next steps.* Resources for the Future.

Atabey, S., & Toprak, Z. F. (2024). *A criticism of the Kyoto Protocol with an objective approach.* Journal of Advanced Research in Natural and Applied Sciences, 10(3), 520–529. https://doi.org/10.28979/jarnas.1452226

Auer, M. R. (2000). *Who participates in global environmental governance? Partial answers from international relations theory.* Policy Sciences, 33(2), 155–180. https://doi.org/10.1023/A:1026563821056

Ayhan, D. (2010). *Global climate change problem and the Kyoto Protocol in the context of energy, environment, and sustainable development: A case study on Turkey.* Doctoral dissertation, Marmara University, Institute of Social Sciences, Department of International Economics, Istanbul.

Azad, M. A. (2025). *The implications of the Kyoto Protocol for COP: Why is global environmental governance political? A study in environmental anthropology.* Open Journal of Social Sciences, 13(8), 145–157. https://doi.org/10.4236/jss.2025.138009

Babiker, M. H., Jacoby, H. D., Reilly, J. M., & Reiner, D. M. (2002). *The evolution of a climate regime: Kyoto to Marrakech and beyond.* Environmental Science & Policy, 5(3), 195–206. https://doi.org/10.1016/S1462-9011(02)00035-7

Babuş, D. (2005). *Examining the global warming issue in international environmental policy and Turkey's position.* Master's thesis, Çukurova University, Institute of Science, Department of Landscape Architecture, Adana.

Bayrak, M. R. (2012). *Low-carbon economy in Turkey for sustainable development and financing sources of the Kyoto Protocol.* Journal of History, Culture and Art Research, 1(4, Special Issue), 1–15. https://doi.org/10.7596/taksad.v1i4

Berkes, F. (2012). *Sacred ecology* (3rd ed.). Routledge.

Böhringer, C., & Vogt, C. (2003). *Economic and environmental impacts of the Kyoto Protocol.* Canadian Journal of Economics, 36(2), 475–496. https://doi.org/10.1111/1540-5982.t01-1-00010

Brulle, R. J. (2022). *Advocating inaction: A historical analysis of the Global Climate Coalition.* Environmental Politics. https://doi.org/10.1080/09644016.2022.2058815

Brulle, R. J. (2022). *Climate change and society: Critical analyses of organizations and movements.* Sociological Inquiry, 92(3), 587–612.

Buanawatyy, P., & Hastiadi, F. F. (2017). *The impact of the Kyoto Protocol on environment quality in the free trade era: Case of G20 countries.* International Journal of Economics and Financial Issues, 7(3), 36–42.

Bulkeley, H., & Moser, S. C. (2007). *Responding to climate change: Governance and social action beyond Kyoto.* Global Environmental Politics, 7(2), 1–10. https://doi.org/10.1162/glep.2007.7.2.1

Caneill, J.-Y., & Cassen, C. (2025). *From the Kyoto Protocol to Article 6: The troubled history of the cooperation mechanisms.* HAL Open Science. https://halshs-05033809

Coskun, H. G., Alganci, U., Eris, E., Agiralioglu, N., Cigizoglu, H. K., Yilmaz, L., & Toprak, Z. F. (2010). *Remote sensing and GIS innovation with hydrologic modelling for hydroelectric power plant (HPP) in poorly gauged basins*, Water Resources Management, 24(14), 3757–3772. https://doi.org/10.1007/s11269-010-9632-x

Depledge, J. (2022). *The top-down Kyoto Protocol? Exploring caricature and misrepresentation in literature on global climate change governance.* International Environmental Agreements: Politics, Law and Economics, 22, 673–692. https://doi.org/10.1007/s10784-022-09580-9

Dessai, S., Lacasta, N. S., & Vincent, K. (2003). *International political history of the Kyoto Protocol: From The Hague to Marrakech and beyond.* International Review for Environmental Strategies, 4(2), 183–205.

Egorov, D., Manoilova, M., Strakhov, V., & Egorov, G. (2021). *On the Coase theorem as a theoretical basis for the Kyoto and Paris Protocols.* Society. Integration. Education. Proceedings of the International Scientific Conference, 6, 245–254. https://doi.org/10.17770/sie2021vol6.6141

Gökpınar, F. (2020). *Global climate change and climate justice debates: An assessment in the context of vulnerable societies.* Journal of Sociological Research, 23(1), 141–168.

Gupta, J. (2010). *A history of international climate change policy.* WIREs Climate Change, 1(5), 636–653. https://doi.org/10.1002/wcc.67

Güneş, Ş. A. (2011). *Ensuring compliance with climate change obligations: Kyoto Protocol compliance mechanism.* International Relations, 8(31), 69–94.

Hongyuan, Y. (2015). *Evolution of the global climate governance system and its implications.* China Quarterly of International Strategic Studies, 1(3), 423–446. https://doi.org/10.1142/S2377740015500220

IPCC. (2007). *Climate change 2007: Synthesis report. Contribution of Working Groups I, II and III to the Fourth Assessment Report of the Intergovernmental Panel on Climate Change.* IPCC.

IPCC. (2014). *Climate change 2014: Synthesis report. Contribution of Working Groups I, II and III to the Fifth Assessment Report of the Intergovernmental Panel on Climate Change.* IPCC.

IRENA. (2023). *World energy transitions outlook 2023.* International Renewable Energy Agency.

Karakaya, E. (Ed.). (2008). *Global warming and the Kyoto Protocol: Scientific, economic, and political analysis of climate change.* Bağlam Publishing.

Kaya, H. E. (2020). *Global climate policies from Kyoto to Paris.* Meriç International Journal of Social and Strategic Studies, 4(10), 165–191.

Kim, R. E., von Schomberg, R., & Biber-Freudenberger, L. (2020). *Climate justice and technology.* Environmental Science & Policy, 112, 465–474.

Kim, Y., Tanaka, K., & Matsuoka, S. (2020). *Environmental and economic effectiveness of the Kyoto Protocol.* PLoS ONE, 15(7), e0236299. https://doi.org/10.1371/journal.pone.0236299

Lopez, T. M. (2003). *A look at climate change and the evolution of the Kyoto Protocol.* Natural Resources Journal, 43(1), 285. https://digitalrepository.unm.edu/nrj/vol43/iss1/9

Ma, Z. (2010). *The effectiveness of the Kyoto Protocol and consummating the legal institution for international technology transfer.* Asian Social Science, 6(4), 80–85.

Maamoun, N. (2019). *The Kyoto Protocol: Empirical evidence of a hidden success.* Journal of Environmental Economics and Management, 95, 227–256. https://doi.org/10.1016/j.jeem.2019.03.001

Madubuegw, C. E., Okechukwu, G. P., Emeka, O., Samuel, N., & Kyrian, U. (2021). *Climate change and challenges of global interventions: A critical analysis of Kyoto Protocol and Paris Agreement.* Journal of Policy and Development Studies, 5(6), 127–140. https://doi.org/10.12816/0059151

Morin, J.-F., Orsini, A., Trudeau, H., Duplessis, I., Lalonde, S., Van de Graaf, T., De Ville, F., O'Neill, K., Roger, C., Dauvergne, P., Oberthür, S., Biermann, F., Ohta, H., & Ishii, A. (2013). *Insights from global environmental governance.* International Studies Review, 15(4), 562–589.

OECD. (2011). *Towards green growth.* OECD Publishing.

OECD. (2017). *Investing in climate, investing in growth.* OECD Publishing. https://doi.org/10.1787/9789264273528-en

Ockwell, D., & Mallett, A. (Eds.). (2012). *Low-carbon technology transfer: From rhetoric to reality.* Routledge.

Öztürk, Ş. T., & Toprak, Z. F. (2025). *The success of the Kyoto Protocol in reducing carbon emissions in the EU.* International Journal of Global Warming, 36, 53–66.

Page, E. (2007). *Equity and the Kyoto Protocol.* Politics, 27(1), 8–15. https://doi.org/10.1111/j.1467-9256.2007.00273.x

Toprak, Z. F., Eris, E., Agiralioglu, N., Cigizoglu, H. K., Yilmaz, L., Aksoy, H., Coskun, H. G., & Andic, G. (2009). *Modeling monthly mean flow in a poorly gauged basin using fuzzy logic*.
CLEAN – Soil, Air, Water, 37(7), 555–564. https://doi.org/10.1002/clen.200800152

CHAPTER 5

SUSTAINABILITY OF NUCLEAR ENERGY IN TERMS OF WASTE MANAGEMENT

Nesli AYDIN[1], Gül KAYKIOĞLU[2]

1 Doç. Dr. Tekirdag Namik Kemal University, Faculty of Corlu Engineering, Department of Environmental Engineering, 59860 Corlu, Tekirdag, Turkey (Corresponding author, https://orcid.org/0000-0002-7561-4280
2 Prof. Dr. Tekirdag Namik Kemal University, Faculty of Corlu Engineering, Department of Environmental Engineering, 59860 Corlu, Tekirdag, Turkey, https://orcid.org/0000-0003-3271-211X

1. The Role of Nuclear Energy in Meeting Global Energy Demand

Rapidly increasing global energy demand and the increasingly severe impacts of climate change are driving the global shift toward clean and sustainable energy sources. In this context, nuclear energy stands out as a key enabler of the energy transition, offering zero carbon emissions during electricity generation and lower lifecycle emissions compared to fossil fuels (Çelik and Selçuklu, 2025). Nuclear energy has become an integral part of civilisation, with numerous applications ranging from medicine, diagnostics and medical therapy, to large-scale nuclear power plants and space exploration. Globally, nuclear power plants account for nearly 10% of the world's electricity (IAEA, 2025). As demand for "low-carbon" energy sources revives, interest in electricity generation through nuclear fission is also expected to grow considerably (Pershukov et al., 2022). However, nuclear energy production inherently generates radioactive waste. Safe, long-term, and sustainable management of this waste is critical to the future role of nuclear energy and its public acceptance (Erdoğdu, 2025; Jewell and Ateş, 2015; Kurniawan et al., 2022). An integrated, transparent waste management strategy encompassing both technical and social dimensions is crucial, especially for countries entering the new nuclear energy landscape (Kurniawan et al., 2022). The 433 nuclear power reactors currently in operation have a total net installed capacity of 387,998 MW of electricity (World Nuclear Association, 2025a). The growing use of nuclear energy is reflected in the 57 new power reactors under construction worldwide, totalling an additional 59,009 MW (Dalton, 2023).
The success of this nuclear revival will inevitably depend on addressing a number of known challenges, including plant safety, costs, liabilities, and successful site selection. This study aims to evaluate waste management policies in terms of sustainability by considering the basic principles of nuclear waste management and existing and developing technologies.

2. Environmental Dimension of Nuclear Energy

As is known, nuclear energy is produced by a process called fission, which means the splitting of 235U atoms by a slow neutron (n) impact (Eq-1) (Lyman, 2011; World Nuclear Association, 2025a).

$$^{235}_{92}\mathrm{U} + {}^{1}_{0}\mathrm{n} \longrightarrow \mathrm{A} + \mathrm{B} + \mathrm{x}\,{}^{1}_{0}\mathrm{n} + 200\ \mathrm{MeV} \quad \text{(Eq-1)}$$

The energy released by the fission of the 235U atom is used to generate steam that drives electricity-generating turbines. This fission also releases neutrons, which can then split further 235U nuclei, making the reaction called a chain reaction (Lyman, 2011; Massachusetts Institute of Technology, 2025). When a uranium atom fissions, it forms two smaller, unstable atoms, labelled (A + B). These smaller atoms include fission products and the highly radioactive smaller actinides, shown in Figure 1 (Lyman, 2011; Massachusetts Institute of Technology, 2025; World Nuclear Association, 2025a).

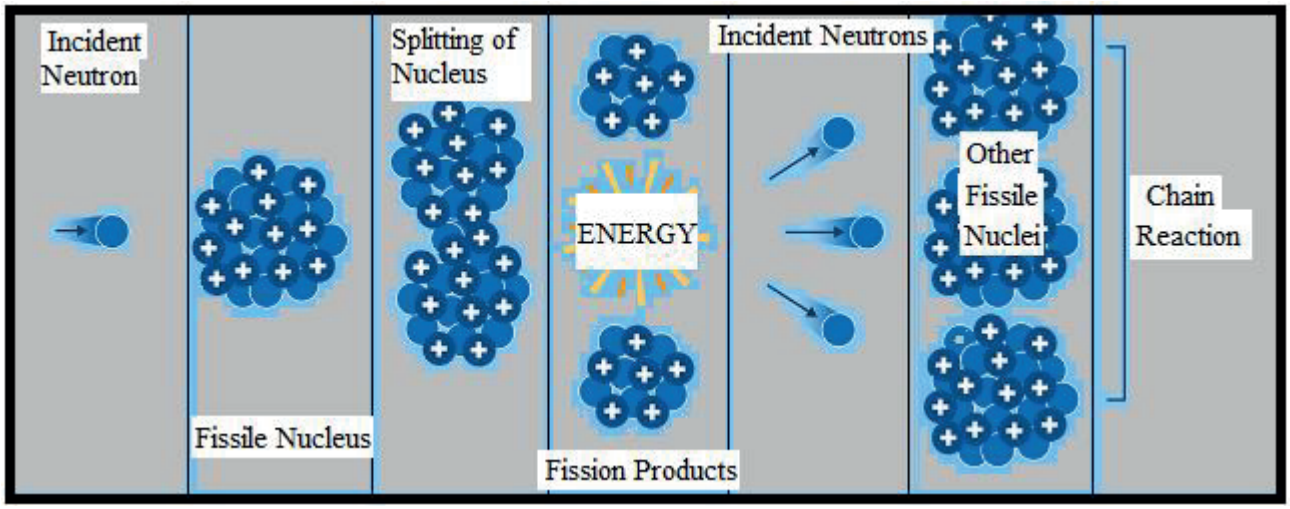

Figure 1. Nuclear Fission (IAEA, 2025)

Managing nuclear waste is similar to managing toxic chemicals from other industrial processes, with one exception: the waste generated by the decay of 235U into unstable nuclear elements is radioactive (Kochkin et al., 2021). This means that the processes used to handle, treat, and store the waste must minimise the effects of radioactivity on human health and the environment (Harvego et al., 2009). Uniquely, the hazard of this radioactivity will diminish over time due to the decay of radionuclides (radioactive isotopes) within the waste into stable isotopes (Chapman and Hooper, 2012). This process takes at least a million years, making nuclear waste management one of the most important and long-term challenges (Chapman, 2019; IAEA, 2006).

The use of nuclear energy inevitably results in the production of some radioactive or contaminated materials. When not considered a resource for recycling, these materials are referred to as nuclear waste (IAEA, 2009). The volume of nuclear waste generated by the nuclear industry is much smaller than that produced by non-nuclear applications. For instance, a typical nuclear power plant producing approximately 1 GW annually produces an average of 25 tonnes of waste (Ojovan, 2023). This waste includes several hundred cubic metres of low- and medium-level nuclear waste material that must be disposed of accordingly (IAEA, 2017). On the other hand, a coal-fired power plant of the same capacity produces approximately 6.5 million tonnes of CO_2 and over 300,000 tonnes of ash annually (UCS, 2019). It is noteworthy that ash waste from coal-fired power plants contains approximately 400 tonnes of toxic heavy metals, containing radioactivity, and over 5,000 tonnes of harmful gases that must be treated before discharge (EPA, 2025a).

However, integrated nuclear waste management planning must be comprehensive, requiring consideration of all waste from existing facilities, as well as waste from decommissioning and remediation of nuclear plants and potential accident waste (IAEA, 2020). Consequently, these plans also require the development of different planning scenarios and control phases to allow for sufficient flexibility to adapt to changes (IAEA, 2022).

In 2009, the International Atomic Energy Agency published a specific guidance document on radioactive waste management policies and strategies after extensive consultation with member countries (IAEA, 2009). This guidance outlines how to establish a nationally agreed-upon position on nuclear waste management and how to manage such waste appropriately.

Based on this guidance, member countries then began developing their national policies and strategies to define the objectives and requirements for the safe management of this waste.

3. Definition and Classification of Nuclear Waste

According to the definition of International Atomic Energy Agency (IAEA) within the framework of basic international safety standards, nuclear waste is material containing radionuclides above authorisation levels established by the authorities and for which no other use is intended (IAEA, 2009). The terms "radioactive waste" and "nuclear waste" are generally used synonymously in the context of safety and waste management. As is well known, all materials have a certain background radioactivity level. The focus of this guide is to identify materials and activities that significantly exceed this radioactivity level and integrate them into a regulatory control system.

It is internationally recognised that each country legally and ethically is obligated to take care of the radioactive waste generated within its borders. Government processes determine what constitutes radioactive waste, the parties responsible, and the institutions responsible for regulating its use and ultimate disposal. Authorisation and/or exemption levels of nuclear waste are always determined by national authorities.

Nuclear waste, like other wastes, could be composed of materials with different origin, chemical composition, and physical state (Baisden and Choppin, 2001; IAEA, 2014). However, what distinguishes radioactive waste from other types of waste is that it includes unstable components due to radioactive decay (Ahn and Apted, 2017; IAEA, 2022). Managing radioactive waste properly requires various approaches to ensure the protection of the environment from radiation.

To manage nuclear waste, waste is classified according to its characteristics, such as high, medium, or low based on its present radioactivity level; by the predominant type of radiation emitted (alpha, beta, gamma, or X-ray); or by its half-life (the time required for the material to decay to half its original value) (Defra, 2007). Radioactive waste could also be grouped according to its physical properties (primarily solid, liquid, or gas) (Metcalf and Batandjieva, 2013). In addition to providing an assessment covering various waste types and disposal solutions, the International Atomic Energy Agency has developed a general nuclear waste classification system (IAEA, 2009). According to this system, nuclear waste is evaluated in six groups as follows.

3.1 Exempt Nuclear Waste

These are wastes that meet the criteria for exclusion from regulatory control for radiation protection purposes (IAEA, 2009). Once removed from regulatory control, such wastes are not considered radioactive waste.

3.2 Very Short-Lived Waste

This type of waste could be left to degrade for a limited period of up to several years. Then, it is removed from regulatory control and disposed of according to regulations approved by the regulatory agency. This class includes waste that often contains radionuclides with very short half-lives and is typically used for research and medical purposes (IAEA, 2009; IAEA, 2014).

3.3 Very Low-Level Waste

This type of waste does not require a high level of containment and isolation, and hence, it is suitable for disposal in subsurface storage facilities with limited regulatory control (IAEA, 2009). Such storage facilities could also include other hazardous wastes. Typical wastes in this class include soil and debris with low activity concentrations (IAEA, 2009; IAEA, 2014; Rohlig, 2022a).

3.4 Low-Level Waste (LLW)

Waste containing limited amounts of long-lived radionuclides. This sort of waste necessities isolation and containment for up to several hundred years, but is suitable for disposal in engineered near-surface facilities (IAEA, 2014). This class encompasses a very broad spectrum of wastes (IAEA, 2003; IAEA, 2014). It could contain short-lived radionuclides at higher activity concentration levels, as well as long-lived radionuclides at relatively low activity concentration levels (IAEA, 2009).

All facilities that use or process radioactive materials, inevitably generate this type of waste. These include clinics, research laboratories, hospitals that use radionuclides for diagnostic and therapeutic purposes, and nuclear power plants (World Nuclear Association, 2025b). Paper, tools, masks, protective clothing, filters, and other lightly contaminated materials containing small amounts of short-lived nuclides are generally categorised in this group. For these wastes, depending on the nature of the waste, both the "decay delay" and "dilution and dispersion" principles could be used for disposal (Crossland, 2012; IAEA, 2003).

While they constitute approximately 90% of the global nuclear waste volume, they comprise only 1% of the radioactivity in all nuclear waste (World Nuclear Association, 2025b). Depending on their radioactivity level, these wastes are disposed of by storage near the surface (Crossland, 2012).

3.5 Intermediate-Level Waste (ILLW)

These wastes, particularly those containing long-lived radionuclides, require greater protection and isolation than those provided by near-surface disposal (IAEA, 2003; IAEA, 2014). However, they require only limited, if any, regulation for heat dissipation during storage and disposal (Crossland, 2012). These wastes, while long-lived, may contain alpha-emitting radionuclides that will not decay to an acceptable activity concentration level for near-surface disposal over extended periods (Ojovan, 1999). Therefore, this class of waste requires disposal at greater depths, up to several hundred meters (Muller, 2019).

Reactor modules, polluted materials from reactor dismantling operations, sludge and resins from fuel cooling and loading areas, and materials used to disinfect cooling systems, such as filters and screens, generally fall into this group. The most common management option for short-lived solid waste is "decay retardation," while long-lived waste requires the "concentrate and contain" principle (solidification for deep geological disposal) (IAEA, 2014). Wastes in this group constitute approximately 7% of the volume and 4% of the radioactivity of all radioactive waste (World Nuclear Association, 2025b).

3.6 High-Level Waste (HLW)

This group includes wastes with activity concentrations high enough to produce significant amounts of heat through radioactive decay, as well as wastes containing long-lived radionuclides (IAEA, 2003; IAEA, 2014). Disposal typically requires disposal in deep, stable

geological formations, several hundred meters or more below the surface (World Nuclear Association, 2025b).

This type of waste generally refers to high levels of radioactive nuclides originating from nuclear power generation or irradiated materials associated with nuclear weapons production (Cohen, 1977; Rohlig, 2022a). These wastes are highly radioactive, generate significant amounts of heat, and contain long-lived radionuclides. Typically, these wastes are processed using vitrification or the "condense and store" principle, solidifying them into a ceramic matrix waste (Rohlig, 2022a, 2022b). Spent nuclear fuel, which is not reprocessed, also falls into this category. Due to the highly radioactive fission products contained in spent fuel, it must be put in storage for "cooling" for many years before final disposal, isolated from the environment (Rohlig, 2022b). Final disposal of these wastes is achieved by placing them in deep geological formations (Cohen, 1977; Rohlig, 2022b).

4. Nuclear Waste Handling and Disposal

Generally, three options are available for radioactive waste management (Ojovan and Steinmetz, 2022). These are concentration and containment (concentrating and isolating the waste in a suitable environment), dilution and dispersion (diluting to regulatory-acceptable levels and then discharging into the environment), and decay delay (allowing radioactive components to decay to acceptable or background levels) (Freeze at al., 2019; Freeze at al., 2020; IAEA, 2003; IAEA, 2014). The first two options are common in the management of non-radioactive waste, while the third is specific to radioactive waste. All radioactive waste eventually becomes harmless as it decays into stable elements, while non-radioactive hazardous waste remains hazardous indefinitely or until its chemical form changes (IAEA, 2009).

The processing of nuclear waste consists of several steps. These are pre-treatment, treatment, conditioning, storage, and disposal processes (World Nuclear Association, 2025b). Pre-treatment encompasses all processes preceding waste treatment to enable the selection of technologies (treatment and conditioning) for subsequent waste processing (Baisden and Choppin, 2001). The treatment phase includes processes aimed at improving safety or economics by modifying the properties of nuclear waste (Kochkin et al., 2021). Some treatment processes could result in the conversion of nuclear waste into another waste form (Drace et al., 2022). The conditioning phase involves the production of a suitable waste package for the transport, storage, and/or disposal of nuclear waste (Baisden and Choppin, 2001; IAEA, 2014). Storage involves the preservation of waste packages for a specified period, ensuring containment, isolation, environmental protection, and monitoring (Corkhill and Hyatt, 2018). Disposal is the final stage of the nuclear waste life cycle and involves the placement of the waste in a suitable facility without the intention of recovery (Bracke et al., 2019).

The retention times required to safely isolate waste radionuclides are estimated based on the radiotoxicity of the nuclear waste (Bracke et al., 2019). The fundamental principle of disposal facilities is based on a multi-barrier defence system (IAEA, 2014; Freeze et al., 2020; Pershukov et al., 2022) to isolate the waste from the environment. This system consists of a natural or engineered geological barrier (Freeze et al., 2020; Ojovan et al., 1999). The depth of the disposal facility's location is related to the hazard level (Pershukov et al., 2022).

There is a global consensus among all countries using nuclear energy that disposal is the ultimate safe solution for the long-term management of nuclear waste (Ojovan, 2022). Disposal is the placement of waste in a suitable facility without the intention of recovery (Pershukov et al., 2022). Disposal is also considered the nearly complete removal of hazardous substances from the biological cycle (biosphere) (Muller et al., 2019).

Many sources find recommendations for disposing of nuclear waste in space or deep within bodies of water, such as the sea or ocean (Pershukov et al., 2022). Disposal typically involves nuclear waste in solid form, placed in suitable containers. Furthermore, the waste is initially stabilised in a durable waste form (Freeze et al., 2020). Safe storage forms part of a multi-barrier approach (Figure 2) consisting of engineered geological configurations that aim to minimise the risk of radionuclide migration within the biosphere (Muller et al., 2019; Pershukov et al., 2022).

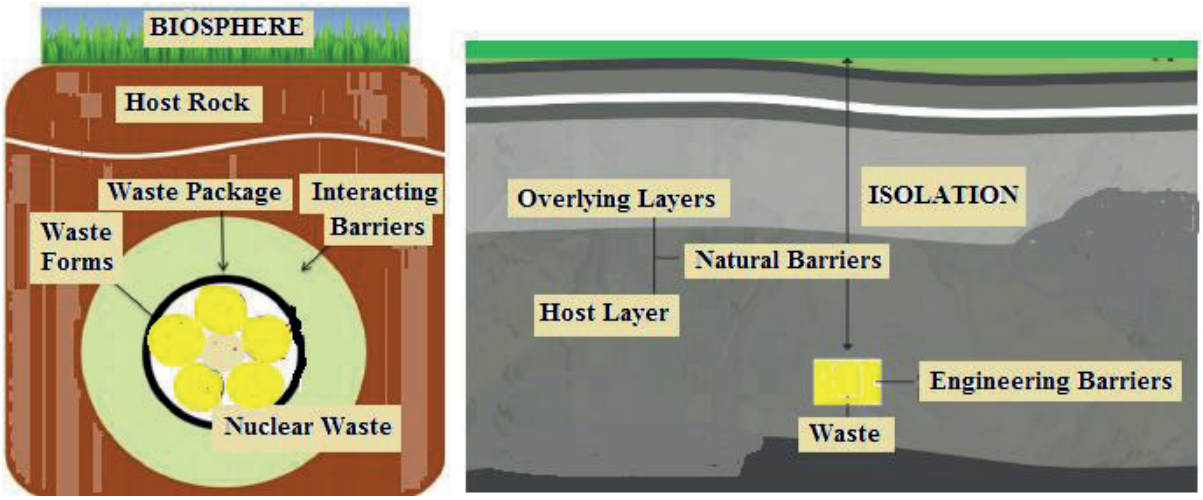

Figure 2: Multi-Barrier Approach for Nuclear Waste Disposal (Jantzen and Ojovan, 2019; Pilania and Dube, 2023)

Nuclear waste disposal with a deep geological repository is considered the most ideal and permanent long-term disposal solution for high-level waste and spent nuclear fuel (Kurniawan et al., 2022). This method aims to permanently isolate radioactive waste from the biosphere for thousands of years (Unokiwedi et al., 2025). Deep geological repository systems use a combination of engineered barriers and natural geological barriers to isolate waste from the environment (Unokiwedi et al., 2025).

4.1. Solidification Technologies

One of the fundamental goals in radioactive waste management is to reduce waste volume, limit the mobility of radionuclides, and ensure long-term safety during storage and transportation. In this context, the processing and solidification technologies developed play a critical role in the safe disposal of high-level nuclear waste and intermediate-level nuclear waste.

Solidification technologies primarily make storage and disposal processes more manageable by significantly reducing waste volume. Immobilising waste in a solid matrix minimises the risk of radioactive isotopes leaking or dispersing into the environment, thereby reducing potential radiological exposure for both current and future generations. This method not only

provides physical encapsulation but also increases the chemical and structural stability of the waste, making it resistant to corrosion, degradation, or deterioration due to environmental conditions.

The products obtained through the solidification process form a durable barrier against environmental influences, preventing the transmission of radioactive substances into the biosphere. Furthermore, this method simplifies the transportation and storage of nuclear waste, allows for safer packaging of solid waste, and significantly reduces risks during transportation and storage. This type of stabilisation and immobilisation strategy is considered essential for meeting radiological safety standards, especially for highly radioactive waste (Barbhuiya et al., 2024).

Glass Solidification

Radioactive waste is melted at high temperatures by mixing it with glass components (e.g., SiO_2, P_2O_5, B_2O_3, etc.) in specific proportions. The resulting molten glass is injected into storage vessels and cooled, creating a stable solid form. This process physically traps radioactive nuclides within the glass matrix. Furthermore, during the melting process, radioactive components undergo thermal decomposition and oxidation (Kurniawan et al., 2022). This method is one of the most common and effective techniques for solidifying high-level waste. It also demonstrates high immobilisation performance for intermediate-level waste (Dong et al., 2025).

During the vitrification process, waste is stabilised by embedding it in chemically stable glass matrices such as borosilicate or iron phosphate glass. This method allows for safe waste storage, transport, and placement in facilities. All components of high level waste could be incorporated into the glass matrix as it has an average loading of 30% w/w, provides a high volume reduction ratio, and the solidified structure maintains its stability over long periods. Furthermore, vitrification can immobilise radioactive nuclides and other contaminants such as heavy metals, and the properties of these contaminants remain constant in solid form (Kurniawan et al., 2022).

However, because glass is a metastable phase that tends to dissolve or crystallise under high temperature and humidity conditions, cooling and humidity control in storage facilities are essential. Fragmentation or pulverisation of the glass matrix could significantly increase leaching rates. Furthermore, harmful gases could be generated during the vitrification process; therefore, gas purification systems should be integrated into the process design (Dong et al., 2025). The industrial application of the vitrification technique was first achieved in France in 1978 and has subsequently been commercialised and widely implemented in countries such as the United States, China, the United Kingdom, Russia, Italy, Japan, Belgium, and India (Dong et al., 2025).

Cement Solidification

Cement is a binder commonly used in the solidification of radioactive waste. The waste is mixed with cement in specific proportions, creating a hard matrix through cement hydration and coagulation, physically trapping radioactive components within the cement structure

(Hossen et al., 2025; Dong et al., 2025; Barbhuiya et al., 2024). This method is particularly preferred for low- and medium-level waste.

The solidification process typically uses materials such as Portland cement, sand, fly ash, and slag to create a stable matrix. It is highly suitable for the immobilisation of waste resins or waste slurries from nuclear power plants (Luhar et al., 2023). The simplicity of the process allows for the straightforward processing of radioactive waste with high moisture content, the equipment used is relatively inexpensive, and solidification/disposal costs are low. The cement matrix is resistant to heat and mechanical stress, providing long-term stability (Hossen et al., 2025).

However, the cement solidification method also has some disadvantages. The solidified material has a relatively low density and poor leaching resistance; moreover, the resulting solidified form increases in volume by approximately twice that of the initial radioactive waste. This could lead to increased disposal costs (Dong et al., 2025).

Cement-based solidification technology is being implemented on an engineering scale in countries such as the US, France, Germany, China, and Japan and is considered a widespread disposal solution (Dong et al., 2025).

Asphalt Solidification

In the solidification method using asphalt, radioactive waste is mixed with asphalt at a specific temperature, and as a result of the saponification reaction, it is evenly distributed throughout the waste asphalt matrix. This physically traps the radioactive components within the asphalt, resulting in a stable solid form. This method is particularly suitable for the immobilisation of intermediate-level long-lived waste.

The most significant advantages of the asphalt solidification method include low porosity, low leaching rate, and high retention capacity for radioactive waste. The waste-to-asphalt ratio is generally between 0.5 and 1, making this method highly efficient in terms of volume and reducing disposal costs. Furthermore, the high corrosion resistance of the asphalt matrix provides advantages in terms of long-term stability (Dong et al., 2025).

However, the asphalt solidification method has several disadvantages. There is a risk of secondary pollution during the disposal process. Furthermore, radioactive waste with high water content requires pre-treatment (e.g., dehydration by melting, centrifuging, or freezing), which increases equipment investment costs. The asphalt matrix has relatively low ageing resistance and chemical stability. Furthermore, because asphalt is a flammable material, fire risk must be carefully managed during the solidification process (Dong et al., 2025).

Various engineering-scale studies on asphalt solidification have been conducted in countries such as the USA, France, Germany, Russia, and China, and limited applications have been implemented (Dong et al., 2025).

Polymer Solidification

In the polymer-based solidification method, polymers are mixed with intermediate-level long-lived waste at normal temperature or between 100–170°C. The unique three-dimensional network structure of the polymers enables the physical confinement of radioactive waste or its

adsorption through ion exchange (Dong et al., 2025). This method is particularly suitable for the immobilisation of intermediate-level long-lived waste.

The most significant advantage of the polymer solidification method is its lower nuclide leaching rate compared to cement and asphalt solidification methods. Furthermore, this method achieves high encapsulation and high volume reduction performance. With these features, the long-term stability of disposed radioactive waste could be increased (Dong et al., 2025; Houhou et al., 2025).

However, the polymer solidification method also has several disadvantages. The initial strength of the solidified material is low, and it exhibits a significant tendency to erode when exposed to salt solutions. The process flow is complex, safety levels are relatively low, and the required equipment costs are high. Furthermore, polymers have limited ageing resistance and chemical stability, making it critical to evaluate their long-term performance (Dong et al., 2025; Houhou et al., 2025).

Polymer-based solidification techniques have been implemented on an industrial scale in the United States, France, Japan, and some other countries, and have been developed as an alternative method, particularly for the disposal of intermediate-level waste (Dong et al., 2025).

Artificial Rock Solidification

A multi-mineral solid solution is obtained from a mixture of radioactive waste and minerals using high-temperature heat treatment technology. In this process, radioactive waste is incorporated into the mineral lattice voids or lattice regions, and upon cooling, a stable multi-mineral phase forms (Dong et al., 2025). This method is considered one of the most suitable solidification technologies for the immobilisation of high-level radioactive waste.

The advantages of this technique include a simple synthesis process, the creation of a stable geological envelope, excellent thermal and physicochemical properties, and strong leaching and radiation resistance. The solidified structure has a low volume and a high radioactive load capacity; it could be loaded with an average of 45% w/w oxide minerals and 60% w/w oxygen salt minerals (Dong et al., 2025).

However, this method also has some disadvantages. The high reaction temperature and complexity of the process place significant demands on process control and equipment performance. Furthermore, the solidification matrix in high-level radioactive waste processing has limitations; only a portion of a single mineral phase could encapsulate the waste, which could lead to radiation damage to the partial minerals, resulting in volume expansion and increased leaching rates (Dong et al., 2025). Research on this technology has been conducted in Australia, the United States, and China, and pilot-scale plants have been established (Dong et al., 2025).

Suitable waste types, loading capacities, and advantages and disadvantages of solidification methods are summarised in Table 1.

Table 1. Comparison of nuclear waste solidification technologies

Process	**Waste Type**	**Loading Capacity** (w/w)	**Advantages**	**Disadvantages**
Vitrification	HLW, ILLW	30 % (high)	High stability, low leakage, high volume reduction, long-term durability	Metastable phase, dissolution at high temperature and humidity, harmful gas during processing
Cement Solidification	ILLW	10–15 % (low)	Simple process, low cost, direct application to high moisture waste, good mechanical strength	Low density, poor leak resistance, volume increase (almost 2 times)
Asphalt Solidification	ILLW	0.5–1 % (Medium)	Low porosity, high retention capacity, low disposal cost, good corrosion resistance	High water content requires pre-treatment, risk of aging and fire, low stability
Polymer Solidification	ILLW	Medium-High	Low leakage rate, high volume reduction, high enveloping performance	Complex process, low initial strength, high equipment cost, low aging resistance
Artificial Rock Solidification	HLW	45-60 % (High)	Excellent thermal and chemical stability, high leach resistance; low volume	High temperature and equipment requirements, risk of radiation damage, complex process

4.2 Fundamental Principles and Challenges of Nuclear Waste Management

Nuclear waste management is based on sustainability principles that consider not only current environmental and technological requirements but also the safety and well-being of future generations. Sustainability principles can be summarised as follows.

- The hazardous nature of radioactive waste has a potential impact that could last for thousands of years. Therefore, waste management strategies must be designed to prevent future generations from incurring additional burdens (Kurniawan et al., 2022). This approach also brings about a shared responsibility aligned with sustainable development goals.

- The fundamental goal of waste management is to safely isolate radionuclides from the biosphere (Unokiwedi et al., 2025). Deep geological storage systems are designed with a combination of engineering and natural barriers to ensure this isolation for thousands of years. Nuclear waste management programmes require sustainable financing mechanisms due to their high capital and long-term operating costs. Factors such as energy pricing, the establishment of waste funds, and government support are particularly critical in this context (Kurniawan et al., 2022; Erdoğdu, 2025).

-
- The site selection and operation of landfills require the trust and acceptance of local communities. Therefore, transparency, compensation mechanisms for affected communities, and principles of social justice should be prioritised in decision-making processes (Sanders and Sanders, 2021; Tohver et al., 2025; Alinejad et al., 2025).

Implementing these principles presents numerous technical, economic, social, and geopolitical challenges.

Long-Term Safety and Isolation

Ensuring the isolation of radioactive waste from the human environment for thousands of years is the most critical challenge. This process involves not only engineering solutions but also the intergenerational transfer of knowledge (Tohver et al., 2025). In deep geological storage facilities, the goal is to ensure that the biosphere is not exposed to radiation exceeding 0.15 millisieverts annually for 10,000 years (Kurniawan et al., 2022). This goal requires comprehensive risk assessments and continuous monitoring.

Nuclear waste disposal aims to isolate waste from both human activities and natural dynamic processes. The impacts of disposal facilities are analysed in terms of potential doses caused by potentially emitted and migrated radionuclides (Koplik et al., 1982; OECD, 2000).

In accordance with recommendations from the International Atomic Energy Agency, exposures resulting from natural processes are generally <0.3 mSv/year, while exposures resulting from human intervention are assessed as <10 mSv/year (IAEA, 2016). If these doses exceed 10 mSv/year, the design of the storage facility should be reconsidered. The adequacy of a system's safety is determined by a "safety analysis report."

A nuclear waste disposal facility's "safety analysis report" includes an assessment of the facility's performance and radiological effects on the environment and humans, and concludes with data demonstrating compliance with safety standards (Koplik et al., 1982; OECD, 2000). While the primary focus of safety is generally on radiological criteria, these criteria include limited doses or risks (Chapman and Hooper, 2012; OECD, 2000).

The most challenging aspect of preparing safety analysis reports is the long-term uncertainty inherent in geologically barrier-based waste disposal facilities, the only solution for high-level waste disposal (Chapman and Hooper, 2012; OECD, 2000). Recent research raises questions about the limitations of waste materials and the range of prediction models used (Chapman and Hooper, 2012; IAEA, 2011; World Nuclear Association, 2025b).

Site Selection

Site selection for storage facilities encompasses technical parameters such as geological stability, seismic risk, and hydrogeological characteristics, as well as public acceptance and socioeconomic impacts. The Yucca Mountain Project in the US, despite being technically feasible, was cancelled due to public outcry (Kurniawan et al., 2022). A study in Turkey identified Seydişehir as the most suitable location for small modular reactor facilities, demonstrating the importance of comprehensive site assessments (Ayyildiz et al., 2025).

Public Acceptance and Social Factors

The Chernobyl (1986) and Fukushima (2011) accidents severely undermined public confidence in nuclear energy. Therefore, transparent communication, independent oversight,

and participatory decision-making processes are critical to addressing public concerns (Jewell and Ates, 2015; Kok and Benli, 2017).

Financing and Economic Liability

Nuclear waste management projects involve operating costs spanning decades coupled with high investment costs. Therefore, meeting long-term financial obligations is a major challenge for the financial sustainability of energy policies (Erdoğdu, 2025).

Knowledge and Institutional Capacity

The success of waste management strategies depends on the preservation of technical know-how across generations. The continuity of institutional capacity and regulatory frameworks is a critical factor for long-term safety (Tohver et al., 2025).

Geopolitical Vulnerabilities

Nuclear technology transfer and waste management carry a geopolitical dimension in international relations. International cooperation mechanisms, particularly those such as the "Build-Own-Operate" model, have the potential to create external dependency (Jewell and Ates, 2015; Duru, 2025).

5. Emerging Technologies and Innovative Approaches

Nuclear waste management and the sustainability of the nuclear energy sector are being reshaped by the continuous development of advanced technologies and innovative approaches. These developments contribute to both the safer and more efficient management of radioactive waste and the strengthening of nuclear energy's role in the future global energy portfolio.

5.1 Small Modular Reactors

Small modular reactors stand out as a promising solution for the low-carbon energy transition by overcoming the limitations of traditional large-scale nuclear power plants (Ayyıldız et al., 2025; Tohver et al., 2025). These reactors offer shorter construction times and the ability to increase capacity based on demand thanks to their modular design, enhanced passive safety mechanisms, flexibility, and cost-effectiveness. Small modular reactors, expected to play a strategic role in future energy production, are critical for appropriate site selection and operational safety, especially in developing countries like Turkey, where energy demand is rapidly increasing.

5.2 Thorium Fuel Cycle

The thorium-based nuclear fuel cycle is an innovative approach that stands out as an alternative to uranium-based systems. It offers advantages such as lower toxicity, shorter half-life waste production, and greater resistance to nuclear proliferation (Kurniawan et al., 2022). Additionally, the widespread availability of thorium worldwide offers strategic potential for long-term fuel supply.

Small modular reactors stand out as a promising solution for the low-carbon energy transition by overcoming the limitations of traditional large-scale nuclear power plants (Tohver et al., 2025; Ayyıldız et al., 2025). These reactors offer shorter construction times and the ability to increase capacity based on demand with their modular design, improved passive safety mechanisms, flexibility, and cost-effectiveness. Small modular reactors, expected to play a

strategic role in future energy production, are critical for site selection and operational safety, especially in developing countries like Turkey, where energy demand is rapidly increasing.

5.3 Recycling of Spent Nuclear Fuel

Reprocessing of spent nuclear fuel maximises the energy potential of existing fuel and optimises the management process by reducing the final radioactive waste volume (Kurniawan et al., 2022). This approach also contributes to minimising the radioactive properties of high-level waste

5.4 Digitalisation and Artificial Intelligence Applications

Digital technologies and artificial intelligence offer revolutionary opportunities in terms of operational efficiency, safety, and traceability in nuclear waste management (Kurniawan et al., 2022; Hu and Pfingsten, 2023). Data-driven machine learning algorithms and computer-based modelling methods are effective tools for understanding complex system behaviour and developing optimisation processes. Furthermore, prototype tracking systems developed by integrating Block Chain and Internet of Things technologies provide transparency and data integrity throughout the waste lifecycle (Alinejad et al., 2023). Additionally, Material Flow Analysis software is widely used for calculating radioactive waste loads and optimising waste management systems during the preliminary design phase (Tohver et al., 2025).

6. Conclusions

Nuclear energy stands out as a low-carbon solution to increasing global energy demand and climate change, but it also brings with it complex environmental and societal responsibilities, such as radioactive waste management. This study examines the definition, classification, management approaches, and disposal methods of nuclear waste from a sustainability perspective, comprehensively evaluating existing and emerging technologies.

Nuclear waste disposal refers to the final storage of radioactive waste, which aims to permanently house it in a specialised disposal facility. Disposal facilities utilise a multi-barrier approach, effectively containing radionuclides and providing environmental protection. Nuclear waste disposal involves a well-established set of practices, primarily for low and medium level waste. Disposal facilities incorporating these practices have been in operation for decades.

Safe management of radioactive waste could be achieved through the integration of multi-barrier engineering systems and natural geological barriers, with deep geological storage methods emerging as a long-term solution, particularly for high-level waste. Solidification technologies (glass, cement, asphalt, polymer, and mineral-based methods) play a critical role in reducing waste volume and immobilising radioactivity. However, each technology has its limitations in terms of cost, technical difficulty, and long-term stability.

Emerging technologies and innovative approaches, small modular reactors, the thorium fuel cycle, spent nuclear fuel recycling, and artificial intelligence and digitalisation-based monitoring systems have the potential to increase the sustainability of the nuclear energy sector. These technologies offer future perspectives in terms of reducing waste, improving safety, and ensuring traceability.

However, nuclear waste management is not limited to technical solutions. It also encompasses multifaceted factors such as financing, public acceptance, social justice, and geopolitical risks. Long-term success will be achieved through transparent communication, strong regulatory

frameworks, intergenerational knowledge transfer, and the development of sustainable financing mechanisms.

The most challenging aspect is the disposal of high-level waste. Countries such as the US, Finland, and Sweden currently utilise disposal facilities constructed using multiple geological barriers (EPA, 2025b; Ministry of Economic Affairs and Employment of Finland, 2020; Swedish Radiation Safety Authority, 2025). Improving the safety levels of these facilities through diverse engineering approaches will be a significant step toward the safe and peaceful use of nuclear energy.

Ultimately, the future role of nuclear energy depends on the effective implementation of a safe and environmentally responsible waste management strategy. This strategy is key to a sustainable energy transition that will ensure the safety not only of current but also of future generations.

References

Ahn, J., Apted, M.J., 2017, Geological Repository Systems for Safe Disposal of Spent Nuclear Fuels and Radioactive Waste, Elsevier, Cambridge, UK.

Alinejad, S., Khoshsepehr, Z., Alimohammadlou, M., 2025, Strategic nuclear waste management for reducing environmental impacts: Innovative decomposed fuzzy methods, Journal of Cleaner Production, 513, 145728. https://doi.org/10.1016/j.jclepro.2025.145728

Ayyildiz, E., Yildirim, B., Erdogan, M., Aydin, N., 2025, Strategic site selection methodology for small modular reactors: A case study in Türkiye, Renewable and Sustainable Energy Reviews, 215, 115545. https://doi.org/10.1016/j.rser.2025.115545

Baisden, P.A., Choppin, G.R., 2001, Nuclear Waste Management and the Nuclear Fuel Cycle, Radiochemistry And Nuclear Chemistry – Vol. Il - Nuclear Waste Management And The Nuclear Fuel Cycle, Available at: https://www.eolss.net/sample-chapters/c06/E6-104-11.pdf

Barbhuiya, S., Das, B.B., Qureshi, T., Adak, D., 2024, Cement-based solidification of nuclear waste: Mechanisms, formulations and regulatory considerations, Journal of Environmental Management, 356, 120712, https://doi.org/10.1016/j.jenvman.2024.120712.

Bracke, G., Kudla, W., Rosenzweig, T., 2019, Status of Deep Borehole Disposal of High-Level Radioactive Waste in Germany. Energies, 12, 2580.

Chapman, N., Hooper, A., 2012, The disposal of radioactive wastes underground, Proc. Geol. Assoc., 123, 46–63.

Chapman, N.A., 2019, Who Might Be Interested in a Deep Borehole Disposal Facility for Their Radioactive Waste? Energies, 12, 1542

Cohen, B.L., 1977, High-level radioactive waste from light-water reactors. Rev. Mod. Phys., 49, 1–20.

Corkhill, C., Hyatt, N., 2018, Nuclear Waste Management, Available at: https://iopscience.iop.org/book/mono/978-0-7503-1638-5.pdf

Crossland, I., 2012, Disposal of radioactive waste. In Nuclear Fuel Cycle Science and Engineering; Woodhead Publishing Series in Energy; Woodhead Publishing: Sawston, UK, Chapter 18; pp. 531–557.

Çelik, E., Selçuklu, S.B., 2025,. Analysis and optimization of Türkiye's nuclear energy policies in achieving the net-zero emission target, Progress in Nuclear Energy, 188, 105898. https://doi.org/10.1016/j.pnucene.2025.105898

Dalton, D., 2023, Nuclear Status / 438 Reactors in Operation, With Six New Units Online In 2022, Available at: https://www.nucnet.org/news/438-reactors-in-operation-with-six-new-units-online-in-2022-2-1-2023

Defra, 2007, Policy for the Long Term Management of Solid Low Level Radioactive Waste in the United Kingdom; Department for Environment, Food and Rural Affairs: London, UK.

Dong, D., Wang, Z., Guan, J., Xiao, Y., 2025, Research on safe disposal technology and progress of radioactive nuclear waste, Nuclear Engineering and Design, 435, 113934. https://doi.org/10.1016/j.nucengdes.2025.113934

Drace, Z., Ojovan, M. I., Samanta, S. K., 2022, Challenges in planning of integrated nuclear waste management, Sustainability, 14, 21, 14204. https://doi.org/10.3390/su142114204

Duru, A.A., 2025, The implementation of Türkiye's nuclear energy policy, Energy Strategy Reviews, 59, 101737. https://doi.org/10.1016/j.esr.2025.101737

EPA, U.S. Environmental Protection Agency, 2025a, Available at: https://www.epa.gov/coalash/coal-ash-basics#:~:text=Coal%20ash%20contains%20contaminants%20like,drinking%20water%2C%20and%20the%20air.

EPA, U.S. Environmental Protection Agency, 2025b, Nuclear Power Plants, Available at: https://www.epa.gov/radtown/nuclear-power-plants

Erdogdu, E., 2025, The role of nuclear energy in competitive power markets: Policy solutions applied to Türkiye, Journal of Policy Modeling, https://doi.org/10.1016/j.jpolmod.2025.07.003

Freeze, G.A., Stein, E., Brady, P.V., Lopez, C., Sassani, D., Travis, K., Gibb, F., Beswick, J., 2019, Deep borehole safety case, Energies, 12, 2141.

Freeze, G., Sassani, D., David, O.K.B., Calvo, R., Peer, G., 2020, Borehole Disposal of Radioactive Waste in Israel–20388. In Proceedings of the WM2020 Conference, Phoenix, AZ, USA, 8–12.

Harvego, E.A., Schultz, R.R., 2009, Generation IV Technologies. In Nuclear Engineering Handbook, Ed.; Kok, K.D., CRC Press, Taylor & Francis Group: Boca Raton, USA, pp. 227–242.

Hossen, A., Rayhan, M. M., Sarker, M. S. A., Saha, A., Hamrani, A., McDaniel, D., 2025, A systematic review on grout in nuclear waste management: Advancement, composition and performance, Nuclear Engineering and Design, 443, 114281, https://doi.org/10.1016/j.nucengdes.2025.114281

Houhou, M., Leklou, N., Ranaivomanana, H., Penot, J. D., de Barros, S., 2025, Geopolymers in nuclear waste storage and immobilization: Mechanisms, applications, and challenges. Discover Applied Sciences, 7, 126, https://doi.org/10.1007/s42452-025-06536-x

Hu, G., Pfingsten, W., 2023, Data-driven machine learning for disposal of high-level nuclear waste: A review, Annals of Nuclear Energy, 180, 109452, https://doi.org/10.1016/j.anucene.2022.109452

IAEA, 2003, Scientific and Technical Basis for Near-surface Disposal of Low and Intermediate Level Waste, Vienna, Austria.

IAEA, 2006, Fundamental Safety Principles, Vienna, Austria, Available at: https://www-pub.iaea.org/MTCD/Publications/PDF/Pub1273_web.pdf

IAEA, 2009, Classification of Radioactive Waste; General Safety Guide GSG-1; IAEA: Vienna, Austria, Available at: https://www-pub.iaea.org/MTCD/Publications/PDF/Pub1419_web.pdf

IAEA, 2011 Disposal of Radioactive Waste Specific Safety Requirements, Vienna, Austria, Available at: https://www-pub.iaea.org/MTCD/Publications/PDF/Pub1449_web.pdf

IAEA, 2014 Radiation Protection and Safety of Radiation Sources: International Basic Safety Standards, Vienna, Austria, Available at: https://www-pub.iaea.org/MTCD/Publications/PDF/Pub1578_web-57265295.pdf

IAEA, 2017 Selection of Technical Solutions for the Management of Radioactive Waste, Vienna, Austria, Available at: https://www.iaea.org/publications/12217/selection-of-technical-solutions-for-the-management-of-radioactive-waste

IAEA, 2020, Design Principles and Approaches for Radioactive Waste Repositories, Vienna, Austria, Available at: https://www.iaea.org/publications/13510/design-principles-and-approaches-for-radioactive-waste-repositories

IAEA, 2022, Nuclear Safety and Security Glossary, Vienna, Austria, Available at: https://www.iaea.org/publications/15236/iaea-nuclear-safety-and-security-glossary

IAEA, 2025, Joint Convention on the Safety of Spent Fuel Management and on the Safety of Radioactive Waste Management, Vienna, Austria, Available at: https://www.iaea.org/topics/nuclear-safety-conventions/convention-nuclear-safety

Jantzen, C.M., Ojovan, M.I., 2019, On selection of matrix (wasteform) material for higher activity nuclear waste immobilisation, Russ. J. Inorg. Chem., 64, 1611–1624. Available at: https://link.springer.com/article/10.1134/S0036023619130047

Jewell, J., Ates, S.A., 2015, Introducing nuclear power in Turkey: A historic state strategy and future prospects, Energy Research & Social Science, 10, 273–282, https://doi.org/10.1016/j.erss.2015.07.011

Kochkin, B., Malkovsky, V., Yudintsev, S., Petrov, V., Ojovan, M., 2021, Problems and perspectives of borehole disposal of radioactive waste, Prog. Nucl. Energy, 139, 103867.

Kok, B., Benli, H., 2017, Energy diversity and nuclear energy for sustainable development in Turkey, Renewable Energy, 111, 870–877, https://doi.org/10.1016/j.renene.2017.05.001

Koplik, C.M.; Kaplan, M.F., Ross, B., 1982, The safety of repositories for radioactive wastes. Rev. Mod. Phys., 54, 269–312.

Kurniawan, T.A., Othman, M.H.D., Singh, D., Avtar, R., Hwang, G.H., Setiadi, T., Lo, W.H., 2022, Technological solutions for long-term storage of partially used nuclear waste: A critical review, Annals of Nuclear Energy, 166, 108736, https://doi.org/10.1016/j.anucene.2021.108736

Luhar, I., Luhar, S., Abdullah, M.M.A.B., Sandu, A.V., Vizureanu, P., Razak, R.A., Burduhos-Nergis, D.D., Imjai, T., 2023, Solidification/Stabilization technology for radioactive wastes using cement: An appraisal, Materials, 16, 954, https://doi.org/10.3390/ma16030954

Lyman, E.S., 2011, Nuclear Energy and Human Health, Eds: J.O. Nriagu, Encyclopedia of Environmental Health, 185-192, https://doi.org/10.1016/B978-0-444-52272-6.00185-9.

Massachusetts Institute of Technology, 2025, The Fission Process, Available at: https://nrl.mit.edu/reactor/fission-process/

Metcalf, P., Batandjieva, B., 2013, International safety standards for radioactive waste (RAW) management and remediation of contaminated sites. In Radioactive Waste Management and Contaminated Site Clean-up: Processes, Technologies and International Experience, Eds. Lee, W.E., Ojovan, M.I., Jantzen, C.M., Woodhead Publishing Series in Energy, 48, Woodhead Publishing, Cambridge, UK, Chapter 3, 73–114.

Ministry of Economic Affairs and Employment of Finland, 2020, Nuclear facilities include nuclear power plants and facilities for nuclear waste management, Available at: https://tem.fi/en/nuclear-facilities-and-projects

Muller, R.A., Finsterle, S., Grimsich, J., Baltzer, R., Muller, E.A., Rector, J.W., Payer, J., Apps, J., 2019, Disposal of high-level nuclear waste in deep horizontal drillholes, Energies, 12, 2052.

OECD, 2000, Features, Events and Processes (FEPs) for Geologic Disposal of Radioactive Waste; An International Database, Paris, France.

Ojovan, M.I., Guskov, A.V., Prozorov, L.B., Arustamov, A.E., Poluektov, P.P., Serebriakov, B.E., 1999, Safety assessment of bore-hole repositories for sealed radiation sources disposal, MRS Online Proc. Libr., 608, 141–146.

Ojovan, M.I., 2022, Challenges in the long-term behaviour of highly radioactive materials. Sustainability, 14, 2445

Ojovan, M.I., Steinmetz, H.J., 2022, Approaches to disposal of nuclear waste, Energies, 15, 20, 7804, Available at: https://doi.org/10.3390/en15207804

Ojovan, M.I., 2023, Nuclear Waste Disposal. Encyclopedia, 3, 2, 419-429. https://doi.org/10.3390/encyclopedia3020028

Pershukov, V., Artisyuk, V., Kashirsky, A., 2022, Paving the Way to Green Status for Nuclear Power. Sustainability, 14, 9339.

Pilania, R.K., Dube, C.L., 2023, Matrices for radioactive waste immobilization: a review, Front. Mater., Ceramics and Glass, 10, https://doi.org/10.3389/fmats.2023.1236470

Rohlig, K.J., 2022a, Disposal and other conceivable strategy ‘endpoints’ for different types of waste. In Nuclear Waste: Management, Disposal and Governance, IOP Publishing Ltd., Bristol, UK, Chapter 7; pp. 7.1–7.19.

Rohlig, K.J., 2022b, Geologic (‘deep’) disposal of high-level and other long-lived waste: Host rocks, concepts, current international status, In Nuclear Waste: Management, Disposal and Governance, IOP Publishing Ltd., Bristol, UK, Chapter 8, 8.1–8.25.

Sanders, M.C., Sanders, C.E., 2021, A world's dilemma 'upon which the sun never sets': The nuclear waste management strategy (part III), Australia, Belgium, Czech Republic, Netherlands, and Romania, Progress in Nuclear Energy, 142, 104014, https://doi.org/10.1016/j.pnucene.2021.104014

Swedish Radiation Safety Authority, 2025, Nuclear power, Available at: https://www.stralsakerhetsmyndigheten.se/en/areas/nuclear-power/

Tohver, H., Salupere, S., Jeltsov, M., 2025, Operational radioactive waste management strategies for small reactors in nuclear newcomer countries, Nuclear Engineering and Design, 443, 114327. https://doi.org/10.1016/j.nucengdes.2025.114327

UCS, 2019, Coal Power Impacts, Available at: https://www.ucs.org/resources/coal-power-impacts#:~:text=Coal%20impacts:%20water%20pollution,waterways%20and%20drinking%20water%20supplies.

Unokiwedi, O.P., Gao, J., Bethune, T., Awolayo, A.N., 2025, Deep geological repositories — A review of design concepts, near-field evolution, and their implications for nuclear waste containment, Journal of Environmental Radioactivity, 289, 107750, https://doi.org/10.1016/j.jenvrad.2025.107750

World Nuclear Association, 2025a, Physics of Uranium and Nuclear Energy, Available at: https://world-nuclear.org/information-library/nuclear-fuel-cycle/introduction/physics-of-nuclear-energy#:~:text=The%20total%20binding%20energy%20released,is%20about%2082%20TJ/kg

World Nuclear Association, 2025b, Total Operable Reactor Net Capacity, Available at: https://world-nuclear.org/nuclear-reactor-database/summary

CHAPTER 6

STRUCTURAL DESIGN AND ANALYSIS OF EXPOSED COLUMN BASE PLATE CONNECTIONS IN INDUSTRIAL STEEL BUILDING[1]

Günnur YAVUZ[2] , Pinar Salahaldin Hussein HUSSEIN[3]

1 This book chapter is based on a section of Pinar Salahaldin Hussein Hussein's master's thesis titled "Analytical Investigation of Column Base Plates Used in Steel Structures," completed under the supervision of Assoc. Prof. Dr. Günnur Yavuz.

2 Assoc.Prof. Dr., Konya Technical University, Faculty of Engineering and Natural Sciences, Department of Civil Engineering, ORCID:0000-0002-8725-7129

3 Asst.Lect., Northern Technical University, Polytechnic College Kirkuk, Construction and Building Techniques Department , Iraq, ORCID: 0000-0002-1489-0214

1. INTRODUCTION

In general, column base plate connections consist of a steel column, base plate, and anchor bolts. Column base plates are used as unstiffened base plates, but when the highest bending moment was required to transfer, the stiffened column base plate was used [1]. This connection type is the most important part of a steel structure, so it influences the total behaviour of structures. The column base plate connections have a complex behaviour because of many factors, such as existence of two different materials, like contact between steel and concrete. The complexity becomes so difficult when an additional component is added to the connection in order to increase rigidity [2].

When the exposed column base plate was laterally loaded, deformation in these connections was caused by rotations under bending moments and shear forces. Under lateral loading, the behaviour of this part of the connections was of great significance in the overall structural behaviour [3]. Previous studies present that the semi-rigid behaviour was shown in connections between the steel column and concrete foundation and in many situations extremely influenced the overall structural system [3-6].

Many researches about exposed column base plate connections show that when the exposed column base plate was a semi-rigid connection, the behaviour of frames subjected to significant lateral loads was more accurately represented. In the static analysis of frames, theoretical support conditions are usually taken as hinged or fixed. This simplification of using support conditions not only leads to the use of easier models, but also the codes actually promote their use [4].

In this study, the behaviours of five different column base plate connection models under axial and horizontal loads were examined by two stress types. First, support reactions of a steel industrial building were obtained by two-dimensional analysis in the SAP2000 program [7], and then by these support reactions, dimensions of the exposed column base plate were determined according to AISC (American Institute of Steel Construction) Base Plate and Anchor Rod Design Guide No. 1 [8]. The design guide includes design procedures for base plates under concentric compressive axial loads and under moments (small and large moments) effects and also includes anchor rod design for tension axial loads and shear loads. In this guide, the design procedure was presented for the W-section column base plate, but summary information about the design of base plates for rectangular hollow structural section (HSS) columns, round HSS columns, and pipe columns was given. Additionally, in Guide No. 1 there is no design method or information about stiffened column base plate connections. Hence, in this study, base plate dimensions were determined for the W section column-base plate, and this base plate dimensions were used for five different column base plate models for nonlinear finite element analysis purposes. Nonlinear finite element analyses of the models were performed using the Picard method. The connection models incorporated three column section types—W-sections, square HSS, and circular HSS—while variations in base plate thickness were considered and stiffeners were welded to selected configurations. From finite element analysis, two types of stress distributions on column base plate connection models and top column displacement were obtained and evaluated for two support types (rigid and hinged). In this study, the column base connection was designed to resist moments, so it models as rigid supports. In practise, because in some cases anchor bolts may not act as fully rigid, sometimes when a column base plate designed as a fixed support acts as a hinge support, therefore the changed column base plate behaviour was studied. For this purpose, the same column sections and base plate dimensions that were obtained in the case of fixed support were used with bolts modeled as a hinge supports.

2. TYPES OF COLUMN BASE PLATES

In general, there are two column base plate types: exposed column base plates and embedded column base plates [4]. In the exposed column base plate, a steel base plate is welded to the steel column end, and it is connected into the concrete block by anchor bolts to obtain a hinged situation to transfer axial compression, axial tension, and shear loads from the whole structure to the concrete block. Exposed column base plates can be especially used for steel industrial buildings [4]. An embedded column base plate contains steel columns embedded into a reinforced concrete block or in a grade beam. Embedded column base plates are especially used in office and other commercial structure applications[4]. In Figure 1, typical exposed and embedded column base plates are shown. In the exposed column base plate, bearing on the foundation in the compression case and tension case in the anchor rods are used to resist moment and axial loads, while shear in the anchor rods and friction between the steel base plate and foundation (concrete block) are used to resist shear forces [9]. In the embedded column base plate, the bearing of the column and the base plate against the concrete is used to resist moments, axial and shear forces [4]. The anchor rods have an important influence on the whole behaviour only in the case of shallowly embedded column bases used in a steel structure [4]. In AISC-Guide No. 1, there is no detailed design requirement about these types of connections. The embedded column base plates require the coordination of many construction trades so that they take more time in construction and are more expensive than exposed column base plates [9].

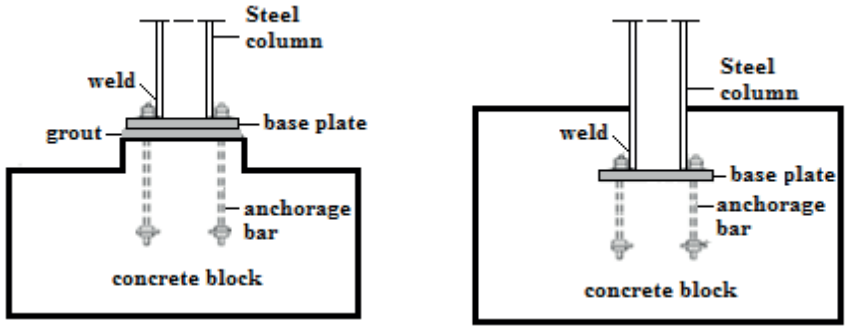

Exposed column base plate Embedded column base plate

Figure 1. Steel column base plate types

3. COLUMN BASE PLATE CONNECTION DETAILS OF A SINGLE STOREY STEEL INDUSTRIAL BUILDING

The column and beam sections of a single storey steel industrial building were selected as W18x119 (W460x177) (column depth d=18.97 in (482 mm), column flange width b_f =11.265 in (286 mm). Steel material Grade 36 was used; yield stress (F_y) equals to 36 ksi (244.8 MPa), and compressive strength for concrete block (f_c') equals 4 ksi (27.2 MPa). The applied load on the frame (without self-weight) and column and beams profile sections are shown in Figure 2 [10].

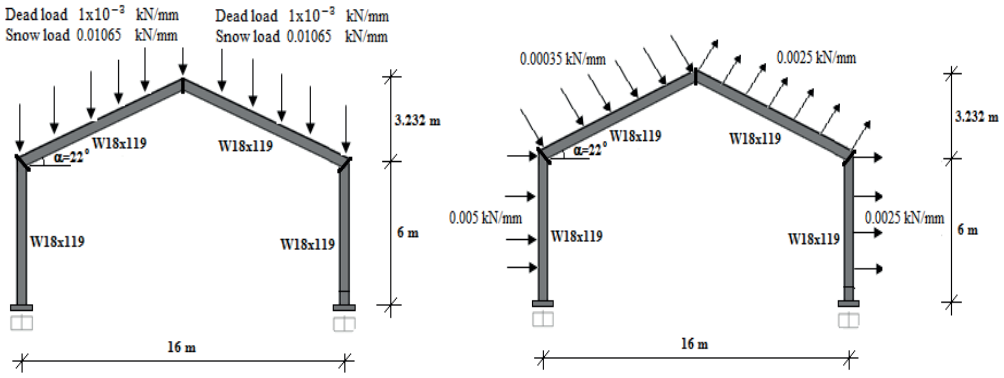

(a) (b)

Figure 2. Loads applied on industrial building (a) D: dead load, S: snow load, (b) W: wind load [11]

In the SAP2000 program, frame supports were assigned as fixed, and two-dimensional analysis was done. Load and Resistance Factor Design (LRFD) load combinations were used in analysis. The highest support reactions was achieved from "1.2D+1.6S+0.8W" load combination. According to analysis results, the highest support reactions values were M_u = -2350.279 kip.in (-265.55 kN.m), P_u = 39.076 kip (173.82 kN), and V_u = -22.136 kip (-98.466 kN). These support reactions were used to design the column base plate connections according to the LRFD method in AISC Base Plate and Anchor Rod Design Guide No. 1. In Table 1, the design procedure of a steel column-base plate under large moment effect was explained [12]. Also, force distribution under base plate in large moment case was given in Figure 3. The final details of steel column base plate connection are shown in Figure 4.

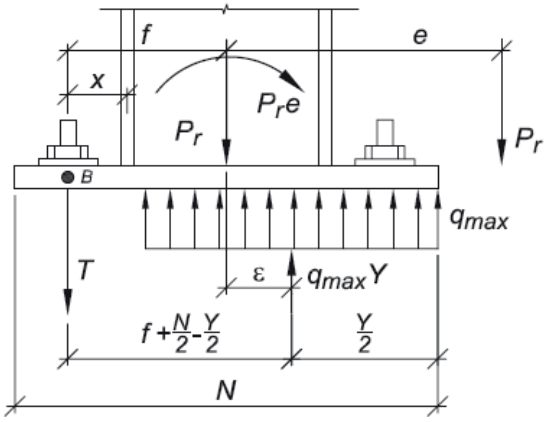

Figure 3. Force distribution under base plate in large moment case [8]

Table 1. Design of column base plate connection under large moment case

1) Trial dimensions

$N > d + 2\ (3\ in)$; 18.97+ 2*3 = 24.97 in (634.2 mm)

$B > b_f + 2\ (3\ in)$; 11.265 + 2*3 = 17.267 in (438.5 mm)

Take dimensions as; 30x25 in (762x635 mm)

2) Eccentricity comparison

$e = \frac{Mu}{Pu} = \frac{2350.279}{39.076}$ = 60.15 in (1527.81 mm)

$f_{p(max)} = \Phi c\,(0.85\,fc')\sqrt{\frac{A_2}{A_1}}$ = 0.65 *0.85*4 * 1 = 2.21 ksi (15.028 MPa)

$q_{(max)} = f_{p(max)} . B$ = 2.21 * 25 = 55.25 kip/in (9.675 kN/mm)

$e_{crit} = \frac{N}{2} - \frac{Pu}{2\,q_{max}} = \frac{30}{2} - \frac{39.076}{2*55.25}$ = 14.65 in (372.11 mm) → $e > e_{crit}$ (large moment)

3) Anchor bolt details

Assume that the anchor bolts edge distance is *2.5 in (63.5 mm)* therefore,

$f = \frac{N}{2} - 2.5 = \frac{30}{2} - 2.5 = 12.5\ in\ (317.5\ mm)$

$(f + \frac{N}{2})^2 \geq \frac{2\,Pu\,(e+f)}{q_{max}}$, $(f + \frac{N}{2})^2 = (12.5 + \frac{30}{2})^2 = 756.25\ in^2\ (487902\ mm^2)$

$\frac{2\,Pu\,(e+f)}{q_{max}} = \frac{2*39.076*(60.15+12.5)}{55.25} = 102.76\ in^2\ (66297\ mm^2) \rightarrow 756.25\ in^2 > 102.76\ in^2$

The condition is satisfied, so the base plate dimensions are true.

$Y = (f + \frac{N}{2}) \pm \sqrt{\left(f + \frac{N}{2}\right)^2 - \frac{2\,Pu\,(e+f)}{q_{max}}} = (12.5 + \frac{30}{2}) \pm \sqrt{\left(12.5 + \frac{30}{2}\right)^2 - \frac{2*39.076(60.15+12.5)}{55.25}}$

$= 27.5 + 25.56 = 53.06\ in\ (1347.7\ mm)$

$= 27.5 - 25.56 = 1.94\ in\ (49.3 mm)$

$T_u = q_{max}\,Y - P_u = (55.25*1.94) - 39.076 = 68.109\ kip\ (302.96\ kN)$

4) Base plate minimum thickness calculation : when $Y < m$

a) At bearing interface:

The calculation of m and n dimensions which shown in In Figure 4 .

$m = \frac{N - 0.95\,d}{2} = \frac{30 - (0.95*18.97)}{2} = 5.99\ in\ (152.1\ mm)$, $n = \frac{B - 0.8\,bf}{2} = \frac{25 - (0.8*11.265)}{2} = 7.994\ in\ (203.0\ mm)$

The maximum concrete bearing stress $f_{p(max)} = f_p$ = 2.21 ksi (15.028 MPa).

$tp_{(req)} = 2.11\sqrt{\frac{f_{p(max)}\,Y\,(m - \frac{Y}{2})}{Fy}} = 2.11\sqrt{\frac{2.21*1.94*(5.99 - \frac{1.94}{2})}{36}} = 1.63\ in\ (41.4\ mm)$

b) At tension interface:

$x = \frac{N}{2} - \frac{d}{2} + \frac{t_f}{2} - 2.5 = \frac{30}{2} - \frac{18.97}{2} + \frac{1.06}{2} - 2.5 =$ 3.545 in (90.04 mm)

$tp_{(req)} = 2.11\sqrt{\frac{T_u\,x}{B\,Fy}}$ $tp_{(gerekli)} = 2.11\sqrt{\frac{68.109*3.545}{25*36}} = 1.09\ in\ (27.7\ mm)$

c) Thickness control

$tp_{(req)} = 2.11\sqrt{\frac{f_{p(max)}\,Y\,(n - \frac{Y}{2})}{Fy}} = 2.11\sqrt{\frac{2.21*1.94*(7.994 - \frac{1.94}{2})}{36}} = 1.93\ in\ (49.0\ mm)$

According to the largest $tp_{(req)}$, use 2 in (50.8 mm) as a base plate thickness.

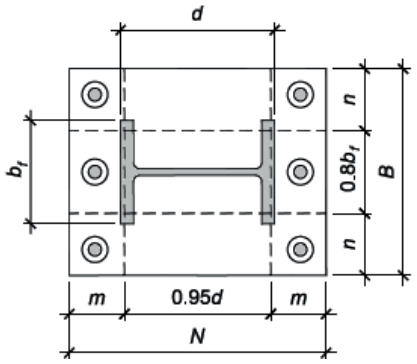

Plate dimensions : N ve B	(30x25) in (762x 635) mm
Plate edge distance: m,n	5.99 in(152.1 mm), 7.994 in(203 mm)
Anchor rods:	6 anchor rods 1 $^1/_4$ in (31.75 mm)
Rod hole diameter:	2 $^1/_{16}$ in (52.4 mm)
Column depth, d:	18.97 in (482 mm)
Column flange width, b_f:	11.265 in (286 mm.)
Base plate thickness, t:	2 in (50.8 mm)

Figure 4. Details of steel column-base plate connections

4. ANALYSIS OF STEEL COLUMN BASE PLATE CONNECTION MODELS

The determined column base plate connection details of a single storey industrial building were used in nonlinear finite element analysis. In this study, five types of column base plate model behaviours for bolts taken as rigid supports were obtained in the RFEM 5.05 program [13]. Then the bolts were taken as hinge supports in order to investigate the changes that occur in the column-base plate models and to estimate the difference in the behaviour between the rigid and hinged connections of all five models. Three types of column sections were selected to use in analysis; the selected column sections were sufficient in static analysis of industrial buildings. The column types that were used were W, square, and round hollow sections; the thickness of the base plate has been taken as 2 in (50.8 mm) as calculated in Table 1. The section properties of base plates and columns of analysed models are shown in Table 2.

Table 2. Section properties of the analysed models

Model No	Model type	Base plate		Column sections	
		Thickness (mm)	Stiffeners height, thickness (mm)	Section type	Dimensions (mm)
1	MW_1	50.8	-	W18x119	482x286
2	MW_2	25.4	-	W18x119	482x286
3	MS_3	50.8	300x20	W18x119	482x286
4	MSH_4	50.8	-	HSS 16x16x5/8	406.4x406.4x15.87
5	MRH_5	50.8	-	HSS 12.75x0.50	323.85x12.7

In the analyses, in addition to the use of three different column sections, a stiffened column base plate was also used, and in the other model, base plate thickness was reduced from that calculated according to AISC Guide No. 1-LRFD method (2 in (50.8 mm)) to 1 in (25.4 mm). Under the same load effect, nonlinear finite element analysis for five types of connections was performed in the program. For analysis, column height was taken as 39.37 in (1000 mm). In all five models, concrete block was modeled as a Winkler foundation type. The column base plate acted as a support to transfer building loads into a foundation. In this study, the column was bolted into bases by fixed supports, as that used in the industrial building, which carried lateral loads, so it must be resisting moments. But the actual column base plate connection behaviour may not act as a full rigidity. So, the same column and base plate dimensions were used with hinge supports (not resisting moment) to know how the stress distribution would be if the same column base connection details under the same forces applied were used. The five models were subjected to axial and horizontal loads. The axial load value was taken as 40 kip (177.92 kN), which was obtained from static analysis of the single storey building, and the lateral load was selected as 22.046 kip (100 kN) to show stress distributions according to these loads.

The Von Mises and Tresca stress distributions for each model were performed. There are many types of stresses in the analysis of steel structures, such as Von Mises, Tresca, Rankine, and Bach stresses. Often the Von Mises stress gives the best results in steel structures, and it is commonly used. In this study, because the Tresca stress was similar to the Von Mises stress and both are used for ductile materials, it is given beside the Von Mises stresses. Shape modification hypothesis is another name for Von Mises stress. These stress types assumed that when the shape-modifying energy exceeded an appointed limit, the material failed. When Von Mises stress was greater than the material yielding

stress, yielding was caused at that point. Tresca stress is also called maximum shear stress theory, and it assumes that the material fails when maximum shear stress is exceeded [13].

In the RFEM 5.05 program, the three-dimensional model of the column base plate connection was created. The base plate was modeled as 30x25 in (762x635 mm), and steel material A36 was selected. The yield stress of this material (F_y) value is 36 ksi (244.8 MPa), and Poisson's ratio is 0.3. The concrete compressive strength (f_c') has been taken as 4 ksi (27.2 MPa). For the column section, W18x119 was selected, and the column height considered has been taken as 39.37 in (1000 mm), and the anchor bolt hole diameter was 2 $^1/_{16}$ in (52.4 mm). Meshing the model was done by choosing the mesh length of 0.7 in (17.8 mm); also, the bolt mesh size was entered, with a node circular radius of 3.5 in (88.9 mm), a target finite element length, an inner of 0.14 in (3.56 mm), and an outer of 0.70 in (17.8 mm). In model three, the stiffener edge mesh was entered as a node rectangular side length of 0.5 in (12.7 mm) and a target finite element length (inner) of 0.14 in (3.56 mm) (Figure 5). The top of the column was covered by a rigid plate, and axial and lateral loads were applied to the center of a rigid plate; then nonlinear finite element analysis by the Picard method was performed.

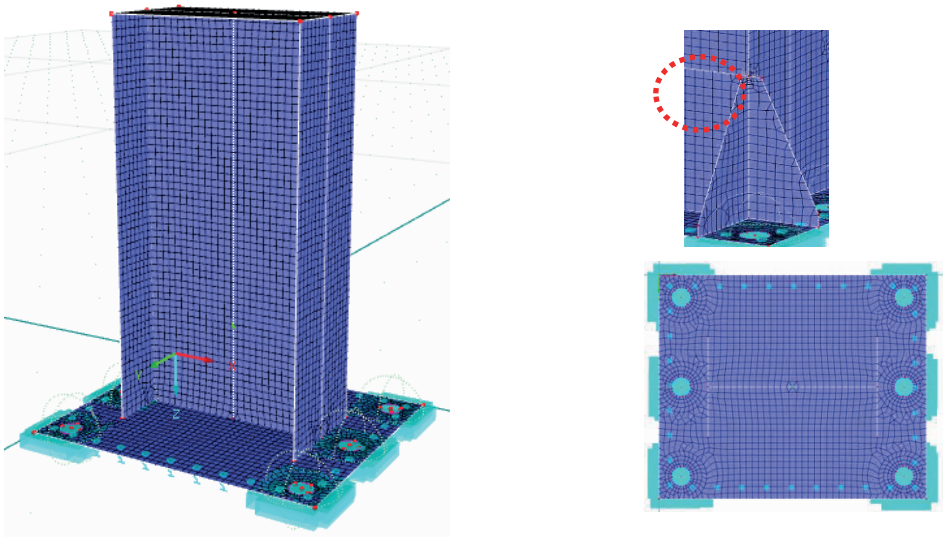

Figure 5. The details on meshing column base plate connection

4.1 Results

4.1.1 Rigid column base plate connections

Von Mises and Tresca stress distributions on five types of column base plate connection models where bolts were modeled as rigid supports, as shown in Figures 6 and 7, respectively. The column top displacement was measured, and the smallest value was obtained when the stiffened column section was W18X119 and the base plate thickness was 2 in (50.8 mm) (MS_3 model), and the largest displacement value was obtained when the column section was W18X119 and the base plate thickness was 1 in (25.4 mm) (MW_2 model).

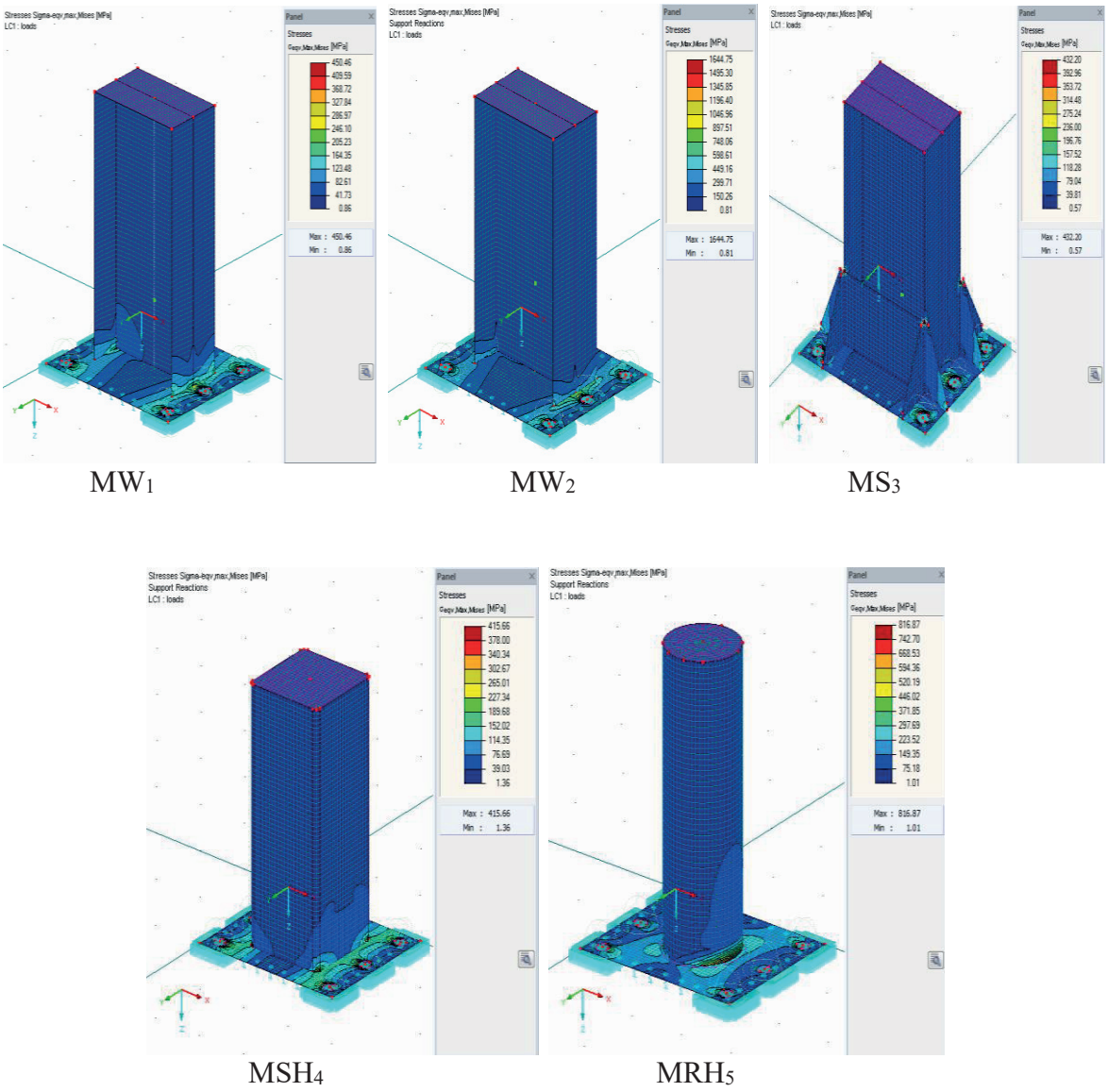

Figure 6. Von Misses stress distributions for five column base plate connection models (rigid bolts)

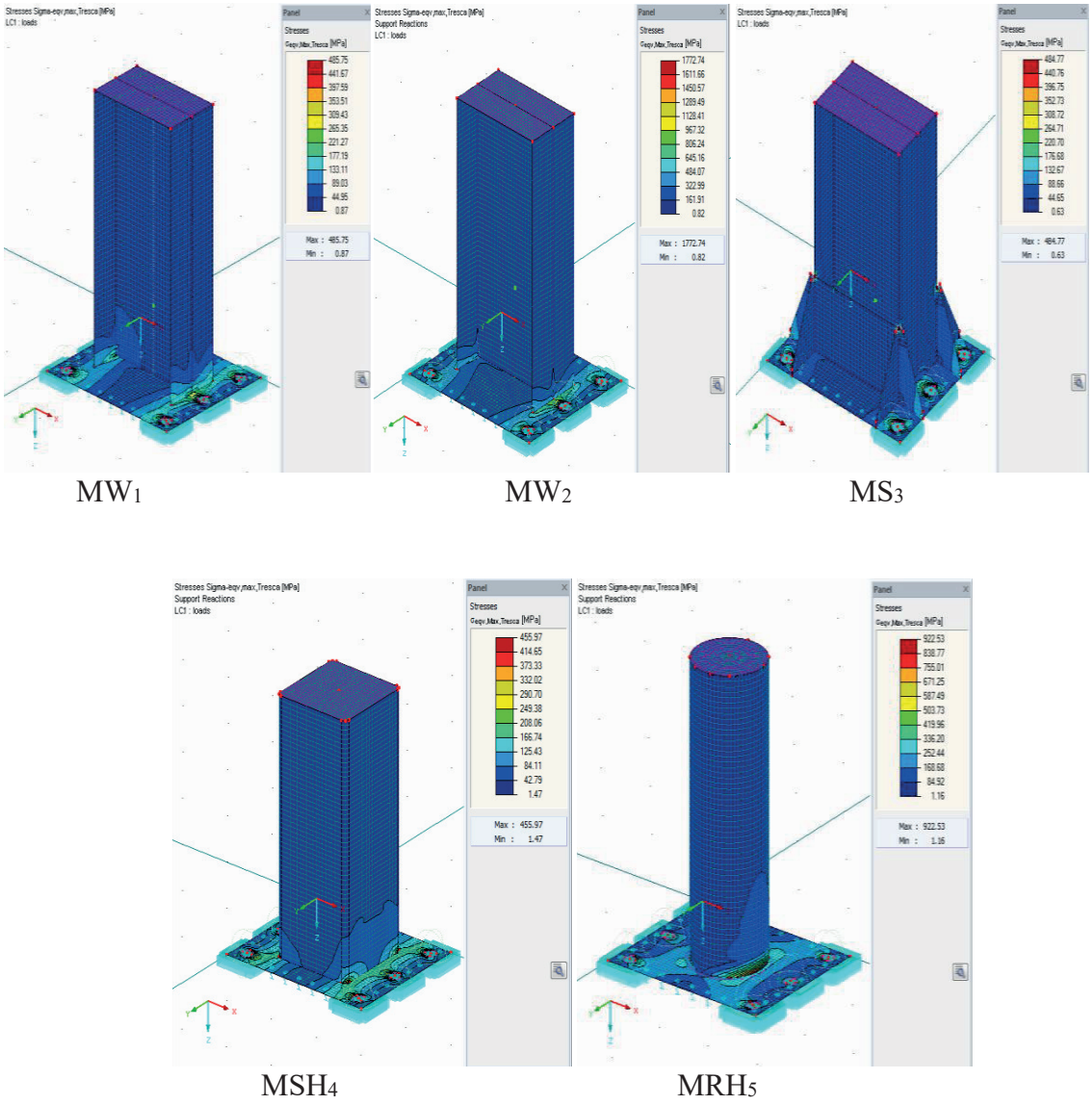

Figure 7. Tresca stress distributions for five column base plate connection models (rigid bolts)

Von Mises and Tresca stress distributions on three-column section types were less than the stress distribution over the base plates. The stress distributions were generally concentrated around the anchor bolts as expected. The Von Mises and Tresca stress distributions on the base plates for five connection models were shown in Figures 8 and 9, respectively.

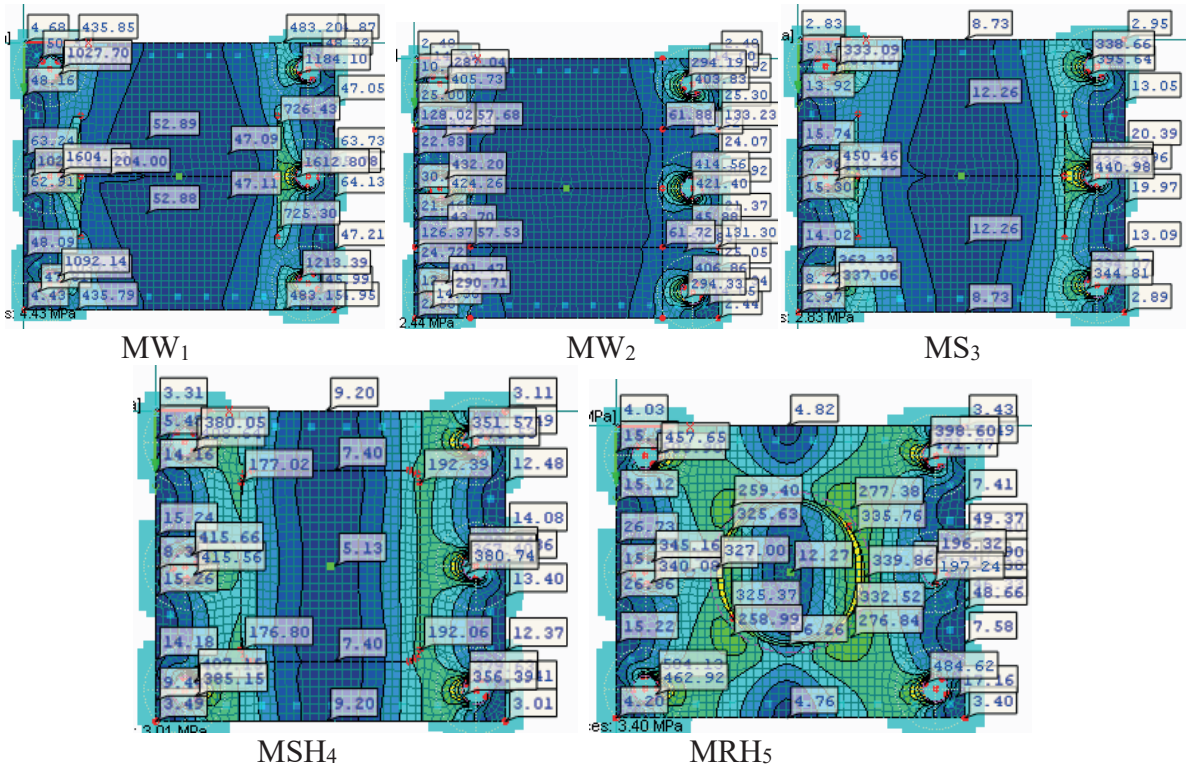

Figure 8. Von Misses stress distributions on the base plate for five models (rigid bolts)

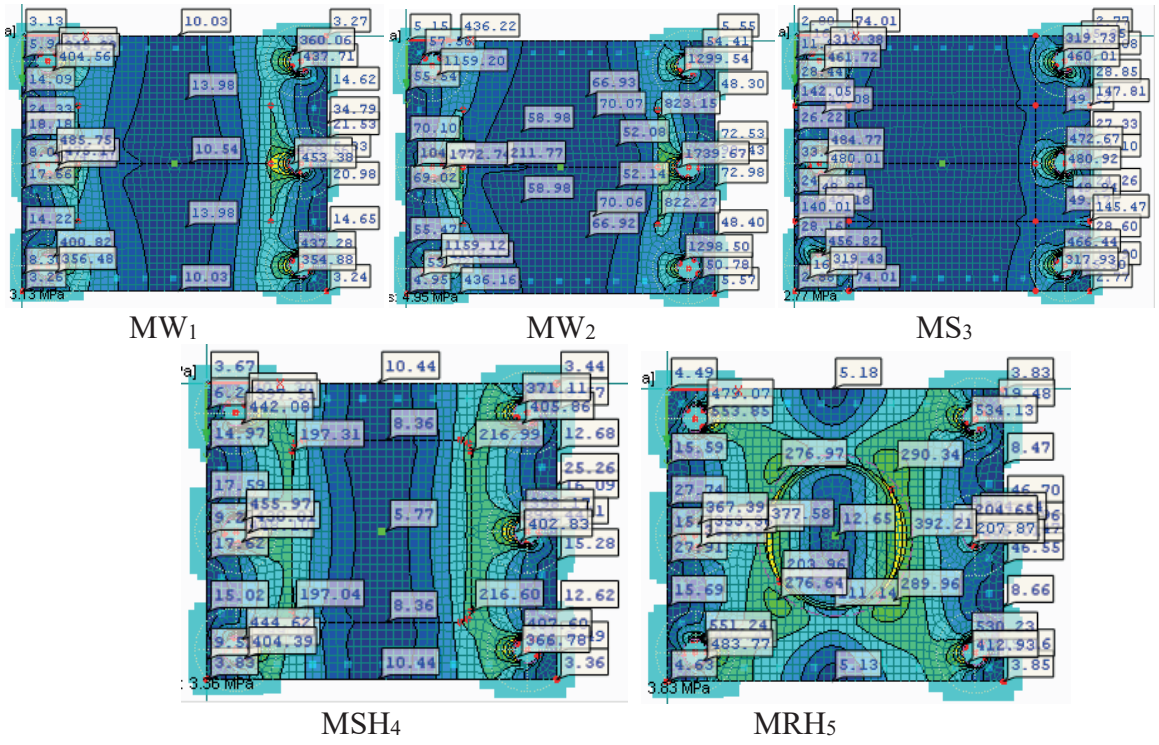

Figure 9. Tresca stress distributions on the base plate for five models (rigid bolts)

4.1.2 Hinged column base plate connections

The industrial building in this study was resisting lateral loads, so in this type of buildings, the column base plate should be fixed in order to resist axial forces, shear forces, and moments. The actual behaviour of the column base connection may not be fully rigid. To investigate the changing in the behaviour of column base plate models from rigid to hinged support, the bolts were modeled as hinge supports. In this case, the same column base model details were used. The Von Mises and Tresca stress distributions on five different types of models are shown in Figures 10 and 11, respectively. Also, the column top displacement values were achieved from analysis results; the smallest value was obtained when the stiffened column section was selected as W18X119 and the base plate thickness was 2 in (50.8 mm) (MS_3 model), and the largest displacement value was obtained when the round HSS12.75x0.50 column section and base plate thickness were 2 in (50.8 mm) (MRH_5 model).

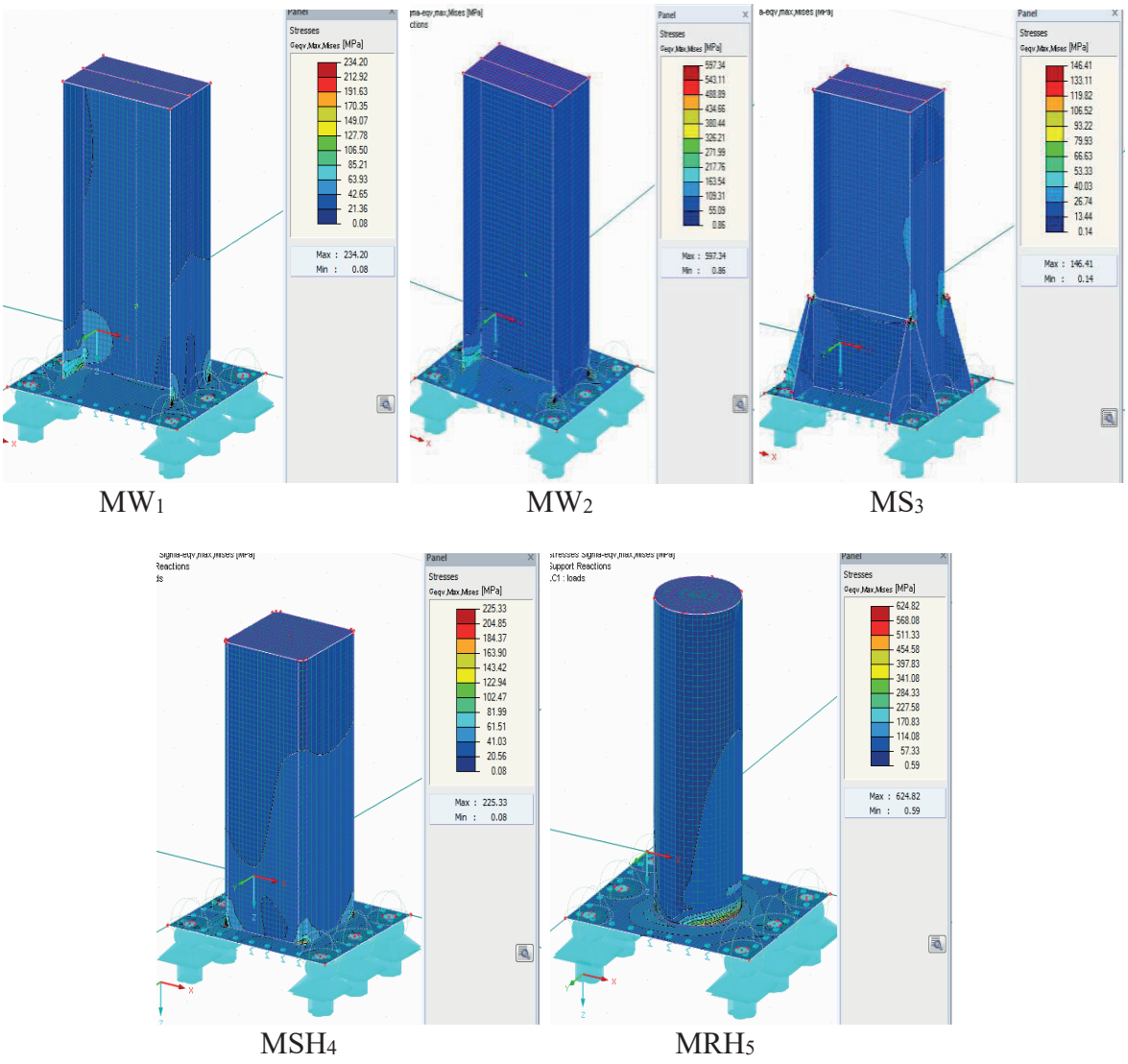

Figure 10. Von Misses stress distributions for five column base plate connection models (hinge bolts)

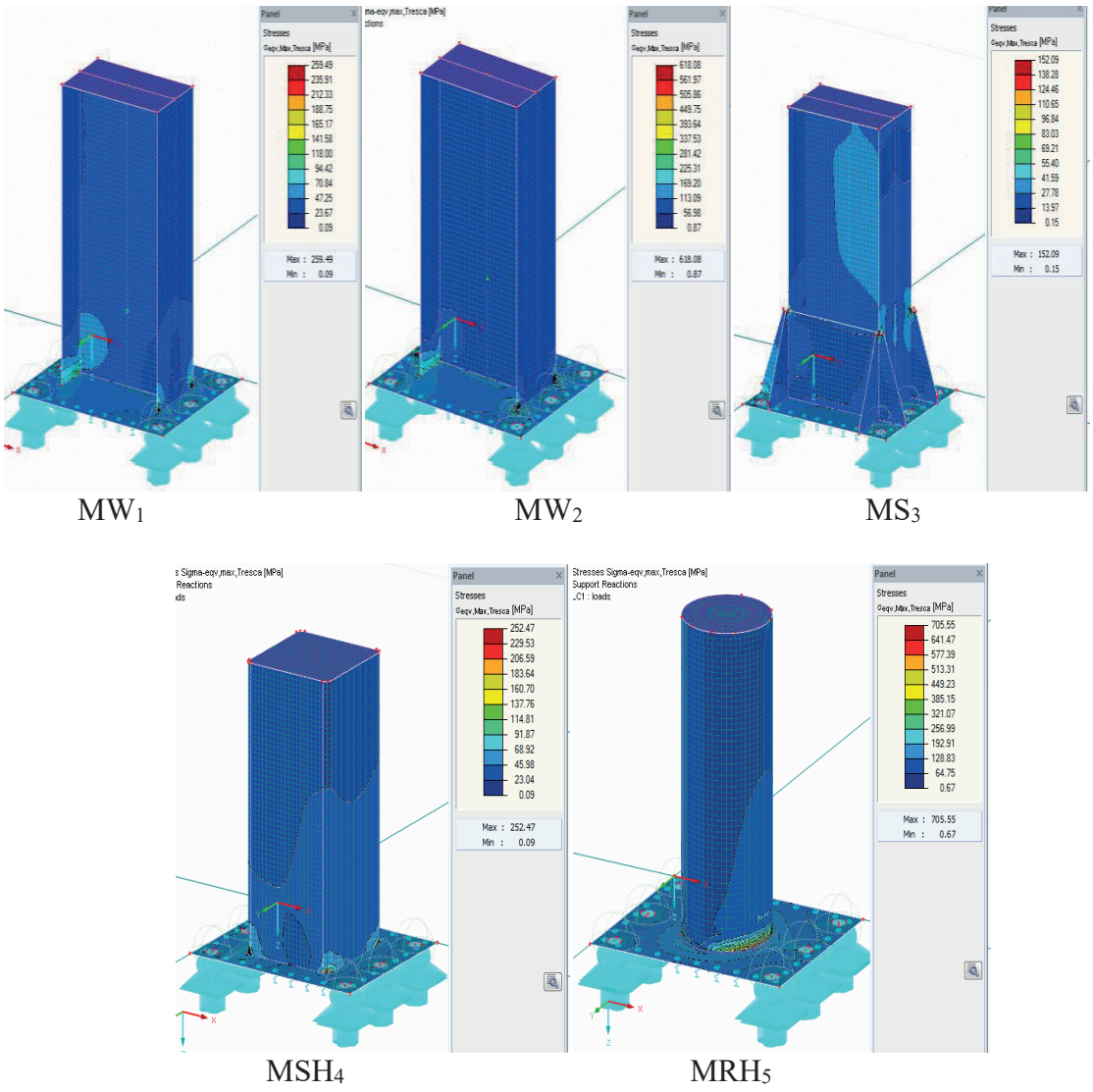

Figure 11. Tresca stress distributions for five column base plate connection models (hinge bolts)

The Von Mises and Tresca stress distributions on base plates for five connection models were shown in Figures 12 and 13, respectively. The critical stresses that occurred in column base connections were shown in the contact area between the column and base plate or around anchor bolts over the base plates. Here, stress distribution was less than in models in which rigid bolts were used.

In Table 3, due to applied axial and lateral loads, upper-end column displacement and ratios, and maximum Von Mises and Tresca stress values and ratios for all models were given. In Tables 4 and 5, the two types of stress distribution shapes for five models were explained as stress distribution behaviour on column sections and over the base plates for rigid and hinged bolts, respectively.

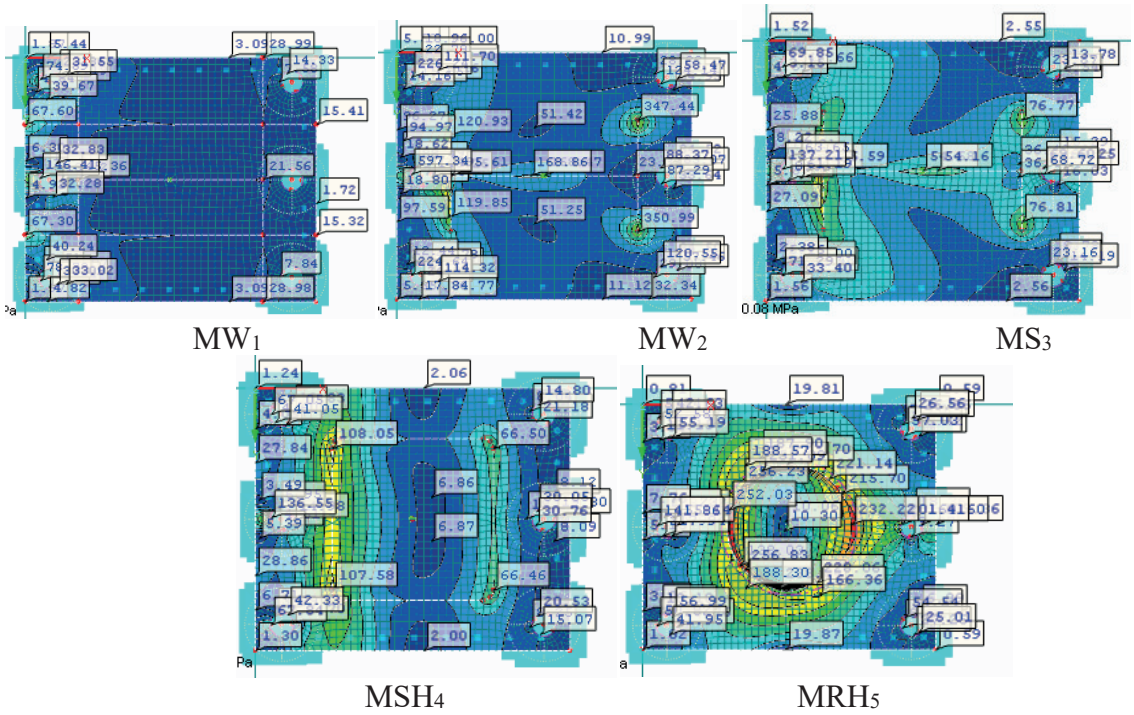

Figure 12. Von Misses stress distributions on base plate for five models (hinge bolts)

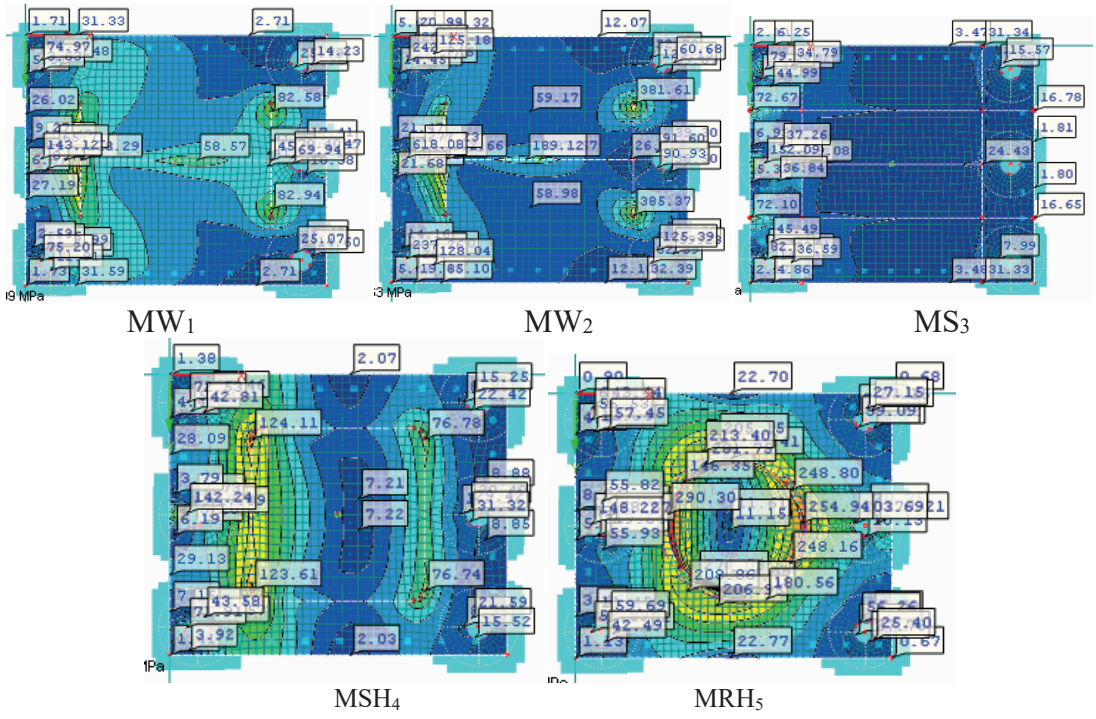

Figure 13. Tresca stress distributions on base plate for five models (hinge bolts)

Table 3. Comparison of analysed models

Model type	Column top lateral displacement (mm)		Displacement ratio		Max. Von Misses stresses (MPa)		Stresses Ratio		Max. Tresca stresses (MPa)		Stresses Ratio	
	rigid	*hinge*	*rigid*	*hinge*	*rigid*	*hinge*	*rigid*	*hinge*	*rigid*	*hinge*	*rigid*	*hinge*
MW_1*	5.3	43.9	1.00	1.00	450.46	234.20	1.00	1.00	485.75	259.49	1.00	1.00
MW_2	25.9	46.4	4.89	1.06	1644.75	597.34	3.65	2.55	1772.74	618.08	3.65	2.38
MS_3	3.2	43.3	0.60	0.99	432.20	146.41	0.96	0.63	484.77	152.09	0.99	0.59
MSH_4	6.6	44.3	1.25	1.01	415.66	225.33	0.92	0.96	455.97	252.47	0.94	0.97
MRH_5	13.2	55.5	2.49	1.26	816.87	624.82	1.81	2.67	922.53	705.55	1.90	2.72

* Reference column base plate connection model

Table 4. Column base plate models behaviour according to two stresses types (rigid supports)

Model type	Stresses distribution on the column section	Von Mises stress distribution heights on the column (mm)	Tresca stress distribution heights on the column (mm)	Stresses distribution over the base plate
MW_1	Stress distribution at the lower end of the column and along the column flange line	177.8	195.58	Moderate stress distribution along the column flanges and around the anchor bolts
MW_2	Less stress distribution at the column lower end and along the column flange line	106.68	106.68	Less distribution on column flanges and around anchor bolts
MS_3	Stress distribution on small portion of stiffeners	No stress on the column	No stress on the column	Most distribution was around anchor bolts
MSH_4	Stress distribution at the column lower end and along the column–base plate contact line	231.14	213.36	More distribution on base plate
MRH_5	Less stress distribution at the column lower end	373.38	320.04	Excessive stress distribution on the base plate

The largest value of top column lateral displacement in rigid column base connections was obtained in model two, in which a W-profile column section was used and the base plate thickness was 1 in (25.4 mm), whereas in hinged column base connections, it was obtained in model five, in which a round HSS12.75x0.50 column section was used and the base plate thickness was 2 in (50.8 mm) (Table 3). But the smallest value of top column lateral displacement in rigid and hinged column base connections was obtained in model three (MS_3), in which a stiffened W column section was used and the base plate thickness was 2 in (50.8 mm). The W column sections and base plate thickness of 2 in (50.8 mm) (MW_1 model) were selected as the reference model, and the other column base models were compared with it. The largest values of Von Mises and Tresca stresses in rigid column base connections were obtained in model two (MW_2), in which the W profile column section was used and the base plate thickness was 1 in (25.4 mm), whereas in hinged column base connections, they were obtained in model five (MRH_5), in which the round HSS12.75x0.50 column section was used and the base plate thickness was 2 in (50.8 mm). The smallest stress values in rigid column base connections

were obtained in model four (MSH_4), in which square HSS16x16x5/8 was used and the base plate thickness was 2 in (50.8 mm). In Tables 4 and 5, the Von Mises and Tresca stress distributions over column sections and the base plates for five column base plate connection models and for two support types (rigid and hinged support) were displayed. Von Mises and Tresca stress distributions were similar, but the stress distribution height over the column section was different; this height was larger in the case of using hinged supports. The more stresses distributed on the base plate were shown when square and round HSS column sections were used (MSH_4 and MRH_5 models).

Table 5. Column base plate models behaviour according to two stresses types (hinge supports)

Model type	Stresses distribution on the column section	Von Mises stress distribution heights on the column (mm)	Tresca stress distribution heights on the column (mm)	Stresses distribution over the base plate
MW_1	Stress distribution in whole column and concentrated in the lower end corner	1000	1000	Moderate distribution on column flanges less distribution around anchor bolts
MW_2	Less stress distribution in column lower end	177.8	195.58	Less distribution on column flanges and around anchor bolts
MS_3	Stress distribution on the column and on the stiffeners	1000	1000	Less stress distribution on the plate and around anchor bolts
MSH_4	Stress distribution on the column and concentrated in the lower end corner	693.42	640.08	More distribution on base plate
MRH_5	stress distribution on the column and concentrated in the column lower end	586.74	533.4	Too much distribution on base plate

5. CONCLUSIONS

In this study, a column base plate design was performed according to AISC Base Plate and Anchor Rod Design Guide No. 1—LRFD method. In the studied steel industrial building, large moment cases have been obtained. In this study, for the W section column, rectangular base plate dimensions according to Guide No. 1—the LRFD method—were determined. These base plate dimensions were used in different cases, such as with different column sections and in the case of reduced base plate thickness in the column base plate connection. The anchor bolts are modeled as rigid and hinged supports to estimate the intermediate behaviour between these support types of column base plate connections. For this purpose, in the first model (MW_1), the Von Mises stresses in actual must be between 450.46 MPa and 234.20 MPa and the column lateral displacement between 5.3 mm and 43.9 mm. The Von Mises and Tresca stresses were obtained from nonlinear finite element analysis; the two stress distributions were similar, but the stress values were different. In this study, the Tresca stress values on five column base plate models for two support types were greater than the Von Mises stress values. When hinged supports were used, the stresses on the connection were less, but column lateral displacements were greater than those values that were obtained in the case of rigid supports. The three column sections used in finite element analysis were sufficient, but in model two (MW_2), when base plate thickness was reduced to 1 in (25.4 mm), the column base plate was not

sufficient, and large values of stresses and displacements were obtained. In the first three models (MW_1, MW_2, and MS_3), in which the column section was W, the best behaviour was achieved in the stiffened column base plate connection. In other models (MSH_4, MRH_5) in which column sections are used as HSS sections, the best behaviour is obtained in square HSS section columns. When comparing the value of top column displacements of all five models, the least top column displacement was shown in the W section column with stiffened base plate model MS_3. According to the stresses and column top lateral displacement values, which were obtained from finite element analysis, the base plate thickness was one of the effective parameters in column base plate connections. Although the best results were obtained in stiffened column base plate connections, in AISC Guide No. 1, there are no calculation details about these connection types. Also, the least information about the design of base plates for rectangular and round hollow structural section columns and pipe columns was given.

NOTATIONS

A1 : Area of base plate
A2 : Maximum area of the portion of the supporting surface that is geometrically similar to and concentric with the loaded area
B : Base plate width
b_f : Column flange width
d : Overall column depth
D : Dead load
e : Eccentricity
e_{crit} : Critical eccentricity
f : Distance from the column face to the resultant compressive force on the compression side of the base plate.
f_c' : Concrete compressive strength
F_y : Base plate or anchor bolts yield strength
f_p : Bearing stress between plate and concrete
M_u : Factored bending moment
m : Cantilever length of the base plate in the direction of bending
n : Cantilever length of the base plate perpendicular to the axis of bending
N : Base plate length
P_u : Factored axial force
P_r : P_u changed from the original work by Drake and Elkin
q_{max} : Maximum bearing force
S : Snow loads
T :Tension force
T_u : Factored tension forces
$t_{p(req.)}$: Minimum plate thickness
t_f : Column flange thickness
V_u : Factored shear force
W : Wind load
X : Eccentricity from the column (or base plate) centerline to the resultant concrete bearing force
Y : Bearing length
φ : Strength reduction factor for bearing

6. REFERENCES

[1] Moore, D.B., Wald, F., editor (2003). Design of structural connections to Eurocode 3 –frequently asked questions. Building Research Establishment Ltd, Watford. Project Continuing Education in Structural Connections, No. CZ/00/B/F/PP-134099, Leonardo Da Vinci, Programme.

[2] Shafieifar, M.R., Khonsari, S.V. (2012). Studying the behaviour of base plates with high degree of rigidity. In Proceedings of the 15th World Conference on Earthquake Engineering. Lisbon, Portugal.

[3] Melenciuc, S.C., Ştefancu, A.I., Budescu, M. (2011). Experimental studies on the behavior of steel column base connections. Bulletin of the Polytechnic Institute of Iaşi, 57(3), 149–156.

[4] Grauvilardell, J. E., Lee, D., Hajjar, J. F., Dexter, R. J. (2005). Synthesis of design, testing and analysis research on steel column base plate connections in high-seismic zones (Structural Engineering Report No.ST-04-02). Department of Civil Engineering, University of Minnesota, USA.

[5] Hamizi, M., Hannachi, N.E. (2007). Evaluation by a finite element method of the flexibility factor and fixity degree for base plate connections commonly used. Strength of Materials, 39(6), 588–599.

[6] Stamatopoulos, G.N., Ermopoulos, J.C. (2011). Experimental and analytical investigation of steel column bases. Journal of Constructional Steel Research, 67(9), 1341–1357. https://doi.org/10.1016/j.jcsr.2011.03.007.

[7] Computers and Structures Inc. (2015). SAP2000-Version 15: Integrated finite element analysis and design of structures—Basic analysis reference manual. Computers and Structures Inc. Berkeley, CA. USA.

[8] Fisher, J.M., Kloiber, L.A. (2010). AISC Steel Design Guide No. 1: Base plate and anchor rod design (2nd ed., 2nd printing). American Institute of Steel Construction, USA.

[9] Kingsley, A. M. (2005). Experimental and analytical investigation of embedded column base connections for concrete-filled high-strength steel tubes, Master's thesis, University of Washington, USA.

[10]Hussein, P.S.H. (2015). Analytical investigation of column base plates used in steel structures, Master's thesis, Selçuk University, Konya, Turkey (In Turkish).

[11]Hussein, P.S.H., Yavuz, G. (2019). An Investigation of Base Plate Connections of a Steel Industrial Building Having Different Column Cross-Sections. Natural and Engineering Sciences, 4(2), 84-91. https://doi.org/10.28978/nesciences.567052

[12]Yavuz, G., Hussein, P.S.H., (2015). Designing the Column Base Plate of a Steel Industrial Building according to AISC-LRFD Method. International Journal of Natural and Engineering Sciences, 9 (2), 7-16.

[13]Dlubal Software (2015). RFEM 5.05: Spatial models calculated according to the finite element method—Program description, Dlubal-company, Tiefenbach, Germany.

CHAPTER 7

ASSESSMENT OF SOLAR ENERGY POTENTIAL IN EDUCATIONAL BUILDINGS USING OPENSTREETMAP-BASED 3D BUILDING MODELS

Ahmet USLU[1]

1 Dr. Öğr. Üyesi; Kütahya Dumlupınar Üniversitesi Tavşanlı Meslek Yüksekokulu Mimarlık ve Şehir Planlama Bölümü. ahmet.uslu1@dpu.edu.tr ORCID No: 0000-0001-8745-423X

Introduction

Increasing energy demand on a global scale, dependence on fossil fuels, and the negative effects of climate change have made energy efficiency and the use of renewable energy sources mandatory in the construction sector (Pérez-Lombard et al., 2008; Rey-Hernández et al., 2018; Ahmed Ali et al., 2020). The construction sector constitutes a significant share of global energy demand and greenhouse gas emissions, thereby playing a decisive role in environmental impacts. These environmental impacts have led to the necessity of sustainable building design as a major research area (Li et al., 2019; Min et al., 2022; Olabi et al., 2022). Among different renewable and clean energy sources, solar energy is the most accessible and applicable in buildings (Fremouw et al., 2019; Liu et al., 2023). Especially the roofs and facades of buildings directly contribute to energy production in urban areas by offering large areas for solar panels (Redweik et al., 2013; Reffat & Ezzat, 2023; Xu et al., 2025). Educational buildings; It is one of the most ideal building types for the use of solar energy because its energy needs are concentrated during daylight hours and it has large roof surfaces (Ascione et al., 2017). In addition, educational buildings play an important role in making sustainability practices visible and increasing social awareness thanks to their public nature (Ascione et al., 2017; Altassan, 2023). In this context, evaluating the solar energy potential of educational buildings is of strategic importance both environmentally and pedagogically (Hong et al., 2014; Ascione et al., 2017).

Recent advancements in digital design and simulation tools allow for environmental performance analyses of buildings to be conducted right at the design stage (Marzouk, 2022; Kante et al., 2024). Early stage analyses enable the environmental impacts of design decisions to be identified in advance, paving the way for the development of more economical and efficient solutions (Nguyen et al., 2014). Within this context, digital tools support architects and engineers by visualizing technical data, helping them make more accurate and informed design decisions (Nguyen et al., 2014). Autodesk Forma, a cloud-based platform, enables environmental analysis based on the surrounding urban context from the earliest stages of design (Autodesk, 2025). Such tools offer significant advantages as a decision support mechanism in the pre-feasibility and concept design stages (Autodesk, 2025). OpenStreetMap OSM is an open source platform that grows with user contributions, offering a large database of building boundaries and basic building attributes (Neis & Zielstra, 2014). This 3D building data is widely used in city-scale solar energy potential studies. Research in the literature indicates that OSM data can be effectively used in urban analysis and 3D city model production, offering sufficient accuracy, particularly for early-stage assessments (Fan, 2014; Alhamwi et al., 2017; Brovelli & Zamboni, 2018; Hadimlioglu & King, 2019; Nusantara & Dewanto, 2020; Katal et al., 2022; Biljecki et al., 2023; Demirel et al., 2025). Research in the literature has focused on estimating solar energy potential by utilizing technologies such as Geographic Information Systems (GIS) (Biljecki vd., 2015; Kara & Koç, 2020; Idrovo-Macancela vd., 2025; Hafizh & Prarikeslan, 2025), 3D CAD-based modeling (Beltran-Velamazan vd., 2021; Shirinyan & Petrova-Antonova, 2024), UAV Photogrammetry (Baghani, 2023; Mitka, 2023; Yadav et al., 2024; Ekawita et al., 2025; Jaczewska et al., 2025) and LiDAR (Adjiski et al., 2023; Waqas et al., 2023; Ni et al., 2024; Soha et al., 2024; Mahir et al., 2025; Rees et al., 2025). These studies have been conducted at the level of residential buildings, neighborhoods, or entire cities. 3D CAD-based modeling software, LiDAR, photogrammetry, and remote sensing techniques have been used to extract the 3D geometric characteristics of buildings in the study area.

In this study, it was aimed to evaluate the potential of solar energy in educational buildings by using the integration of OpenStreetMap-based 3D building models and Autodesk Forma software. The study examines the roof and facade-based solar energy analyses of the Tavşanlı Hayme Ana Vocational and Technical Anatolian High School building, aiming to assess the applicability of combining open-source data and early design tools. In this respect, the study offers a method proposal that can be used in the early design phase for educational buildings and similar public buildings.

MATERIALS AND METHODS

Study Area

For this study, a school campus was chosen as the application area. School buildings are considered quite appropriate building types in assessing solar energy potential due to their usually large and uninterrupted roof surface area, operating hours that predominantly fall within daytime, and public accessibility. In addition, educational buildings are spread all over the city and possess similar spatial characteristics; therefore, the results of such an analysis can also be generalized to other schools. The Tavşanlı Hayme Ana Vocational and Technical Anatolian High School, selected as the study area, is situated at a high topographic location and is surrounded by limited urban development. This minimizes shading effects, allowing the solar energy potential of roof and façade surfaces to be assessed more accurately. In this context, the school site presents a highly representative case study area for solar energy potential analyses, in terms of both technical suitability and sustainability, as well as educational awareness. The geographic location of the study area is illustrated in Figure 1.

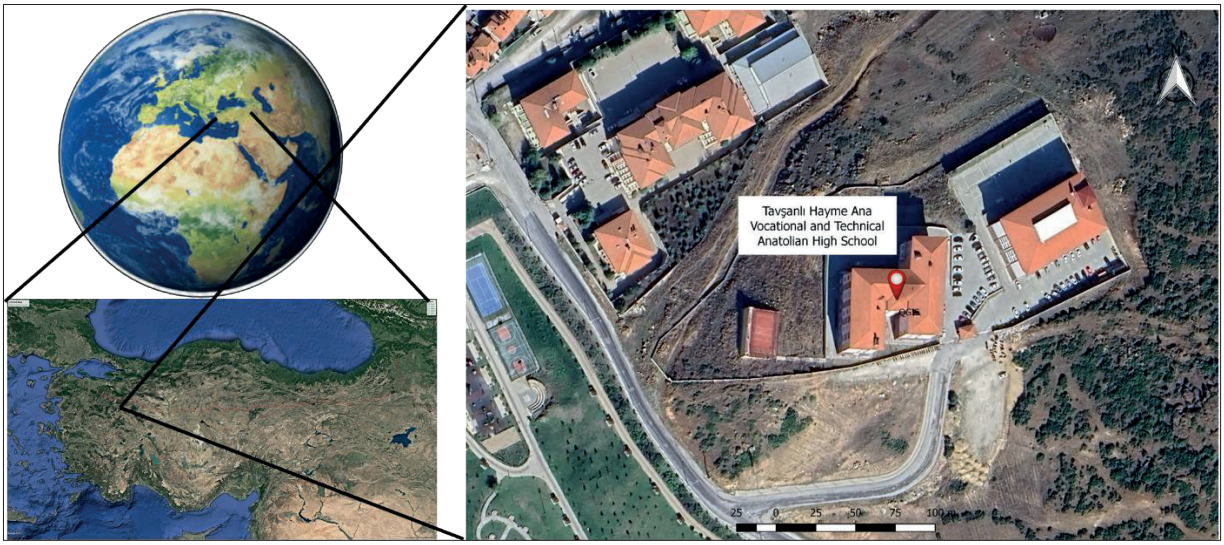

Figure 1. Geographical location of the study area.

Study Materials

The three-dimensional (3D) building models of the study area at the LOD-1 (Level of Detail 1) were derived from crowdsourced geospatial data available on the OpenStreetMap (OSM) platform. Based on the building footprints and structure height information found in the OSM database, a simple mass model representing the general geometry of the building has been created. This model does not take into account the roof slopes and the detailed architectural elements. However, it does provide enough geometric precision for the surface-based analyses when the latter are aimed at the assessment of solar energy potential at the urban scale. In this connection, the entire building envelope which consists of the roofs and all vertical facades of the 3D model created for the study was analyzed to find out the solar photovoltaic energy potential. Hence, the 3D building models were imported into the Autodesk Forma software. This software provides a wide range of tools for conducting solar and energy analysis on 3D geometries and it is also the most common software used for the preliminary urban scale solar radiation and shadowing analyses.

Methodology

Using the OpenStreetMap platform, the LOD-1 three-dimensional (3D) building model of the study area was created. The building heights and footprints provided in the OSM database were analyzed in the context of this framework to produce a simple mass model. This model was designed specifically for surface-based analyses that attempt to evaluate the potential of urban solar photovoltaics. The LOD-1 model consists of a 3D representation of the basic building geometry. It

lacks detailed features such as roof slopes or architectural elements, but it is still precise enough for urban energy potential assessments. Hence, the sunlight and energy analysis features of Autodesk Forma were used to compute the building surfaces in terms of sunshine duration, total incident solar radiation, and shading effects. During the analysis stage, surface-based solar radiation calculations were carried out taking into consideration the location characteristics of the building (latitude, longitude), the orientation (aspect) and slope of the surfaces, and the effects of shading. Consequently, the results obtained were evaluated in order to reveal the annual total solar photovoltaic energy potential of the building; thus, the suitability levels of façade surfaces to produce solar energy were analysed comparably. The obtained results were evaluated to determine the building's annual total solar photovoltaic energy potential. This allowed for a comparative analysis of the suitability of the façade surfaces for solar energy generation. This approach enabled the generation of numerical and visual outputs for assessing the solar energy potential of educational buildings. Figure 2 shows the method of studying.

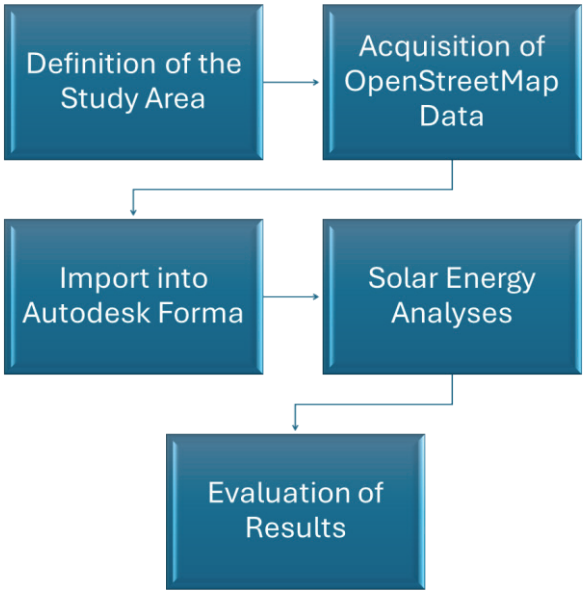

Figure 2. The framework of the proposed method

RESULTS

Since OSM data does not include detailed information on roof geometry, the building's roof was assumed to be flat. The analyses were performed via Autodesk Forma, evaluating both the roof surfaces and the cardinal building facades (north, south, east, and west).

Results of the OSM-Based 3D Building Model

Based on building footprints and height information derived from OSM data, a 3D mass model was created. The surroundings were included in the model to correctly represent the urban context for the simulations. This approach allows for the assessment of the solar energy potential not just at the single building scale but also considering the environmental interactions.

Figure 3. OSM-based 3D Building Model of the Study Area

The building in the study area is at a high topographical position on a hill and does not have any dense development around its vicinity. This spatial situation constitutes a considerable advantage when evaluating its potential for solar energy. Analysis of the OSM-based 3D building model shows the shading effects of surrounding structures to be very limited. Facades and roof surfaces are largely exposed to direct solar radiation, especially during noon time. In contrast to areas with high urban density, there is the possibility of receiving more homogeneous and higher insolation values. The fact of buildings being on a high hill has a positive effect on the angle of incidence of solar radiation and allows longer sunshine during the day, notably on south, east, and west facades. Furthermore, the open topography minimizes the shading effect of natural elements (trees, small constructions) in the far environment. Results indicated that the location of educational buildings in open and high elevation areas provides an extremely favorable environment for roof and facade-based solar energy applications.

Analysis of Solar Energy Potential for Rooftop Areas

Roof pitch and orientation information is not consistently available for every building in the OSM database. For this reason, in the study, roof surfaces were assumed to be flat, and solar gain and shading analyses were performed based on the building's upper levels. In the study, the roof surface of the structure was created using a 3D building model based on OSM data and analysed assuming a flat roof. Solar radiation analyses conducted using Autodesk Forma software indicate that the roof surfaces are exposed to direct sunlight throughout the year and that shading effects are minimal. This situation results from the building’s location on a high hill and the lack of dense development in its surroundings. The open topography ensures an uninterrupted horizon, increasing the duration of sunlight on the roof surfaces, particularly during the morning and evening hours.

The solar radiation values generated by Autodesk Forma visually illustrate the potential of the roof surfaces (Figure 4). Areas with high potential are shown in yellow tones, medium-potential areas in orange tones, and low-potential areas in brown tones. The roof surface exhibits a homogeneous solar exposure profile throughout the year. Especially at midday, the roof surface reaches its maximum radiation value. The annual average solar radiation values calculated for the roof surfaces of the study area are presented in Table 1.

Table 1. Annual total and average solar radiation values calculated for roof surfaces

Study Area	Roof Area (m^2)	Annual Total Solar Energy (kWh)	Annual Average Solar Energy (kWh/m^2)
Tavşanlı Hayme Ana Vocational and Technical Anatolian High School	1.431,00	2.430,000	1.698,00

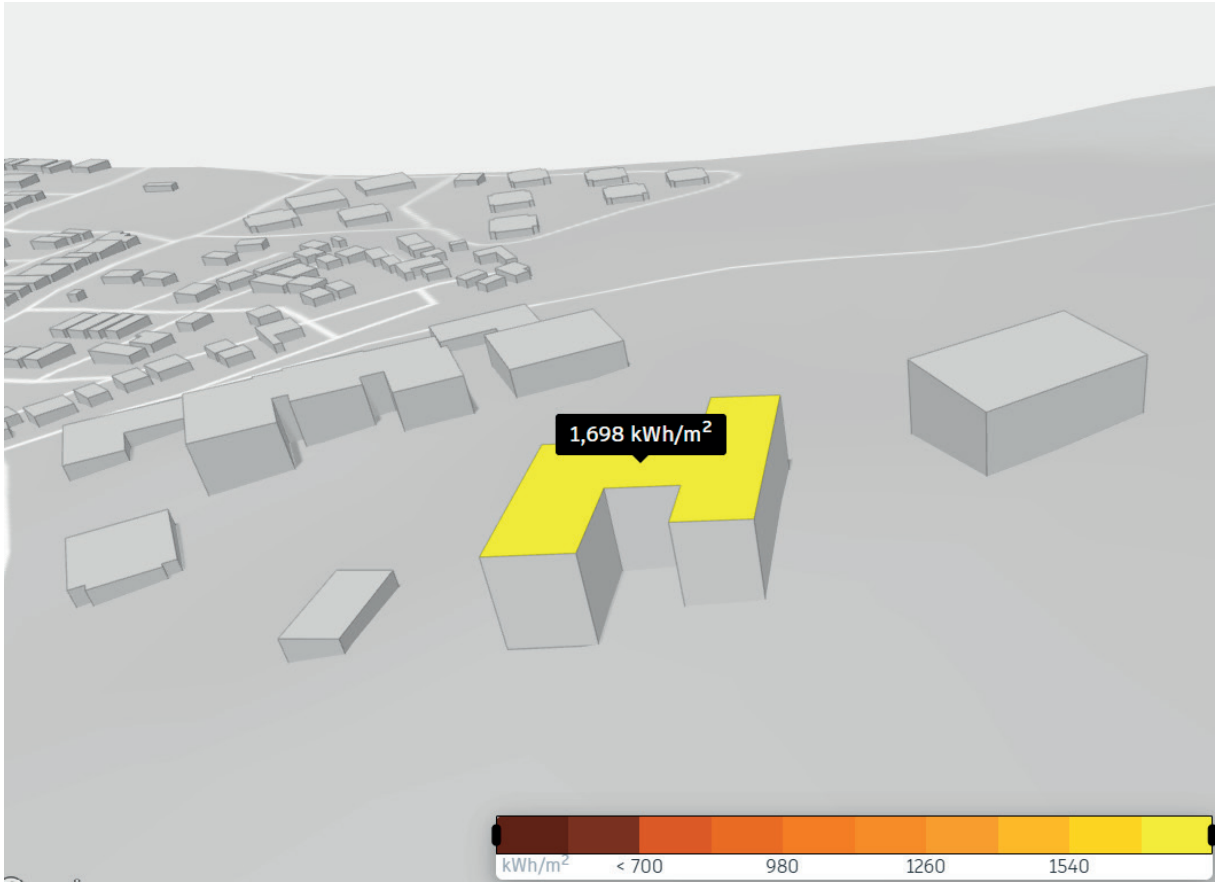

Figure 4. Solar energy potential of the roof surfaces in the study area

Analysis of Solar Energy Potential for Vertical Facades

The building facades were analyzed according to their orientations (north, south, east, and west) using Autodesk Forma software. The location of the workspace on the hilltop and the absence of dense development in the surrounding area increase the exposure of the facades to solar radiation. However, differences in orientation lead to significant variations in the total energy potential of the facades. The solar radiation values generated by Autodesk Forma visually illustrate the potential distribution of the facades according to their orientations. Areas with high potential are indicated in yellow tones, areas with medium potential in orange tones, and areas with low potential in brown tones (Figure 5, 6) The rooftop and facade solar potentials show that the roof surfaces have better and more homogenous energy potential than all other building envelopes. The roof receives direct solar radiation all year round without being subjected to shading. So, it becomes the main residential area for PV systems. The south facade represents the second-best solar energy potential after the roof and is a suitable area, particularly for BIPV (Building Integrated Photovoltaics). East and west facades are in medium level positions regarding annual total energy potential, though they are subjected to high radiation during morning and afternoon hours. These facades have a complementary potential compared to roofs and south facades. The north facade has the lowest energy potential because of its short sun duration and is considered an area of low priority for PV systems. Supported visualizations with a color scale

rapidly provide a clear overview of these differences and visually illustrate the energy potential variations both for roofs and facades due to orientation and topographic positioning.

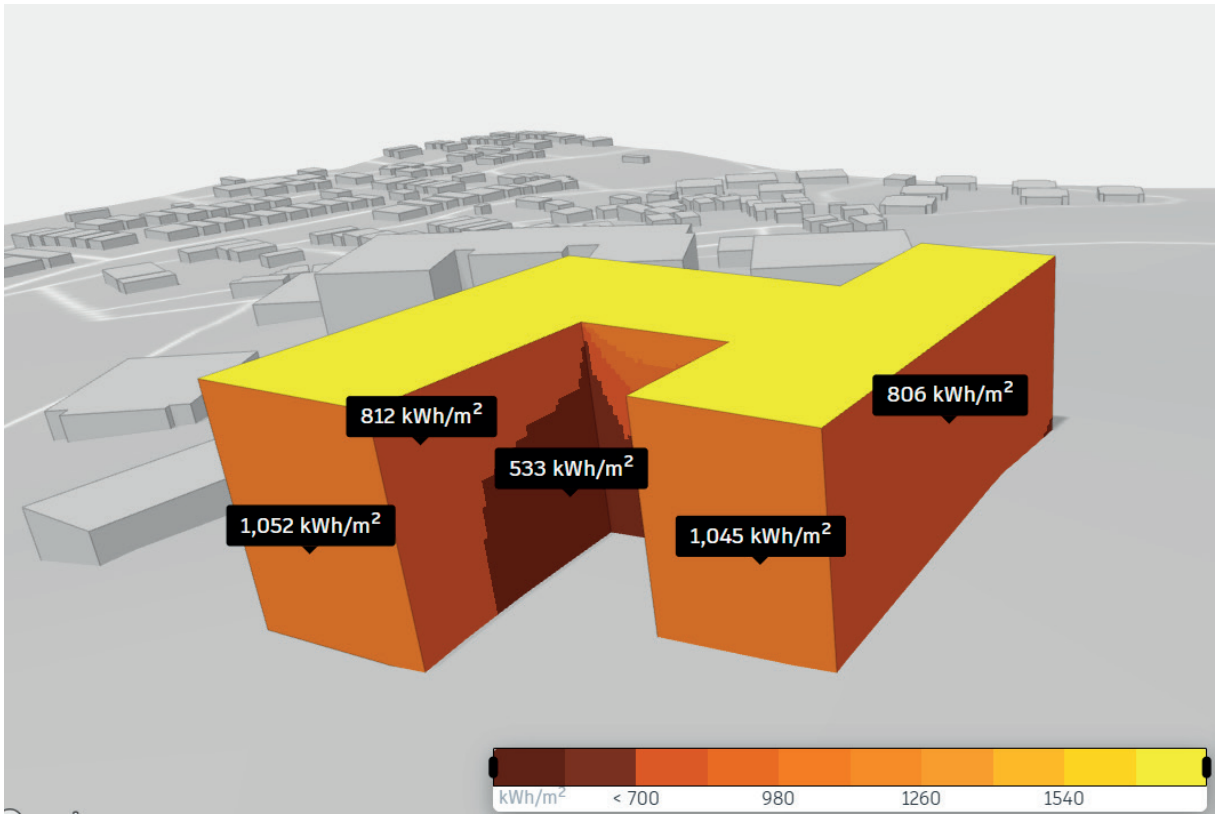

Figure 5. Southeast perspective of the study area

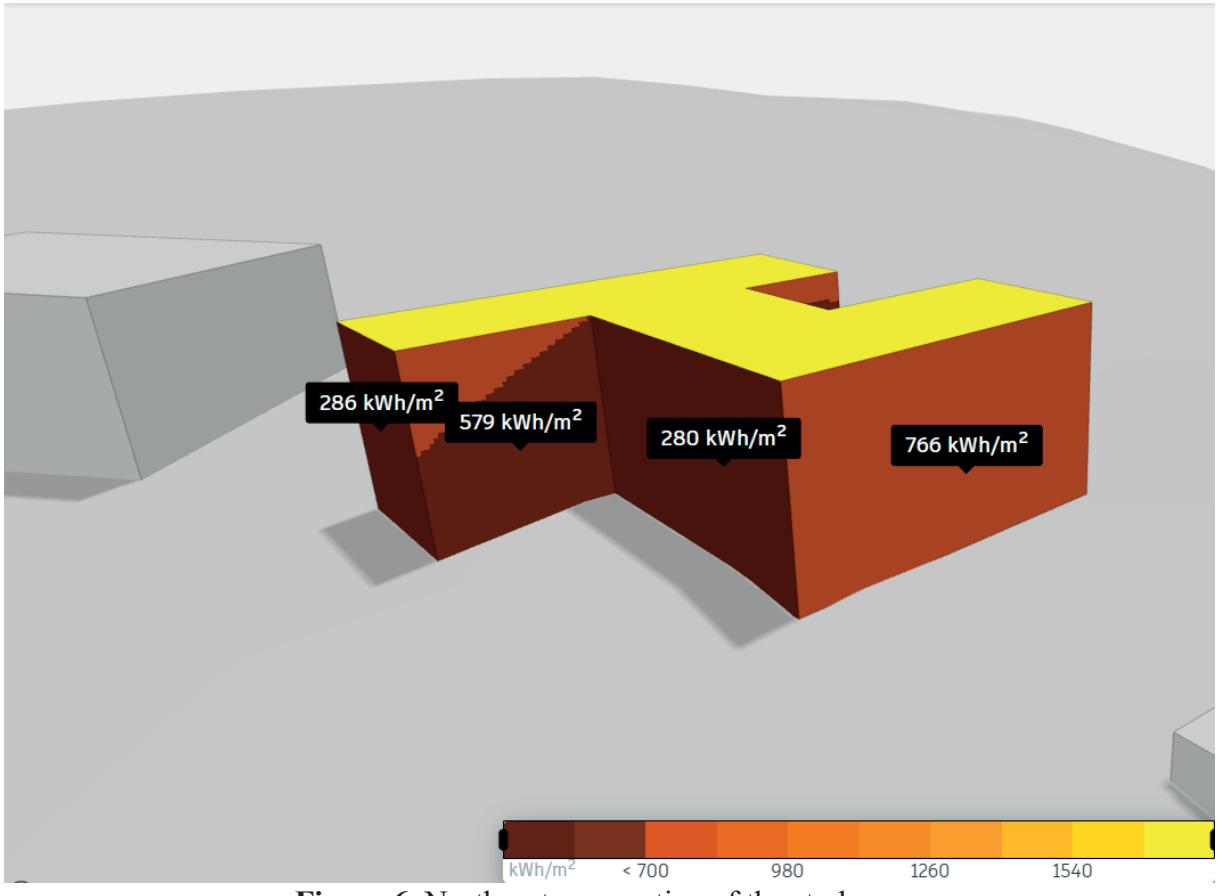

Figure 6. Northeast perspective of the study area

South-facing facades benefit from the advantage of their elevated position, receiving sunlight for longer periods throughout the day and offering the highest energy potential among all facades. The unobstructed topography allows the east and west facades to capture direct solar radiation during the morning and afternoon periods. Nevertheless, their cumulative annual energy yield remains lower than that of the rooftop surfaces. Despite the positive influence of the topography, the north facades exhibit limited potential in terms of solar exposure duration and radiation values. Table 2 shows a comparison of the solar energy potential of roofs and facades.

Table 2. Comparative Table of Roof and Facade Solar Energy Potential

Surface Type	**Orientation**	**Average Annual Solar Radiation (kWh/m²/year)**	**Relative Energy Potential**
Roof (flat)	-	1.698,00	Very high
Facade	South	1.052,00	High
Facade	East	806,00	Medium
Facade	West	932,00	Medium
Facade	North	280,00	Low

CONCLUSION AND DISCUSSION

In this study, the solar energy potential of Tavşanlı Hayme Ana Vocational and Technical Anatolian High School was analysed using Autodesk Forma, based on a 3D building model derived from OpenStreetMap (OSM). The analyses revealed how rooftop and facade surfaces exhibit specific energy distribution patterns influenced by orientation, shading effects, and topographic positioning. Studies addressing the usability of open-source spatial data (specifically OpenStreetMap) in early-stage energy analyses reveal that OSM-based 3D building models provide sufficient accuracy in representing mass and environmental context (Alhamwi et al., 2017; Hadimlioglu & King, 2019; Nusantara & Dewanto, 2020; Katal et al., 2022; Demirel et al., 2025). In this study as well, the 3D building model generated using OSM data provided a reliable foundation, particularly for shading and orientation analyses. As frequently emphasized in the literature, it has been identified that the roof surfaces have higher and more homogeneous solar energy potential than the facades (Wendel et al., 2017; Schiefelbein et al., 2019; Demirel et al., 2025). Assuming flat roofs, the results obtained in this study also confirm that the roof surfaces are subjected to high annual solar radiation and therefore should be considered as priority surfaces where photovoltaic systems could be installed. Similarly, the findings are supportive of literature reports that Autodesk Forma and similar early design tools can be effectively used in decision support before detailed engineering calculations have been conducted (Demirel et al., 2025). The location of the study area on a hilltop and the low-density development in its surroundings minimized shading effects, allowing the roof's solar potential to reach its maximum. The facades exhibit varying energy potentials depending on their orientation. Among those, the south facade has the highest potential after the roof, while the east and west facades have a medium potential, and the north facade presents low potential. This situation indicates that a roof-focused strategy should be prioritized in PV system design for educational buildings, with facades serving a complementary function.

This research proposes a rapid and systematic approach to solar energy planning in educational buildings, highlighting the significance of a PV placement strategy that integrates both roof and facade components. Nonetheless, the study has certain limitations, including the restricted detail of OSM data regarding roof slopes and features, as well as the hypothetical consideration of actual PV efficiency and atmospheric conditions. It is expected that analyses supported by field measurements and actual PV performance data in the future will increase the accuracy of the results. Another limitation of this study is that roof surfaces were assumed to be flat. In future studies, modelling

detailed roof geometries using CAD-based (Shirinyan & Petrova-Antonova, 2024), LiDAR (Yilmaz & Uysal, 2017) or photogrammetric data (Ekawita et al., 2025)[1] will enable more accurate calculations of building-based solar energy potential. One of the novel contributions presented in this study is that it shows very clearly the effect of topographical location. While the majority of studies in the literature have focused on highly urban-dense areas, this present study indicates that locations on hilltops and open areas for educational buildings minimize shading effects and increase roof and facade potential. In this respect, the present study contributes to the limited number of studies underlining topography as one of the most important parameters in solar energy analyses and extends this discussion specifically to educational buildings. The conclusion is that the PV layout strategy in educational buildings considers the whole roof and facade with the goal of making sustainable design choices in regard to solar energy efficiency.

REFERENCES

Adjiski, V., Kaplan, G., & Mijalkovski, S. (2023). Assessment of the solar energy potential of rooftops using LiDAR datasets and GIS-based approach. *International Journal of Engineering and Geosciences, 8*(2), 188–199.

Ahmed Ali, K., Ahmad, M. I., & Yusup, Y. (2020). Issues, impacts, and mitigations of carbon dioxide emissions in the building sector. *Sustainability*, *12*(18), 7427.

Alhamwi, A., Medjroubi, W., Vogt, T., & Agert, C. (2017). OpenStreetMap data in modelling the urban energy infrastructure: a first assessment and analysis. *Energy Procedia*, *142*, 1968-1976.

Altassan, A. (2023). Sustainable integration of solar energy, behavior change, and recycling practices in educational institutions: a holistic framework for environmental conservation and quality education. *Sustainability*, *15*(20), 15157.

Ascione, F., Bianco, N., De Masi, R. F., Mauro, G. M., & Vanoli, G. P. (2017). Energy retrofit of educational buildings: Transient energy simulations, model calibration and multi-objective optimization towards nearly zero-energy performance. *Energy and Buildings*, *144*, 303-319.

Autodesk. (2025). *Autodesk Forma: Environmental analysis documentation*.

Baghani, A. (2023). Assessment of rooftop solar power potential in rural areas using UAV photogrammetry and GIS. *Renewable Energy Research and Applications, 4*(2), 251-258.

Beltran-Velamazan, C., Monzón-Chavarrías, M., & López-Mesa, B. (2021). A method for the automated construction of 3D models of cities and neighborhoods from official cadaster data for solar analysis. *Sustainability*, *13*(11), 6028.

Biljecki, F., Stoter, J., Ledoux, H., Zlatanova, S., & Çöltekin, A. (2015). Applications of 3D city models: State of the art review. *ISPRS International Journal of Geo-Information, 4*(4), 2842–2889.

Biljecki, F., Chow, Y. S., & Lee, K. (2023). Quality of crowdsourced geospatial building information: A global assessment of OpenStreetMap attributes. *Building and Environment*, *237*, 110295.

Brovelli, M. A., & Zamboni, G. (2018). A new method for the assessment of spatial accuracy and completeness of OpenStreetMap building footprints. *ISPRS International Journal of Geo-Information*, *7*(8), 289.

Demirel, H., Koçyiğit, A., Alpagut, B., & Muhcu, D. (2025). Evaluating the solar energy potential for Positive Energy Districts (PED) through advanced 3D Geographic Information System (GIS) analysis. *Open Research Europe*, *5*, 81.

Ekawita, R., Almadi, I. F., & Yuliza, E. (2025). Investigating rooftop solar energy potential in coastal area with unmanned aerial vehicle technology. *Journal of Energy Systems*, *9*(1), 1-11.

Fan, H., Zipf, A., Fu, Q., & Neis, P. (2014). Quality assessment for building footprints data on OpenStreetMap. *International Journal of Geographical Information Science*, *28*(4), 700-719.

Fremouw, M., Bagaini, A., & De Pascali, P. (2020). Energy potential mapping: Open data in support of urban transition planning. *Energies*, *13*(5), 1264.

Hadimlioglu, I. A., & King, S. A. (2019). City maker: reconstruction of cities from openstreetmap data for environmental visualization and simulations. *ISPRS International Journal of Geo-Information*, *8*(7), 298.

Hafizh, S., & Prarikeslan, W. (2025). *High-Resolution Rooftop Solar PV Potential Assessment using Open-Source Remote Sensing Data and Cloud Computing: A Case Study in Padang Utara Subdistrict*. Inderaja, 19(2), 90–100.

Hong, T., Koo, C., Kwak, T., & Park, H. S. (2014). An economic and environmental assessment for selecting the optimum new renewable energy system for educational facility. *Renewable and Sustainable Energy Reviews*, *29*, 286-300.

Idrovo-Macancela, A., Velecela-Zhindón, M., Barragán-Escandón, A., Zalamea-León, E., & Mejía-Coronel, D. (2024). *GIS-based assessment of photovoltaic solar potential on building rooftops in equatorial urban areas*. Heliyon, 11(1), e41425.

Jaczewska, P., Sybilski, H., & Tywonek, M. (2025). Assessment of the Solar Potential of Buildings Based on Photogrammetric Data. *Energies*, *18*(4), 868.

Kante, M., Pattanaik, A., & Moharana, B. R. (2024). An Insight of Digital Technology's Role in the Solar Energy Sector and Its Implications for Sustainable Energy Generation. In *Digital Technology Enabled Circular Economy* (pp. 1-19). CRC Press.

Kara, F., & Koç, A. (2020). Kentsel alanlarda çatı üstü güneş enerjisi potansiyelinin CBS ile analizi. *Gazi Üniversitesi Fen Bilimleri Dergisi, 33*(2), 412–425.

Katal, A., Mortezazadeh, M., Wang, L. L., & Yu, H. (2022). Urban building energy and microclimate modeling–From 3D city generation to dynamic simulations. *Energy*, *251*, 123817.

Li, Y. L., Han, M. Y., Liu, S. Y., & Chen, G. Q. (2019). Energy consumption and greenhouse gas emissions by buildings: A multi-scale perspective. *Building and Environment*, *151*, 240-250.

Liu, K., Xu, X., Zhang, R., Kong, L., Wang, W., & Deng, W. (2023). Impact of urban form on building energy consumption and solar energy potential: A case study of residential blocks in Jianhu, China. *Energy and Buildings*, *280*, 112727.

Mahir, I. H., Bachour, D. A., Abedrabboh, K., Perez-Astudillo, D., & Al Fagih, L. (2025). Processing airborne LiDAR point cloud for solar cadasters: A review. *Applied Energy*, *382*, 125325.

Marzouk, O. A. (2022). Facilitating digital analysis and exploration in solar energy science and technology through free computer applications. *Engineering Proceedings*, *31*(1), 75.

Min, J., Yan, G., Abed, A. M., Elattar, S., Khadimallah, M. A., Jan, A., & Ali, H. E. (2022). The effect of carbon dioxide emissions on the building energy efficiency. *Fuel*, *326*, 124842.

Neis, P., & Zielstra, D. (2014). Recent developments and future trends in volunteered geographic information research: The case of OpenStreetMap. *Future intern*

Nguyen, A. T., Reiter, S., & Rigo, P. (2014). A review on simulation-based optimization methods applied to building performance analysis. *Applied energy*, *113*, 1043-1058.

Ni, H., Wang, D., Zhao, W., Jiang, W., Mingze, E., Huang, C., & Yao, J. (2024). Enhancing rooftop solar energy potential evaluation in high-density cities: A Deep Learning and GIS based approach. *Energy and Buildings*, *309*, 113743.

Nusantara, G. C., & Dewanto, B. G. (2020). Analisis Potensi Tenaga Surya Pada Permodelan Bangunan Tiga Dimensi Berdasarkan Data Open Street Map (Studi Kasus: Universitas Gadjah Mada Yogyakarta). *Elipsoida: Jurnal Geodesi dan Geomatika*, *3*(01), 38-45.

Olabi, A. G., & Abdelkareem, M. A. (2022). Renewable energy and climate change. *Renewable and Sustainable Energy Reviews*, *158*, 112111.

Pérez-Lombard, L., Ortiz, J., & Pout, C. (2008). A review on buildings energy consumption information. *Energy and buildings*, *40*(3), 394-398.

Redweik, P., Catita, C., & Brito, M. (2013). Solar energy potential on roofs and facades in an urban landscape. *Solar energy*, *97*, 332-341.

Rees, G., Hebryn-Baidy, L., & Good, C. (2025). Estimating the Potential for Rooftop Generation of Solar Energy in an Urban Context Using High-Resolution Open Access Geospatial Data: A Case Study of the City of Tromsø, Norway. *ISPRS International Journal of Geo-Information*, *14*(3), 123.

Reffat, R. M., & Ezzat, R. (2023). Impacts of design configurations and movements of PV attached to building facades on increasing generated renewable energy. *Solar Energy*, *252*, 50-71.

Rey-Hernández, J. M., Yousif, C., Gatt, D., Velasco-Gómez, E., San José-Alonso, J., & Rey-Martínez, F. J. (2018). Modelling the long-term effect of climate change on a zero energy and carbon dioxide building through energy efficiency and renewables. *Energy and Buildings*, *174*, 85-96.

Schiefelbein, J., Rudnick, J., Scholl, A., Remmen, P., Fuchs, M., & Müller, D. (2019). Automated urban energy system modeling and thermal building simulation based on OpenStreetMap data sets. *Building and environment*, *149*, 630-639.

Shirinyan, E., & Petrova-Antonova, D. (2024). Large-Scale Solar Potential Analysis in a 3D CAD Framework as a Use Case of Urban Digital Twins. *Remote Sensing*, *16*(15), 2700.

Soha, T., Sugár, V., & Hartmann, B. (2024). City-scale analysis of PV potential and visibility in heritage environment using GIS and LiDAR. *Energy and Buildings*, *311*, 114124.

Uslu, A., & Tuğcu, A. (2024). Sürdürülebilir Binalar İçin Güneşlenme Süresinin 3B Modellenmesi ve Simülasyonu Üzerine Bir Araştırma. *Kirklareli University Journal of Engineering and Science*, *10*(2), 387-401.

Wendel, J., Simons, A., Nichersu, A., & Murshed, S. M. (2017, November). Rapid development of semantic 3D city models for urban energy analysis based on free and open data sources and software. In *Proceedings of the 3rd ACM SIGSPATIAL Workshop on Smart Cities and Urban Analytics* (pp. 1-7).

Waqas, H., Jiang, Y., Shang, J., Munir, I., & Khan, F. U. (2023). An integrated approach for 3D solar potential assessment at the city scale. *Remote Sensing*, *15*(23), 5616.

Xu, C., Chen, S., Ren, H., Xu, C., Li, G., Li, T., & Sun, Y. (2025). A novel deep learning and GIS integrated method for accurate city-scale assessment of building facade solar energy potential. *Applied Energy*, *387*, 125600.

Yadav, Y., Harshit, Kushwaha, S. K. P., Zlatanova, S., Boccardo, P., & Jain, K. (2024). Assessing Photo-Voltaic Potential in Urban Environments: A Comparative Study between Aerial Photogrammetry and LiDAR Technologies. *The International Archives of the Photogrammetry, Remote Sensing and Spatial Information Sciences*, *48*, 533-539.

Yilmaz, M., & Uysal, M. (2017). Comparing uniform and random data reduction methods for DTM accuracy. *International Journal of Engineering and Geosciences*, *2*(1), 9-16.

CHAPTER 8

CONSTRUCTION ERRORS IN STEEL COLUMN BASE PLATE CONNECTIONS[1]

Pinar Salahaldin Hussein HUSSEIN[2], Günnur YAVUZ[3]

1 This book chapter is based on a section of Pinar Salahaldin Hussein Hussein's master's thesis titled "Analytical Investigation of Column Base Plates used in Steel Structures," completed under the supervision of Assoc. Prof. Dr. Günnur Yavuz.

2 Asst.Lect., Northern Technical University, Polytechnic College Kirkuk, Construction and Building Techniques Department , Iraq, ORCID: 0000-0002-1489-0214

3 Assoc.Prof. Dr., Konya Technical University, Faculty of Engineering and Natural Sciences, Department of Civil Engineering, ORCID:0000-0002-8725-7129

1. INTRODUCTION

Column base plate connections are critical and important types of connections in steel structures, which carry the whole structure loads to the foundation. There are many requirements for the design and construction of the column base plate connections, and there are standards that include the requirement for this connection types.

Column base plates and anchor rods are the first components of steel structures to be installed in site construction, despite being the last components that will be designed. These connection types influence the overall behaviour of steel structures, so they must not be design only for strength requirements [1].

In steel column base plate connection design, material costs should be minimised where possible. Economical solutions can often be achieved by using thicker base plates instead of incorporating stiffeners or additional reinforcement to achieve equivalent strength with a thinner plate [1].

The strength, stiffness, and failure mode of a column base connection are directly influenced by the base plate thickness. The size of the base plate has an effect on the maximum bearing stress that the concrete foundation can reach [2].

Experimental studies have been done to test the influence of different anchor rod types, including round bars, J-type anchors, and deformed bars (with and without plates at the end of the bolt) on the last resistance of column base plates [3]. The highest resistance was achieved when using deformed bars with end plates [2].

The column base plates are the most important part of a steel structure, mostly when the column base is used for the purpose of resisting bending moments [4]. The anchor bolts and base plate transfer the applied loads to the foundation. Despite their important role in the behaviour of steel structures, their design is often negligent. This lack of attention results in costly engineering solutions, while poor design practices can lead to unsafe structures [4].

The base plate, a structural steel element welded to the column base, distributes column forces to the foundation through bearing and anchor rod connections. It increases the contact area between the steel column and the concrete foundation, which reduces compressive stress and prevents concrete crushing. Additionally, the base plate carries tension forces from the column to the anchor bolts. The column foundation consists of a concrete block that distributes the loads to the ground. Anchor bolts are used for fixing the column by transferring tensile loads into the foundation [4].

A mortar layer is placed to fill all voids and create a friction surface between the steel base plate and the concrete foundation to transfer shear forces by the friction from the column to the concrete block. The typical mortar layer thickness is taken as 0.1 times the base plate width, with a maximum of 0.2 times the width [4-5]. In exposed column base plate construction, the mortar layer is installed last, filling the space between the base plate and concrete foundation. For thicker base plates, holes are often provided to allow trapped air to escape during grout injection [4-6].

2. COLUMN BASE PLATE CONNECTION DETAILS ACCORDING TO AISC STEEL DESIGN GUIDE 1

Details of a typical steel column base plate connection are shown in Figure 1. The details to be considered for steel column base plates according to American Institute of Steel Construction-AISC Steel Design Guide 1: Base Plate and Anchor Rod Design are summarised below [1].

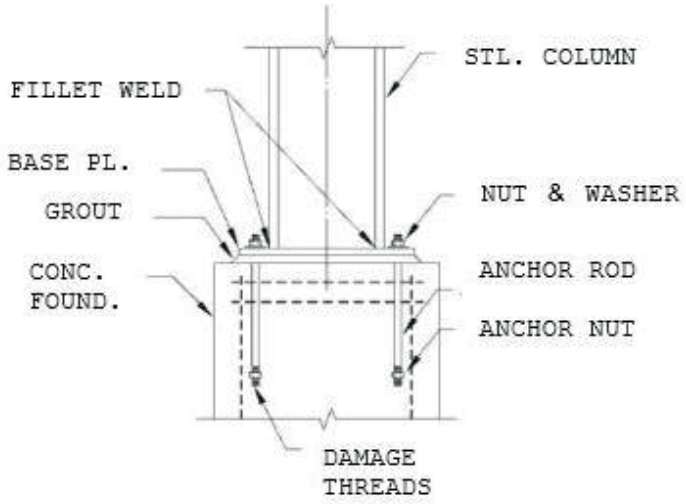

Figure1. Steel column base plate connection details [1]

- Since the compressive strength of grout is higher than the foundation concrete strength, column base plates are often placed directly on a grout layer. AISC Design Guide 1 [1] recommends specifying the grout strength to be at least twice the concrete strength for optimal load transfer.
- It is critical to adhere to the manufacturer's specifications for grout mixing, placement, and curing. In cold weather conditions, protective measures must be implemented as specified by the manufacturer to ensure proper grout performance. The non-shrink grout must develop adequate compressive strength to fully transfer the steel bearing stresses to the foundation. Per industry standards, its specified compressive strength shall exceed at least twice that of the supporting concrete foundation.
- The design thickness of the grout space depends on two key factors: the fluidity of the grout mixture and the placement accuracy of the concrete surface elevation. For columns installed on finished floors, a grout space of 25.4 mm is typically sufficient. Conversely, for columns supported by footings or piers, a greater grout thickness of 25.4-12.7 to 50.8 mm is generally required. Additionally, larger base plates or those incorporating shear lugs often necessitate even thicker grout spaces to ensure proper load transfer and accommodate construction tolerances.
- When determining base plate dimensions based on strength requirements, the designer must consider optimal anchor rod positioning within the plate geometry and minimum clearances for nut tightening operations.
- Current engineering practice favours headed anchor rods or threaded rods with heavy hex nuts for base plate connections, as hooked bars demonstrate significantly inferior pullout resistance. The anchorage system should utilise either a heavy hex nut or an anchor rod head. However, in exceptional cases involving high-strength anchor rods or potential concrete blowout conditions, the use of plate washers may be permitted.
- Anchor rod installation must ensure proper nut rotation during assembly. Three primary elevation adjustment methods are commonly employed: adjustable nuts with washers, setting plates, and shim stacks.
- Special applications requiring enhanced connection details may utilise specialized anchor rod configurations, including double-nut systems, sleeved anchor rods, pretensioned applications, and moment-resisting base connections.
- Special structures employ double-nut anchor rods as active load-bearing components in compression, contrasting with standard building practice where setting nuts function merely as temporary positioning elements during erection, with permanent compressive forces

transferred through base plate bearing. In contrast, double-nut anchor rod connections are robust and reliable, particularly effective in transmitting moments to the foundation.

- When using double-nut anchor rods in ungrouted base plates for light poles and sign structures, the anchor rods must resist all structural loads (tension, compression, and shear) without relying on grout for load transfer. The foundation system must be explicitly designed to transfer all applied loads through the anchor rod assembly.
- The pullout strength of anchor rods cannot be increased by using additional plate washers or similar devices. It is noted that these modifications may create field installation conflicts with reinforcement steel and prevent adequate concrete consolidation beneath the base plate. Therefore, anchorage should generally be limited to either a heavy hex nut or an integral head on the rod. Plate washers should only be considered in specific cases involving high-strength anchor rods or where concrete blowout is a potential concern.
- For anchor rods designed to resist shear forces in column base connections, the washers must be continuously fillet-welded to the base plate to ensure positive load transfer through bearing contact.
- Washer plates for anchor rods should not be hardened.
- The washers shall be either circular or rectangular plates with sufficient thickness to prevent pull-through failure at the anchor rod hole.
- The anchor rod layout must provide adequate clearance for the washers from the column shaft and its welds.
- Additional plate washers are used to accommodate excessively long anchor bolts, allowing the nut to be tightened down to the base plate by providing sufficient thread engagement.
- In high-strength anchor rod applications, bearing washers may be necessary to achieve the full tensile strength of the anchor. However, washer dimensions should be carefully controlled—oversized washers can diminish the effective embedment depth and reduce the anchor's pullout capacity by limiting the concrete's bearing performance.
- The required weld size for column base plates depends largely on the applied moment, shear, and tension forces. For columns subjected only to compression, minimal welding may be sufficient. However, when a column resists moment, shear, or tension, the welds must typically be sized to develop the full tensile capacity of the anchor rods—something that can often be achieved using relatively small fillet welds.
- In double-nut connections, compressive loads from the base plate are transferred through the levelling nuts on the anchor bolts. However, as noted by Fuchs et al. [7], most base plates in practice are installed over a grout layer. In such cases, grout failure typically becomes the governing failure mode [8].
- In load-bearing applications, only non-shrink grout should be used beneath base plates, and it must not contain chlorides or other substances that could lead to anchor bolt corrosion. In double-nut anchor connections, the grout layer must not be relied upon to carry structural loads [8].

Typical double-nut and single-nut connections are given in Figure 2 and Figure 3, respectively.

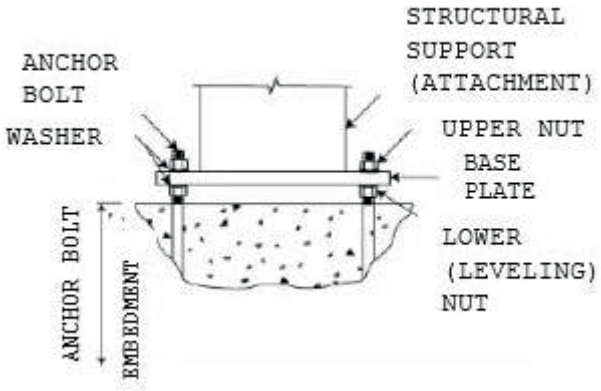

Figure 2. Typical double-nut connection [8]

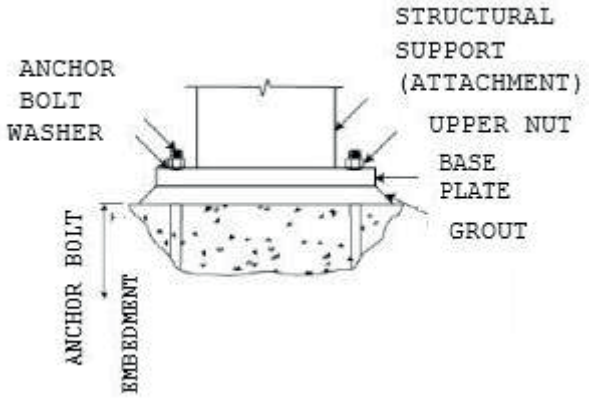

Figure 3. Typical single-nut connection [8]

3. CRITICAL ERRORS AFFECTING THE PERFORMANCE OF STEEL COLUMN BASE PLATE CONNECTIONS

3.1 Design Errors in Steel Column Base Plate Connections

A frequent design error in exposed steel column base plate connections is treating biaxial bending effects through simplified independent checks in orthogonal directions, instead of recognising that biaxial actions change the internal force distribution among anchor rods and the compression block in grout/concrete. Under biaxial bending, additional anchor rods may engage, force patterns become statically indeterminate, and the orientation/extent of the compression zone is not known a priori. If designers apply uniaxial-based assumptions directly, they may underpredict the peak tension in the most critical anchor rod—often the governing design demand—especially when the loading angle and plate aspect ratio amplify force concentration. The result is a connection that may appear adequate in a uniaxial check but becomes vulnerable when real multi-directional demands develop under wind or earthquakes [9]. Another critical design error is underestimating how the axis orientation of bending changes both strength and stiffness. Experimental and numerical evidence shows that the bending resistance, initial rotational stiffness, and rotation capacity can vary markedly with plate thickness and the direction of the resultant moment relative to the column axes. Designs that rely on “one-direction” intuition may neglect unfavourable orientations that increase plate uplift and concentrate anchor tension, leading to premature yielding in the plate or excessive demands in anchors. For book-level guidance, this means design checks should explicitly consider biaxial action rather than assuming the connection response is similar across directions [10].

3.2 Fabrication Errors in Steel Column Base Plate Connections

Fabrication errors commonly manifest as deviations in base plate geometry and detailing (plate thickness tolerances, hole location inaccuracies, and unintended plate out-of-flatness). These imperfections are not merely "workmanship issues"; they directly modify the contact condition between plate and grout/concrete and therefore alter the moment–rotation response measured in tests. When plate flatness and hole tolerances are poor, the base may develop unintended eccentricities, uneven bearing, and earlier uplift on the tension side. This increases local plate bending and can change the stiffness and rotation response compared with the idealised configuration assumed in analysis. From a practical standpoint, fabrication quality becomes part of the mechanical model: if uncontrolled, it reduces the reliability of any design approach calibrated to ideal specimens [11].

3.3 Construction and Installation Errors

Construction and erection errors are dominated by anchor-rod placement tolerances and levelling/grouting execution. Under biaxial moment demands, even small misplacements in anchor layout or deviations in levelling can change the effective lever arms and the engagement sequence of anchor rods, which directly affects the connection's strength and failure mode. If anchor rods are forced into position during erection (field "fit-up"), hidden initial bending or local damage may be introduced, and the connection may show reduced deformation capacity. Likewise, non-uniform grout thickness or incomplete bearing contact creates localised compression zones, increasing rotation and promoting earlier uplift. In biaxial scenarios, these imperfections do not simply "add noise"; they can systematically shift the governing anchor from one corner/row to another, making the response more brittle than expected [12].

3.4 Errors Under Seismic and Cyclic Loading

A recurring error in seismic design is focusing on static strength checks while under-representing cyclic degradation mechanisms. Under cyclic lateral loading, exposed steel column base plate connections can experience repeated uplift and re-contact, progressive concrete/grout cracking, anchor rod yielding accumulation, and stiffness/strength deterioration. If the design does not explicitly target a ductile hierarchy (e.g., controlled yielding in steel components while avoiding brittle concrete breakout), the connection can fail in a brittle mode that severely limits energy dissipation. Extended anchor bolt configurations and cyclic design methodologies highlight that details controlling uplift, anchor elongation demand, and compressive block stability are central to seismic resilience; omitting these considerations can cause an apparently "strong" base to perform poorly under reversed loading histories [13].

3.5 Coordination and Quality Control Errors

A coordination-driven error is treating inspection and verification as administrative steps rather than structural risk controls. The connection comprises interacting components (plate, anchors, grout, concrete) and multiple competing failure modes; inadequate Quality Assurance/Quality Control (QA/QC) allows small deviations to accumulate into a different governing failure mechanism than assumed in design. Data-driven failure-mode identification studies reinforce that column base performance is sensitive to combined parameters and defect patterns, meaning that missing a single critical variable in construction verification (anchor location, pretension condition, grout continuity, plate bearing) can change the failure path and reduce reliability. Consequently, quality control errors should be framed as "mechanism selection errors": they shift the connection from an intended ductile mechanism to a brittle or premature one [14].

4. DEFECTS IN COLUMN BASE PLATE CONNECTIONS

The defects observed in the application of column base plates and connection details that are not in compliance with the AISC code requirements are given in this section between Figure 4 and Figure 18 [15]. In Figure 4, the base plate is placed directly on the concrete block without using a grout layer between the base plate and the concrete block. The grout layer used to transfer shear forces into the foundation and help to distribute the loads came from the column over a large space. Per AISC Design Guide 1, base plate grout must be specifically engineered, properly installed, and achieve a minimum compressive strength of twice the foundation concrete strength to effectively transfer the full bearing pressure from steel to concrete. Also, in Figure 4 and Figure 5, the anchor bolt projections are too long. As noted in AISC Design Guide 1, excessive anchor rod projection can result in inadequate embedment depth, preventing the anchor from achieving its full tensile strength [1].

Figure 4. Column base plate connection directly placed over concrete block [15]

Figure 5. Too long anchor bolt projections [15]

In Figure 6 and Figure 7, the base plate and anchor bolts are not symmetric; it is continuous in one direction. In Figure 6, the stiffeners are not connected (welded) to the column flange. Per the AISC Design Guide 1, if one or two anchor rods in the base plate pattern are misplaced following column fabrication and shipment, the typical fix is to slot the base plate and use a plate washer to cover the slot [1]. When the entire pattern is uniformly out of tolerance, the base plate may be cut and shifted to fit the corrected layout. In such cases, the design must be reviewed to address any resulting eccentricity. Upon removal of the base plate, it may be required to invert it in order to obtain a clean surface suitable for welding the column shaft.

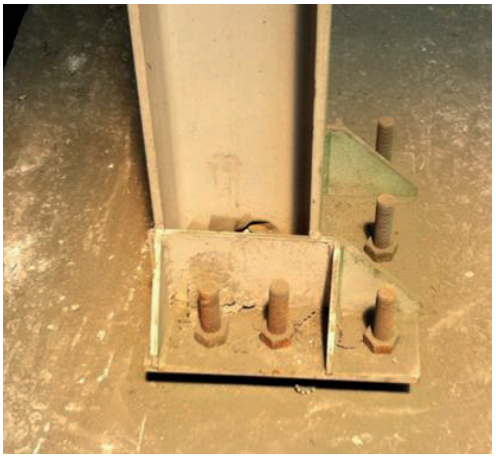

Figure 6. Non-symmetrical base plate connection [15]

Figure 7. The base plate continuous in one direction along the column section [15]

The column base plate is installed in direct bearing contact with the concrete foundation block. Omitting the conventional grout layer between these components, the concrete mixture for this concrete block must be of good quality. If the concrete mixture is bad, the concrete may be cracked and damage the column base plate connection.

In Figure 8, segregation has occured in the concrete block, and the base plate is uprising, and in Figure 9, the concrete block is damaged, and the reinforcement is subjected to corrosion.

Per AISC Design Guide 1 (2nd Edition) [1] and ACI 318-19 [16], anchor rod design must account for enhanced provisions governing pullout and concrete breakout strength, ensuring reliable force transfer from the base plate to the foundation. ACI 318-08, on the other hand, provides the following approach to anchor design [17]:

- Clearly defining failure modes (breakout, pullout, steel failure).
- Incorporating safety factors for different conditions (cracked concrete, edge effects).
- Ensuring anchors perform under service and extreme loads.

Figure 8. Damaged concrete block [15]

Figure 9. Damaged concrete block and corroded reinforcement [15]

The anchor bolts holding by template to not damaged when concrete is placed. After the concrete placed the template must be removed. In Figure 10, it is shown that the template remains in place.

Figure 10. Unremoved template [15]

To ensure proper load transfer from the structural steel system to the concrete foundation, the base plate connection requires a grout layer between the steel plate and concrete surface. In Figure 11, the base plate is connected to the concrete block by four different plates.

Figure 11. Base plate connected into concrete block by four different plates [15]

Addionally many different plate or elements are welded over the base plate (Figure 12). This element may be decrease the strength of base plate connection. The AISC Specification permits sevral plate materials structurally suitable materials for base plate design, with selection typically governed by cost and regional availability.

Figure 12. Different elements welded into the base plate [15]

In Figure 13, the edge space in front of bolts may cause damage and bolts to escape when the column base plate connection is subjected to the largest force effect. The space in the edge of the base plate is not desired, so space may not be made in the base plates.

Figure 13. Edge space in base plate [15]

One of the mistakes in the practice is the use of a different shape of plates as washers, which are used to tighten the anchor bolts. In Figure 14 a base plate is placed upon another base plate, and anchor bolts are tightened by washers and other small plates. The use of these different plates may be due to insufficient base plate thickness.

Figure 14. Base plate placed upon other base plate [15]

In Figure 15, irregular anchor bolts are shown. Here different plates are connected into anchor bolts, and these bolt projections are too long. Also deformation is shown in the concrete block. Per the AISC Design Guide 1 [1], anchor rod specifications should always include ample threaded length. Whenever feasible, the threaded portion should extend at least 76.2 mm beyond the required length to allow for variations in setting elevation. Anchor rods should be arranged in symmetrical

patterns along both axes, and the number of unique configurations should be kept to a minimum. The most common and preferred layout is four anchor rods arranged in a square.

Figure 15. Long anchor bolts and connected by different plates [15]

In Figure 16 and Figure 17, long and short projection bolts are shown. According to AISC Design Guide 1, if the anchor rod projection is too long, the embedment depth may be insufficient to develop the required tensile strength. Conversely, if the rod is too short, it may not extend adequately into the foundation, potentially compromising anchorage [1].

Figure 16. Long anchor rod [15]

Figure 17. Short anchor rod [15]

In column base plate connection application, attention must be paid to the ground level because first the anchor bolts are placed, so when the column base plate is placed, the connection level must be with the pavement. In Figure 18, column base plate connections are under the pavement, and the anchor bolts are too short. According to AISC Design Guide 1, proper placement of anchor rods is essential for the safe, efficient, and cost-effective erection of the structural steel frame [1].

Figure 18. Column base plate under pavement level and too short anchor bolts [15]

5. CONCLUSIONS

In general the steel column base plate connection consists of a steel column, a steel base plate and anchor bolts. The column base plate connection is placed over a concrete block, and a grout layer is placed between the base plate and the concrete block; except in special structures, the grout layer is not used. Because of the importance of column base plate connections on the effect of the structure, these connections are not only important to design for strength requirements. However, errors frequently occur during the installation of column base plates due to lack of experience, oversight, or improper execution, leading to potential connection failures that compromise structural integrity. In this study, the observed errors in the application of column base plate connections for industrial buildings, highway signs and luminaires are given. The procedures that must be followed in practice were explained as those mentioned in AISC Design Guide 1: Base Plate and Anchor Rod Design. This guide gives the details about the design and construction of steel exposed column base plates. So following these guidelines is important to preventing failures, enhancing durability, and maintaining safety in steel structures. Future research could further explore advanced materials or innovative connection techniques to improve the reliability and efficiency of the column base plate connection system.

6. REFERENCES

[1] Fisher, J.M., Kloiber, L.A. (2016). AISC Steel Design Guide 1: Base Plate and Anchor Rod Design. American Institute of Steel Construction, USA.

[2] Grauvilardell, J. E., Lee, D., Hajjar, J. F., Dexter, R.J. (2005). Synthesis of design, testing, and analysis research on steel column base plate connections in high-seismic zones (Structural Engineering Report No. ST-04-02). Department of Civil Engineering, University of Minnesota, USA.

[3] Igarashi, S., Kadoya, H., Nakashima, S., Suzuki, M. (1992). Behavior of exposed-type fixed column base connected to riser foundation. In Proceedings of the Tenth World Conference on Earthquake Engineering. Madrid, Spain.

[4] Amaral, P.M. (2014). Steel column bases under biaxial loading conditions, Master's thesis, University of Porto, Portugal.

[5] Horová, K. (2010). Base plates of hollow sections. Czech Technical University in Prague, Czech Republic.

[6] Correia, R. (2013). Dimensionamento de bases de pilares metálicos: Versão para discussão. Faculdade de Engenharia, Universidade do Porto, Portugal.

[7] Fuchs, W., Eligenhausen, R., Breen, J.E. (1995). Concrete capacity design approach for fastening to concrete. ACI Structural Journal, 92(1), 73–94.

[8] AASHTO (2013). Standard specifications for structural supports for highway signs, luminaires, and traffic signals (6th ed.). American Association of State Highway and Transportation Officials, USA.

[9] Hassan, A. S., Rodas, P. T., Giulietti, L., Kanvinde, A. (2021). Strength characterization of exposed column base plates subjected to axial force and biaxial bending. Engineering Structures, 237, 112165. https://doi.org/10.1016/j.engstruct.2021.112165

[10] Seco, D.S.L., Couchaux, M., Hjiaj, M., Neves, L. C. (2021). Column base plates under biaxial bending moment. Engineering Structures, 231, 111386. https://doi.org/10.1016/j.engstruct.2020. 111386.

[11] Stamatopoulos, G.N., Ermopoulos, J. Ch. (2011). Experimental and analytical investigation of steel column bases. Journal of Constructional Steel Research, 67(9), 1341–1357. https://doi.org/10.1016/j.jcsr.2011.03.007

[12] Cloete, R., Roth, C.P. (2021). Column base connections under compression and biaxial moments: Experimental and numerical investigations. Journal of Constructional Steel Research, 184, 106834. https://doi.org/10.1016/j.jcsr.2021.106834

[13] Torres-Rodas, P., Medalla, M., Zareian, F., Lopez-Garcia, D. (2022). Cyclic behavior and design methodology of exposed base plates with extended anchor bolts. Engineering Structures, 260, 114235. https://doi.org/10.1016/j.engstruct.2022.114235

[14] Kabir, M.A.B., Hasan, A. S., Billah, A.H.M. (2021). Failure mode identification of column base plate connection using data-driven machine learning techniques. Engineering Structures, 240, 112389. https://doi.org/10.1016/j.engstruct.2021.112389

[15] Hussein, P.S.H. (2015). Analytical investigation of column base plates used in steel structures, Master's thesis, Selçuk University, Konya, Turkey (in Turkish).

[16] ACI 318-19 (2019). Building Code Requirements for Structural Concrete. American Concrete Institute: Farmington Hills, Michigan, USA.

[17] ACI 318-08 (2008). Building Code Requirements for Structural Concrete, American Concrete Institute: Farmington Hills, Michigan, USA.

CHAPTER 9

FUNCTIONAL APPLICATION OF SAMBUCUS NIGRA EXTRACT FOR BREAD SHELF-LIFE EXTENSION AND NATURAL COLOR IMPROVEMENT

Tarık Eren BOYLU[1], Fatma İrem ŞAHIN[2], Nil ACARALI[3]

1 Kimya Mühendisi Yildiz Technical University, Department of Chemical Engineering, 34220, Esenler-İstanbul, Türkiye. 0009-0008-8883-0995

2 Kimya Mühendisi Yildiz Technical University, Department of Chemical Engineering, 34220, Esenler-İstanbul, Türkiye. 0000-0001-7670-8871

3 Prof. Dr. Yildiz Technical University, Department of Chemical Engineering, 34220, Esenler-İstanbul, Türkiye. 0000-0003-4618-1540 nilbaran@gmail.com, nbaran@yildiz.edu.tr

1. INTRODUCTION

Food products had been enriched with colorant for centuries. In order to enhance the appearance of their products, candy makers in ancient Egyptian cities added wine and natural extract around 1500 BC [1]. Historically, natural sources such as paprika, turmeric, saffron, and various flowers were used as food coloring agents [2]. The food industry had a significant and fascinating influence on scientific advancement as well as the assurance of health and nutrition as well as the satisfaction of consumers with regard to taste and appearance [3]. Food additives and technological advancements had played critical roles in ensuring that the food supply was cheap, wholesome, tasty, colorful, and safe [4]. There were main reasons for using color additives in food [5].

Food manufacturers typically tried to switch to natural food coloring in place of synthetic food colorin. Elderberry fruit contained high levels of anthocyanin, which was a natural food additives used in industry. However, it was important to note that anthocyanin and soluble solids of elderberry fruit, there were another reasonns to consider when evaluating the compatibility of a specific elderberry variety as an alternative to currently grown ones, such as production yield and resistance [6]. Natural colors were extremely unstable when food was processed under different circumstances. The limited stability of anthocyanins against light, temperature, oxygen, pH changes, heat, and other storage conditions limited their application, both in isolated form and in such concentrates [7]. Although betalains could be found in various plants. These were water-soluble pigments derived from pear fruits that added red to purple (betacyanin) or yellow to orange (betaxanthins) to a variety of products [8].

The elderberry (*Sambucus nigra* L.) belonged to the family *Caprifoliaceae*, which included 20 species. It was native to temperate and subtropical regions [9]. The elderberry was a good source of a number of significant and worthwhile substances. It was high in essential nutrients, including lipids (0.35%), which were mostly found in seeds (~22%), fiber (~7%), proteins (~3%), and carbohydrates (~18%), which were mostly simple sugars [10]. It contained beneficial ingredients for human health. Because of its high anthocyanin content, elderberry extracts were natural food colorants with health benefits [11]. Therefore, consuming elderberries would help regulate the oxidative status of the cells and would improve overall health [12].

The primary goal of this study was to investigate the applicability of utilizing elderberry-based natural colorants to both impart color to bread dough and extend its shelf life. In this context, elderberries were evaluated as a potential sustainable alternative to conventional synthetic additives commonly used in bread production. The study aimed to examine how elderberry-derived pigments influence the physicochemical, microbiological, and sensory properties of bread during storage, with particular attention to color stability, texture, and overall product acceptability over time. A further objective of this research was to explore and optimize preservation methods for elderberries in order to maintain their coloring capacity and functional properties prior to their incorporation into the dough. Overall, this work aimed to contribute to the development of cleaner-label bakery products by providing a natural, environmentally friendly, and potentially health-promoting alternative to synthetic food colorants.

2. MATERIALS AND METHOD

2.1. Materials

The key ingredient used in the experiments of the study was dried black elderberry fruits to extract anthocyanin for obtaining the colorant. Dried black elderberries were gathered from local herbalists. They supplied black elderberries from Bursa in Turkey. The drying process of black elderberries was a traditional drying method of leaving them under the sun for 3 or 4 days.The average particle size of dried black elderberries was 1.02 ± 0.13 mm and moisture content of dried black elderberries was 6.58 ± 0.16%. The other materials to make a bread dough to color were yeast, salt and wheat flour.

2.2. Method

To extract anthocyanin in the dried black elderberries, they were grinded by help of a grinder (kiwi KSPG-4812) with the power of 150 Watt. Grinded black elderberries were taken into beakers with the volume of 50 mL. There were 17 experimental samples and each had 10 g of grinded black elderberries and 20 mL pure water. Each samples were taken on the magnetic stirrer with the different temperature (25, 35, 45°C) and stirring speed (200, 300, 400 rpm) at different durations (5, 10, 15 min). Extracted samples were bottled and labeled according to stirring time, temperature and stirring speed. Bottled samples were taken to investigate the refractive indeces with a refractometer in the laboratory.

All refractive indeces had been processed into Desing Expert (Stat-Ease v.23.1.1). In the processed datas, the optimum value of the refractive index were found. Experimental conditions of this refractive index value were taken as basis for the next samples. At the optimum conditions, grinded black elderberries were prepared for the final sample. In order to see how important the surface area of dried elderberries, dried black elderberries were taken into the beaker without any grinding process at the optimum conditions. Obtained colorant samples (grinded and not grinded) were mixed with the ingredients (flour, yeast, salt and water) while preparing two equivalent bread doughs.

Figure 1 was provided an overview of the experimental workflow and characterization steps employed in this study, from raw material to final product. Dried black elderberries were presented as the natural pigment source. Black elderberries were subjected to extraction under varying process conditions and the resulting elderberry solutions were shown where different combinations of temperature, mixing time, and stirring speed were prepared and subsequently characterized. The "Predicted vs. Actual" plot illustrated the agreement between the experimental refractive index data and the values estimated by the statistical model, confirming the reliability and predictive capability of the optimization approach.

SEM micrographs at multiple magnifications displayed the surface morphology and microstructural features of the elderberry-derived material, providing information on particle size, distribution, and surface texture. Macroscopic and microscopic images of bread dough samples containing elderberry extract demonstrated the visual impact and dispersion of the natural colorant within the dough matrix. Collectively, transition from dried elderberries to optimized extract formulations and their incorporation into bread dough, supported by microstructural and statistical analyses.

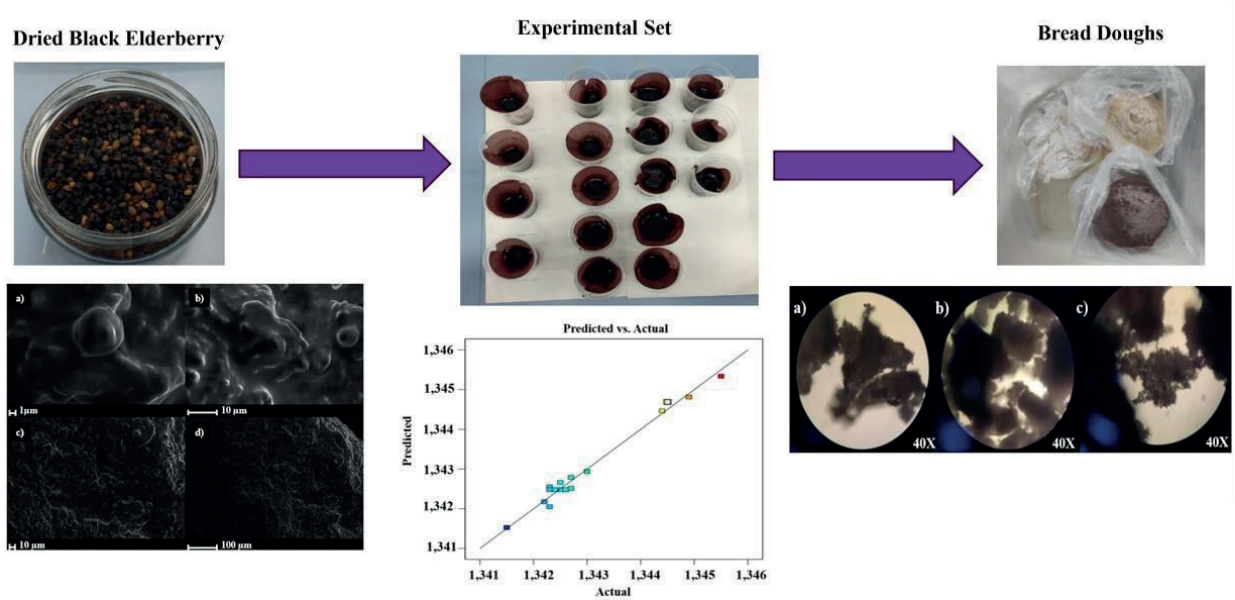

Figure 1. An overview of the experimental study

2.3. Characterization

Stability tests were made to investigate shelf-life and strength of bread doughs which were prepared. Grinded black elderbery were used to make a bread dough with a dark purple color. Another bread dough was made without any additives in order to see the difference. In addition, it was decided that dried black elderberries without grinded could be used to see the effect on elongation of bread dough. Therefore, three samples of bread doughs were prepared.

Firstly, their percent (%) elongation was measured with Force Testing Machine. 10 cm long and 1 cm thick strips were prepared for each sample to attach to the device. Then, the device was started working and was it pulled the bread dough strips as long as they detached. When the strips were detached, device read and transfered the data to the computer. This method was applied on all samples.

Secondly, bread doughs was prepared to determine how much time requires for them to spoil. A small amount of prepared bread doughs were taken to observe on Binocular Microscope (NICON Eclipse E100). Prepared bread doughs were taken into a close and dark room at 25°C.

2.4. Optimization

The response surface methodology was a methodology for designing experiments that made use of the interactions between particular parameters and builds models around these parameters. RSM, in its simplest form, provided statistical and mathematical methods to ensure process optimization.

Chemometris tools allowed to create mathematical models to determine the statistical significance and significance of the factor effects and the interaction effects between the factors. This reduced the number of experiments to perform and the amount of work to do in the laboratory. However, because the level of other variables involved could influence the effect of one of them, this method could not work. Box-Behnken design (BBD) was used in multivariate optimization schemes because it identified important factors and found the optimal operating conditions by changing all variables simultaneously [13].

3. RESULTS

3.1. Determination of Refractive Index of the Natural Colorant

The difference between the speed of light traveling through a medium and the speed of light traveling through a vacuum was known as the refractive index. Because the atoms in a nonvanular medium constantly absorb and emit light particles, light traveling through it has a refractive index. Light speed depends on the optical density of the medium. Electromagnetic wave speeds were affected by the tendency of atoms to reelectronize the absorbed electromagnetic energy. As the density of light increases, light speed decreases. One way of measuring a medium's optical density was to measure its refractive index. Refractive index analysis had chosen to determine the color of the natural food colorant obtained from black elderberries [14].

3.1.1. Effects of System Parameters on Refractive Index of the Natural Colorant

The refractive index results were based on seventeen experiments obtained depending on three basic process parameters: temperature (°C), stirring speed (rpm), and stirring time (minutes). The obtained refractive index values ranged from 1.3415 to 1.3455 (Table 1).

Table 1. Refractive index values obtained from Design Expert

No.	Temperature (°C)	Stirring Speed (rpm)	Mixing Time (min)	Refractive Index
1	25	300	15	1,3445
2	35	200	15	1,3455
3	45	300	5	1,3427
4	35	400	15	1,3444
5	35	200	5	1,3430
6	35	300	10	1,3426
7	25	200	10	1,3422
8	45	200	10	1,3423
9	45	400	10	1,3415
10	35	300	10	1,3424
11	35	300	10	1,3423
12	45	300	15	1,3449
13	35	300	10	1,3425
14	35	400	5	1,3425
15	25	300	5	1,3427
16	35	300	10	1,3426
17	25	400	10	1,3423

In Equation 1, x_1 was temperature, x_2 was stirring speed and x_3 was mixing time. The model included linear effects of each variable, as well as interaction terms and quadratic terms. It showed that the refractive index responded to process parameters in a nonlinear and interrelated manner. Analysis of the coefficients revealed that increasing mixing speed slightly decreased the refractive index, while increasing mixing time increased it. Simultaneous increases in temperature and mixing speed had a reducing effect on the refractive index, while the combined effect of temperature and mixing time slightly increased it.

The negative coefficient of the interaction between mixing speed and mixing time indicated that these two variables together had a negative effect. Analysis of the quadratic terms showed that the refractive index tended to decrease at the extreme values of temperature and mixing speed, while a more pronounced increase occurred at high levels of mixing time. Overall, mixing time had the strongest positive effect, while mixing speed mostly decreased the refractive index. It was observed that a balanced adjustment of all variables was necessary to achieve the optimum refractive index value. The impact of system parameters on the refractive index was displayed in the Quadratic Eq. (1) that followed.

$$\textbf{Refractive Index} = 1.34 - 0.0003 * x_2 + 0.001 * x_3 - 0.0002 * x_1 * x_2 + 0.0001 * x_1 * x_3 - 0.0001 * x_2 * x_3 - 0.0003 * {x_1}^2 - 0.0001 * {x_2}^2 + 0.0015 * {x_3}^2 \quad (1)$$

In Table 2, mixing time and stirring speed had smaller p-value. Therefore, these parameters were more effective on refractive index for the colorant. Parameters with the lowest p-values among the main effects were mixing speed (p=0.0078) and mixing time (p<0.0001). In particular, mixing time was the most dominant parameter of the system in terms of both its linear effect and its second-order (C^2) effect (f=181.32 and f=194.11). In contrast, the linear effect of temperature change was not statistically important (p=0.6452). However, second order effect (A^2) of temperature was found to be significant (p=0.0364). The results showed that temperature exhibited nonlinear behavior on the refractive index. While the significance level in the interaction terms (AB, AC, BC) was close to the limit, the AB term (temperature-speed) in particular showed a moderate level of interaction in the

model (p=0.0807). Design model was Quadratic and it designed the system parameters for refractive index of the colorant. All system parameters affected the refractive index values. R^2 value was 0.9828 and adjusted R^2 value was 0.9607. These values demonstrated that affected of system parameters on refractive index wass defined in Quadratic model successfully.

Table 2. f and p values of parameters

Source	Mean Square	df	f-value	p-value
Model	$2.61x10^{-6}$	9	44.43	<0.0001
Linear				
A-Temperature	$1.125x10^{-8}$	1	0.2313	0.6452
B-Stirring Speed	$6.612x10^{-7}$	1	13.59	0.0078
C-Mixing Time	$8.820x10^{-6}$	1	181.32	<0.0001
Cross Product				
AB	$2.025x10^{-7}$	1	4.16	0.0807
AC	$4.00x10^{-8}$	1	0.8223	0.3946
BC	$9.00x10^{-8}$	1	1.85	0.2159
Quadratic				
A^2	$3.242x10^{-7}$	1	6.67	0.0364
B^2	$6.845x10^{-8}$	1	1.41	0.2742
C^2	$9.442x10^{-6}$	1	194.11	<0.0001
Lack of Fit	$9.083x10^{-8}$	3	5.34	0.0696
R^2	0.9828			
Adj R^2	0.9607			

The amount of time spent mixing had a significant impact on the natural colorant. Therefore, to obtain a more effective natural colorant, it was essential to optimize the value of mixing time. According to Table 1, in a small period of time at a medium level of temperature, it could be said that these parameters affected on refractive index significantly. Figure 2 showed the effect of process parameters and their interaction on the refractive index.

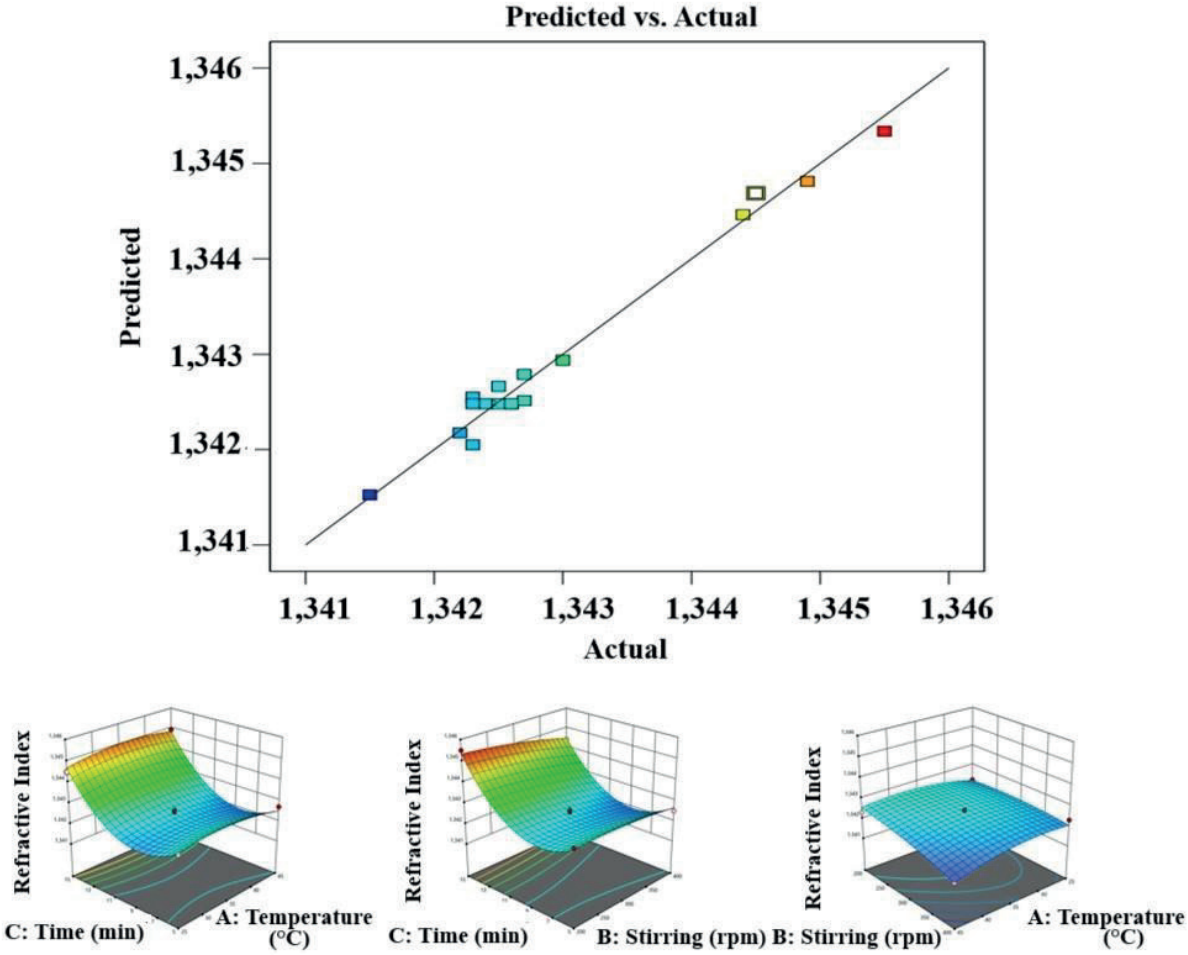

Figure 2. Predicted vs. actual refractive index with color-coded values and 3D graphs of system parameters

3.2. Black Elderberry Powder Characteristics

Black elderberry powder particles often came in very different sizes and shapes. It was common for a mixture of particle size to be formed during the milling and drying process. Black elderberry powder particles could range from very fine to coarse in size. SEM (Scanning Electron Microscope) images of black elderberry powder were shown in Figure 3.

SEM images showing the microstructural characteristics of a powdered black elderberry sample at different magnifications were presented. The surface morphology was evaluated at multiple scales. Images taken at high magnifications, a) 1 µm and b) 10 µm scales showed that the elderberry particles had a rough, wavy, and heterogeneous surface topography. Bubble-like protrusions or rounded structural formations were observed in places. These microstructural irregularities reflected the expected natural variation in pigment-containing biological materials. Images taken at lower magnifications, c) 10 µm and d) 100 µm scales showed how the particles were distributed over larger areas. In these images, the surface texture became more distinct, fibrous or convoluted microstructures were spread over a wide area, and the powder exhibited a heterogeneous agglomeration structure. Overall, the study showed that black elderberry powder had a naturally occurring, irregular, multilayered, and complex surface morphology, and that this structure had significant effects on extraction behavior, pigment release, and incorporation performance into food systems. The natural structure of the plant powder was what gave it its coarse texture. Particle clusters could be seen in SEM images. Remaining moisture or electrostatic attraction caused particles to stick together.

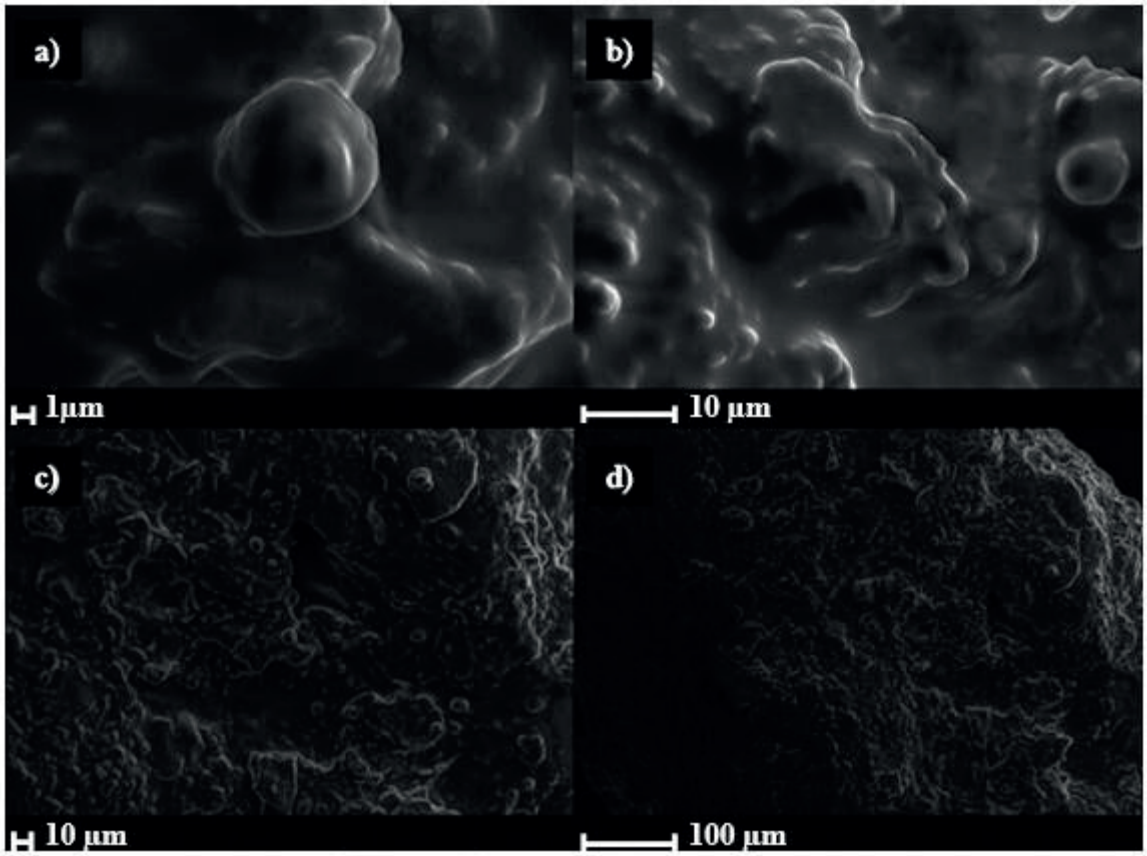

Figure 3. SEM images of powder black elderberry

3.3. Results of Stability Tests

As it appeared in Figure 4, the bread dough with the powdered black elderberry the bread dough with the powdered black elderberry showed more elongation than the other bread dough samples. The bread dough with the powdered black elderberry had 450.85 mm % elongation, the bread dough with black elderberry without grinded had 262.67 mm % elongation and the bread dough without additives had 379 mm % elongation.

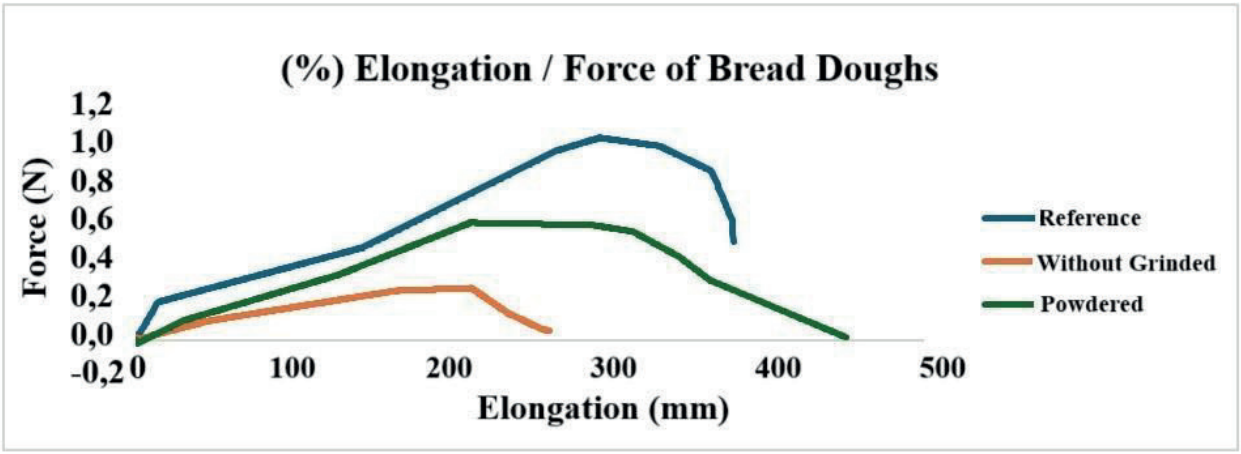

Figure 4. Graph of % elongation / force of bread doughs

To analyze the shelf-life of bread doughs, they were taken into a close and dark room at 25°C. After 72 hours, the bread dough without additives started to mold. However, other bread dough samples with the colorant additives were still fresh. The two days following that the day the first bread dough started to mold, bread dough sample with the additives but not grinded started to mold. The next two days, the bread dough sample with powdered black elderberry colorant additive started to mold. It had been observed with binocular microscope as shown in Figure 5.

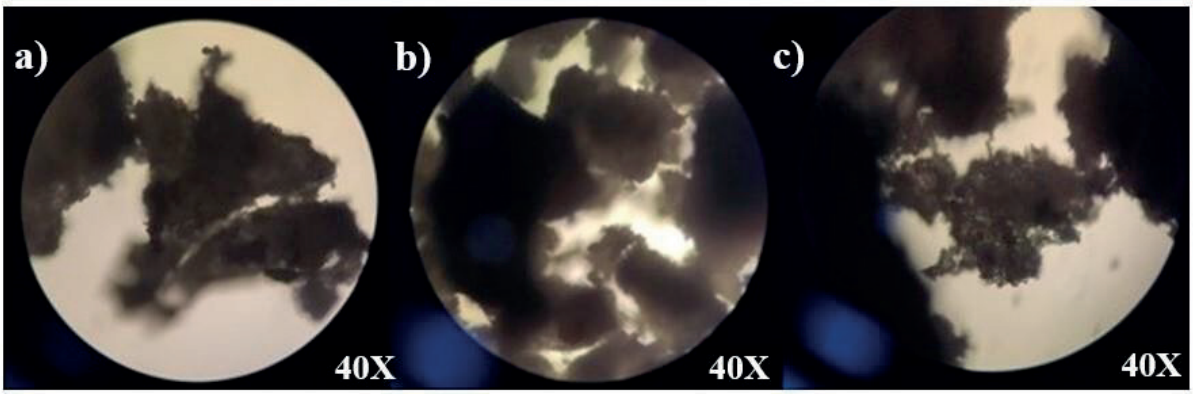

Figure 5. Microscope images of bread dough examples

As a result, it could be seen that the bread dough with black elderberry lasted longer than the bread doughs without additives. Therefore, black elderberry could be used as natural food colorant to increase shelf-life of breads and other patisseries.

4. DISCUSSION

The outcomes of this study were provided important insights into how processing conditions influence both the physicochemical attributes of the elderberry-based natural colorant and its technological performance in a model bakery system. The statistical analysis indicated that the refractive index was highly responsive to variations in the extraction parameters, particularly mixing time. The findings showed that the optical behavior of the extract was tightly coupled with mass-transfer efficiency and the dynamics of pigment release from the plant matrix. Prolonged or intensified mixing likely enhanced molecular dispersion, facilitates pigment diffusion, and induced structural reorganization within the anthocyanin-rich medium. Such reorganization could modify light matter interactions, thereby producing measurable changes in refractive index.

The microstructural observations obtained through SEM imaging offer complementary evidence regarding the physical complexity of the powder material. The presence of irregular particle morphologies, size heterogeneity, and clustered structures was typical of minimally processed botanical powders and reflected the heterogeneous composition of elderberry fruit tissues. Such morphology could influence hydration behavior, the release kinetics of pigments and phenolic compounds, and the interaction of powder particles with gluten networks during dough preparation. These structural characteristics likely contributed to the enhanced extensibility observed in doughs supplemented with powdered elderberry, as the finer particles may promote more uniform dispersion and interaction with the hydration medium.

The shelf-life assessment further highlighted the multifunctional nature of the elderberry-based colorant. The result was consistent with the known bioactive properties of elderberry constituents, which included antioxidant capacity and the presence of naturally occurring compounds capable of inhibiting spoilage mechanisms. The improved stability observed in the powdered form, compared to the non-ground material, suggested that particle reduction enhanced both dispersion and the availability of active components within the dough matrix.

Collectively, these findings showed that the black elderberry extract possesses characteristics that extend beyond its role as a natural colorant. Its physicochemical responsiveness to processing conditions combined with its microstructural attributes and functional impact on dough performance, positions it as a versatile ingredient with potential applicability in clean label bakery formulations. The integration of optical measurements, microstructural analysis, and functional testing provided a comprehensive framework for understanding how such natural extracts behave under processing conditions and how could be optimized for industrial use. Future studies might benefit from linking these technological outcomes more directly to compositional analyses enabling a understanding of how specific molecular constituents contribute to the observed functional behaviors.

5. CONCLUSION

Consequently, this study had demonstrated that black elderberries (*Sambucus Nigra* L.) could be used as natural food colorants with significant benefits for the food industry. The study had demonstrated that not only did anthocyanin extract from black elderberries added color to bread doughs, but it also prolonged their shelf life through careful experimentation and analysis. The use of response surface methodology optimized the extraction conditions, resulting in highly efficient production of anthocyanin containing the desired properties.

The two-stage approach of this study was optimizing the extraction process and applying the colorant to the bread doughs, had yielded promising results. The results showed that bread doughs colored with black elderberry colorant retained their freshness for longer and had more % elongation (450.85 mm) than those without colorant, supporting the preservative properties of natural colorants The effectiveness of anthocyanin in extending the shelf life of bakery products was further validated by microbial growth analysis, anticipation and stability testing, and other methods.

One of the major advances in food technology lied in the ability to combine functional benefits with aesthetic appeal through the use of natural additives. The results of this study suggested that more research should had been conducted on the commercial utilization of the anthocyanin of black elderberries in various food products. As a result, this study suggests that anthocyanin, the elderberry coloring agent, could be used as a natural food colorant, providing appropriate protection by exposing bread dough to moderate heat and depending on a certain mixing time and speed.

As a result, this research opened up new avenues for innovation in modern food industry by providing valuable insights into the development of sustainable and healthy food additives. The use of black elderberry as natural food coloring also promoted eco-friendly practices in food industry.

REFERENCES

[1] M. F. Mohamad, D. J. Dailin, S. E. Gomaa, M. Nurjayadi, H. E. Enshasy. *Int. J. Sci. Technol. Res.* 2019, 8, 3161–3166.

[2] G. T. Sigurdson, P. Tang, M. M. Giusti. *Annu. Rev. Food Sci. Technol.* 2017, 8, 261–280. https://doi.org/10.1146/annurev-food-030216-025923

[3] N. Martins, C. L. Roriz, P. Morales, L. Barros, I. C. F. R. Ferreira. *Trends Food Sci. Technol.* 2016, 52, 1–15. https://doi.org/10.1016/j.tifs.2016.03.009

[4] C. Novais, A. K. Molina, R. M. V. Abreu, C. Santo-Buelga, I. C. F. R. Ferreira, C. Pereira, L. Barros. *J. Agric. Food Chem.* 2022, 70(9), 2789–2805. https://doi.org/10.1021/acs.jafc.1c07533

[5] P. Amchová, H. Kotolová, J. Ruda-Kučerová. *Regul. Toxicol. Pharmacol.* 2015, 73(3), 914–922. https://doi.org/10.1016/j.yrtph.2015.09.026

[6] L. Szalóki-Dorkó, M. Stéger-Máté, L. Abrankó. *Int. J. Food Sci. Technol.* 2015, 50(6), 1317–1323. https://doi.org/10.1111/ijfs.12773

[7] N. J. Nemetz, A. Schieber, F. Weber. *Molecules* 2021, 26(9), 2689. https://doi.org/10.3390/molecules26092689

[8] B. G. Nabi, K. Mukhtar, W. Ahmed, M. F. Manzoor, M. M. N. Ranjha, M. Kieliszek, Z. F. Bhat, R. M. Aadil. *Food Biosci.* 2023, 52, 102403. https://doi.org/10.1016/j.fbio.2023.102403

[9] O. Pascariu, F. Israel-Roming. *Processes* 2022, 10(11), 2288. https://doi.org/10.3390/pr10112288

[10] R. Domínguez, M. Pateiro, P. E. S. Munekata, E. M. S. López, J. A. Rodríguez, L. Barros, J. M. Lorenzo. *Foods* 2021, 10(11), 2713. https://doi.org/10.3390/foods10112713

[11] M. Banach, B. Khaidakov, D. Korewo, M. Węsierska, W. Cyplik, J. Kujawa, L. M. Ahrné, W. Kujawski. *Sustainability* 2021, 13(22), 12702. https://doi.org/10.3390/su132212702

[12] S. S. Ferreira, C. Martins-Gomes, F. M. Nunes, A. M. Silva. *Food Chem. X* 2022, 15, 100437. https://doi.org/10.1016/j.fochx.2022.100437

[13] S. Ferreira, R. Bruns, H. Ferreira, G. Matos, J. David, G. Brandão, E. Da Silva, L. Portugal, P. D. Reis, A. Souza, W. D. Santos. *Anal. Chim. Acta* 2007, 597(2), 179–186. https://doi.org/10.1016/j.aca.2007.07.011

[14] J. C. Espín, C. Soler-Rivas, H. J. Wichers, C. García-Viguera. *J. Agric. Food Chem.* 2000, 48(5), 1588–1592. https://doi.org/10.1021/jf9911390

CHAPTER 10

COMPARATIVE ANALYSIS OF CROSSOVER OPERATORS IN GENETIC ALGORITHMS FOR THE UNCAPACITATED P-MEDIAN PROBLEM

Murat ŞAHIN[1], İsmet SÖYLEMEZ[2]

1 Department of Industrial Engineering, Manisa Celal Bayar University, Manisa, Türkiye Email: sahin.murat@cbu.edu.tr ORCID: 0000-0003-3173-1749
2 Department of Industrial Engineering, Abdullah Gül University, Kayseri, Türkiye Email: ismet.soylemez@agu.edu.tr ORCID: 0000-0002-8253-9389

1. INTRODUCTION

The facility location problem represents one of the most extensively investigated topics in combinatorial optimization. Facility layout and facility location are the two primary categories for the facility location problem. The former relates to internal layout, while the latter concerns external location. The p-median problem is actually an external selection problem. While with the facility selection problem the number of facilities to be established is usually decided, in the p-median problem the number of facilities to be opened is fixed. The problem of placing p facilities in optimal locations under certain constraints, which can be defined as the p-media problem, is widely studied in the literature. In this type of problem, the basic constraints are (1) the number of facilities to be selected is limited to p, (2) each customer point should be assigned to a facility, and (3) each customer point is targeted to be served by the nearest facility at the lowest cost (or distance). Depending on the problem structure, different distance matrices can be used to calculate the total distance such as Euclidian, Manhattan, and weighted distance. However, there may be some additional constraints to the constraints mentioned above. It is often the case in real life that the capacity is not unlimited, i.e., the facilities to be selected may have similar or different capacities, or there may be costs other than the distance of the facility to be built.

As one of the most intensively investigated problems in combinatorial optimization, the p-median problem has generated a vast body of research. Databases such as *Scopus* are widely employed to review and classify these studies. When the keyword "p-median" is entered, it is found that more than 450 000 documents are listed in Scopus. Even when looking only at the year 2024, these numbers are more than 35 000. Similarly, there are over 294,000 studies related to "genetic algorithms" (GAs). In 2024 alone, there are over 19,000. The number of studies in which both keywords appear together is 215. As of 2024, there are 16 such studies. The following are some of the most frequently cited and recently published studies.

Optimal locations for solar-powered charging stations to support the use of electric tractors in agriculture was determined by Macit (2025) and Chance-Constrained model and Genetic Algorithm was applied for solutions. Liang et al. (2025) compared genetic algorithm and novel deep reinforcement learning approach for the p-median problem. Their experimental results showed that the proposed method outperforms genetic algorithms in both accuracy and efficiency, achieving solutions closer to the optimum. An effective and scalable hybrid genetic algorithm for solving the Hamiltonian p-median problem was studied by He et al. (2024). Çelik and Ok (2024) applied a genetic algorithm to solve the p-median problem for site selection and uses Arena simulation to optimize station traffic and charging unit types. The model emphasizes public areas, minimizing travel distances and waiting times. Wang et al. (2024) proposed a distributed localized manufacturing based personalized customization supply chain model with facility siting to enhance sustainability in the context of Industry 5.0. The model was optimized using a p-median approach with a genetic algorithm, while a hybrid simulation combining agent-based modeling and discrete event simulation assesses sustainability metrics. Another study addressed facility location issues, focusing on the p-median problem, by proposing a hybrid fuzzy approach. A bi-objective optimization model was developed, aiming to minimize total transportation costs and maximize demand point coverage. The proposed algorithm was validated using benchmark problems from the existing literature (Varnamkhasti and Varnamkhast. 2024). Farahani et al (2024) provided a comprehensive review of over 40 years

1*
2

of research on hierarchical facility location problems. Pérez-Gosende et al. (2021) reviewed 232 studies on facility layout planning from an operations management perspective. The work was classified by problem type, approach, planning stage, facility characteristics, and material handling system configuration. A review of literature was made by referring to numerous papers about facility layout problems. The study was mainly motivated by the current and prospective trends of research on such points as layout evolution, workshop characteristics, problem formulation, and solution methodologies (Hosseini-Nasab et al., 2018).

This study contributes to literature by comparing different types of crossover methods for the uncapacitated p-median problem. The rest of the paper is organized as follows. General information about genetic algorithms and different types of crossover methods are given at the second section. Section 3 presents the computational results of the test instances. Section 4 gives information about the conclusion and future works.

2. METHODOLOGY

Genetic algorithms are powerful metaheuristic techniques inspired by the process of natural selection, making them effective for solving complex optimization problems. Their performance largely depends on the design of genetic operators, primarily crossover and mutation (Kora and Yadlapalli, 2017). Each chromosome is evaluated using a fitness function, which measures the quality of the solution it represents. This fitness value is crucial for selecting the most promising candidates for reproduction. Chromosomes are selected for reproduction based on their fitness values. Higher fitness scores increase the probability of selection, reflecting the principle of survival of the fittest. Crossover combines features from two parent chromosomes to produce offspring. Various techniques can be used, including one-point, two-point, or uniform crossover, which involve swapping segments of the parent solutions. Mutation introduces random changes to chromosomes, helping to maintain genetic diversity within the population. This prevents premature convergence and allows exploration of new areas in the solution space (Correa et al., 2004). The algorithm iteratively refines the population over multiple generations, with each iteration involving selection, crossover, and mutation, until a satisfactory solution or convergence criterion is reached. The effectiveness of GAs is closely related to the choice and design of genetic operators. By appropriately implementing crossover and mutation, GAs can efficiently explore the solution space and yield high-quality solutions for a variety of optimization problems.

In this study, the effectiveness of the different crossover operators is compared for a well-known, uncapacitated facility location problem, P-median. Totally 6 different crossover operators have been compared to each other. In all GAs which use different crossover operators have the same solution representation. GAs are applied in pure format by only using selection, mutation and crossover operators since this study aims to compare the performances of the crossover operators. The steps of the GAs are given in Figure 1.

Step 1. Generate initial population randomly P(0), set t=0,
Step 2. while (stopping criteria is not met) **do**
Step 2.1. Evaluate P(0);
Step 2.2. Apply selection mechanism P'(t) =Selection P(t);
Step 2.3. Apply reproduction P'(t) =Reproduction with crossover and mutation operators (P'(t));
Step 2.4. Evaluate P'(t);
Step 2.5. Update population P(t +1) = P'(t);
Step 2.6. t = t+1;
Step 3. Output the best solution found

Figure 1. The template of the genetic algorithm (Talbi, 2009)

2.1. Solution representation and initial population

In the solution representation of the suggested GAs *n* continues numbers between 0 and 1 are used where *n* represents the number of locations. The p number of locations with the smallest value are selected as central locations. Supposed that a chromosome with 7 location is given as [0.26 0.42 0.36 0.88 0.75 0.21 0.92], and 2 locations will be selected. The selected locations are 1 and 6 since they have the smallest value. Supposed that the total distance will be calculated according to distance matrix given in Table 1. The total distance is calculated by summing the minimum distances from each location to the central locations. The objective value of the given chromosomes can be determined by summing the specified values: for location 2, *min* (12, 27); for location 3, *min* (14, 19); for location 4, *min* (18, 23); for location 5, *min* (21, 14); and for location 7, *min* (34, 13). It is equal to 71.

In a GA, population size is one of the important parameters and generally varies depending on the size of the problem being addressed. In this study, through the experimental study population size is determined as $10 \cdot n$ and randomly generated.

Table 1. Symmetric distance matrix among the locations.

Locations	1	2	3	4	5	6	7
1	-	12	14	18	21	16	34
2		-	26	19	13	27	24
3			-	22	16	19	21
4				-	17	23	16
5					-	14	22
6						-	13
7							-

2.2. Selection

Selection strategy answers the question that which parents for the next generation are chosen for using production strategy. The basic principle of the selection method is that the individual with better fitness value has a higher chance of becoming a parent of the individual (Talbi, 2009). With this logic, methods such as roulette wheel, stochastic universal sampling and tournament selection are applied for this operator. In this study tournament selection is applied and tournament size was determined as 2. According to this strategy two individuals from the population are randomly chosen and the one who has the better fitness value is selected.

2.3. Crossover

The role of the crossover operators is to produce new individuals which contains both two parents' characteristics. The crossover method, which aims to obtain good individuals (offsprings) by mixing the characteristics of more than one individual in the generation of a new population, is an important component of the genetic algorithm (Talbi, 2009). In this study, the effectiveness of different crossover operators on the GA was tried to be shown by using p-median test problems. In the subsections, information about the crossover methods used is given.

2.3.1 One Point Crossover

In this well-known crossover method, one point is selected for the given parents, the genes on the right side are copied from parent 1, while the other genes are copied from the parent 2 to obtain an offspring. This process is applied in the opposite way to obtain the second offspring (Goldberg, 1989).

				Crossover Point			
Parent1	0.26	0.42	0.36	0.88	0.75	0.21	0.92
Parent2	0.45	0.34	0.28	0.58	0.42	0.94	0.10

Offspring1	0.26	0.42	0.36	0.88	0.42	0.94	0.10
Offspring2	0.45	0.34	0.28	0.58	0.75	0.21	0.92

Figure 2. Illustrative for one point crossover.

An illustrative for one point crossover is given in Figure 2. Since the given p-median problem contains 2 central locations, according to parent1 two locations have the smallest values, location 1 and location 6, should be selected. In parent 2 location 3 and 7 are selected. In the offspring1 that is obtained after the crossover operator location 1 and location 7 are determined as central locations.

2.3.2. Two Point Crossover

In this crossover method, two points are selected for the given parents, the genes between these points are copied from parent 1, while the other genes are copied from the parent 2 to obtain an offspring. This process is applied in the opposite way to obtain the second offspring (Holland, 1975). An example for two point crossover method is given in Figure 3.

		Crossover Point1			*Crossover Point2*		
Parent1	0.26	0.42	0.36	0.88	0.75	0.21	0.92
Parent2	0.45	0.34	0.28	0.58	0.42	0.94	0.10

Offspring1	0.26	0.42	0.28	0.58	0.42	0.21	0.92
Offspring2	0.45	0.34	0.36	0.88	0.75	0.94	0.10

Figure 3. Illustrative for two-point crossover.

2.3.3. Arithmetic Crossover

Arithmetic crossover can be used when the chromosomes contain real-value encoding. Arithmetic crossover operator linearly combines the genes of two chromosomes to generate new offspring. (Kora & Yadlapalli, 2017; Wright, 1991). In this crossover method, the α value indicating the weight of first parent is determined by the decision maker as a continuous number between 0 and 1. Supposed that two offspring will be generated for the given parents in Figure 4 with α=0.25. The first gene of the offspring is obtained by summing the multiplication 0.25 and the value of first gene of parent 1 and the multiplication 0.75 and the value of first gene of parent 2. (0.25*0.26 + 0.45*0.75≈0.40)

α_1=0.25 $1-\alpha_1$ =0.75

Parent1	0.26	0.42	0.36	0.88	0.75	0.21	0.92
Parent2	0.45	0.34	0.28	0.58	0.42	0.94	0.10

Offspring1	40	0.36	0.30	0.66	0.50	0.76	0.31
Offspring2	31	0.40	0.34	0.81	0..67	0.39	0.72

Figure 4. Illustrative for arithmetic crossover.

2.3.4. Linear Arithmetic Crossover

In the linear arithmetic crossover method, unlike the arithmetic crossover method, the value of α is calculated depending on the fitness value of the parents (α_2). This ensures that better individuals have more influence on their offspring (Herrera, Lozano, & Verdegay, 1998). Supposed that the given parents in Figure 5 will be used in solving the problem whose distance matrix is given in Table 1. The fitness values of parent 1 and parent 2 are respectively 71 and 83. Since the objective is minimization the value of α_2 is computed as $\frac{(1/71)}{\left(\frac{1}{71}\right)+\left(\frac{1}{81}\right)}$ =(0,533). Then offspring 1 and offspring 2 can be generated easily.

	α_2=0.533			1-α_2 =0.467			
Parent1	0.26	0.42	0.36	0.88	0.75	0.21	0.92
Parent2	0.45	0.34	0.28	0.58	0.42	0.94	0.10

Offspring1	349	0.383	0.323	0.740	0.596	0.551	0.537
Offspring2	361	0.377	0.317	0.720	0.574	0.599	0.483

Figure 5. Illustrative for linear arithmetic crossover.

2.3.5. Modified Linear Arithmetic Crossover

In this crossover operator the value of α_3 takes different values according to the processing of the algorithm. While in the start of the algorithm this value is smaller in the last of the algorithm it approximates a predetermined value β. Similar adaptive strategies for crossover parameters have been discussed in the literature to improve exploration–exploitation balance (Umbarkar & Sheth, 2015; Abdoun & Abouchabaka, 2012). Through preliminary experiments the value of β is generally in the interval between 0.75 and 0.95. In this study it was taken as 0.85.

$$a_3 = \beta \cdot e^{-\left(\frac{(MaxIter-CurrentIter)}{MaxIter}\right)} \quad (1)$$

The β in Equation 1 is used to determine how likely it is that the offspring will resemble parent1 towards the end of the algorithm. While *MaxIter* shows the number of iterations the algorithm will continue, *CurrentIter* represents the number of iterations has reached. Apart from this, the linear arithmetic crossover performs the same functions as the arithmetic crossover method to obtain the offspring. In other words, the only difference is that the a_3 is used adaptively.

2.3.6. Modified Uniform Crossover

In the uniform crossover method, genes are copied from parent 1 with a certain probability. Genes that do not provide a certain probability value are copied from parent 2 to obtain offspring individuals. In this study, the same probability value is not used from the beginning to the end of the algorithm, which is slightly different from the classical uniform crossover. While the probability of genes being copied from the better of the two parents is kept lower at the beginning of the algorithm, it is aimed for the probability of genes being selected from the good individual to converge to a previously determined β value towards the end of the algorithm. Similar adaptive parameter strategies were previously proposed in real-coded GAs (Deep, Singh, Kansal, & Mohan, 2009). In this way, while diversity is provided at the beginning of the algorithm, it is aimed for the effective use of the intensification mechanism by increasing the copying from the good individuals towards the end of the algorithm. The probability of genes being copied from parent1 is shown as α_4 and an illustrative example for modified uniform crossover operator has been given in Figure 6.

				α_4=0.36			
Parent1	0.26	0.42	0.36	0.88	0.75	0.21	0.92
Parent2	0.45	0.34	0.28	0.58	0.42	0.94	0.10
Random Numbers	0.40	0.28	0.56	0.34	0.48	0.76	0.62

Offspring1							
0.45	0.42	0.28	0.88	0.42	0.94	0.10

Figure 6. Illustrative for modified uniform crossover.

2.4. Mutation

The mutation operator is used in the genetic algorithm to increase diversity. In this study, the value obtained by subtracting the gene value from 1 was used as the mutation operator for a gene. For example, suppose that a gene with 0.25 value is selected for mutation operator. After the mutation process, the value of this gene is updated to 0.75 (1-0.25). In this way, genes with high priority values become low after the mutation process, and genes with low priority values become high priority values after the mutation process. Through the preliminary experiments the mutation probability for a gene is detected as 0.05.

3. COMPUTATIONAL STUDY

The effectiveness of GAs that include 6 different crossover methods have been compared with each other using 36 sample test problems which include from 10 locations to 70 locations. For any algorithm, deviations from the best solution obtained by 6 methods were determined as the performance criterion. And deviations for a solution are computed as given in Equation 2, where $f(sol)$ represents the solution obtained by any algorithm and $f(best)$ shows the best solution.

$$\%gap = 100 * \frac{(f(sol) - f(best))}{f(sol)} \quad (2)$$

Each algorithm was coded using the C# programming language on a computer with an Intel i5 processor (1.3 GHz) and 24 GB of RAM. Each genetic algorithm was run five times for 1,000 iterations, and the best and average solutions from these runs were considered. Table 2 summarizes the computational study based on the best solution among the five runs.

In the table, the first column shows the number of locations, while the second column indicates the number of instances solved within that group. According to first three row, all GAs using different crossover operators found the best solution for the three test instances.

Referring to Table 2, the GA that employs the modified uniform crossover operator outperforms the other methods across all test instance groups. Experimental results indicate that the linear arithmetic crossover achieves superior performance to the arithmetic crossover within the GA structure.

Table 2. Summary of the computational experiments considering best solution according to number of locations.

# of Location	# of Instances	*% gap* for GA with OPC	*% gap* for GA with TPC	*% gap* for GA with AC	*% gap* for GA With LAC	*% gap* for GA with MLAC	*% gap* for GA with MUC
10	3	**0,00**	**0,00**	**0,00**	**0,00**	**0,00**	**0,00**
15	3	**0,00**	**0,00**	**0,00**	**0,00**	**0,00**	**0,00**
20	3	**0,00**	**0,00**	**0,00**	**0,00**	**0,00**	**0,00**
25	3	**0,00**	**0,00**	0,55	**0,00**	0,13	**0,00**
30	3	**0,00**	**0,00**	1,06	**0,00**	0,43	**0,00**
35	3	**0,00**	0,02	0,02	0,06	**0,00**	**0,00**
40	3	0,05	**0,00**	0,36	0,05	0,64	**0,00**
45	3	0,00	0,09	1,31	0,18	0,91	**<0,01**
50	3	0,31	0,12	1,36	0,02	0,61	**<0,01**
55	3	0,25	0,31	1,52	0,32	1,39	**<0,01**
60	3	0,16	0,05	2,04	0,16	0,78	**<0,01**
70	3	0,57	0,09	2,21	0,50	1,55	**<0,01**

GA: genetic algorithm, OPC: one-point crossover, TPC: two-point crossover, AC: arithmetic crossover, LAC: linear arithmetic crossover, MLAC: modified linear arithmetic crossover, MUC: modified uniform crossover
Bold values show the best performance.

The averages of the solutions are summarized in Table 3 according to number of locations. According to this table, the GA uses modified uniform crossover operator, appears to be less efficient than the analysis considering the best solutions. On the other hand, it seems that it is more logical to use linear arithmetic crossover rather than the GA using arithmetic crossover method, because linear arithmetic crossover was superior to arithmetic crossover in all test problem groups.

Table 3. Summary of the computational experiments considering average solution according to number of locations.

# of Location	# of Instances	*% gap* for GA with OPC	*% gap* for GA with TPC	*% gap* for GA with AC	*% gap* for GA with LAC	*% gap* for GA with MLAC	*% gap* for GA with MUC
10	3	**0,00**	**0,00**	**0,00**	**0,00**	**0,00**	**0,00**
15	3	**0,00**	**0,00**	0,13	**0,00**	**0,00**	**0,00**
20	3	**0,00**	**0,00**	0,81	**0,00**	0,40	**0,00**
25	3	0,06	0,06	1,72	**0,02**	0,66	0,10
30	3	0,22	**0,18**	2,41	0,37	1,67	0,26
35	3	0,27	0,47	2,71	0,57	1,95	**0,30**
40	3	0,50	0,32	2,44	0,83	1,79	**0,21**
45	3	**0,36**	0,64	2,82	0,50	2,00	0,65
50	3	0,59	**0,50**	1,89	0,54	1,61	0,59
55	3	0,74	0,71	2,73	1,11	2,89	**0,64**
60	3	**0,50**	0,58	3,86	0,88	1,93	0,70
70	3	1,06	0,86	3,97	1,61	3,20	**0,78**

GA: genetic algorithm, OPC: one-point crossover, TPC: two-point crossover, AC: arithmetic crossover, LAC: linear arithmetic crossover, MLAC: modified linear arithmetic crossover, MUC: modified uniform crossover
Bold values show the best performance.

All calculation results are presented in Table 4 by specifying the algorithms according to the deviation of the obtained solutions (both best and average) from the best-found solution and the number of the best solution was obtained. As a result, the genetic algorithm that uses the modified uniform crossover operator is more effective in terms of both the number of best solutions and the deviation value from the best solution.

Table 4. Summary of all computations.

# of Instances	GA with OPC	GA with TPC	GA with AC	GA with LAC	GA with MLAC	GA with MUC
# of Best Solution	24	24	14	21	18	**28**
Mean of Average % gap	0,3589	0,361	2,12	0,537	1,509	**0,352**
Mean of Best % gap	0,1118	0,0568	0,8695	0,1083	0,5368	**0,0006**

GA: genetic algorithm, OPC: one-point crossover, TPC: two-point crossover, AC: arithmetic crossover, LAC: linear arithmetic crossover, MLAC: modified linear arithmetic crossover, MUC: modified uniform crossover
Bold values show the best performance.

4. CONCLUSION AND FUTURE RESEARCH

This study compares the effectiveness of different crossover methods used in genetic algorithms. These methods are applied to solve the p-median problem, which is commonly addressed in literature and is relevant to many real-world problems. A total of six different crossover methods were employed in genetic algorithms with the same parameter values, and their effectiveness was evaluated across 36 test instances. Experimental study shows that the modified uniform crossover method performs greater effectiveness than the other crossover methods for the specified encoding schema. The literature includes various distinct variations of p-median problems, making this study significant in terms of comparing the effectiveness of crossover methods.

Future studies could focus on the development and comparison of more advanced crossover operators specifically designed for complex optimization problems. For example, adaptive or self-adjusting crossover operators that dynamically change their behavior according to the progress of the algorithm may further improve solution quality. Another promising direction is the design of hybrid crossover operators that combine the advantages of arithmetic, uniform, and order-based methods, aiming to balance exploration and exploitation more effectively. In addition, problem-specific crossover operators tailored to different variations of the p-median problem (such as capacitated or dynamic versions) could be proposed and tested. Finally, examining how the encoding scheme influences the performance of different crossover operators could open up new avenues for more efficient and reliable applications of genetic algorithms.

REFERENCES

Abdoun, O., & Abouchabaka, J. (2012). A comparative study of adaptive crossover operators for genetic algorithms to resolve the traveling salesman problem. *arXiv preprint arXiv:1203.3097*.

Çelik, S., & Ok, Ş. (2024). Electric vehicle charging stations: Model, algorithm, simulation, location, and capacity planning. *Heliyon*, *10*(7).

Correa, E. S., Steiner, M. T. A., Freitas, A. A., & Carnieri, C. (2004). A genetic algorithm for solving a capacitated p-median problem. *Numerical Algorithms*, *35*, 373-388.

Deep, K., Singh, K. P., Kansal, M. L., & Mohan, C. (2009). A real coded genetic algorithm for solving integer and mixed integer optimization problems. *Applied Mathematics and Computation*, 212(2), 505–518.

Farahani, R. Z., Hekmatfar, M., Fahimnia, B., & Kazemzadeh, N. (2014). Hierarchical facility location problem: Models, classifications, techniques, and applications. *Computers & Industrial Engineering*, *68*, 104-117.

Goldberg, D. E. (1989). *Genetic Algorithms in Search, Optimization and Machine Learning*. Addison-Wesley.

He, P., Hao, J. K., & Wu, Q. (2024). A hybrid genetic algorithm for the Hamiltonian p-median problem. *Networks*, *83*(2), 348-367.

Herrera, F., Lozano, M., & Verdegay, J. L. (1998). Tackling real-coded genetic algorithms: Operators and tools for behavioural analysis. *Artificial Intelligence Review*, 12(4), 265–319.

Holland, J. H. (1975). *Adaptation in Natural and Artificial Systems*. University of Michigan Press.

Hosseini-Nasab, H., Fereidouni, S., Fatemi Ghomi, S. M. T., & Fakhrzad, M. B. (2018). Classification of facility layout problems: a review study. *The International Journal of Advanced Manufacturing Technology*, *94*(1), 957-977.

Kora, P., & Yadlapalli, P. (2017). Crossover operators in genetic algorithms: A review. International Journal of Computer Applications, 162(10).

Liang, H., Wang, S., Li, H., Pan, J., Li, X., Su, C., & Liu, B. (2025). AIAM: Adaptive interactive attention model for solving p-Median problem via deep reinforcement learning. *International Journal of Applied Earth Observation and Geoinformation*, *138*, 104454.

Macit, I. (2025). Determination of The Location Layout of Electricity Agriculture Tractors In Open Landscape Conditions with The P-Median Chance Constrained Mixed Integer Mathematics Model. *International Journal of Industrial Engineering: Theory, Applications and Practice*, *32*(4).

Pérez-Gosende, P., Mula, J., & Díaz-Madroñero, M. (2021). Facility layout planning. An extended literature review. *International Journal of Production Research*, *59*(12), 3777-3816.

Wright, A. H. (1991). Genetic algorithms for real parameter optimization. *Foundations of Genetic Algorithms*, 1, 205–218.

Talbi, E. G. (2009). Metaheuristics: From Design to Implementation. *John Wiley & Sons google schola*, *2*, 268-308.

Umbarkar, A. J., & Sheth, P. D. (2015). Crossover operators in genetic algorithms: a review. *ICTACT journal on soft computing*, *6*(1).

Varnamkhasti, M. J., & Varnamkhast, M. J. (2025). New Technique for Solving P-Median Problems based on Fuzzy System and Genetic Algorithm. *Journal of Intelligent Decision and Computational Modelling*, *1*(1), 15-26.

Wang, X., Xue, Y., Zhang, J., Hong, Y., Guo, S., & Zeng, X. (2024). A sustainable supply chain design for personalized customization in Industry 5.0 era. *IEEE Transactions on Industrial Informatics*, *20*(6), 8786-8797.